

**AN INVESTIGATION OF THE WAVE ENERGY RESOURCE
ON THE SOUTH AFRICAN COAST, FOCUSING ON THE
SPATIAL DISTRIBUTION OF THE SOUTH WEST COAST**

by

J.R Joubert

Thesis presented in partial fulfilment of the requirements
for the degree of Master of Science in Civil Engineering
at the University of Stellenbosch

Mr. D.E. Bosman
Study leader

DECLARATION

I, the undersigned, hereby declare that the work contained in this thesis is my own original work and that I have not previously in its entirety or in part submitted it at any other university for a degree.

Signature: R. Joubert

Date: 27/02/2008

ABSTRACT

This thesis is an investigation of the wave power resource on the South African coast, focusing on the spatial distribution of wave power of the coastal region exposed to the highest wave power. The study's main objective is to provide a detailed description of the spatial distribution of wave power to assist in the selection of locations for deployment of Wave Energy Converter (WEC) units in this zone. The study methodology employed to achieve this main objective entails an analysis of measured wave data recorded at wave recording stations distributed along the South African coast. The analysis provided a general description of wave power at locations for which wave data exist. From this analysis it was found that the South West Coast is exposed to the highest wave power, with an average wave power of approximately 40 kW per meter wave crest. The rest of the South African coast is exposed to average wave power between approximately 18 kW/m to 23 kW/m.

The wave power characteristics on the South West Coast region (from Cape Point to Elands Bay) were therefore the focus of this thesis. The study objective was achieved by transferring deep sea wave data into the nearshore South West Coast study area with the Simulating WAVes Nearshore (SWAN) wave model. The deep sea wave data was obtained from a 10 year period of available hindcast data. A simplified simulation procedure was required in order to make the study practically feasible. A sensitivity analysis was carried out to determine the validity of the simplified simulation procedure and it was found that the procedure slightly overestimate wave power in the shallower water regions due to the underestimation of energy dissipation processes. This overestimation was deemed acceptable for the dominant wave conditions and the simplified model was therefore applied in the study. An appropriate programming system was developed and used to transfer the available 10 year deep sea wave data into the selected South West Coast region. From this exercise spatial distribution of wave power and related statistical parameters were obtained for the study area. The accuracy of the modelled output was investigated by directly comparing it to wave data recorded during the overlapping recording period. It was found that the model slightly overestimates the monthly wave power resource compared to the measured data with a maximum overestimation of 9%; which is sufficiently accurate for the purpose of the study.

The results of this investigation can be used for the identification of areas of high wave power concentration within the study area for the location of WEC units. Further

numerical modelling is required for the detailed design of wave farms, especially if potential sites are located in shallow water (shallower than approximately 50 m).

SAMEVATTING

In hierdie tesis is die golfdrywing-hulpbron aan die Suid-Afrikaanse kus ondersoek met fokus op die ruimtelike verspreiding van golfdrywing van die kusgebied waar die mees intensiewe golfdrywing voorkom. Die studie se hoofdoel is om 'n gedetailleerde beskrywing te verskaf van die ruimtelike verspreiding van golfdrywing wat kan dien as 'n hulpmiddel vir die identifisering van areas vir die onttrekking van seegolf-energie. Die studie metodiek wat gevolg is ten einde hierdie doel te bereik, behels onder andere, die analiese van historiese golf data soos gemeet by golfstasies langs die Suid-Afrikaanse kus. Hierdie analiese dien as 'n algemene beskrywing van die Suid-Afrikaanse golfdrywing hulpbron by gebiede waar golfdata beskikbaar is. Vanaf hierdie analiese is daar gevind dat die grootse golfdrywing aan die Suid-Wes kus voorkom, met 'n benaderde gemiddelde golfdrywing van 40 kW/m. Die res van die Suid-Afrikaanse kus word blootgestel aan gemiddelde golfdrywing van tussen 18 kW/m tot 23 kW/m.

Die golfdrywing eienskappe van die Suid-Wes Kus (van Kaappunt tot Elandsbaai) was dus die fokus van hierdie tesis. Die studie se hoofdoel is bereik deur die transformasie van beskikbare diepsee golf data tot in die nabyliggende kusgebied van die Suid-Wes Kus studie area met die "Simulating WAves Nearshore (SWAN)" golf model. Die diep see golf data is verkry van 'n 10 jaar periode van beskikbare historiese data van 'n globale golfmodel. 'n Vereenvoudigde simulasiemasjienprosedure was gebruik om die studie prakties uitvoerbaar te maak. 'n Sensitiwiteitsanaliese is gedoen om die akkuraatheid van hierdie vereenvoudigde simulasiemasjienprosedure te bepaal en daar is gevind dat die model golfdrywing effens oorskakel in vlak water weens die onderskatting van energieverliese. Die akkuraatheid van die model was aanvaarbaar vir die dominante golf kondisies en die vereenvoudigde model kon dus toegepas word in die studie. 'n Toepaslike programmeringsstelsel was ontwikkel en gebruik vir die transformasie van die beskikbare 10 jaar diepsee golfdata. Vanuit laasgenoemde prosedure is die ruimtelike verspreiding van golfdrywing en verwante statistiese parameters verkry vir die studie-area. Die gemodelleerde uitvoer data is geverifieer deur dit te vergelyk met gemete golfdata. Daar is bevind dat die model die maandelikse golfdrywing oorskakel met 'n maksimum van 9% wat beskou is as voldoende akkuraat vir die doeleindes van die studie.

Die resultate van die studie kan dien as 'n hulpmiddel vir die identifisering van areas met hoë golfdrywing konsentrasies vir kragopwekking binne die studie area. Verdere numeriese

modellering sal benodig word vir die gedetailleerde ontwerp van golf-aangedrewe kragstasies, veral as die stasies in vlak water geleë is (vlakker as ongeveer 50 m).

ACKNOWLEDGEMENTS

I would like to express my gratitude to a number of people who contributed to the successful completion of this thesis:

I would firstly like to thank the Transnet National Ports Authority of South Africa for their permission to use the collection of recorded wave data recorded along the South African coast. I am indebted to the CSIR personnel for making available the recorded wave data and their friendly support and willingness to help, in particular, Mr. Marius Rossouw. I would like to express my gratitude to the Centre for Renewable and Sustainable Energy Studies and Prof Wikus van Niekerk (Director of the Centre) for their support.

I would like to express my sincere appreciation to Mr. Cobus Rossouw of ZHL consulting engineers. Without his willingness to help and expert advice on numerical modelling, this study would not have been possible. I would also like to thank Mr. Albert Strasheim who greatly contributed to the computer programming to enable a vast number of computer simulations and who helped transform billions of numbers into a visual splendour. Thank you to my family and friends for their support throughout the course of the last two years.

Lastly, I would like to thank my mentor and the single biggest contributor to my study, Mr. Eddie Bosman. Mr Bosman was ever willing to help and provide expert advice throughout this study.

TABLE OF CONTENTS

ABSTRACT	i
SAMEVATTING	iii
ACKNOWLEDGEMENTS	v
TABLE OF CONTENTS	vi
LIST OF TABLES	xi
LIST OF FIGURES	xiii
LIST OF APPENDICES	xviii
NOMENCLATURE	xix
DEFINITION OF TERMS	xx
1. INTRODUCTION	1-1
1.1. Problem statement	1-1
1.2. Existing work	1-1
1.3. Aims of study	1-1
1.4. Scope and limitations	1-3
1.5. Main sources of information	1-3
1.6. Thesis overview	1-4
2. LITERATURE REVIEW	2-1
2.1. Origins of wave power and its global distribution (Boud, 2003)	2-1
2.2. South African meteorology (Rossouw, 1989)	2-2
2.3. Numerical weather prediction (NWP)	2-4
2.4. Wave parameters relevant to ocean wave power (CEM, 2002)	2-7
2.4.1. Basic wave mechanics	2-7
2.4.2. Energy density	2-8
2.4.3. Wave power (wave energy flux)	2-10
2.4.4. Spectral analysis	2-10
2.4.4.1. One dimensional wave energy density spectrum	2-10
2.4.4.2. Two dimensional wave energy density spectrum	2-12
2.4.5. Wave energy density spectra shapes and the peak-enhancement factor	2-13
2.4.6. Wave power calculation procedure	2-15
2.5. Wave Energy Conversion technology	2-16

2.5.1.	Introduction	2-16
2.5.2.	Classification of WEC's	2-16
2.5.3.	Oscillating Water Column WEC types	2-17
2.5.3.1.	Description	2-17
2.5.3.2.	Conclusions on Oscillating Water Column WEC types	2-21
2.5.4.	Reservoir storage WEC types	2-22
2.5.4.1.	Description	2-22
2.5.4.2.	Conclusions on reservoir storage WEC types	2-22
2.5.5.	Relative motion WEC types	2-23
2.5.5.1.	Description	2-23
2.5.5.2.	Conclusions on relative motion WEC types	2-27
2.5.6.	Cost comparison	2-28
3.	WAVE POWER CONDITIONS ON THE SOUTH AFRICAN COAST BASED ON RECORDED DATA	3-1
3.1.	Description of wave recording stations and available wave data	3-1
3.1.1.	Port Nolloth	3-3
3.1.2.	Slangkop	3-3
3.1.3.	Cape Point	3-4
3.1.4.	FA platform	3-5
3.1.5.	Durban	3-5
3.2.	Percentage coverage of recording stations	3-6
3.2.1.	Port Nolloth	3-6
3.2.2.	Slangkop	3-8
3.2.3.	Cape Point	3-10
3.2.4.	FA platform	3-11
3.2.5.	Durban	3-12
3.3.	Wave height and -period exceedance analysis	3-14
3.3.1.	Wave height	3-14
3.3.2.	Wave period	3-15
3.4.	Peak-enhancement factor analysis	3-17
3.5.	Directional distribution	3-18
3.6.	Annual and seasonal wave power	3-20
3.6.1.	Introduction	3-20
3.6.2.	Port Nolloth	3-21
3.6.3.	Slangkop	3-22

3.6.4.	Cape Point	3-24
3.6.5.	FA platform	3-26
3.6.6.	Durban	3-28
3.7.	Wave energy development index (WEDI) = $\frac{\bar{P}}{P_{\max}}$	3-30
3.8.	Probability of exceedance- and frequency of occurrence of wave power	3-31
3.8.1.	Introduction	3-31
3.8.2.	Port Nolloth	3-32
3.8.3.	Slangkop	3-33
3.8.4.	Cape Point	3-35
3.8.5.	FA platform	3-36
3.8.6.	Durban	3-37
3.9.	Wave energy scatter diagrams	3-39
3.9.1.	Port Nolloth	3-39
3.9.2.	Slangkop	3-40
3.9.3.	Cape Point	3-41
3.9.4.	FA platform	3-41
3.9.5.	Durban	3-44
3.10.	Summary and conclusions of recorded wave data analysis	3-45
3.10.1.	Summary	3-45
3.10.1.1.	Port Nolloth	3-45
3.10.1.2.	Slangkop	3-46
3.10.1.3.	Cape Point	3-46
3.10.1.4.	FA platform	3-46
3.10.1.5.	Durban	3-47
3.10.1.6.	Comparison of wave power distribution at all recording stations	3-47
3.10.2.	Conclusions	3-49
4.	SPATIAL WAVE POWER DISTRIBUTION ON THE SOUTH AFRICAN SOUTHWEST COAST BASED ON HINDCAST DATA	4-1
4.1.	Introduction	4-1
4.2.	Hindcast wave data used in the study	4-2
4.3.	Analysis of NCEP deep sea data at selected deep sea location	4-4
4.3.1.	Directional distribution	4-4
4.3.2.	Wave energy scatter analysis	4-6

4.3.3.	Frequency of occurrence of concurrent wave period and wave direction	4-6
4.3.4.	A comparison of wave power at Base and Cape Point recording station	4-7
4.4.	Background of the SWAN wave model	4-8
4.4.1.	Functionality of SWAN	4-9
4.4.2.	General formulation	4-9
4.5.	SWAN assumptions	4-10
4.6.	Input requirements for SWAN model analyses	4-12
4.6.1.	Computational grid for SWAN simulations	4-12
4.6.2.	Bathymetric grid	4-13
4.6.3.	Boundary conditions	4-15
4.6.3.1.	Peak wave period (T_p)	4-15
4.6.3.2.	Peak wave direction (D_p)	4-15
4.6.3.3.	Peak-enhancement factor (γ) and wave directional spreading (m)	4-15
4.6.3.4.	Significant wave height (H_s)	4-16
4.7.	Simulation process	4-20
4.7.1.	Automated file generation and simulation	4-20
4.8.	Simulate NCEP wave data	4-21
4.9.	Results of model study	4-23
4.9.1.	Mean annual wave power	4-24
4.9.2.	Mean seasonal wave power	4-26
4.9.3.	Mean monthly wave power	4-29
4.10.	Comparison of model hindcast- to measured data	4-32
4.10.1.	A comparison of monthly wave power distribution at Cape Point with SWAN transferred hindcast data close to the latter recording station	4-32
5.	SUMMARY AND CONCLUSIONS OF STUDY	5-1
5.1.	Literature study	5-1
5.2.	Wave power conditions on the South African coast based on recorded data	5-1
5.3.	Spatial wave power distribution on the South African South West Coast based on hindcast data	5-3
6.	RECOMMENDATIONS	6-1

LIST OF TABLES

Table 2-1:	Capital cost comparison of WEC units	2-28
Table 3-1:	Relevant information of wave recording stations	3-1
Table 3-2:	Overlapping of recording periods of wave recording stations and percentage coverage	3-6
Table 3-3:	Coverage of Port Nolloth wave data	3-7
Table 3-4:	Coverage of Slangkop wave data	3-9
Table 3-5:	Coverage of Cape Point wave data	3-11
Table 3-6:	Coverage of FA platform wave data	3-12
Table 3-7:	Coverage of the Durban wave data	3-13
Table 3-8:	Mean annual frequency of occurrence of T_p	3-16
Table 3-9:	Probability of exceedance of 90-, 50- and 10% for T_p	3-17
Table 3-10:	Seasonal statistical parameters of the wave power (kW/m) at Port Nolloth	3-22
Table 3-11:	Statistical seasonal parameters of the wave power (kW/m) at Slangkop recording station	3-24
Table 3-12:	Statistical seasonal parameters of the wave power (kW/m) at Cape Point (Slangkop recording station)	3-26
Table 3-13:	Statistical parameters of the wave power (kW/m) at FA platform	3-28
Table 3-14:	Statistical parameters of the wave power (kW/m) at Durban recording station	3-29
Table 3-15:	WEDI of the various recording stations	3-30
Table 4-1:	Frequency of occurrence of concurrent values of T_p and D_p	4-7
Table 4-2:	A comparison of mean annual wave power (kW/m) at Base and Cape Point	4-7
Table 4-3:	5% and 1% probability of exceedance for extreme seasonal wave power events at model grid point closest to Cape Point recording station	4-29
Table 4-4:	Percentage difference in mean monthly average wave power of measured and modelled data	4-33
Table 4-5:	1% and 5% probability of exceedance of extreme wave power events for the modelled and measured data	4-34

Tables in Appendices:

- Table A- 1: Wave power calculation results
- Table D- 1: UTM coordinates of comparative locations
- Table D- 2: Percentage overestimation of wave power as determined by method 2
- Table D- 3: Peak-enhancement factor values
- Table E- 1: Wave height conditions at Base on the model boundary
- Table E- 2: Wave height conditions at Pt1 on model boundary
- Table E- 3: Wave height conditions at South Eastern corner of model boundaries
- Table E- 4: Wave height conditions at north western corner of model boundaries

LIST OF FIGURES

Figure 1-1:	The main and sub-objectives, overall methodology and structure of the thesis	1-2
Figure 2-1:	Global distribution of deep sea average annual ocean wave power (www.oceanpd.com/Resource/Worldresourcemap.html , 17/4/07)	2-2
Figure 2-2:	Composite diagram showing the important typical features of the surface atmospheric circulation over South Africa (Tyson et al, 2000)	2-3
Figure 2-3:	Tropical cyclone occurrence and intensity map for the Southern African east coast (Rossouw, 1999).	2-4
Figure 2-4:	Wind field at 10m elevation	2-5
Figure 2-5:	Resulting wave field	2-5
Figure 2-6:	Wave period dispersion from storm generation zone http://polar.ncep.noaa.gov/waves/main_text.html , 26/11/2007)	2-6
Figure 2-7:	A simple sinusoidal wave (WMO, 1998)	2-8
Figure 2-8:	3D representation of parameters relevant to specific energy (Massie et al, 2001)	2-9
Figure 2-9:	1D irregular sea state (WMO, 1998)	2-11
Figure 2-10:	2D irregular sea state (Carbon Trust UK, 2007)	2-11
Figure 2-11:	2D spectrum (CEM 2002)	2-13
Figure 2-12:	Direction distribution function (van Tonder, 1992)	2-13
Figure 2-13:	PM and JONSWAP spectrums (CEM, 2002)	2-13
Figure 2-14:	Classification by deployment location (Falnes, 2005)	2-17
Figure 2-15:	Classification by size and orientation (Falnes, 2005)	2-17
Figure 2-16:	Cross sectional view of LIMPET	2-19
Figure 2-17:	LIMPET (The Queen's University Belfast, 2002)	2-19
Figure 2-18:	Parabolic wall OWC (Previsic, 2004)	2-19
Figure 2-19:	SWEC (Retief, 2007)	2-20
Figure 2-20:	Pressure increase caused by wave crest (Retief, 2007)	2-21
Figure 2-21:	Pressure reduction caused by wave trough (Retief, 2007)	2-21
Figure 2-22:	Schematic representation of a WAVEDRAGON unit (Previsic, 2004)	2-23
Figure 2-23:	PELAMIS - Sea snake (bottom photograph) and WEC (top photograph)	2-24
Figure 2-24:	PELAMIS specifications	2-24
Figure 2-25:	AQUABUOY displacer, reactor and hose pump	2-25

Figure 2-26:	Sea trials of IPS buoy	2-25
Figure 2-27:	AWS prototype at sea	2-26
Figure 2-28:	Components of AWS	2-27
Figure 2-29:	Submerged depth of AWS (Previsic, 2004)	2-27
Figure 3-1:	Contours of the Southern African seabed to 3000 m depth and the distribution of wave recording stations (van der Westhuysen, 2002)	3-2
Figure 3-2:	South African sea storm regions (MacHutchon, 2006)	3-2
Figure 3-3:	Locations of Slangkop and Cape Point wave recording stations	3-4
Figure 3-4:	Arial view of the FA platform in 113 m water depth	3-5
Figure 3-5:	Bar chart representation of the degree of completeness of Port Nolloth wave data	3-8
Figure 3-6:	Bar representation of degree of completeness of the Slangkop wave data	3-10
Figure 3-7:	Bar representation of degree of completeness of the Durban wave data	3-13
Figure 3-8:	Probability of exceedance of H_s for South African recording stations	3-14
Figure 3-9:	Frequency of occurrence of H_s	3-15
Figure 3-10:	Mean annual frequency of occurrence of T_p	3-16
Figure 3-11:	Scatter plot of γ and T_p measured at Cape Point recording station	3-18
Figure 3-12:	Scatter plot of m and T_p values recorded at Cape Point	3-19
Figure 3-13:	The relationships of T_p and m as observed at Cape Point and after Rossouw (2007)	3-20
Figure 3-14:	Annual and mean annual wave power at Port Nolloth	3-21
Figure 3-15:	Seasonal wave power distribution at Port Nolloth recording station	3-21
Figure 3-16:	Annual- and mean annual wave power at Slangkop recording station	3-22
Figure 3-17:	A comparison of wave power at Slangkop- (SK) and Port Nolloth recording station (PN) during overlapping recording years	3-23
Figure 3-18:	Seasonal wave power distribution at Slangkop recording station	3-24
Figure 3-19:	Annual- and mean annual wave power at Cape Point recording station	3-25
Figure 3-20:	Available seasonal wave power at Cape Point recording station	3-25
Figure 3-21:	Annual- and mean annual wave power at FA platform	3-26
Figure 3-22:	A comparison of wave power at Cape Point (CP) and FA platform (FA) during overlapping recording years	3-27
Figure 3-23:	Seasonal wave power at FA platform	3-27
Figure 3-24:	Annual- and mean annual wave power at Durban	3-28
Figure 3-25:	Seasonal variability of wave power at Durban recording station	3-29
Figure 3-26:	A comparison of the WEDI of each station	3-30

Figure 3-27: Probability of exceedance of different power levels at Port Nolloth recording station	3-32
Figure 3-28: Frequency of occurrence of different power levels at Port Nolloth recording station	3-33
Figure 3-29: Probability of exceedance of different power levels at Slangkop recording station	3-34
Figure 3-30: Frequency of occurrence of different power levels at Slangkop recording station	3-34
Figure 3-31: Probability of exceedance of different power levels at Cape Point recording station	3-35
Figure 3-32: Frequency of occurrence of different power levels at Cape Point recording station	3-36
Figure 3-33: Probability of exceedance of different power levels at the FA platform	3-36
Figure 3-34: Frequency of occurrence of different power levels at FA platform	3-37
Figure 3-35: Probability of exceedance of different power levels at the Durban recording station	3-37
Figure 3-36: Frequency of occurrence of different power levels at Durban	3-38
Figure 3-37: Wave energy scatter diagram at Port Nolloth recording station	3-40
Figure 3-38: Wave energy scatter diagram at Slangkop recording station	3-40
Figure 3-39: Wave energy scatter at Cape Point	3-41
Figure 3-40: Wave power scatter at FA platform	3-42
Figure 3-41: High frequency spectrum development	3-43
Figure 3-42: Wave exposure from opposing directions at the platform (www.buoyweather.com , 01/02/1997)	3-44
Figure 3-43: Dual directional exposure at the FA platform (http://polar.ncep.noaa.gov/waves/main_text.html , 26/08/2007)	3-44
Figure 3-44: Wave energy scatter at Durban	3-45
Figure 3-45: A comparison of statistical parameters of wave power of all stations	3-47
Figure 3-46: Probability of exceedance comparison of all stations	3-48
Figure 3-47: Frequency of occurrence comparison of all stations	3-48
Figure 4-1: Presentation of objective, methodology, output and investigation area	4-2
Figure 4-2: Frequency of occurrence of wave direction	4-4
Figure 4-3: NCEP wave direction rose	4-5
Figure 4-4: Wave energy scatter diagram of Base	4-6
Figure 4-5: A comparison of monthly wave power distribution at Cape Point (CP) and Base (NCEP)	4-8

Figure 4-6:	An overview of the wave transfer process with SWAN	4-11
Figure 4-7:	Illustration of the SWAN model grid spacing relative to seabed depth contours	4-13
Figure 4-8:	Digitisation and bathymetric grid generation process	4-14
Figure 4-9:	Peak-enhancement factor (CEM, 2002)	4-16
Figure 4-10:	Directional spreading	4-16
Figure 4-11:	Procedure employed to determine H_s conditions on model boundaries	4-17
Figure 4-12:	Determination of H_s variation for example NCEP record	4-18
Figure 4-13:	Areas affected by erroneous boundary conditions (Shaded zones)	4-19
Figure 4-14:	Automated file generation and simulation process	4-21
Figure 4-15:	NCEP simulation process for an example case	4-22
Figure 4-16:	Bathymetry contour map of the study area	4-23
Figure 4-17:	Mean annual average wave power distribution (kW/m) of the South West coastal zone based on 10 years of hindcast wave data	4-25
Figure 4-18:	Spatial distribution of mean seasonal average wave power (kW/m) for summer	4-27
Figure 4-19:	Spatial distribution of mean seasonal average wave power (kW/m) for autumn	4-27
Figure 4-20:	Spatial distribution of mean seasonal average wave power (kW/m) for winter	4-27
Figure 4-21:	Spatial distribution of mean seasonal average wave power (kW/m) for spring	4-27
Figure 4-22:	Seasonal probability of exceedance of wave power at model grid point closest to Cape Point recording station	4-28
Figure 4-23:	Mean monthly average wave power distribution (kW/m) for January	4-30
Figure 4-24:	Mean monthly average wave power distribution (kW/m) for April	4-30
Figure 4-25:	Mean monthly average wave power distribution (kW/m) for July	4-30
Figure 4-26:	Mean monthly average wave power distribution (kW/m) for October	4-30
Figure 4-27:	Statistical parameters of mean monthly modeled wave power	4-31
Figure 4-28:	Monthly measure and modeled wave power	4-33
Figure 4-29:	Probability of exceedance of wave power measured at Cape Point recording station and modeled data (hindcast data transferred)	4-34
Figure 5-1:	Wave power exposure of each wave recording station	5-2
Figure 5-2:	Mean annual average wave power distribution (kW/m) of the South West coastal zone based on 10 years of hindcast wave data	5-5

Figures in Appendices:

- Figure A- 1: 100% wave reflection by non-absorbing vertical barrier (Chadwick et.al, 2004)
- Figure A- 2: Superimposed wave due to 100% reflection (Port and Coastal Engineering lecture notes, 2007)
- Figure A-3: Typical "snap-shot" of an ocean wave train
- Figure A-4: Dominant measured wave spectrum for Slangkop
- Figure B- 1: Design wave heights for Port Nolloth recording station
- Figure B- 2: Design wave heights for Cape Point recording station
- Figure B- 3: Design wave heights for FA platform wave recording station
- Figure B- 4: Design wave heights for Durban recording station
- Figure C- 1: A comparison of monthly average wave power
- Figure C- 2: Comparison of monthly 90% exceedance of wave power
- Figure C- 3: Comparison of monthly standard deviation of wave power
- Figure D- 1: Locations in deep, intermediate, shallow and sheltered water considered in the sensitivity analysis
- Figure D- 2: Wave power at deep water location as determined by method 1 and 2 for $H_s = 2.6\text{m}$
- Figure D- 3: Wave power at shallow water location as determined by method 1 and 2 for $H_s = 2.6\text{m}$
- Figure D- 4: Wave power at sheltered location as determined by method 1 and 2 for $H_s = 2.6\text{m}$
- Figure F- 1: Mean monthly average wave power distribution (kW/m) for January
- Figure F- 2: Mean monthly average wave power distribution (kW/m) for February
- Figure F- 3: Mean monthly average wave power distribution (kW/m) for March
- Figure F- 4: Mean monthly average wave power distribution (kW/m) for April
- Figure F- 5: Mean monthly average wave power distribution (kW/m) for May
- Figure F- 6: Mean monthly average wave power distribution (kW/m) for June
- Figure F- 7: Mean monthly average wave power distribution (kW/m) for July
- Figure F- 8: Mean monthly average wave power distribution (kW/m) for August
- Figure F- 9: Mean monthly average wave power distribution (kW/m) for September
- Figure F- 10: Mean monthly average wave power distribution (kW/m) for October
- Figure F- 11: Mean monthly average wave power distribution (kW/m) for November
- Figure F- 12: Mean monthly average wave power distribution (kW/m) for December

LIST OF APPENDICES

- APPENDIX A: Calculation of wave energy and wave power related parameters
- APPENDIX B: Design wave heights at wave recording stations along the South African coast as determined by (MacHutchon, 2006)
- APPENDIX C: Monthly wave power distribution at wave recording stations
- APPENDIX D: Validation and sensitivity analysis of simplified simulation procedure and the consequential impact on energy dissipation
- APPENDIX E: Wave height conditions on model boundaries for concurrent wave period and –direction conditions
- APPENDIX F: Spatial maps of monthly average wave power of the study area
- APPENDIX G: A comparison of monthly average probability of exceedance of measured- and modelled wave power
- APPENDIX H: Index of electronic appendix

NOMENCLATURE

Symbols

C	wave celerity (m/s)
C_g	group velocity (m/s)
c_x, c_y	wave propagation velocity (celerity) in the x- and y space respectively
c_σ	wave propagation velocity in frequency space
c_θ	wave propagation velocity through the directional space
Dir or D_p	peak wave direction
d	water depth (m)
\bar{E}	specific energy or energy density (Joules/m ²)
f	wave frequency (Hz)
H_s	significant wave height, H_{mo} if calculated in the frequency domain
H_{RMS}	root mean square wave height (time domain)
J or \bar{P}	wave energy flux or wave power (Joules/s/m length of wave crest) or (kW/m)
L	wavelength in intermediate and shallow water depth (m)
m	power of the $\cos^m \theta$ function directly related to directional spreading around the peak direction
ρ	sea water density = 1025kg/m ³
S	source term which represents all effects of wave generation and dissipation
S_{surf}	source term for dissipation of wave energy due to depth induced breaking
$S_{ds,b}$	source term for dissipation of wave energy due to bottom friction
T_p	spectral peak wave period (s)
θ	mean wave direction
γ	peak-enhancement factor of the JONSWAP wave spectrum
σ	relative (intrinsic) wave frequency
ω	wave frequency

Acronyms

JONSWAP	Joint North Sea Wave Project
NCEP	National Centers for Environmental Prediction
SWAN	Simulation WAVes Nearshore (Numerical model of the Delft University of Technology, 2006)
WEC	Wave energy converter

DEFINITION OF TERMS

Wind and wave direction

Wind and wave directions indicate the directions from which the wind blows and from which the waves approach. The direction convention is clockwise from North = $0^\circ = 360^\circ$. According to this convention, the direction range starts from North (0°) and increases over 90° (East), 180° (South) and 270° (West) back to $360^\circ = 0^\circ$ (North).

Peak wave direction (D_p)

The peak wave direction is defined as the direction associated with the peak spectral frequency of $E(\sigma, \theta)$

Peak wave period (T_p)

The wave period calculated as the inverse of the spectral peak frequency (the frequency in the wave energy spectrum at which maximum energy occur).

(van der Westhuysen, 2004)

Significant wave height (H_s)

A wave parameter derived statistically from the wave time series (i.e. $H_s = 4 \times$ standard deviation).

Numerical modelling or numerical simulation

“The determination of a numerical solution to the governing equations of fluid flow whilst advancing the solution through space or time to obtain a numerical description of the complete flow field of interest”. (NASA glossary)

The numerical model

Referring to the collective components required for successful numerical wave modelling.

Wave farms

Consists out of one or more wave energy converter devices, but generally refers to arrays of wave energy converter devices.

1. INTRODUCTION

1.1. Problem statement

Currently the global energy demand is predominantly being met by our exhaustible resource of fossil fuels. A diminishing supply and increasing demand has seen significant increases in oil prices in the last decade. These high prices in conjunction with the negative environmental impacts of fossil fuel combustion and the consequential threat of global warming, has opened the market for emerging energy sectors. Renewable (solar, wind, geothermal and ocean) energies aim to enter this market by providing power at competitive prices, from inexhaustible sources, in a sustainable manner.

South Africa, as a member of the global community, has pledged its support for sustainable power generation by setting a target of 10 million MWhr energy per annum to be produced by renewable energy sources by 2013. Due to South Africa's close proximity to the storm generation zones in the lower latitudes its 3000 km coastline is exposed to a significant wave energy resource. The focus of this study is to describe this resource for energy conversion purposes to contribute towards assisting the government in reaching its renewable energy goals.

1.2. Existing work

Research on South Africa's wave power resource and wave energy conversion devices was done at Stellenbosch University in the late seventies to mid eighties due to high oil prices. During this time, G. de F. Retief developed the Stellenbosch Wave Energy Converter (refer to §2.5.3). Under Retief, L. Geustyn published his M.Sc thesis on South Africa's wave power resource entitled "*An evaluation of the time and spatial distribution of seawave energy along the South African coastline*" (1983). A portion of this study will focus on the revision of Geustyn's work by analysing the additional 23 years of wave data.

1.3. Aims of study

An energy resource can only be successfully exploited if the resource itself is well understood, defined and harnessed. This study aims to provide a comprehensive description of the spatial distribution of wave power along the South African coastline, focusing on the area with the highest wave power levels. The study comprises of a literature study and

wave data analyses of measured- and modelled hindcast wave data. The overall study objective and the aims of each subset of the study are presented in Figure 1-1 below.

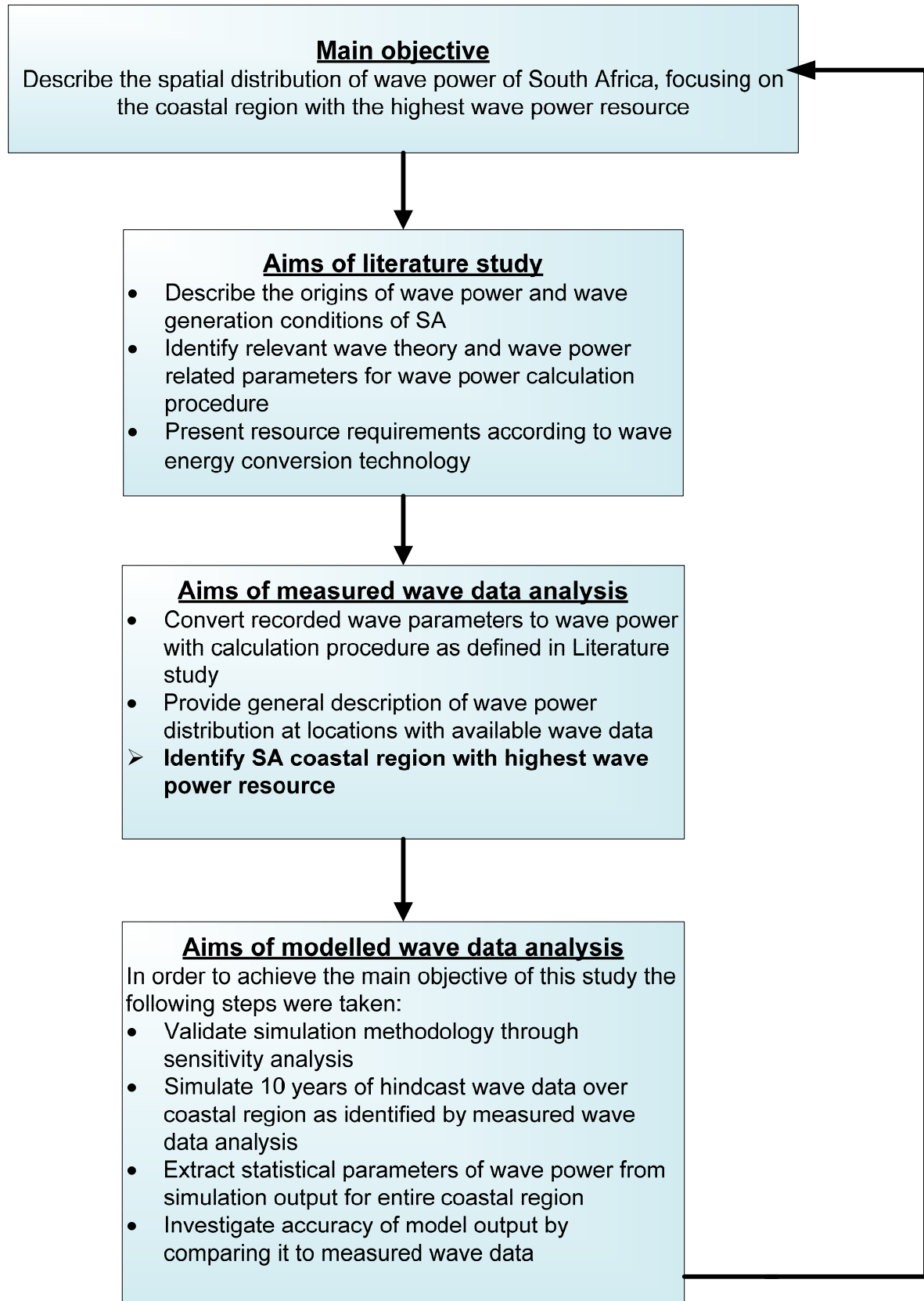


Figure 1-1: The main and sub-objectives, overall methodology and structure of the thesis

Figure 1-1 presents the main and sub-objectives, overall methodology and structure of the thesis. With the main objective realised, the statistical output from the modelled hindcast wave data analysis can serve as a guideline to the identification of sites best suited for wave energy conversion. Potential users of this guideline include wave farm developers such as national-, regional governments or private developers and/or wave energy conversion device manufacturers.

1.4. Scope and limitations

The resolution of the spatial distribution of wave power, as output from the main objective of the study, is such that it describes the general (expected) wave power conditions over the investigated coastal region. For site specific designs further numerical simulation is required, especially at shallow water sites.

1.5. Main sources of information

A wide spectrum of relevant literature and expertise in the study field were consulted. However, it is considered necessary to list the main sources/inputs:

- In preparation for this investigation of wave power resource mapping the thesis of (Geustyn, 1989) was consulted (as mentioned in §1.2) and also the thesis of (Hagerman, 2001).
- The data analysed in the measured wave data analysis was made available by the National Ports Authority via the CSIR. The thesis of (MacHutchon, 2006) on storm characterisation was consulted for the analysis of the measured wave data and also for the South African meteorological discussion in §2.2.
- The hindcast data used in the numerical simulation portion of the study was obtained from the National Centers for Environmental Prediction (NCEP) website. C Roussouw assisted with mentoring the numerical modelling process by providing expert advice and original programming code. During the statistical analysis of the model output A Strasheim was consulted. The last, and most influential, source of information was the promoter of this study, E Bosman.

1.6. Thesis overview

The literature study of Chapter 2 comprises of a brief description of the origins of wave power followed by a discussion of the South African meteorological conditions. Consequently, the relevant wave theory and wave power related parameters are presented in a wave power calculation procedure. The literature study is concluded with a discussion of the current wave energy conversion technology.

The result of the wave power analysis of measured wave data recorded at wave recording stations along the South African coast is presented in Chapter 3. In the analysis recorded wave parameters are converted to wave power by employing the wave power calculation procedure as defined in §2.4.6. The statistical output from the wave power analysis provided a general description of the wave power distribution along the South African coastline. This chapter is concluded with the identification of the coastal zone with the greatest wave power resource.

In Chapter 4 the deep sea NCEP hindcast wave data is initially analysed and compared to the wave data recorded at the shallower water location of the Cape Point recording station. The SWAN wave model (Booj et. al., 2004) and the simulation procedure required to transfer deep sea waves into the coastal zone, as identified in the measured wave power analysis, is subsequently described. Examples of output from the modelling procedure are presented. The accuracy of the model output is investigated by comparing the measured wave data of Cape Point recording station to the transferred deep sea hindcast wave data for the period during which these two data sets overlap.

Chapters 5 and 6, present the conclusions drawn from this wave power resource investigation and recommendations made from the findings and conclusions of the study, respectively.

2. LITERATURE REVIEW

This review of literature related to global wave power distribution, South African meteorology, wave power calculations and wave energy conversion device technology provide background on the study topic of wave power.

2.1. Origins of wave power and its global distribution (Boud, 2003)

Wave energy is an indirect result of solar radiation. Winds are generated by the differential heating of the earth, and as they blow over large areas of ocean, part of the wind energy is converted to water waves. The amount of energy transferred, and the size of the resulting waves, depends on the wind speed, the length of time for which the wind blows, and the distance over which it blows, (the 'fetch'). In oceanic areas, wind energy is transferred to wave energy and concentrated at each stage in the conversion process, so that original uniformly distributed solar radiation power levels of typically $\sim 100 \text{ W/m}^2$ of earth surface can be converted to waves with locally concentrated power levels in the order of 10 to 50 kW per meter of wave crest length, (the standard form of measurement) in ocean zones where relative high wave energy occurs. Within or close-to the wave generation area, storm waves known as the 'seas', exhibit a very irregular pattern, and continue to travel in the direction of their formation, even after the wind change direction or subside. In deep water, waves can travel out of the storm areas (wind fields) with a minimal loss of energy, and progressively becoming regular, smooth waves or a 'swell', which can persist for great distances (i.e. tens of thousands of kilometers) from the origin.

Consequently, coasts with exposure to the prevailing wind direction towards the coast and long fetches tend to have the most energetic wave climates—e.g. the Northwest coasts of North America, South West coast of South America, Europe, Africa, Australia and New Zealand, as shown in Figure 2-1.

The global wave power potential has been estimated to be 8^6 - 8^7 kWh/year (which is equivalent to an installed power generation capacity of 1 to 10 million MW), which is of the same order of magnitude as world electrical energy consumption in the 1970's (Isaacs and Seymour, 1973; WEC, 1993). Figure 2-1 below shows that the highest wave climates, with annual average power levels between 20 to 70 kW/m or higher, are found in the temperate zones (30 to 60 degrees north and south latitude) where strong storms occur. However,

significant wave climates are still found within $\pm 30^\circ$ latitude where regular trade winds blow; the lower power levels being compensated by the smaller wave power variability.

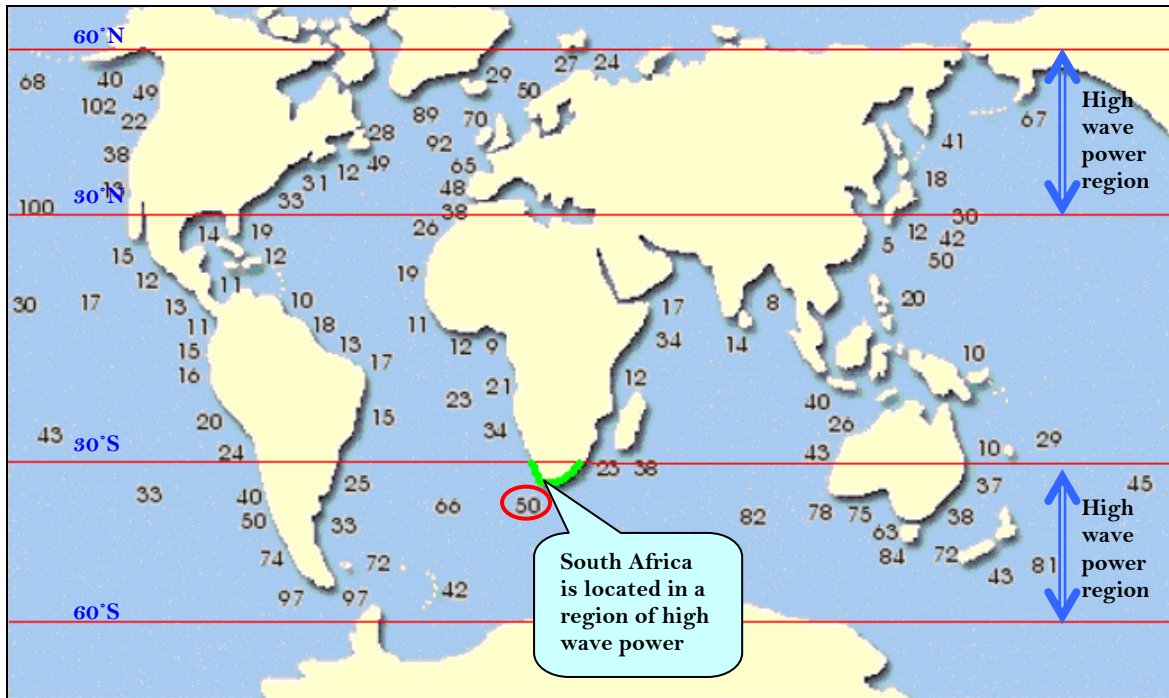


Figure 2-1: Global distribution of deep sea average annual ocean wave power kW/m
(www.oceanpd.com/Resource/Worldresourcemap.html, 17/4/07)

Figure 2-1 above shows that South Africa has a substantial wave power resource compared to the rest of the world. The reasons for its large resource can be contributed to its prevailing meteorological conditions. A brief discussion of the relevant South African meteorology is described in the next section.

2.2. South African meteorology (Rossouw, 1989)

The wind and therefore the wave regime in the South Atlantic and South Indian oceans are influenced by a number of dominant meteorological features. Heated air which rises in the tropics near the equator moves southwards and descends in the vicinity of the 30°S to form the so-called Hadley cell. This descending air causes two semi-permanent high pressure systems, the South Atlantic high and the South Indian high, with the air moving in an anti-clockwise rotation around the centre of the high pressure system. South of the Hadley cell the air sinks and moves towards the poles creating prevailing westerly winds known as the Ferrel westerlies which spiral eastwards around the globe. Disturbed air in the Ferrel westerlies creates the low pressure systems of the South Atlantic. Once formed, these low pressure systems moves from west to east within the Ferrel westerly wind system. It is the

passage of these depressions with their associated cold fronts and wind fields that are the main cause of ocean waves approaching the South African coastline (see Figure 2-2).

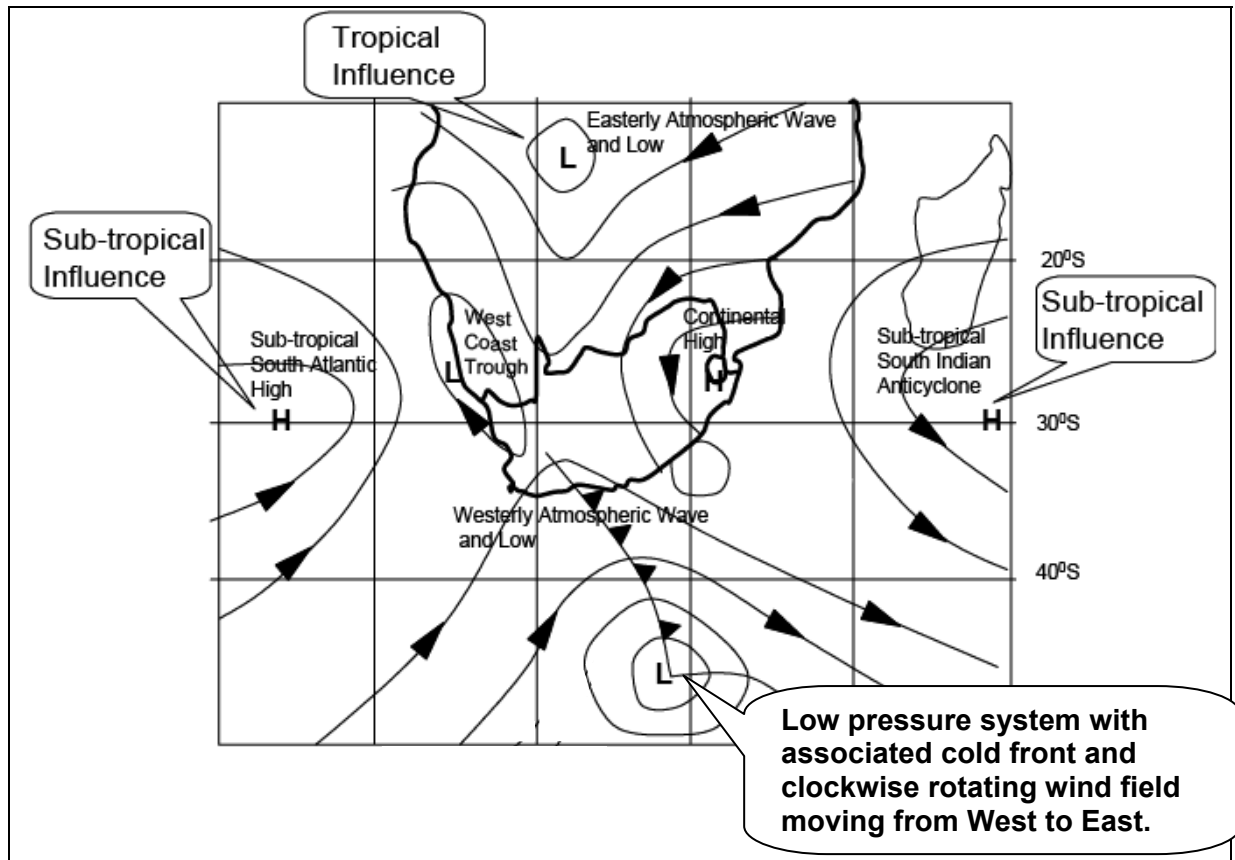


Figure 2-2: Composite diagram showing the important typical features of the surface atmospheric circulation over South Africa (Tyson et al, 2000)

These low pressure systems pass the southern tip of Africa at an approximate frequency of 3 to 5 days. In winter the path of these depressions is frequently intersected by the southern tip of the African continent. In summer the path of these systems shift further south and the depressions mostly pass south of the continent. More severe wave conditions can therefore be expected to occur more frequently in winter along the southern Cape coast than in summer. The occasional northerly excursion of a cold front does however occur in summer resulting in occasional high waves along this coast during this season as well.

On the South West coast the wind direction during the passing of these cold fronts (i.e. low pressure systems) normally swings from NW through SW to SE as it passes the southern tip of the African continent. The South African west and south coasts are the most exposed coastal regions to the waves generated by the easterly movement of these low pressure systems.

A secondary source of high waves along the eastern extremity of the South African coast is the presence of tropical cyclones (low pressure systems) in the Western Indian Ocean. These usually occur in the months October to May (summer). The tropical cyclone tracks/paths usually pass to the North of Richards Bay, but the waves generated in these systems do affect the coastline north of Durban (refer to Figure 2-3 for the occurrence and intensity map of tropical cyclones along the South African coast).

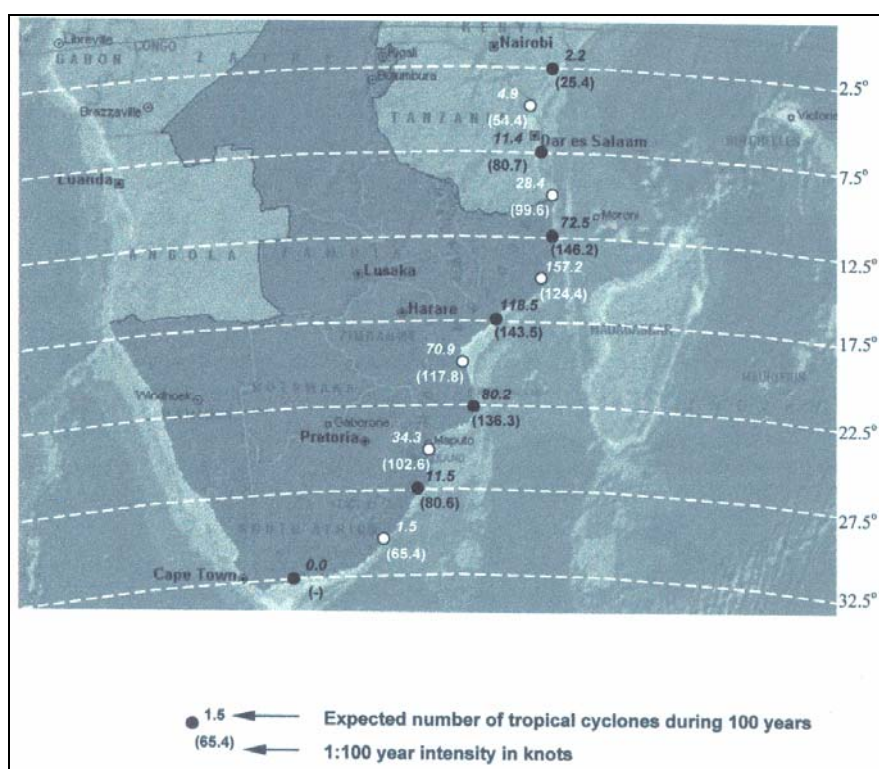


Figure 2-3: Tropical cyclone occurrence and intensity map for the Southern African east coast (Rossouw, 1999). [Black dots and associated black values are indicated on the dashed latitude lines and the white dots and associated white values are indicated midway between dashed latitude lines]

Future meteorological conditions are accurately predicted with global weather models. A brief discussion of numerical weather prediction and examples of forecast wind and wave conditions are discussed in the next section.

2.3. Numerical weather prediction (NWP)

According to the UK Meteorological Office (British weather bureau), numerical weather prediction concentrates upon two problems: “diagnosing the current state of the atmosphere and numerically modelling of how the atmosphere will evolve with time”. Observations of weather conditions are input into the NWP model and are representative of the current state

of the atmosphere. From these observations weather forecasts are made. Forecasts are continually updated with observations and satellite input.

Satellite imagery is employed to observe meteorological variables such as wind speed and direction, cloud height and cloud amount, surface temperature, sea ice cover, vegetation cover, precipitation, ect. Forecast of wave conditions can be derived from predicted wind fields which are derived from forecast atmospheric conditions. A few examples of wind- and wave forecast models of the following organisations can be found on their respective websites: Buoyweather.com, Oceanweather.com, Stormsurf.com and NOAA NCEP. Examples of NCEP output are presented in Figure 2-4, Figure 2-5 and Figure 2-6 below.

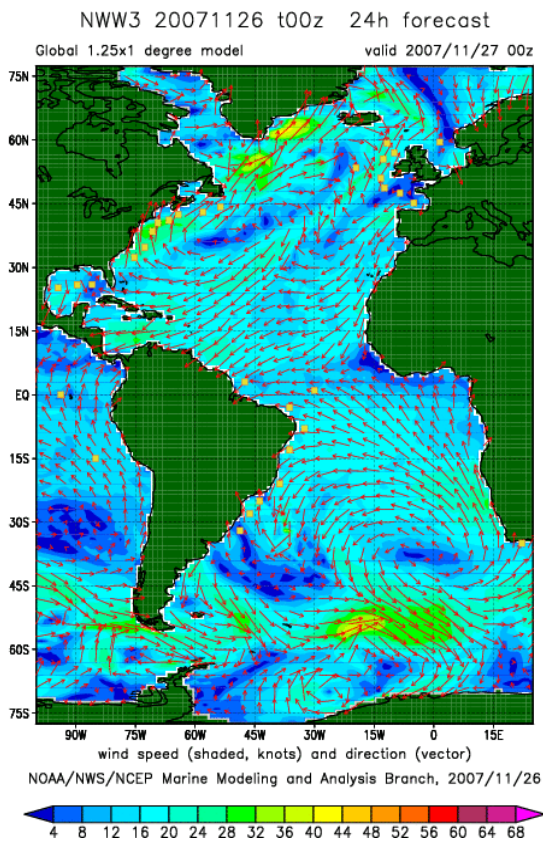


Figure 2-4: Wind field at 10m elevation

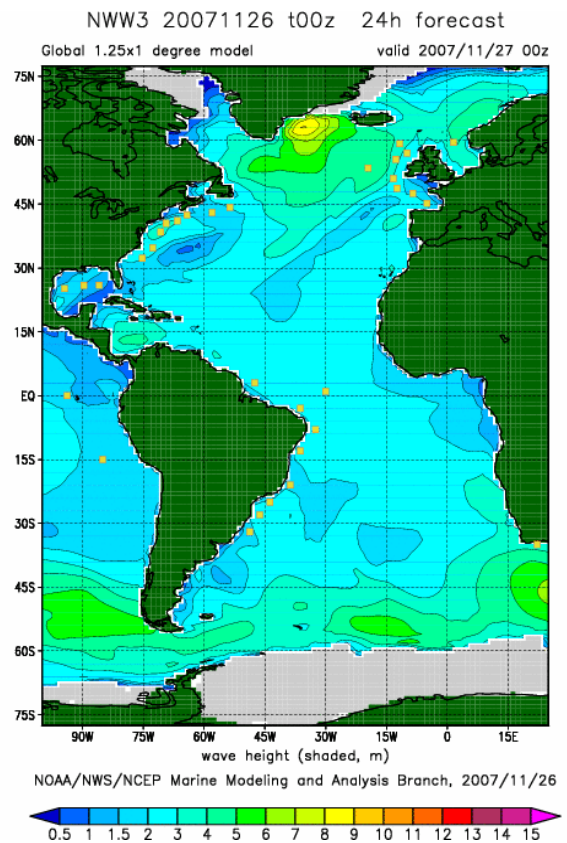


Figure 2-5: Resulting wave field

Figure 2-4 shows the 30h forecast of wind fields at 10m elevation. High wind intensities are found in 40° to 60° southern- and northern latitude, for example note the 40 knot wind concentration south of the African continent. This high wind intensity produces 7m wave heights in deep sea (see Figure 2-5). Figure 2-6 demonstrates the process of wave period dispersion. This is when the faster moving long period waves propagate out of the storm generation zone and reach the coastline before the slower, short period waves which also tend to dissipate over time and distance. Note the longer period waves near the coast compared to further offshore.

In the following section basic wave parameters relevant to ocean wave power are discussed.

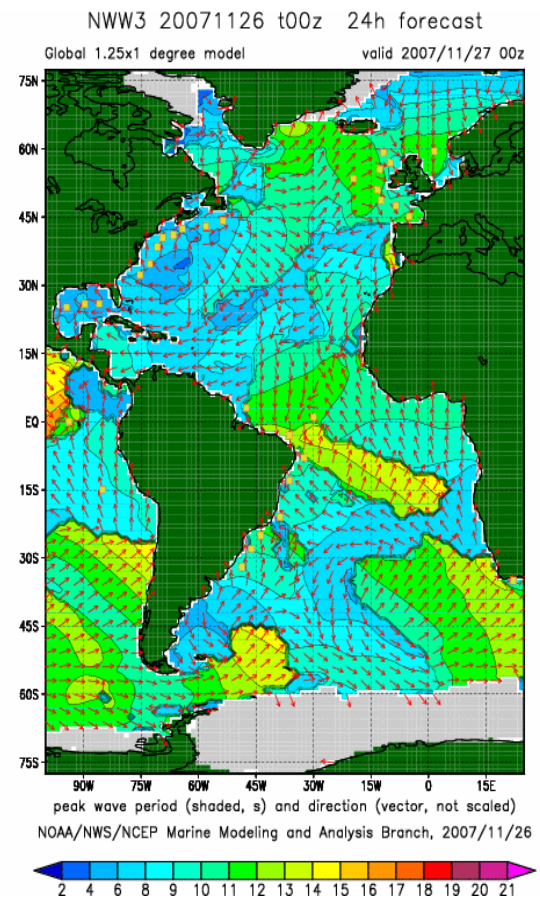


Figure 2-6: Wave period dispersion from storm generation zone

(http://polar.ncep.noaa.gov/waves/ma_in_text.html, 26/11/2007)

2.4. Wave parameters relevant to ocean wave power (CEM, 2002)

2.4.1. Basic wave mechanics

Since this investigation deals with wave power in deep sea and intermediate water depth where linear wave theory describes wave parameters sufficiently accurate, the linear wave theory was used to define the parameters relevant to wave power below.

Linear (or Airy) wave theory describes ocean waves as simple sinusoidal waves. The part of the wave profile with the maximum elevation above the still water level (SWL) is called the wave crest and the part of the wave profile with the lowest depression is the wave trough (refer to Figure 2-7). The distance from the SWL to the crest or the trough is the amplitude (a) of the wave and the wave height (H) is defined as the total distance from the trough to the crest. The wavelength (L) of a regular wave at any depth is the horizontal distance between successive points of equal amplitude and phase for example from crest to crest or trough to trough and is defined according to the linear theory by:

$$L = \frac{gT^2}{2\pi} \tanh\left(\frac{2\pi d}{L}\right) \quad \text{Eqn 2.1.}$$

Where: g = gravitation constant

T = wave period (the time required for one wavelength to pass a fixed point)

d = water depth (distance from ocean floor to SWL)

In deep water where d is large, the hyperbolic *tanh* function tends to unity and Eqn 2.1. simplifies to:

$$L_0 = \frac{gT^2}{2\pi} \quad \text{Eqn 2.2.}$$

Where: L_0 = deep sea wave length

Deep sea = $d/L \geq \frac{1}{2}$

These basic parameters are presented in Figure 2-7.

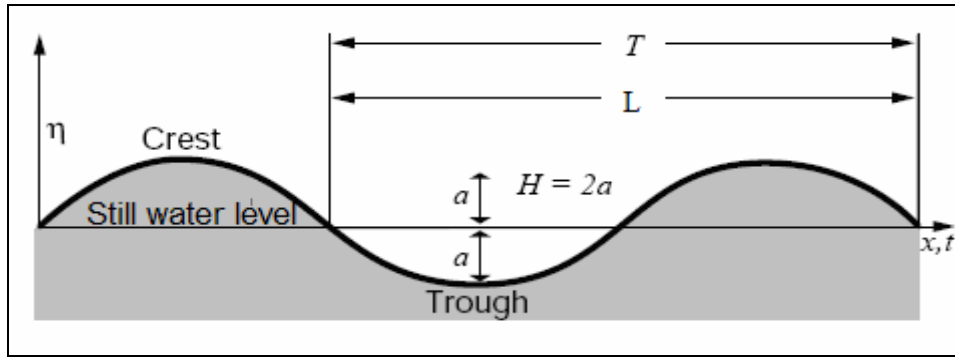


Figure 2-7: A simple sinusoidal wave (WMO, 1998)

The equation describing the free surface as a function of time t and horizontal distance x for a simple sinusoidal wave can be shown to be

$$\eta = \frac{H}{2} \cos\left(\frac{2\pi x}{L} - \frac{2\pi t}{T}\right) \quad \text{Eqn 2.3.}$$

Where η is the elevation of the water surface relative to the SWL. The propagation speed or celerity of a regular wave is given by:

$$C = \frac{L}{T} = \frac{gT}{2\pi} \tanh\left(\frac{2\pi d}{L}\right) \quad \text{Eqn 2.4.}$$

Wave power is dependent on energy density and equations to determine energy density is therefore derived in the following section.

2.4.2. Energy density

The total energy of a wave system is the sum of its kinetic energy and its potential energy. The kinetic energy is that part of the total energy due to water particle velocities associated with wave motion. Potential energy is that part of the energy resulting from part of the fluid mass being above the trough: the wave crest. The total energy (E) of an ocean wave is given by

$$E = E_k + E_p = \int_x^{x+L} \int_{-d}^{\eta} \rho \frac{u^2 + w^2}{2} dz dx + \int_x^{x+L} \rho g \left[\frac{(\eta + d)^2}{2} - \frac{d^2}{2} \right] dx \quad \text{Eqn 2.5.}$$

Where:

E_k = kinetic energy (Joules)

E_p = potential energy (Joules)

ρ = density of sea water (1025 kg/m³)

u = fluid velocity in x-direction

w = fluid velocity in z-direction

Refer to Appendix A for the derivation of energy density equations from first principles.

According to the Airy theory, if the potential energy is determined relative to SWL, and all waves are propagated in the same direction, potential and kinetic energy components are equal, and the total wave energy in one wavelength per unit crest width (w_c) is given by:

$$E = E_p + E_k = \frac{\rho g H^2 L}{16} + \frac{\rho g H^2 L}{16} = \frac{\rho g H^2 L}{8} \quad \text{Eqn 2.6.}$$

Where: H = wave height

The total average wave energy per unit surface area is called the specific energy or energy density (\bar{E}) and is given by:

$$\bar{E} = \frac{E}{L} = \frac{\rho g H^2}{8} \quad \text{Eqn 2.7.}$$

A 3D representation of the parameters relevant to energy density (specific energy) of a deep sea ocean wave is shown in Figure 2-8.

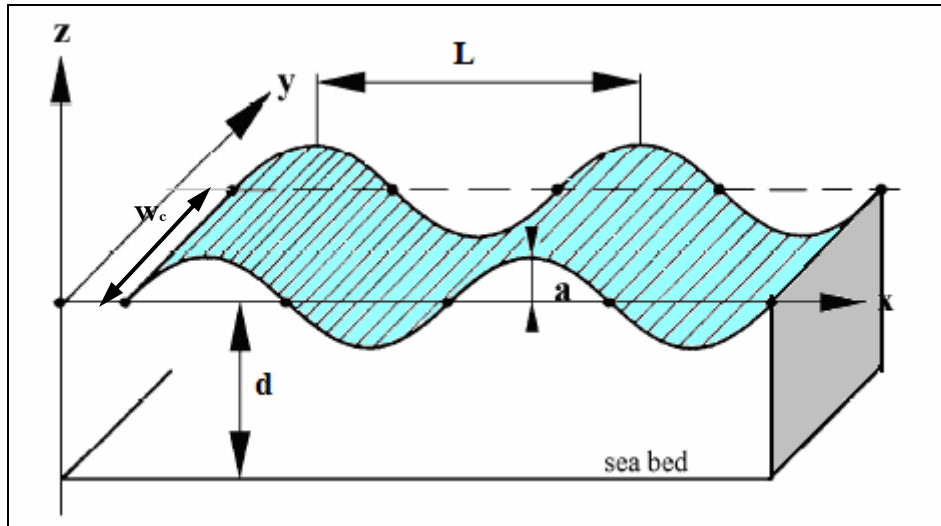


Figure 2-8: 3D representation of parameters relevant to specific energy (Massie et al, 2001)

The rate at which wave energy propagates is directly dependant on the group velocity of the wave. The group velocity (C_g) is given by:

$$C_g = nC \quad \text{Eqn 2.8.}$$

Where: C = wave celerity Eqn 2.4.

n = constant as determined by:

$$n = \frac{1}{2} \left[1 + \frac{4\pi d/L}{\sinh(4\pi d/L)} \right] \quad \text{Eqn 2.9.}$$

In deep water Eqn 2.9. simplifies to $n = 0.5$ and $C_{go} = 0.5 \frac{L_o}{T}$.

All wave power related parameters are now defined and in the following section an equation for wave power is derived.

2.4.3. Wave power (wave energy flux)

Wave energy flux is the rate at which energy is transmitted in the direction of wave propagation across a vertical plane perpendicular to the direction of wave advance and extending down the entire depth. Assuming linear theory holds, the average energy flux per unit wave crest width (\bar{P}) transmitted across a vertical plane perpendicular to the direction of wave advance is

$$\bar{P} = \frac{1}{T} \int_t^{t+r} \int_{-d}^{\eta} p u dz dt \quad \text{Eqn 2.10.}$$

Where: p = gauge pressure
 t = start time
 r = end time

Integration of Eqn 2.10. simplifies to:

$$\bar{P} = \bar{E} n C = \bar{E} C_g \quad \text{Eqn 2.11.}$$

In deep water wave energy density is transmitted in the zone from the surface to $L_o/2$ below SWL. Wave energy flux (\bar{P}) is also called **wave power**. The wave theory described indicates that wave power is dependant on three basic wave parameters: Wave height, wave period and water depth. How these parameters are determined and applied to calculate wave power is discussed in the following section.

2.4.4. Spectral analysis

2.4.4.1. One dimensional wave energy density spectrum

Linear wave theory describes idealised wave conditions. Actual sea states are however irregularly and randomly distributed. Examples of real, irregular sea states are presented in Figure 2-9 and Figure 2-10. These figures show how random surface elevation records can be deconstructed into a series of sinusoidal components using a Fourier series analysis. Each sinusoidal component has unique basic parameters, as discussed in § 2.4.1. Its amplitude and frequency is used to produce a distribution of wave energy density as a function of frequency. This distribution indicates the variation of the surface elevation of the record from the mean and is called the one dimensional- or frequency spectrum ($E(f)$).

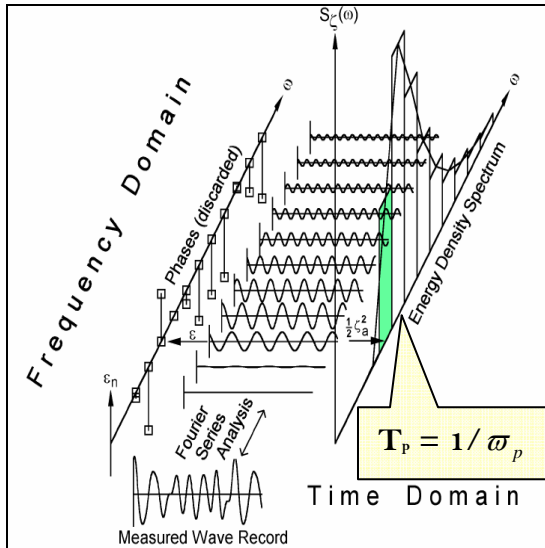


Figure 2-9: 1D irregular sea state (WMO, 1998)

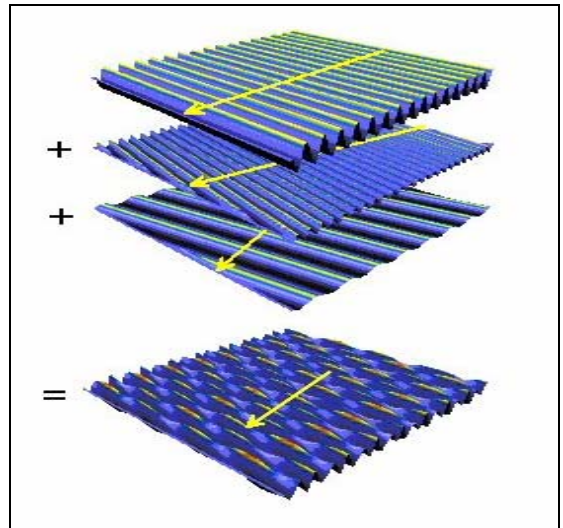


Figure 2-10: 2D irregular sea state (Carbon Trust UK, 2007)

The inverse of the frequency ($1/\omega_p$ in Figure 2-9) in the recorded wave energy density spectrum at which maximum energy density occurs is known as the peak period (T_p) of the record. This is a very important parameter frequently used in coastal engineering applications. Another important wave parameter that can be derived from the $E(f)$ is the significant wave height (H_s). H_s (also $H_{1/3}$) is defined as the average height of the highest third wave heights recorded over the sampling period. H_s can also be derived from the variance of the record or the integral of the variance in the spectrum and is then denoted H_{m0} . It is generally assumed that $H_s \approx H_{m0}$ and therefore H_s can be determined by:

$$H_s \approx 4\sqrt{m_0} \quad \text{Eqn 2.12.}$$

Where m_0 is defined as:

$$m_0 = \int_0^{\infty} E(f)df = \sigma_{\eta}^2 \quad \text{Eqn 2.13.}$$

Where σ_{η}^2 is the variance of surface elevation over the recording period.

$$H_s \approx 4\sigma_{\eta} \quad \text{Eqn 2.14.}$$

Where σ_{η} is the standard deviation of surface elevation over the recording period.

In order to determine wave power for a measured wave record a regular wave height parameter is required containing the same wave energy density as the measured irregular

wave record. This equivalent wave height is known as the root-mean-square wave height (H_{RMS}) and can be determined from

$$H_{RMS} = \frac{H_s}{\sqrt{2}} \quad \text{Eqn 2.15.}$$

Refer to Appendix A for the derivation of Eqn 2.15. from first principles.

Similarly to the equivalent wave height parameter, H_{RMS} , a regular wave period parameter is required with equivalent energy density to that of the irregular wave record. The wave period parameter that will be used in the wave power analysis of this study is called the energy period (T_e) and is defined by:

$$T_e = \frac{\sum \frac{E(f_i)}{f_i}}{\sum E(f)} \quad \text{Eqn 2.16. (Geustyn, 1983)}$$

Where: $\frac{E(f_i)}{f_i}$ = the ratio of the energy density to frequency interval f_i .

$$\sum E(f) = m_0 = \text{the total energy in the wave spectrum}$$

T_e effectively divides the energy density spectrum in two halves of equal area. Eqn 2.16. shows that T_e is determined by integrating the wave energy density spectrum.

2.4.4.2. Two dimensional wave energy density spectrum

Figure 2-10 above shows that each sinusoidal component of an irregular sea state has a propagation direction. Wave energy density is thus also a function of direction. Energy density as a function of direction and frequency is called a directional energy - or 2D spectrum. An example of a 2D spectrum is shown in Figure 2-11 below. The $\cos^m \theta$ model is one of many models used to describe the directional distribution (see Figure 2-12):

$$D(\theta) = A \cos^m(\theta) \quad \text{Eqn 2.17.}$$

Where:

$D(\theta)$ = directional distribution

m = the power of m controls the width of the directional distribution and is an indication of the energy spreading around the peak direction.

θ = mean wave direction

A = normalised coefficient and is derived from:

$$A = \Gamma\left(\frac{1}{2}m + 1\right) / \left[\Gamma\left(\frac{1}{2}m + \frac{1}{2}\right)\sqrt{\pi}\right]$$

Where:

$\Gamma(\cdot)$ = gamma function

Directional spreading is an important input parameter for numerical simulation and will be discussed in further detail in §4.6.3.

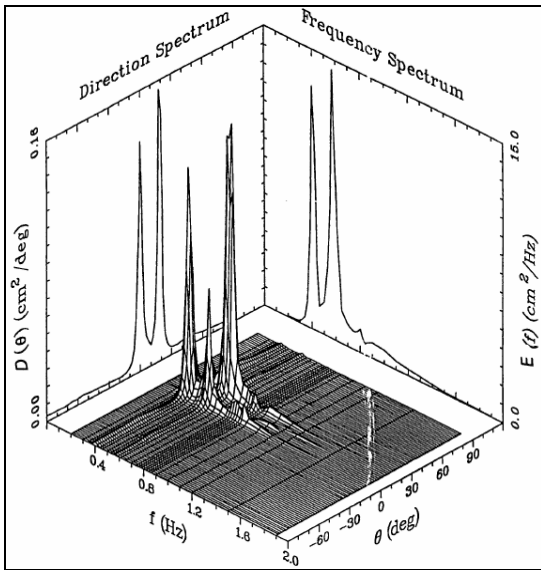


Figure 2-11: 2D spectrum (CEM 2002)

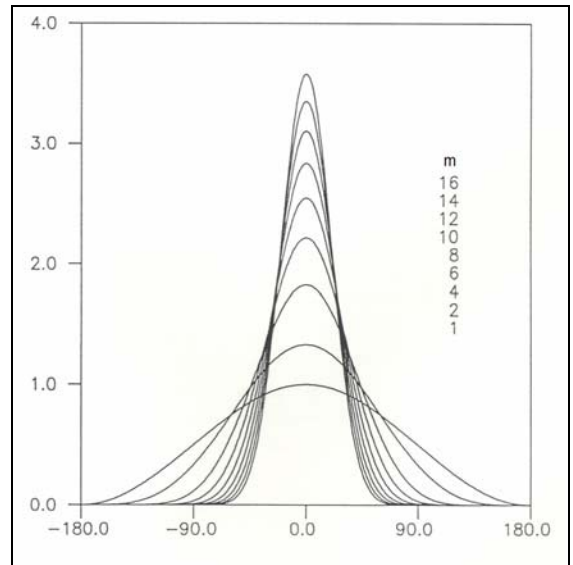


Figure 2-12: Direction distribution function (van Tonder, 1992)

2.4.5. Wave energy density spectra shapes and the peak-enhancement factor

The wave energy density spectra discussed in §2.4.4.1 can be represented by standard spectral shapes, the two most common are the Pierson-Moskowitz- (PM) and JONSWAP spectrum see Figure 2-13. The shape of a wave energy density function is defined in terms of its peak-enhancement factor (γ). γ is the ratio of the maximum energy density of a JONSWAP- and PM spectrum (see Figure 2-13). A PM spectrum is therefore a JONSWAP spectrum with $\gamma = 1$.

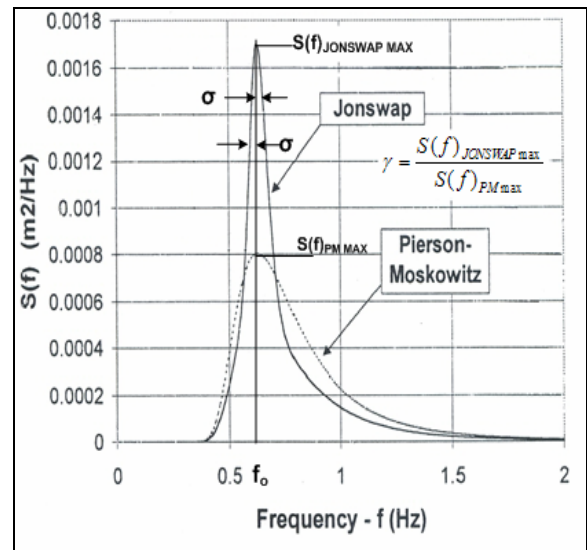


Figure 2-13: PM and JONSWAP spectrums (CEM, 2002)

The PM spectrum describes a wave-field which have reached a state of saturation for a given wind speed i.e. where no more wind energy is transferred to wave energy within the wind field, this wave-field-state is generally termed as a fully-developed sea. It is defined with one parameter, the wind speed, and assumes that both the fetch and duration are infinite. Its low γ -value of one is thus an indication of energy spreading over a large range of frequencies around the peak frequency. The JONSWAP distribution on the other hand is fetch limited and its peak energy density is spread over a narrower range of frequencies. Similarly to the m -value of Eqn 2.17., γ is an important input parameter in numerical modelling and will be discussed in further detail in §3.4.

A spectrum is generated by prescribing its shape in terms of its γ -value. From the generated spectrum parameters relevant to wave power, such as T_e , are derived. Dominant γ -values will therefore be determined from the analysis of representing γ -values of wave records recorded at a wave recording station on the South West Coast in §3.4.

This concludes the discussion of equations and parameters relevant to wave power. The application of these equations and parameters to determine wave power is demonstrated in the outlined calculation procedure in the following section.

2.4.6. Wave power calculation procedure

The wave power calculation procedure used in this thesis is similar to that as defined in the thesis of (Geustyn, 1983). Measured wave data generally consist of wave parameters such as H_s , T_p and the mean wave direction. The following seven step procedure is employed to calculate wave power from these recorded wave parameters:

1. H_{RMS} from **Eqn 2.15**.
2. \bar{E} (Joule/m²) from **Eqn 2.7**. using H_{RMS}
3. Determine γ from measured spectra in § 3.4
4. T_e from **Eqn 2.16**.
5. L from **Eqn 2.1**. using T_e
6. C , n and C_g from **Eqn 2.4.**, **Eqn 2.9**. **Eqn 2.8**.
7. \bar{P} (kW/m) from **Eqn 2.11**.

$$\text{In deep water: } \bar{P} = \bar{E} C_{go} = \frac{\rho g H_{RMS}^2}{8} \frac{g T_e}{4\pi} = \frac{\rho g^2 H_{RMS}^2 T_e}{32\pi}$$

The seven step wave power calculation procedure outlined above will be employed to calculate wave power in the measured- and modeled wave data analysis of Chapters 3 and 4. It was found that this procedure is sufficiently accurate (refer to Appendix A for a comparison with integration of the recorded spectrum to determine wave power).

In the following section wave energy conversion technology is discussed. It gives a background of different types of wave energy converter units (either under development or in operation) which could be considered for wave energy conversion on the South African coastline.

2.5. Wave Energy Conversion technology

2.5.1. Introduction

Wave energy conversion is not a new concept with the first patented **Wave Energy Converter** (WEC) dating back to the early 18th century. High oil prices in the 1980's forced governments of the world to consider alternative sources of energy. During this period ocean energy was identified as one of a number of alternative extractable sources. This led to world-wide research in the field of wave energy conversion. It was during this period (1980's) that South Africa invented and researched a WEC (called the SWEC, refer to §2.5.3) at the University of Stellenbosch (Retief, 1982). However, the implementation of a pilot plant in the ocean was not realised after the oil price stabilised in the late 1980's.

Recently focus has again fallen on renewable energy sources, because of factors such as:

- Predicted global climate change
- Exhaustion of conventional resources, including fossil fuels
- Human population explosion
- Increased development
- Energy security
- Economic stability

(depts.washington.edu/poeweb/gradprograms/envmgt/2004symposium/wavetext.pdf, 5/2/2007)

2.5.2. Classification of WEC's

There are various ways of classifying WEC's. The most common classification in literature is to describe a WEC in terms of its deployed location. The three main location categories are on-, near- and offshore. This classification type demonstrates the need to describe the available wave power resource at all the possible deployment locations from offshore to shore. Figure 2-14 presents a schematic representation of the deployment locations relative to the shoreline.

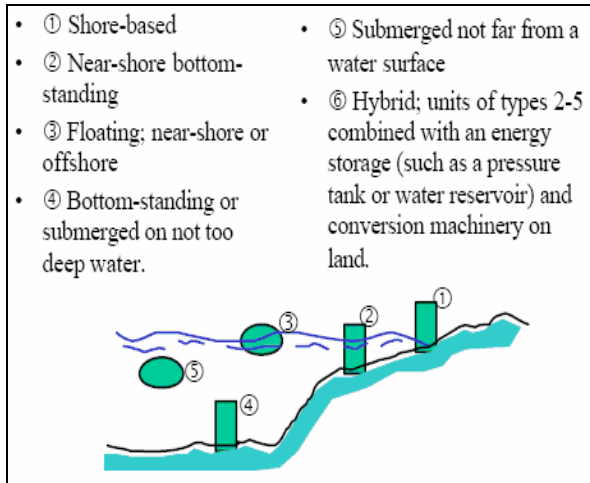


Figure 2-14: Classification by deployment location (Falnes, 2005)

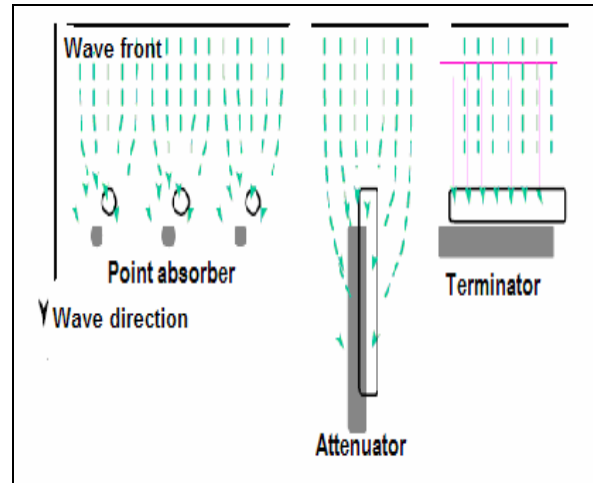


Figure 2-15: Classification by size and orientation (Falnes, 2005)

Another classification method is to describe the WEC in terms of its size and orientation. In this classification type there are three categories. A WEC can be classified as a point absorber, attenuator or terminator (see Figure 2-15). A point absorber is a relatively small device compared to a typical wavelength. An attenuator is a floating device with a length equal to/ or greater than one wavelength. This type of device is aligned in the direction of wave propagation. If this same device is aligned perpendicular to the direction of wave propagation it is called a terminator device.

The last classification of WEC units that will be discussed and used throughout this technology overview is the categorisation of a WEC unit with regards to its basic principle of energy extraction. The classification categories include:

- Oscillating water column
- Reservoir storage
- Relative motion.

The WEC technology will now be discussed in further detail under the categories of the last mentioned classification. Costs presented for the different WEC units mainly included capital cost (manufacturing/construction) and excludes maintenance and operating costs.

2.5.3. Oscillating Water Column WEC types

2.5.3.1. Description

An Oscillating Water Column (OWC) WEC type essentially comprises of a partly submerged structure, open below the water surface, inside which air is trapped above the

free water surface. Incident waves cause the height of the water surface to oscillate, and the air can be channeled through a turbine to drive an electric generator.

- **The collector structure.** In addition to the requirement for survivability, the collector geometry may strongly influence the power capture and must be designed to suit the prevailing wave climate.
- **The turbine.** A bi-directional, axial-flow Wells turbine has been used in some OWC prototypes, notably those developed by Queen's University Belfast and Wavegen. (Boud, 2003)

An OWC is a terminator device with little to no wave energy transmitting through the device to shore.

a) **LIMPET**

- **Specifications**

The LIMPET is a 500 kW OWC developed by the Queen's University of Belfast and Wavegen Ltd in the United Kingdom. It was installed on the Isle of Islay off the west coast of Scotland and was commissioned in November 2000. The LIMPET system is the first commercial, grid connected WEC.

The collector structure consists of reinforced concrete and has cross sectional dimensions of 21 by 7.16 m. The structure is very robust in order to survive extreme loadings with 0.75 m thick walls (see Figure 2-16 and Figure 2-17). As mentioned in § 2.5.3, the airflow caused by the oscillating water column drives two Wells turbines each with a 250 kW capacity and a blade diameter of 2.6 m. The available annual average wave power resource in the deployment area is 20 kW/m and the water depth is six meters.

The generator systems offer an average conversion efficiency of 35% of the power incident on the collector width. (The Queen's University of Belfast, 2002)

- **Costs**

An exchange rate of U\$ 1 = R 6.50 was used to obtain an order of magnitude of cost in local currency of the WEC's considered in this study. According to Wavegen, the total capital cost of the LIMPET project was \$ 1.6 million (R 10.4 million, <http://www.nsc.org/ehc/climate/ccu0101.htm>, 29/10/2007).

Another European oscillating water column pilot plant was constructed on the Portuguese island of Pico. This system has a maximum rated capacity of 400 kW.

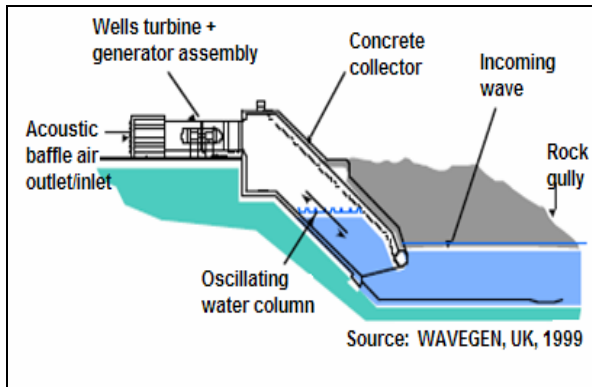


Figure 2-16: Cross sectional view of LIMPET



Figure 2-17: LIMPET (The Queen's University Belfast, 2002)

b) **ENERGETECH**

• **Specifications**

ENERGETECH is an Australian based company who designed a parabolic wall OWC. The parabolic wall focuses the incident waves onto an OWC unit (see Figure 2-18). This device was original designed to be shore based, but after certain mooring innovations it can now be deployed in depths of up to 50 m. A Denniss-Auld variable pitch turbine is used for energy conversion.

The maximum width available for power extraction is 35m per unit and the capacity of such a device can range from 500 kW to 2 MW depending on the wave climate and device dimensions. The structure consists of steel components which can be manufactured locally in South Africa. The power take off of this system was designed to adjust the damping of the OWC and effectively tune the device to real time conditions.

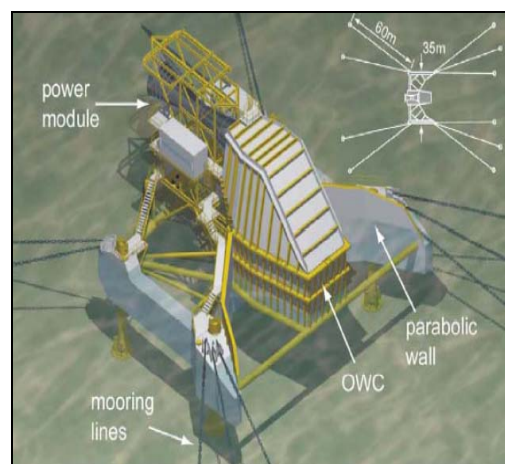


Figure 2-18: Parabolic wall OWC (Previsic, 2004)

- **Costs**

The costs of one such unit can range from \$ 2.5 to \$ 3 million (R 16.25 to R 19.5 million) after Previsic (2004). This cost does not include mooring and grid connection.

c) **Stellenbosch WEC (SWEC)**

- **Specifications**

SWEC was developed at Stellenbosch University (Deon Retief et al, 1989). The SWEC comprises of a pair of collectors (arms) coupled in a V-formation to a single air turbine and power generator mounted above water level in a tower at the apex of the V. Each collector arm has OWC chambers and the pressurised air is send along the arm to the power generator in the tower (See Figure 2-19, Figure 2-20 and Figure 2-21). This is a near shore system founded on the seabed in water depth of between 15 to 20 m.

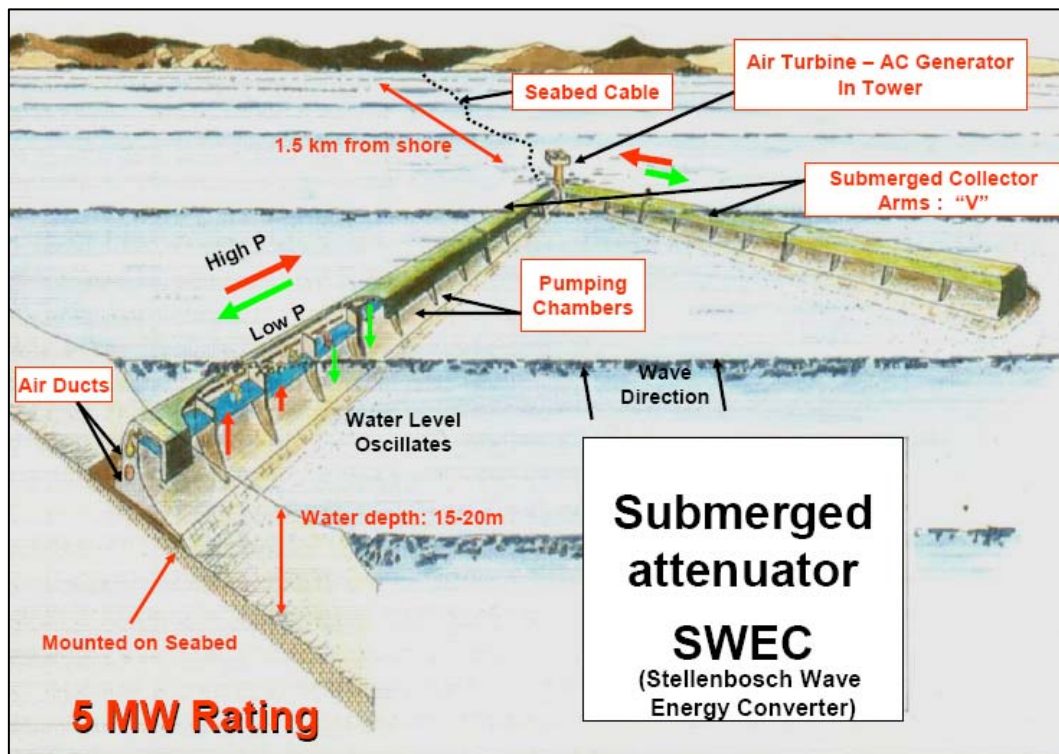


Figure 2-19: SWEC (Retief, 2007)

The design length of a collector arm is 300 m with a 30° inclination angle to the shore. This gives the system an effective width of 350 m for power extraction. The collector arms consist of prefabricated concrete units. The rated power capacity for such a system is 5 MW and a 40 km stretch of coastline is required for a 770 MW power plant on the South African South West coast.

- **Costs**

A 770 MW power plant is estimated to cost between 60 to 75 c/kWhr (Retief, 2007); therefore assuming the plant generates electricity at full capacity for 50% of the year the total cost of the power plant is R3.4 billion. This power plant will comprise of 154 5 MW units which is estimated to cost approximately R 1 million per unit.

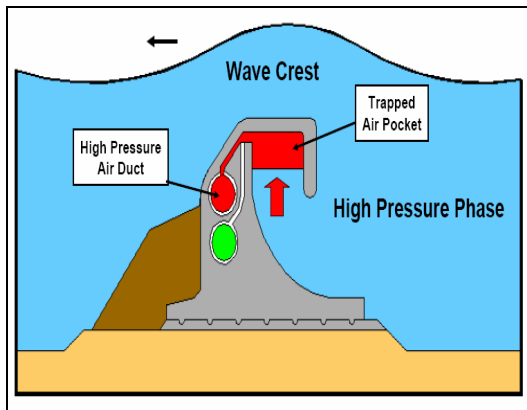


Figure 2-20: Pressure increase caused by wave crest (Retief, 2007)

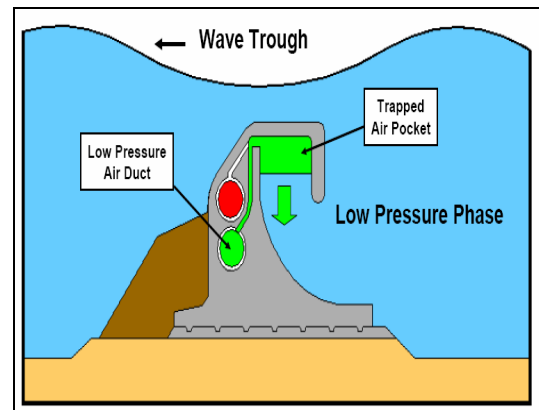


Figure 2-21: Pressure reduction caused by wave trough (Retief, 2007)

2.5.3.2. Conclusions on Oscillating Water Column WEC types

The main advantages of OWC technology include the following:

- Shore based OWC devices provide easy access for operation and maintenance work.
- The near shore location reduces transmission costs.
- OWC devices can be incorporated into existing breakwaters and can be used to create calm sea areas.

Some disadvantages associated with OWC devices include:

- The available wave power resource is less in the near shore zone compared to offshore in deeper water due to energy dissipation processes.
- An OWC, being a terminator device, can disrupt sediment transport processes by reducing the wave power reaching the shore.
- Most OWC devices (except Energetech) are non-tuneable and this reduces the system's overall efficiency.
- Shore based OWC structures can have a visual impact if it's not submerged like the SWEC.

- Foundation requirements make the construction cost of these types of WEC devices very dependant on local site conditions such as water depth and ocean sub-bottom properties.

2.5.4. Reservoir storage WEC types

2.5.4.1. Description

Reservoir storage WEC devices focus waves into a storage reservoir and from here the stored water flows through low head turbines to generate power, similar to a small hydro power scheme. This system can either be deployed onshore (local site conditions permitting) or offshore. An example of such an offshore system is discussed below.

a) WAVEDRAGON

- **Specifications**

The WAVEDRAGON is a floating, offshore, overtopping WEC device. It consists out of two parabolic reflecting arms, a double curved overtopping ramp, a storage basin and multiple low head turbines (see Figure 2-22). The reflecting arms focus waves onto the overtopping ramp and into the storage basin above sea level. From the basin the water flows through modified Kaplan-turbines and generates electricity. This device is slack moored and can orientate itself to face into the dominant wave direction.

The structural components of the WAVEDRAGON consist out of steel and reinforced concrete. The rated maximum capacity ranges from 4 to 11 MW with a width of 260 to 390 m and a length of 150 to 220 m. The reservoir storage ranges from 5 000 to 14 000 m³. This device is physically large with a total weight of up to 54 000 tons. It is designed to operate in water depths greater than 25 m.

- **Costs**

A 4MW unit is estimated to cost between \$ 10 and \$ 12 million (R 65 to R 78 million) after Previsic (2004). This is only the capital cost of the device. The mooring and power transmission costs are excluded from the latter cost.

2.5.4.2. Conclusions on reservoir storage WEC types

The following can be concluded on reservoir storage WEC devices:

- Power storage and output smoothing is possible due to the reservoir storage.

- The efficiency of the hydro power plant component of the system is high (up to 80%) and this will minimise overall losses throughout the system.
- This device can utilise a broad bandwidth of frequencies and therefore requires less tune-ability.
- Mooring and structural integrity of this device is important to ensure survivability during extreme storm events.

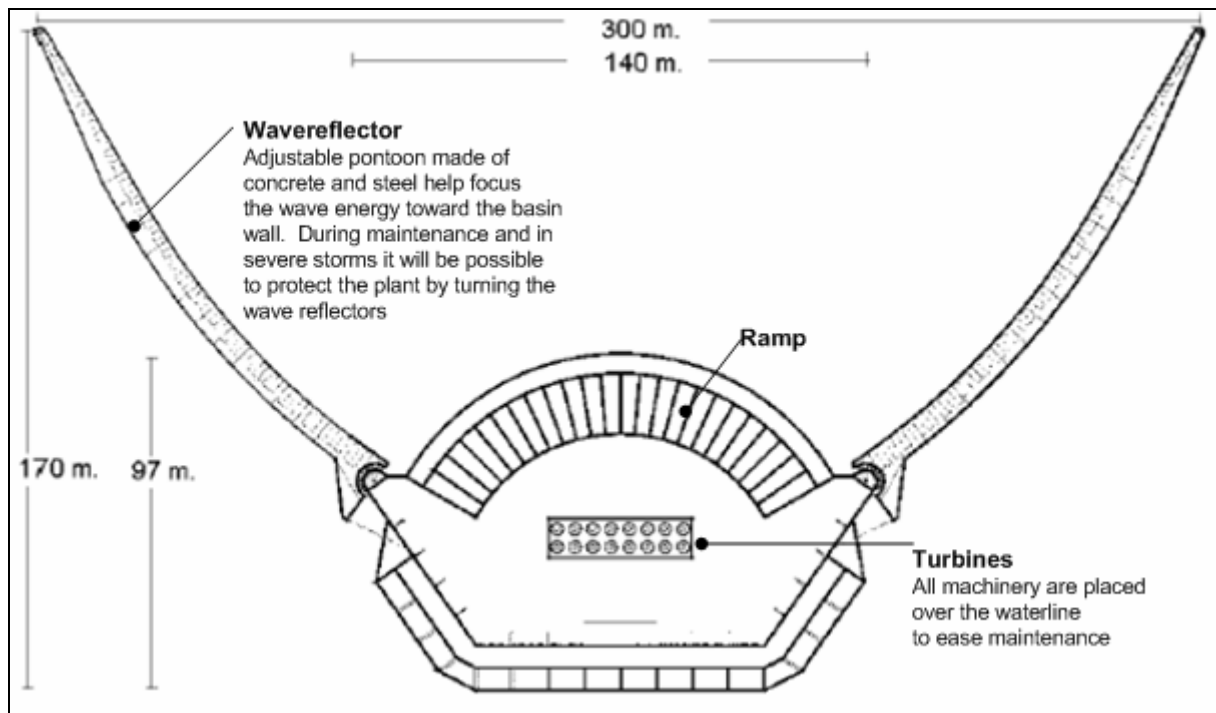


Figure 2-22: Schematic representation of a WAVEDRAGON unit (Previsic, 2004)

2.5.5. Relative motion WEC types

2.5.5.1. Description

A relative motion device is one where wave action displaces an object which then moves relative to another device component. This relative motion is then used to pump fluid through a turbine or motor that generates electricity. Examples of such types of WEC devices are discussed in further detail below.

a) PELAMIS

• Specifications

The word “pelamis” is Latin for sea snake and the similarities between this snake and its namesake WEC are clear (see Figure 2-23). The PELAMIS WEC is a floating device consisting of four tubular sections connected at three hinges. These tubular sections move

relative to each other as a wave crest passes under it and power is generated through a digitally controlled hydraulic power conversion system. The device is slack moored enabling it to orientate itself into the direction of the most dominant wave conditions. It is thus classified as an attenuator device (see Figure 2-15).



Figure 2-23: PELAMIS - Sea snake (bottom photograph) and WEC (top photograph)

The PELAMIS unit has a diameter of 4.6 m and a length of 150 m. It is designed to be deployed in water depths deeper than 50 m. The maximum power rating for a PELAMIS unit is 750 kW. It is a steel structure and can be manufactured using standard construction techniques at most shipyards. Each hinge contains three hydraulic rams, which convert motion into hydraulic pressure. Through accumulators and two 125 kW generators this hydraulic pressure is converted into electricity. The PELAMIS has high survivability because of its ability to detune during extreme storm loading and also because of its narrow profile.

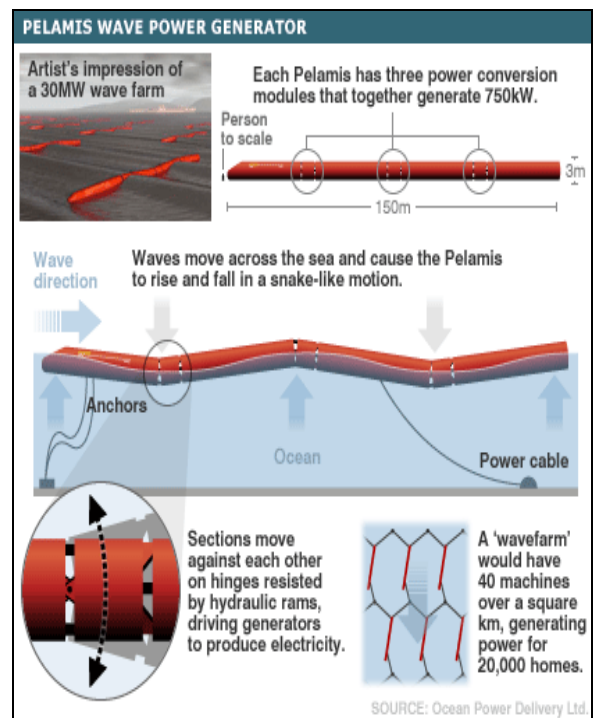


Figure 2-24: PELAMIS specifications

- **Costs**

One PELAMIS unit is estimated to cost \$ 2 to \$ 3 million (R 13 to R 19.5 million) after Previsic (2004). This estimate does not include mooring costs.

b) AQUABUOY

• Specifications

The AQUABUOY is a free floating, heaving point absorber buoy. The buoy displaces relative to a submerged reaction tube. The reaction tube contains a mass of water which drives a piston which in turn drives an elastic, steel reinforced hose pump. An accumulator smoothes the power output and the pressurised water from the pump is discharged into an impulse turbine to generate electricity.

The structure consists of steel and can be manufacture with standard construction techniques. The buoy diameter is six meters and the device has a total draught of 30 m. An AQUABUOY unit has a power rating of 250 kW. The design water depth is larger than 50 m. The device cannot be rapidly tuned to prevailing wave conditions such as could be done for some of the other WEC types.

• Costs

An AQUABUOY unit is estimated to cost \$ 0.75 million (R 4.9 million) after Previsic (2004). This estimate does not include post installation operation, maintenance and monitoring costs.

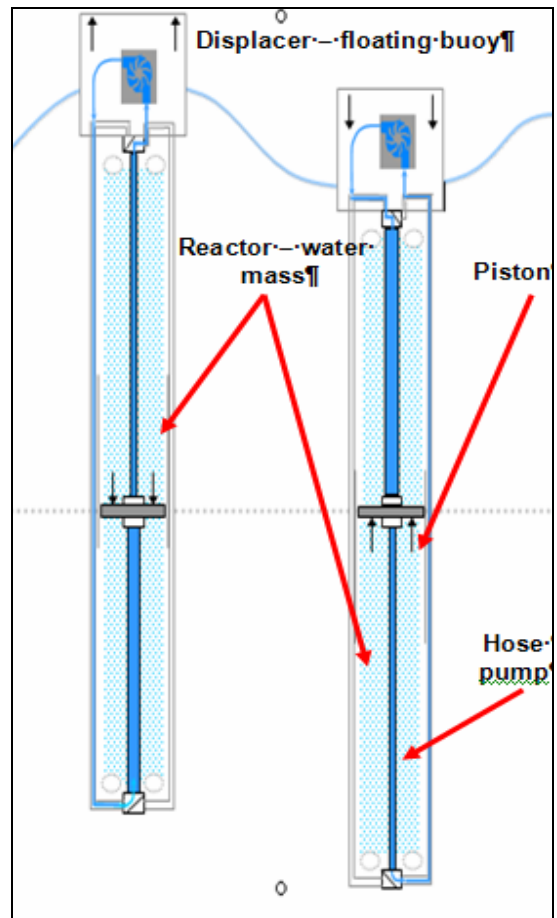


Figure 2-25: AQUABUOY displacer, reactor and hose pump



Figure 2-26: Sea trials of IPS buoy

c) Archimedes Wave Swing (AWS)**• Specifications**

The Archimedes Wave Swing (AWS) is a fully submerged, bottom standing point absorber. It consists out of a cylindrical shaped floater (similar function to the buoy of the AQUABUOY) containing entrapped air which oscillates due to pressure differences caused by surface wave action. The relative motion of the floater is converted into electricity through a linear direct induction generator.

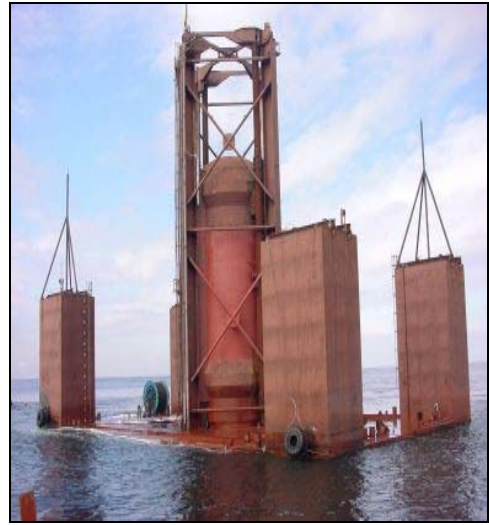


Figure 2-27: AWS prototype at sea

An AWS unit is rated at 4 MW depending on the wave climate. The floater component has a diameter of 9.5 m and the device is designed for deployment in water depths ranging from 50 to 100 m. The device is submerged to at least 6.5 m below the water surface (see Figure 2-29).

• Costs

The AWS unit is estimated to cost \$ 4 to 6million (R 26 to R 39 million) after Previsic (2004). This estimate is for the unit only and further costs will include foundation preparation and transmission cost.

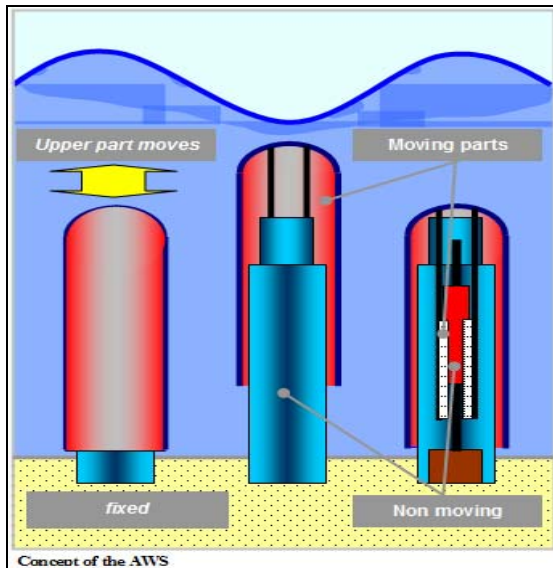


Figure 2-28: Components of AWS
(http://my.fit.edu/~swood/images/wave_2wire_workings.png, 05/2007)

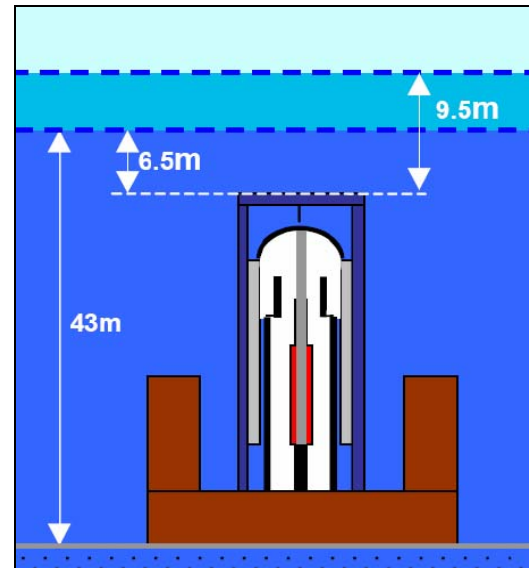


Figure 2-29: Submerged depth of AWS (Previsic, 2004)

2.5.5.2. Conclusions on relative motion WEC types

Conclusions are drawn from the device descriptions presented in § 2.5.5:

PELAMIS

- The WEC device closest to commercialisation (Previsic, 2004).
- High survivability (device submerged during extreme storm events).
- Rapidly tuneable, because of its digital control system.
- High power conversion efficiency (80%).
- This device is designed to generate power optimally in high frequency conditions with maximum relative motion between tubular sections. It will therefore be less suited to long period wave conditions.

AQUABUOY

- Buoy technology (wave recording buoys) is mature and tested.
- The device is modular and easy to transport and repair if required.
- It cannot be rapidly tuned to prevailing sea conditions.
- High mooring and transmission costs.

AWS

- The power takeoff was specifically designed for this device and requires less operation and maintenance.
- Repairs on a sub-sea system are very expensive (Remote Operated Vehicles used).
- No visual impact or interference with shipping (for ships with draughts less than about 9m)
- The direct induction generator does not allow for output smoothing.
- It is a bottom standing device and therefore foundation preparations are required.

2.5.6. Cost comparison

A comparison of the capital construction cost of the various WEC devices discussed in previous section is presented below in Table 2-1.

Table 2-1: Capital cost comparison of WEC units

Energy Source	Capital cost (R/kW)
LIMPET	20 800
ENERGETECH	9 750
SWEC	3 285
WAVEDRAGON	19 500
PELAMIS	26 000
AQUABUOY	19 600
AWS	9 750
Wind	6 500
Nuclear	13 000
Coal	11 538

Conventional energy sources

It is considered appropriate to indicate again that the operation and maintenance cost of the WEC units have not been considered (because of lack of available information in this regard) and that the latter costs should ideally be capitalized and added to the capital construction cost for a more realistic comparison between cost of energy sources.

This concludes the WEC technology overview and the literature review. The results of the wave power analysis of measured wave data on the South African coast is presented in the following chapter.

3. WAVE POWER CONDITIONS ON THE SOUTH AFRICAN COAST BASED ON RECORDED DATA

Wave data of five recording stations along the South African coast was considered during the recorded wave data analysis of this study. These stations are operated by the CSIR on behalf of Transnet, National Port Authority (NPA), who made the data available for this investigation. The main purpose of this data analysis is to determine the magnitude of wave power at each recording station from which the wave power distribution along the South African coast can be derived and the coastal region with the largest wave power potential can be identified. The results of this analysis will also be used to validate the results of the numerical modelling portion of this project.

3.1. Description of wave recording stations and available wave data

The distribution of the wave recording stations along the coastline is shown in Figure 3-1. A brief description of each station and its associated data is presented in Table 3-1 below. It is clear from Figure 3-1 that these recording stations are sparsely distributed on the South African coastline and there are large areas of unknown wave conditions in between stations. The stations are however considered representative of the various coastal regions of South Africa as proposed by (MacHutchon 2006, refer to Figure 3-2)

Table 3-1: Relevant information of wave recording stations

Recording Station	Lat Long coordinates	Distance offshore (km)	Water depth (m)	Description of data	Recording period	% Coverage	Wave recorder
Port Nolloth	29° 46.8'S 16° 46'E	30	100	3 Hourly H_s and T_p	1987/04/08 to 1996/08/31	63%	Waverider
Slangkop	34° 7.6'S 18° 10.6'E	13	170	6 Hourly H_s and T_p	1978/10/03 to 1993/06/12	72%	Waverider
Cape point	34° 12.2'S 18° 17.2'E	7	70	3 Hourly H_s and T_p	2000/07/01 to 2006/06/30	92%	Waverider
FA platform	34° 58.2'S 22° 10.2'E	72.5	113	1 Hourly H_s , T_z and H_{max}	1998/01/01 to 2003/12/31	97%	Radar
Durban	29° 59.2'S 30° 59.9'E	2.3	42	3 Hourly H_s and T_p	1992/08/11 to 2001/10/31	69%	Waverider

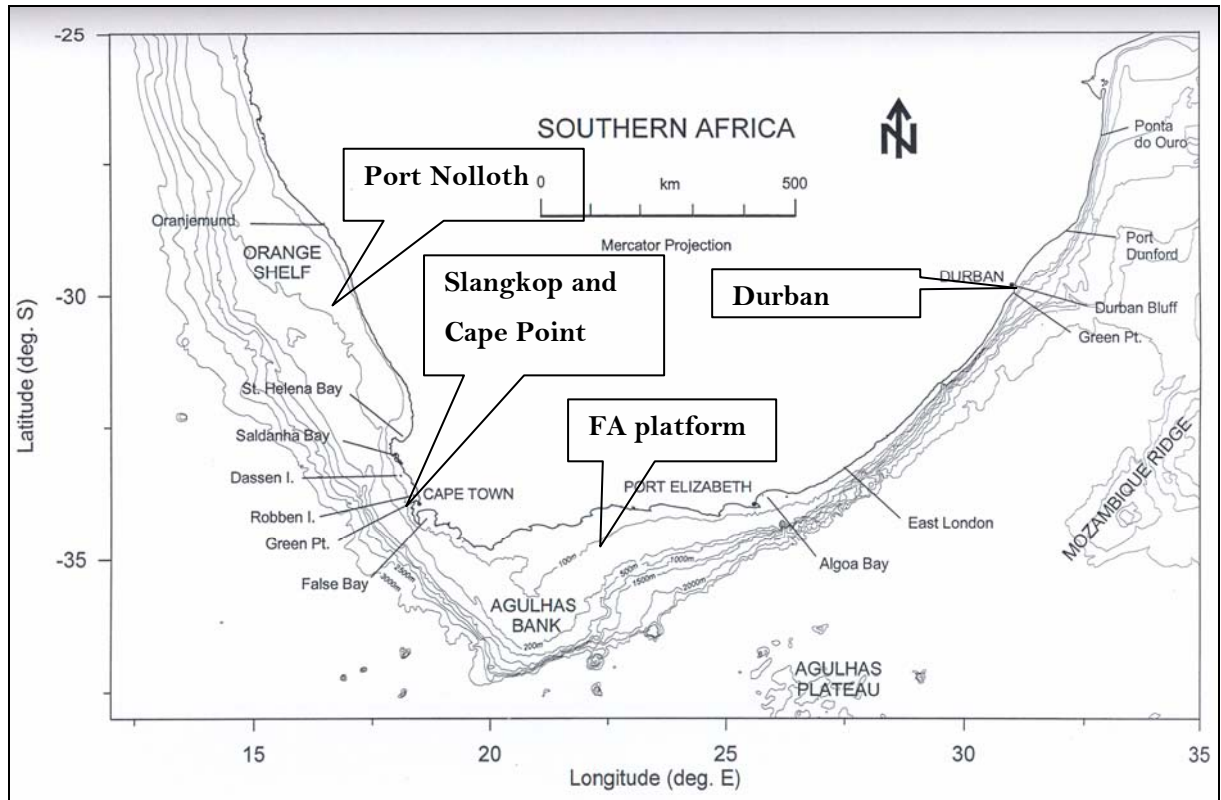


Figure 3-1: Contours of the Southern African seabed to 3000 m depth and the distribution of wave recording stations (van der Westhuysen, 2002)

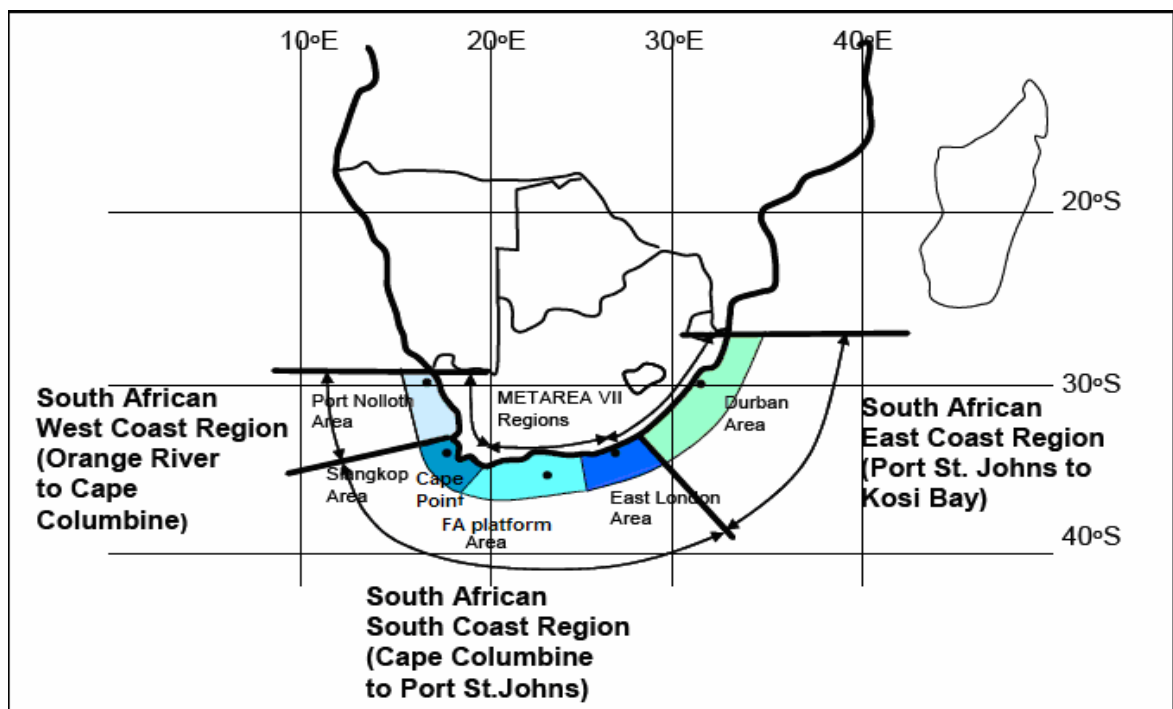


Figure 3-2: South African sea storm regions (MacHutchon, 2006)

Figure 3-1 above shows the locations of the wave recording stations considered in this study. Figure 3-1 also indicates the width of the continental shelf (shelf edge approximately along the 200 m depth contour) at the recording stations. The Slangkop, Cape Point and Durban wave recording stations are located in a zone where the continental shelf is relatively narrow in comparison with the relatively wide continental shelf at the recording stations of Port Nolloth and FA platform. A brief description of the wave recording stations considered is presented below.

3.1.1. Port Nolloth

The Port Nolloth wave data represents the wave power associated with the South African west coast. Waves generated by the extra-tropical cyclone systems (low pressure systems) in the southern ocean (between approximately the 40° and 60° latitude zone) approach the South African west coast, predominantly from the south westerly sector (see § 2.2 for a description of the South African meteorology). It is expected that wave heights and consequent wave power will decline the further north the waves travel from the storm generation zone.

3.1.2. Slangkop

The Slangkop waverider buoy was situated about 13 km directly west of Kommetjie (see Figure 3-3) during the period of 1978 to 1993. The radio signal sent from this buoy was received at the Slangkop lighthouse. In 1994 the Slangkop wave recording station was relocated to the present Cape Point recording station. Slangkop and Cape Point are the most south westerly located stations and the first stations to receive the wave power propagating from the dominant south westerly direction. The water depth at the Slangkop recording station was 170 m only 13 km from shore which confirms that the continental shelf has a very steep gradient in this region (see Figure 3-1).

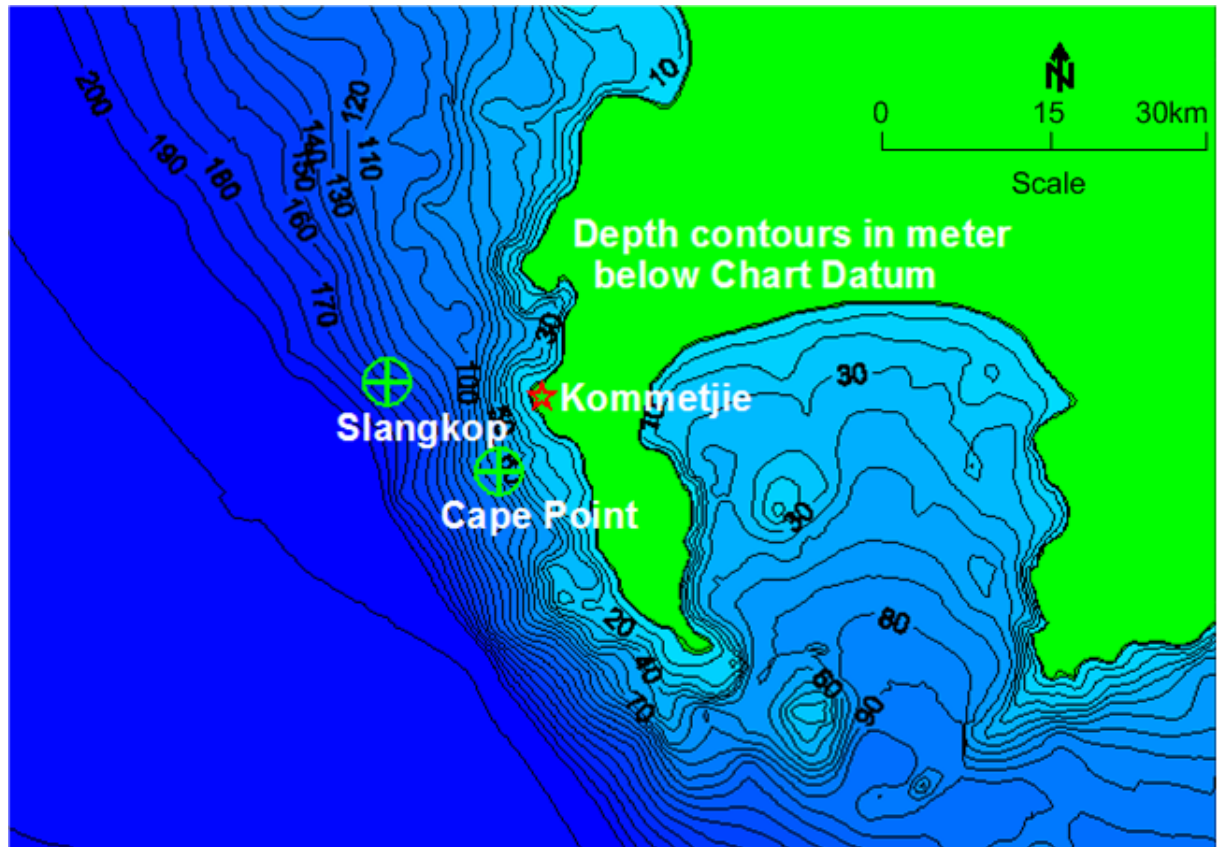


Figure 3-3: Locations of Slangkop and Cape Point wave recording stations

3.1.3. Cape Point

The Waverider buoy at the Cape Point recording station is situated in water depth of 70 m approximately 7 km southwest of Kommetjie. It is expected that the shallower water depth at Cape Point recording station will expose it to lower wave power levels compared to the Slangkop station, but local bathymetry conditions could also focus wave power at the Cape Point station for specific wave conditions, which could increase its wave power exposure compared to Slangkop for those specific wave conditions. A direct comparison between these two stations is not possible since there is no overlapping in their recording periods, but it is expected that the two stations will have similar wave power conditions due to its close proximity.

3.1.4. FA platform

The FA platform is located approximately 73 km offshore at a depth of 113m. The platform produces natural gas from substrata below the seabed. The natural gas is pumped via a sub sea pipeline to the shore based refinery controlled by PetroSA, at Mossel Bay.



Figure 3-4: Aerial view of the FA platform in 113 m water depth

Some important aspects associated with the FA platform include the following:

- a) The FA platform is considered to be a deep sea station, because of its substantial distance offshore and its water depth.
- b) The platform is more exposed than the other stations closer to shore due to its substantial distance from shore (see Figure 3-1).
- c) The main difference between the FA platform and the other recording stations analysed is that the platform is exposed to wave power from the dominant south west and also to wave power from the east.
- d) The recording period of the FA platform overlaps with that of the Cape Point recording station.
- e) The greater width of the continental shelf in the vicinity of the platform require longer electrical transmission cables from an offshore wave farm to shore compared to sites on narrower portions of the continental shelf.
- f) The platform uses a radar wave recording sensor instead of the Waverider buoy used at the other wave recording stations.

3.1.5. Durban

The recorded wave climate at the Durban wave recording station represents the expected wave power along the east and south coast of South Africa. The Durban station is not as exposed to wave power from the south west as the other recording stations. It does however experience wave power generated from tropical storms in the east. The waverider

buoy at the Durban recording station is located offshore of the Durban oil refinery near the Durban Airport.

3.2. Percentage coverage of recording stations

In Table 3-1 the recording period of each station is indicated. The percentage coverage of each station during its recording period is discussed in this section. It is very important to determine the annual percentage of operation time of each recording station. For example if a wave recording buoy was not operational for 50% of the year this will produce unrealistic statistical parameters of wave power for that year. For the purpose of comparison of wave power conditions at the different recording stations the degree of concurrent or overlapping recording periods, is important. The overlapping of recording periods of the wave recording stations is presented in Table 3-2.

Table 3-2: Overlapping of recording periods of wave recording stations and percentage coverage

Stations	Recording year																												
	78	79	80	81	82	83	84	85	86	87	88	89	90	91	92	93	94	95	96	97	98	99	00	01	02	03	04	05	06
Port Nolloth																													
Slangkop																													
Cape Point																													
FA platform																													
Durban																													

For most of the stations the first and last recording years are incomplete and the percentage coverage was therefore determined by excluding these years. A detailed discussion of the percentage coverage is presented in §3.2.1 to §3.2.5.

In the data analysis presented in the following sections wave data of stations with overlapping recording periods will be directly compared, but also entire data sets of stations to indicate general trends in wave conditions and consequent wave power.

3.2.1. Port Nolloth

It is indicated in Table 3-1 above, the wave recording period of the Port Nolloth station covers a ten year period. This is considered to be a long record, only exceeded in length (years recorded) by the Slangkop record. Just considering eight near complete recording years, the average coverage of Port Nolloth is 67%. Table 3-3 (table layout and bar chart

representation based on MacHutchon, 2006) and Figure 3-5 shows the distribution of Waverider buoy operational time at Port Nolloth during its recording period. The highlighted rows (1987 and 1996) are incomplete recording years which were not considered in the coverage calculations.

Table 3-3: Coverage of Port Nolloth wave data

Season	Summer			Autumn			Winter			Spring			Annual	
Months	Dec	Jan	Feb	Mar	Apr	May	Jun	Jul	Aug	Sep	Oct	Nov	Total number of records	% of total
Days	31	31	28	31	30	31	30	31	31	30	31	30		
Max possible records	248	248	224	248	240	248	240	248	248	240	248	240	2920	
Years														
1987	113	0	0	0	68	124	124	113	118	113	87	122	982	34%
1988	115	70	104	114	79	123	116	111	123	117	122	114	1308	45%
1989	120	100	105	115	106	122	86	122	121	118	124	105	1344	46%
1990	120	109	101	124	111	115	120	114	116	114	101	112	1357	46%
1991	238	115	108	121	117	124	120	115	110	166	228	232	1794	61%
1992	242	236	219	233	197	25	0	0	134	221	231	207	1945	67%
1993	220	227	218	242	243	245	162	243	237	222	241	230	2730	93%
1994	230	240	215	242	217	232	198	115	244	228	242	231	2634	90%
1995	239	219	204	206	141	189	214	199	218	177	210	235	2451	84%
1996	0	237	227	247	239	246	234	244	244	0	0	0	1918	66%
Mean monthly	191	165	159	175	151	147	127	127	163	170	187	183	Total recorded	15563
	77%	66%	71%	70%	63%	59%	53%	51%	66%	71%	76%	76%	Max possible	23360
Mean seasonal	71%			64%			57%			74%			Annual mean coverage	67%

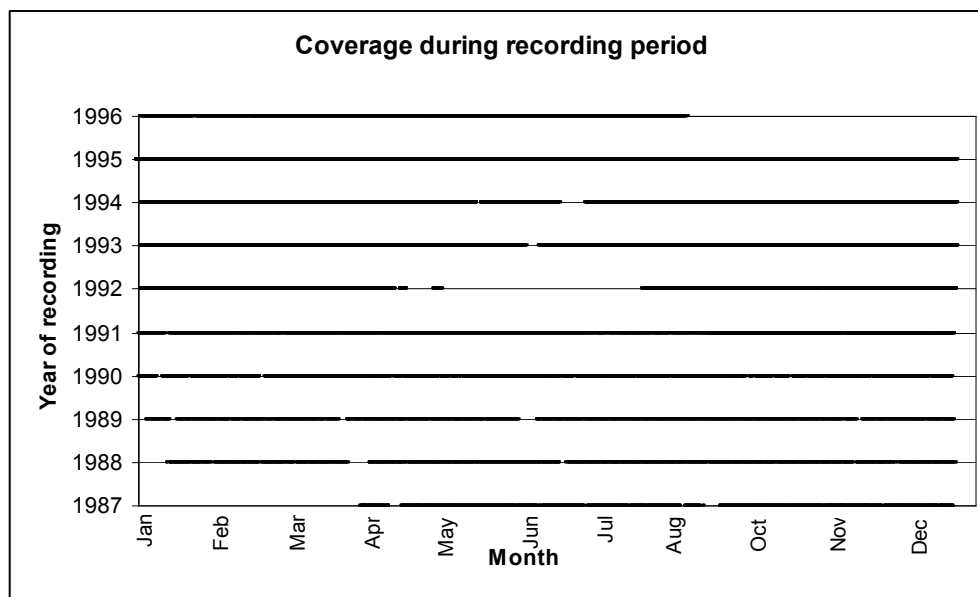


Figure 3-5: Bar chart representation of the degree of completeness of Port Nolloth wave data

3.2.2. Slangkop

As mentioned in the previous section, Slangkop has the longest recording period of 16 years. It does however have a less detailed recording resolution with readings taken at only six hourly intervals, compared to the three hourly records of Cape Point, Port Nolloth and Durban and the hourly records of the FA platform. Again, just considering near complete recording years (excluding highlighted years of 1978 and 1993), the Slangkop station has a coverage of 78% during its recording period. The distribution of measurements taken over its recording period is shown in Table 3-4 and Figure 3-6.

Table 3-4: Coverage of Slangkop wave data

Season	Summer			Autumn			Winter			Spring			Annual	
Months	Dec	Jan	Feb	Mar	Apr	May	Jun	Jul	Aug	Sep	Oct	Nov	Total number of records	% of total
Days	31	31	28	31	30	31	30	31	31	30	31	30		
Max possible records	124	124	112	124	120	124	120	124	124	120	124	120	1460	
Years														
1978	117	0	0	0	0	0	0	0	0	0	105	104	326	22%
1979	0	117	104	113	115	82	105	122	115	11	25	43	952	65%
1980	92	0	0	0	10	101	101	101	124	120	116	99	864	59%
1981	83	79	96	89	114	99	112	109	110	102	107	83	1183	81%
1982	117	94	109	114	116	97	39	120	89	97	53	70	1115	76%
1983	113	122	94	120	120	111	89	85	82	118	115	91	1260	86%
1984	90	121	110	102	120	55	86	114	88	120	98	104	1208	83%
1985	117	114	78	60	60	109	96	89	122	86	124	117	1172	80%
1986	118	85	88	123	104	124	115	50	109	119	123	116	1274	87%
1987	0	105	111	118	113	57	75	123	120	113	124	4	1063	73%
1988	112	0	0	9	113	118	114	108	122	100	114	113	1023	70%
1989	95	111	97	115	74	76	95	102	97	103	108	100	1173	80%
1990	124	103	103	105	89	98	109	89	110	117	108	114	1269	87%
1991	118	109	109	121	115	112	71	106	120	105	109	44	1239	85%
1992	122	122	110	123	108	64	72	94	49	105	120	118	1207	83%
1993	0	120	88	124	113	53	1	0	0	0	0	0	499	34%
Mean monthly	93	92	86	94	98	93	91	101	104	101	103	87	Total recorded	16002
	75%	74%	77%	76%	82%	75%	76%	81%	84%	84%	83%	72%	Max possible	20440
Mean seasonal	75%			77%			80%			80%			Annual mean coverage	78%

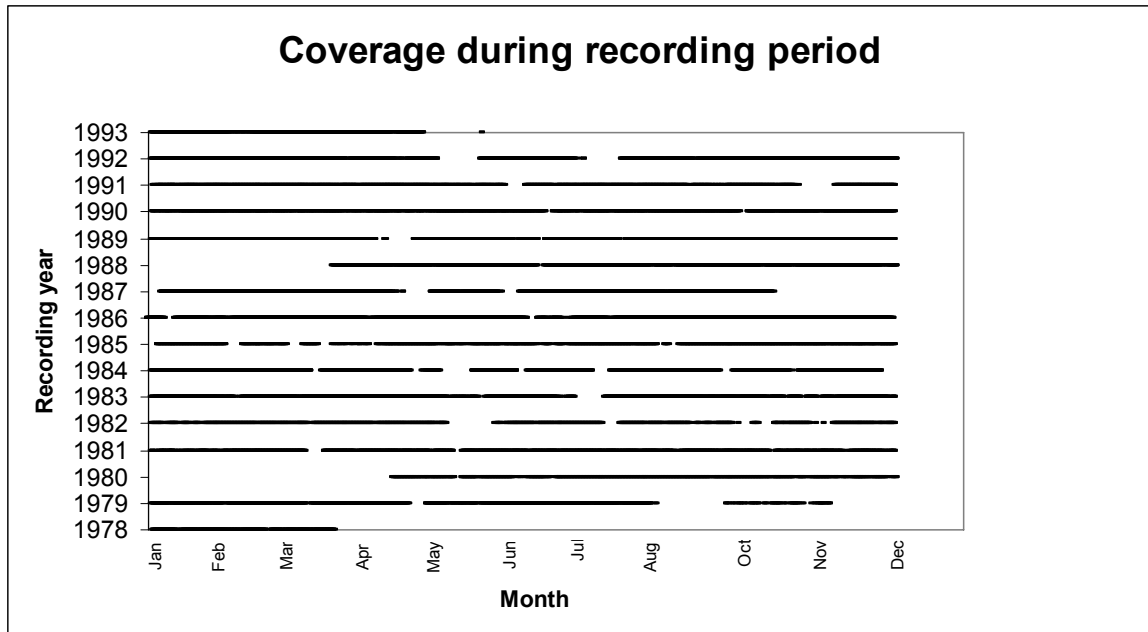


Figure 3-6: Bar representation of degree of completeness of the Slangkop wave data

3.2.3. Cape Point

The Cape Point wave data has an excellent coverage of 93% and the bar chart representation of its measurement distribution is therefore not presented. Its monthly and annual coverage is shown in Table 3-5 below.

Table 3-5: Coverage of Cape Point wave data

Season	Summer			Autumn			Winter			Spring			Annual	
Months	Dec	Jan	Feb	Mar	Apr	May	Jun	Jul	Aug	Sep	Oct	Nov	Total number of records	% of total
Days	31	31	28	31	30	31	30	31	31	30	31	30		
Max possible records	248	248	224	248	240	248	240	248	248	240	248	240	2920	
Years														
2000	161	0	0	0	0	0	0	233	212	165	211	24	1006	34%
2001	247	173	56	223	13	230	237	228	234	216	130	238	2225	76%
2002	247	248	216	240	233	247	231	239	232	216	198	240	2787	95%
2003	237	247	223	248	239	247	240	246	247	239	235	220	2868	98%
2004	236	246	232	248	240	248	240	248	233	240	248	240	2899	99%
2005	242	238	224	247	240	248	239	248	248	240	232	196	2842	97%
2006	0	240	180	237	240	242	240	0	0	0	0	0	1379	47%
Mean monthly	242	230	190	241	193	244	237	242	239	230	209	227	Total recorded	13621
	98%	93%	85%	97%	80%	98%	99%	98%	96%	96%	84%	95%	Max possible	
Mean seasonal	92%			92%			98%			92%				14600
													Annual mean coverage	93%

3.2.4. FA platform

Table 3-6 below shows the excellent coverage that the FA platform had during its six year recording period. Furthermore, readings were taken hourly which makes this data set the most complete and detailed of all the available wave data sets.

Table 3-6: Coverage of FA platform wave data

Season	Summer			Autumn			Winter			Spring			Annual	
Months	Dec	Jan	Feb	Mar	Apr	May	Jun	Jul	Aug	Sep	Oct	Nov	Total number of records	% of total
Days	31	31	28	31	30	31	30	31	31	30	31	30		
Max possible records	744	744	672	744	720	744	720	744	744	720	744	720	8760	
Years														
1998	734	748	668	723	709	729	704	726	712	700	741	714	8608	98%
1999	734	731	668	744	709	729	704	730	733	700	741	714	8637	99%
2000	746	633	552	555	603	411	442	507	744	722	740	721	7376	84%
2001	719	745	681	745	725	741	719	730	755	720	746	716	8742	100%
2002	738	743	681	745	725	748	720	743	755	720	746	720	8784	100%
2003	743	745	681	745	725	748	720	622	755	720	746	720	8670	99%
Mean monthly	736	724	655	710	699	684	668	676	742	714	743	718	Total recorded	50817
	99%	97%	97%	95%	97%	92%	93%	91%	100%	99%	100%	100%	Max possible	52560
Mean seasonal	98%			95%			94%			100%				
													Annual mean coverage	97%

3.2.5. Durban

The Waverider buoy at Durban was infrequently operational during its recording period. Note that the buoy was hardly ever operational for a complete year (see Table 3-7 and Figure 3-7). These infrequent readings are evenly distributed throughout the data set, making conclusions drawn less reliable. Some suspicious measurements (i.e. singular relatively large wave conditions) in the Durban wave data will be highlighted in a later section.

Table 3-7: Coverage of the Durban wave data

Season	Summer			Autumn			Winter			Spring			Annual	
Months	Dec	Jan	Feb	Mar	Apr	May	Jun	Jul	Aug	Sep	Oct	Nov	Total number of records	% of total
Days	31	31	28	31	30	31	30	31	31	30	31	30		
Max possible records	248	248	224	248	240	248	240	248	248	240	248	240	2920	
Years														
1992	245	0	0	0	0	0	0	0	155	235	238	120	993	34%
1993	226	244	212	207	222	208	205	245	246	228	242	226	2711	93%
1994	239	233	217	243	90	172	213	215	213	158	144	232	2369	81%
1995	138	245	91	194	237	238	106	162	145	0	132	182	1870	64%
1996	185	201	108	39	112	241	236	150	234	227	233	198	2164	74%
1997	132	142	190	191	56	139	213	141	243	238	238	225	2148	74%
1998	216	90	179	59	213	245	189	245	244	239	238	191	2348	80%
1999	201	220	211	123	121	208	211	63	247	204	101	194	2104	72%
2000	113	181	86	105	79	212	136	124	0	57	140	124	1357	46%
2001	0	229	156	148	214	229	166	144	220	220	225	0	1951	67%
Mean monthly	181	195	162	145	141	208	189	168	197	169	184	197	Total recorded	17071
	73%	78%	72%	59%	59%	84%	79%	68%	79%	70%	74%	82%	Max possible	23360
Mean seasonal	75%			67%			75%			75%			Annual mean coverage	73%

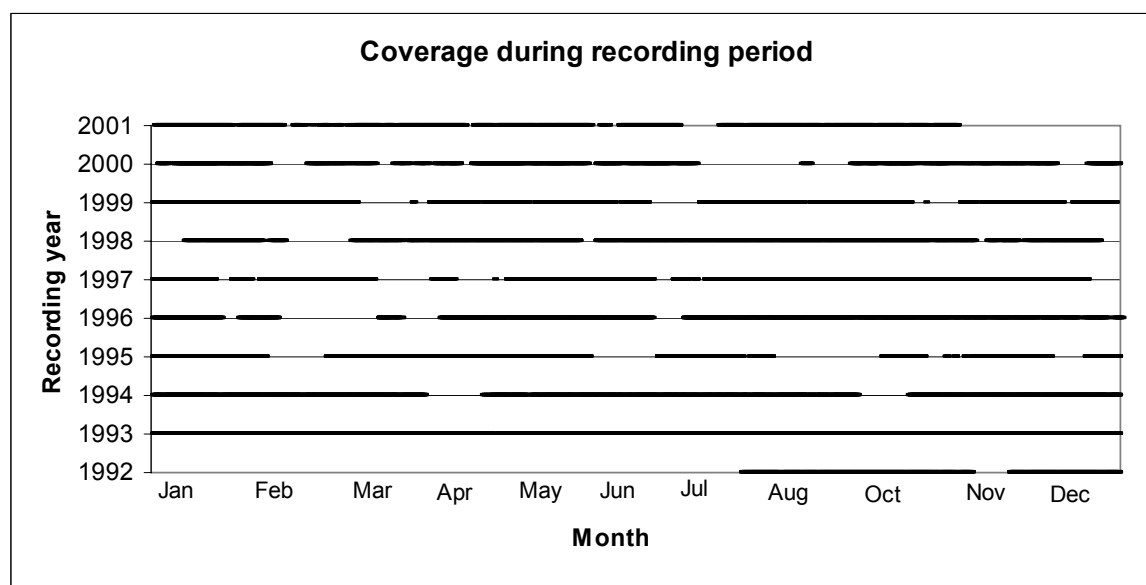


Figure 3-7: Bar representation of degree of completeness of the Durban wave data

3.3. Wave height and -period exceedance analysis

The wave power calculation procedure outlined in §2.4.6 indicated that wave power is proportional to the square of the wave height and linearly proportional to the wave period. This wave data analysis will commence by investigating these two parameters with the purpose to obtain a general indication of the expected wave power conditions at each recording station on the South African coastline.

3.3.1. Wave height

The distribution of H_s at each recording stations is presented in terms of probability of exceedance- and frequency of occurrence of H_s . The probability of exceedance curves for all the stations are presented in Figure 3-8 below.

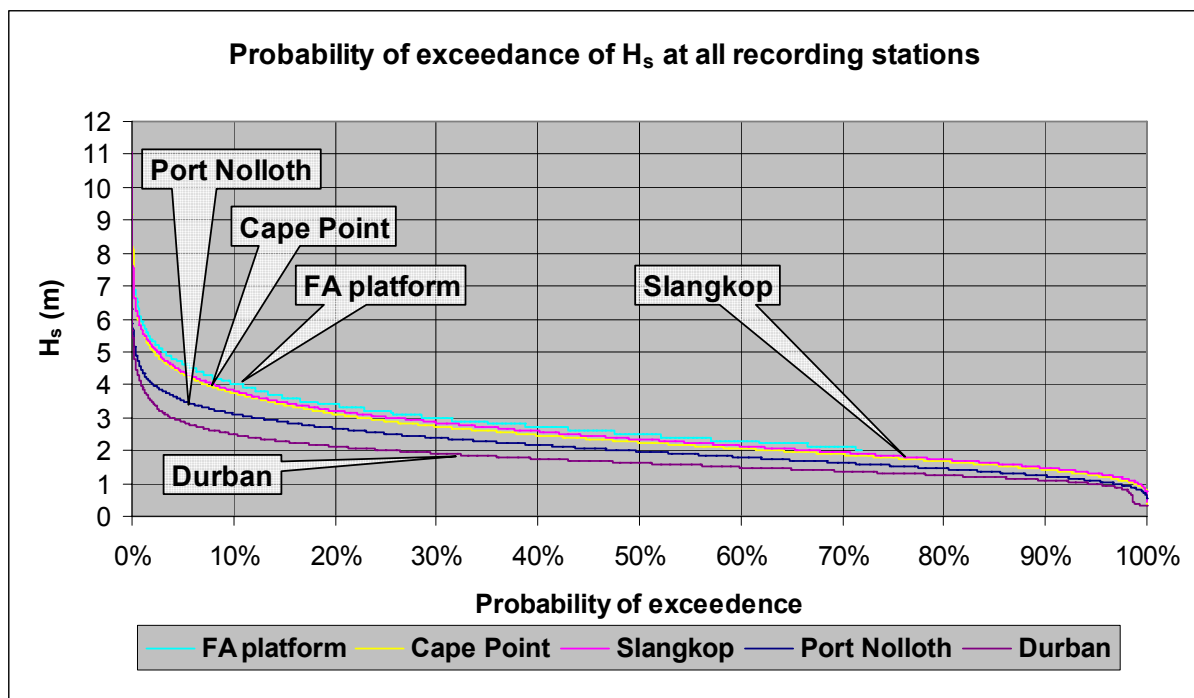


Figure 3-8: Probability of exceedance of H_s for South African recording stations

Figure 3-8 shows that the FA platform is exposed to the greatest H_s values with the highest probabilities of exceedance. Cape Point does however experience larger extreme H_s values at small probabilities of exceedance.

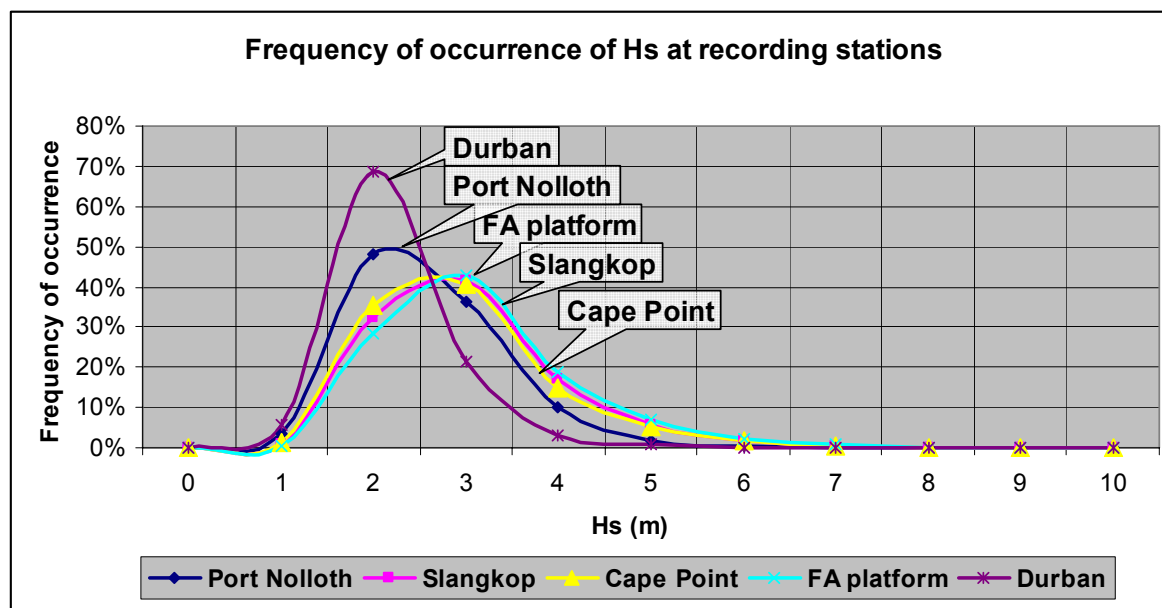


Figure 3-9: Frequency of occurrence of Hs

The frequency of occurrence graph in Figure 3-9 shows that the FA platform is exposed to greater H_s values at greater frequencies compared to the other stations. The Slangkop and Cape Point curves are however only slightly lower. From this analysis of the H_s distribution it is expected that the platform will have the largest wave power resource of all the recording stations.

Extreme wave heights are an important design consideration of wave farms to ensure that WEC units can withstand the extreme loadings of such events. The 1 in 20, 1 in 50 and 1 in 100 year design waves can be derived from the probability of exceedance curves by fitting it to an Extreme I distribution. These design wave heights (MacHutchon, 2006) for all stations except Slangkop are presented in Appendix B.

3.3.2. Wave period

The wave period distribution at the wave recording stations was analysed by investigating the frequency of occurrence of T_p and 90%, 50% and 10% probability of exceedance values of T_p. It is important to note that the data set of FA platform describes wave period in terms of T_z (zero crossing period) and it is assumed that T_p = T_z/0.71 (Massie, 2001). This assumption applies to the Bretschneider spectrum which is especially suited to open ocean areas (like the platform). Implications of this assumption will be discussed in § 3.9.4. The mean annual frequency of occurrence of wave period for the various recording stations is presented in Figure 3-10 and Table 3-8 below.

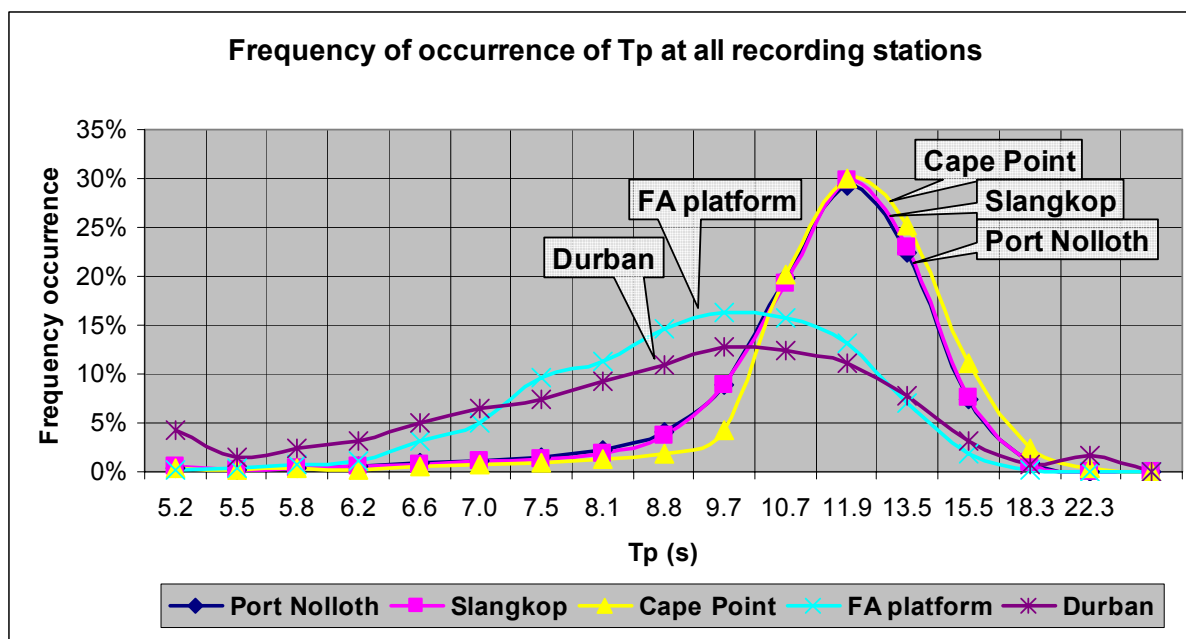


Figure 3-10: Mean annual frequency of occurrence of T_p

Table 3-8: Mean annual frequency of occurrence of T_p

T_p	Port Nolloth	Slangkop	Cape Point	FA platform	Durban
5.2	0%	0%	1%	0%	4%
5.5	0%	0%	0%	0%	2%
5.8	0%	0%	0%	1%	2%
6.2	0%	1%	1%	1%	3%
6.6	1%	1%	1%	3%	5%
7.0	1%	1%	1%	5%	6%
7.5	1%	1%	1%	10%	8%
8.1	1%	2%	2%	11%	9%
8.8	2%	4%	4%	15%	11%
9.7	4%	9%	9%	16%	13%
10.7	20%	20%	19%	16%	12%
11.9	30%	29%	30%	13%	11%
13.5	25%	22%	23%	7%	8%
15.5	11%	7%	8%	2%	3%
18.3	2%	1%	1%	0%	1%
22.3	0%	0%	0%	0%	2%
> 22.3	0%	0%	0%	0%	0%

The intervals of T_p considered in this analysis are as defined in the thesis of (Rossouw, 1989). Figure 3-10 and Table 3-8 indicate that the dominant T_p value for Port Nolloth, Slangkop and Cape Point is approximately 12s. The stations further east, FA platform and Durban, have a lower dominant T_p value of approximately 10s. This lower T_p value at the

platform is expected to reduce the wave power distribution at the platform compared to Slangkop- and Cape Point recording station. Figure 3-10 also indicates that the Cape Point station has the highest frequency of occurrence of high values of T_p .

Table 3-9: Probability of exceedance of 90-, 50- and 10% for T_p

Stations	90%	50%	10%
Port Nolloth	8.8	11.9	13.5
Slangkop	8.8	11.9	13.5
Cape Point	9.1	11.7	14.2
FA platform	6.9	9.0	11.4
Durban	6.2	8.8	13.5

Table 3-9 shows the 90%, 50% and 10% probability of exceedance values of T_p at each station. Slangkop and Port Nolloth have identical T_p distributions, while the T_p distribution at Cape Point recording station is slightly higher.

3.4. Peak-enhancement factor analysis

As indicated in the wave power calculation procedure of §2.4.6, the peak-enhancement factor (γ) of the JONSWAP spectral shape function representing the measured spectrum is required in order to determine the total wave power of the wave record. In the current section the results of an analysis of γ -values derived from measured spectra at the Cape Point recording station will be presented.

γ -values of Cape Point recording station from 2001 to 2006 were made available for this study by the CSIR (personal communication M. Rossouw, 2007). In order to determine an applicable value for γ from basic recorded wave parameters, a relationship is required between T_p and γ . The γ -value has large variability over a significant range. It is dependent on a multitude of variables therefore, assuming one relationship between T_p and γ is considered unrealistic. However, such a relationship is required to calculate wave power and will be determined from a scatter analysis of values of T_p and γ (see § 3.9 for wave energy scatter analysis). A scatter plot reveals the frequency of occurrence of concurrent T_p and γ -values. From the scatter plot the dominant γ -value can be determined for different values of T_p . A contour plot of the scatter analysis is shown in Figure 3-11 below.

Figure 3-11 shows large scatter which implies that a wide range of γ -values apply to a given value of T_p . For example, the dominant wave period of 12s has associated γ -values ranging from 1 to 8. The dominant γ -value for T_p equal to 12s is however 1.5. This γ -value is also the dominant value for T_p values ranging from 8 to 14s (the dominant T_p range). Based on this analysis it was decided to assume a constant γ -value of 1.5 for all values of T_p in the derivation of wave power. The sensitivity of wave power to input γ -values was assessed by means of a sensitivity analysis (refer to Appendix D for results of sensitivity analysis). It was found that wave power is relatively insensitive to small variations of γ using a JONSWAP spectral shape function.

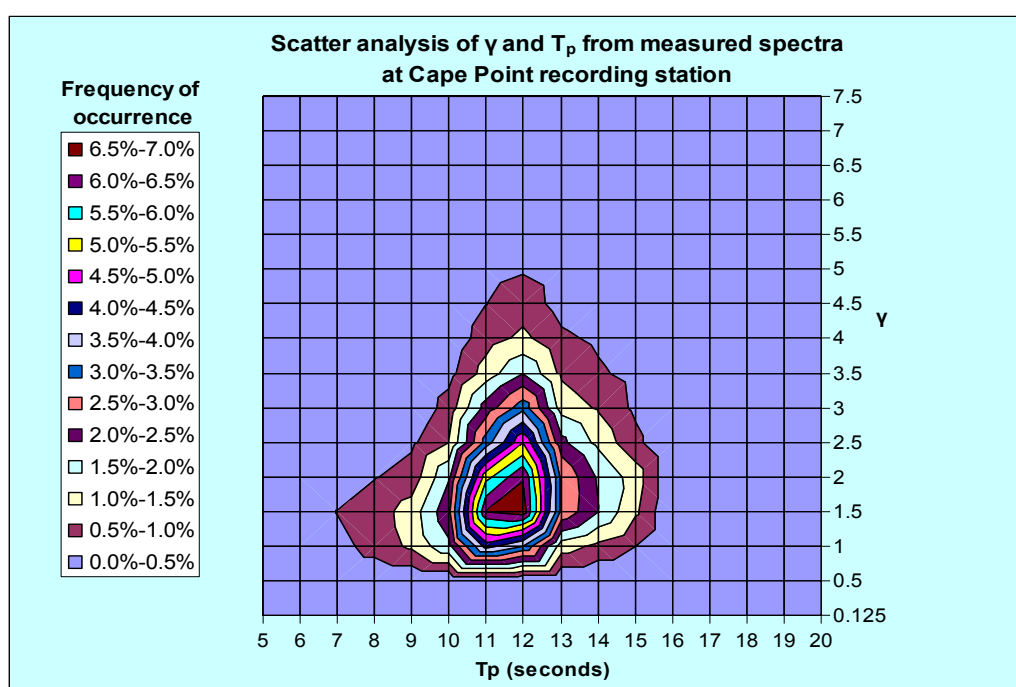


Figure 3-11: Scatter plot of γ and T_p measured at Cape Point recording station

3.5. Directional distribution

All the requirements for the wave power calculation procedure are now accounted for, but before the results of this process is presented a brief description of recorded directional spreading is given.

The data set used in the γ -analysis of § 3.4 also contains measured values of directional spreading at Cape Point recording station. As mentioned above, directional spreading is not required in the power calculation procedure, but is required as input for numerical modeling for setting up a spectral representation. Similarly to the γ -analysis, a scatter analysis of

measured m - and T_p values was conducted. The results of this analysis are shown in the scatter contour plot of Figure 3-12. Figure 3-12 indicates that, unlike the scatter analysis of γ -values, a single, dominant value of m cannot be assumed for all values of T_p .

Further investigation into the relationship of T_p and m was done by consultation with C. Rossouw (personal communication, 2007) who proposed the following relation of m to T_p :

$$m = 0.0582T_p^2 - 0.3988T_p + 3.0546 \quad \text{Eqn 3.1.}$$

A plot of this equation as well as the observed m -values at Cape Point recording station from the scatter analysis is shown in Figure 3-13.

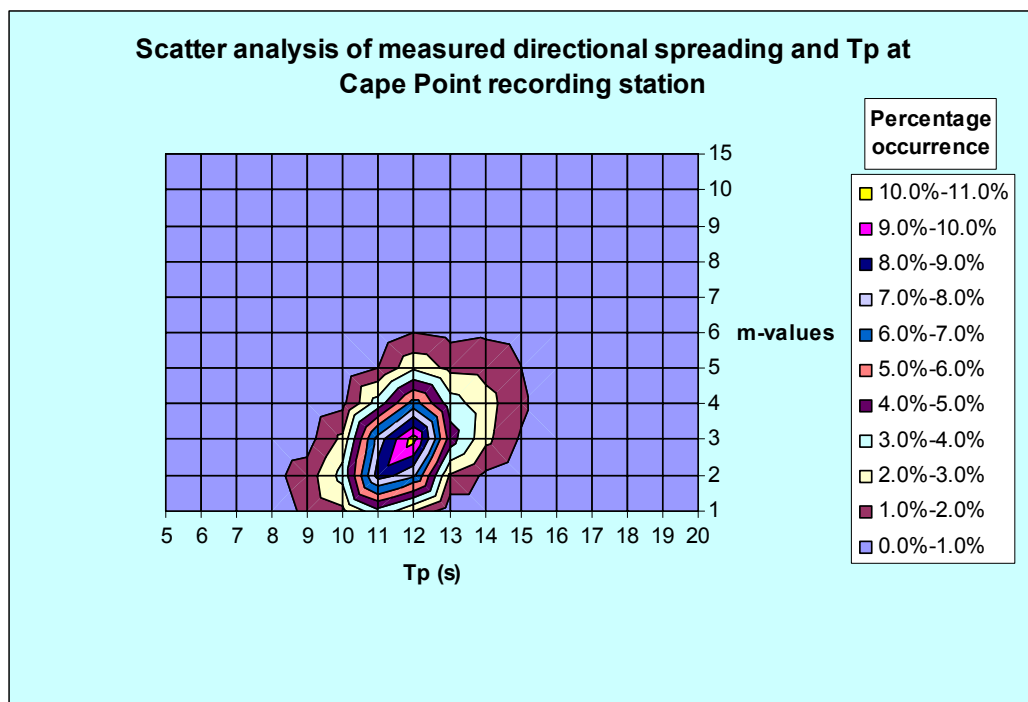


Figure 3-12: Scatter plot of m and T_p values recorded at Cape Point

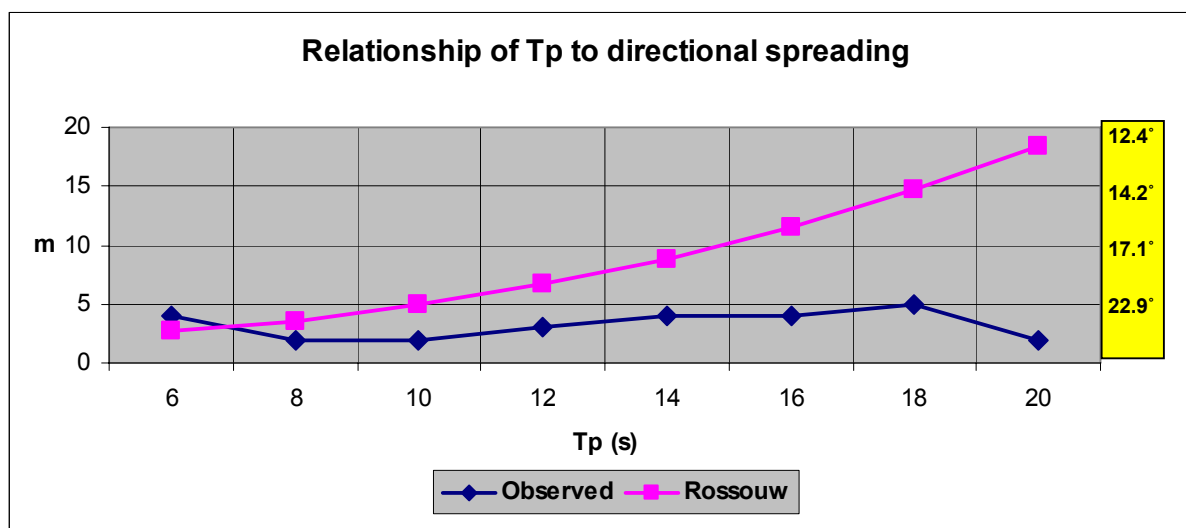


Figure 3-13: The relationships of T_p and m as observed at Cape Point and after Rossouw (2007)

Figure 3-13 shows that the empirical relationship of Rossouw deviates significantly from observed values of m for high values of T_p (≥ 16 s). The difference between observed- and empirical values was however considered acceptable for the dominant T_p range of 10 to 14s. Eqn 3.1. was therefore used to prescribe directional spreading in the numerical modelling portion of the study.

The wave power analysis of the recorded wave data is presented in the following section.

3.6. Annual and seasonal wave power

3.6.1. Introduction

Wave height conditions and consequent wave power is dependant on weather conditions. It therefore varies from day to day, season to season and year to year. In this section the variability of annual wave power of each wave recording station will be described in terms of basic statistical parameters. These parameters include: average wave power over the recording period, 90% probability of exceedance of wave power (represents the lowest expected wave power conditions) and 5% probability of exceedance of wave power (represent the recorded extreme wave power events). All wave power values will be expressed in terms of kW per meter of wave crest and only near completed recording years will be considered for the annual analysis.

3.6.2. Port Nolloth

The graph in Figure 3-14 shows that the annual wave power fluctuation is relatively small as indicated by the average, 90% and 5% probability of exceedance values. These statistical parameters are shown for each season and for the mean annual record in Figure 3-15 and Table 3-10.

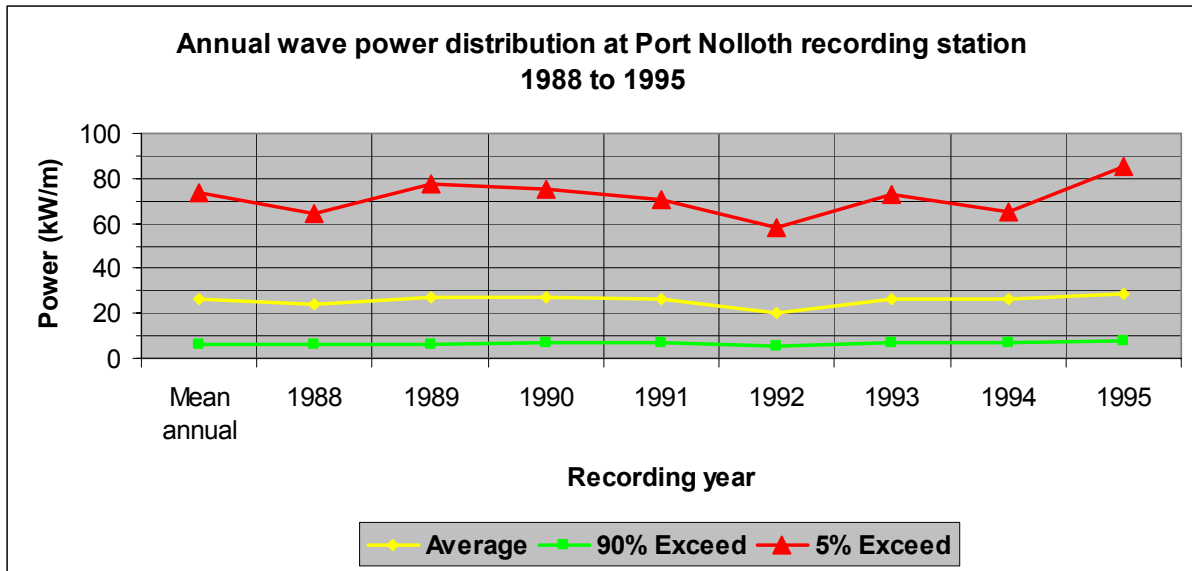


Figure 3-14: Annual and mean annual wave power at Port Nolloth

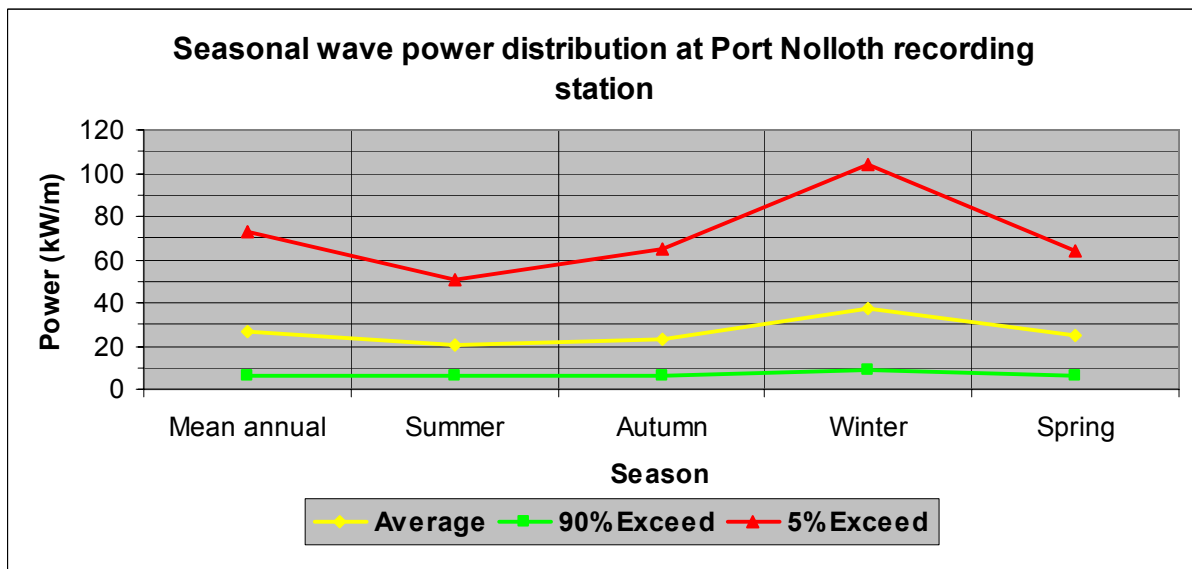


Figure 3-15: Seasonal wave power distribution at Port Nolloth recording station

Table 3-10: Seasonal statistical parameters of the wave power (kW/m) at Port Nolloth

Season	Average	90% Exceedance	5% Exceedance
Mean annual	26.5	6.6	73.3
Summer	20.7	6.1	50.8
Autumn	23.3	6.1	64.6
Winter	37.5	9	104.4
Spring	24.9	6.2	64.3

As expected the maximum wave power occurs in winter, but spring also experiences high levels of wave power at Port Nolloth recording station.

3.6.3. Slangkop

Figure 3-16 indicates that the average annual wave power at Slangkop recording station does not significantly deviate from approximately 40kW/m. The extreme events associated with 5% probability of exceedance vary more significantly annually than the average wave power.

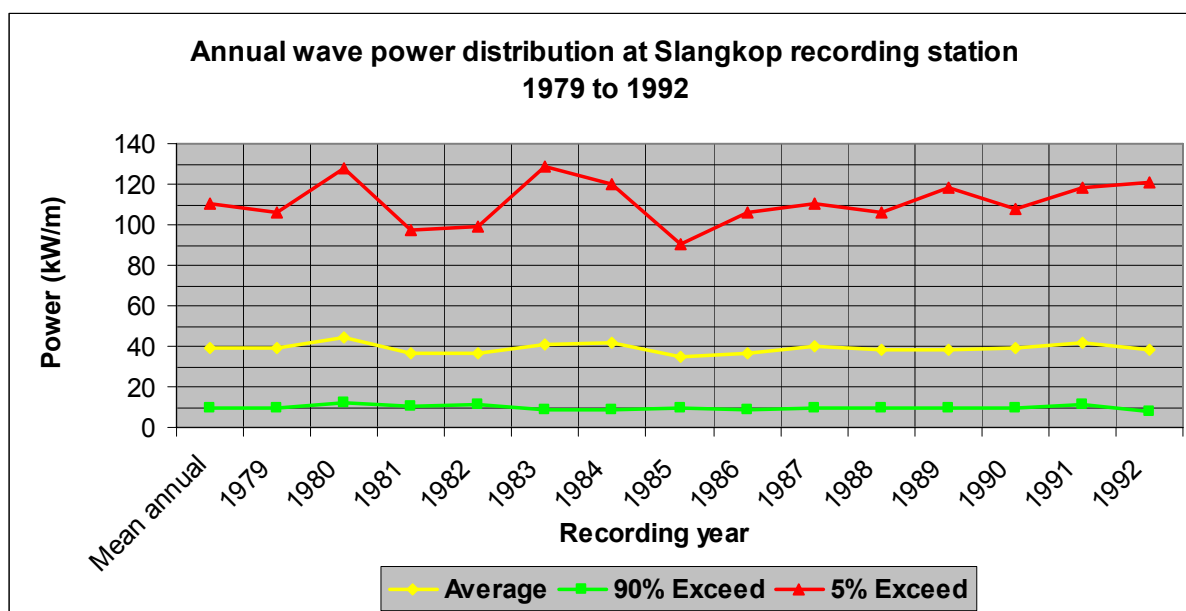


Figure 3-16: Annual- and mean annual wave power at Slangkop recording station

The statistical parameters of the Slangkop wave data are of larger magnitude than that of Port Nolloth wave data. This is a confirmation of the expected reduction in wave power as waves propagate further north from the southern ocean storm generation area. To further

demonstrate the difference in wave power distribution at the Slangkop- and Port Nolloth recording station a comparison was made over the near complete overlapping recording years of these two stations.

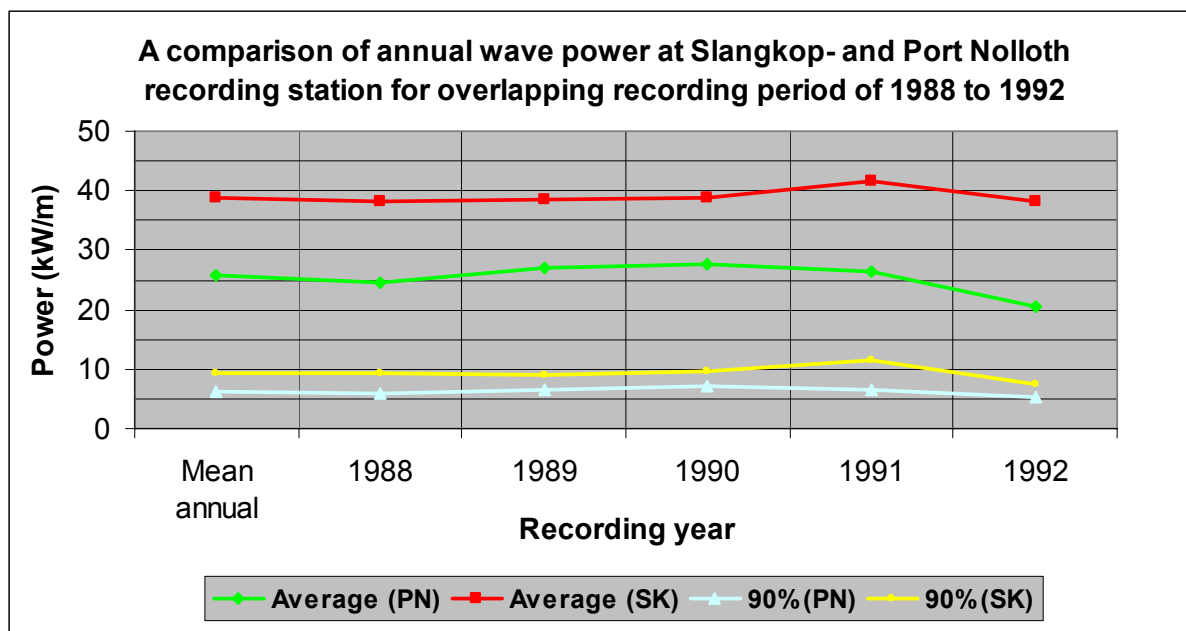


Figure 3-17: A comparison of wave power at Slangkop- (SK) and Port Nolloth recording station (PN) during overlapping recording years

It is interesting to note, in Figure 3-17, that Slangkop- and Port Nolloth recording station experience similar peaks and drops in annual wave power during its overlapping recording years. For example, both the Slangkop- and Port Nolloth recording station experienced a drop in wave power for 1992 compared to the annual wave power of 1991. This confirms that both stations experience similar wave power conditions although of different magnitudes.

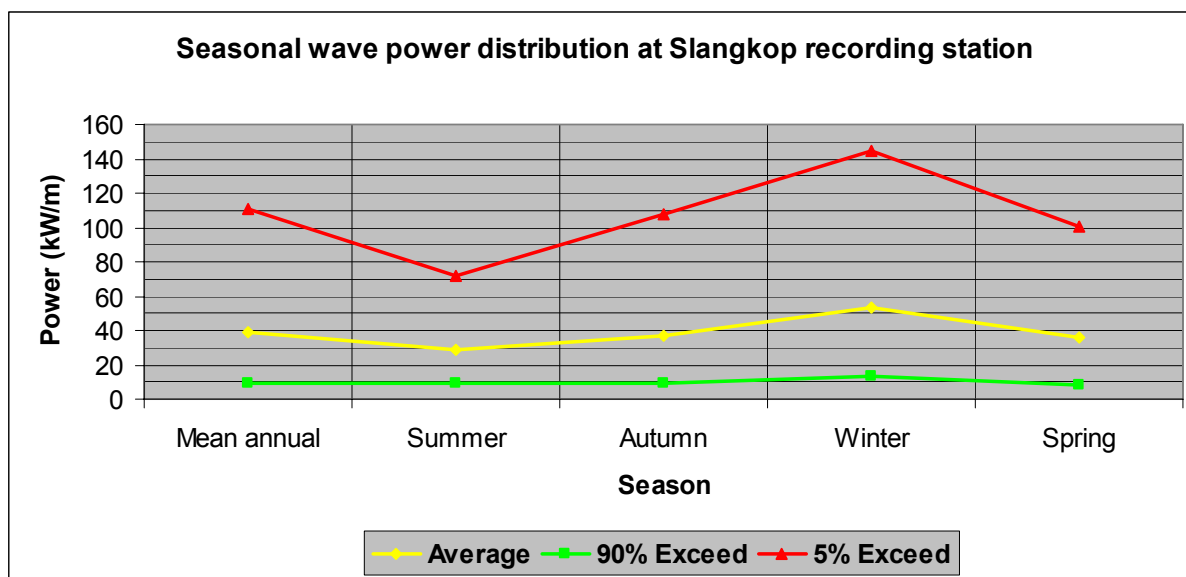


Figure 3-18: Seasonal wave power distribution at Slangkop recording station

Table 3-11: Statistical seasonal parameters of the wave power (kW/m) at Slangkop recording station

Season	Average	90% Exceedance	5% Exceedance
Mean annual	38.7	9.5	110.3
Summer	28.8	8.8	71.8
Autumn	37.2	9.3	108
Winter	52.9	13.1	145.1
Spring	36	8.6	100.1

Figure 3-18 indicates that the maximum and minimum wave power occurs at Slangkop recording station in winter and summer, respectively. Mean annual, autumn and spring have very similar wave power distributions. From a wave energy conversion perspective, a WEC device, deployed in this region, must be able to generate power in periods of low power (summer), survive the storm loadings of the most energetic season (winter) and ideally generate power optimally through the entire year.

3.6.4. Cape Point

Figure 3-19 shows that the Cape Point recording station's mean annual average, -90% and -5% probability of exceedance of wave power is of the same magnitude as Slangkop recording station and also significantly higher than that of Port Nolloth recording station. As

indicated earlier, this comparison is not entirely valid since measurements are from different time periods i.e. do not overlap (see Table 3-2).

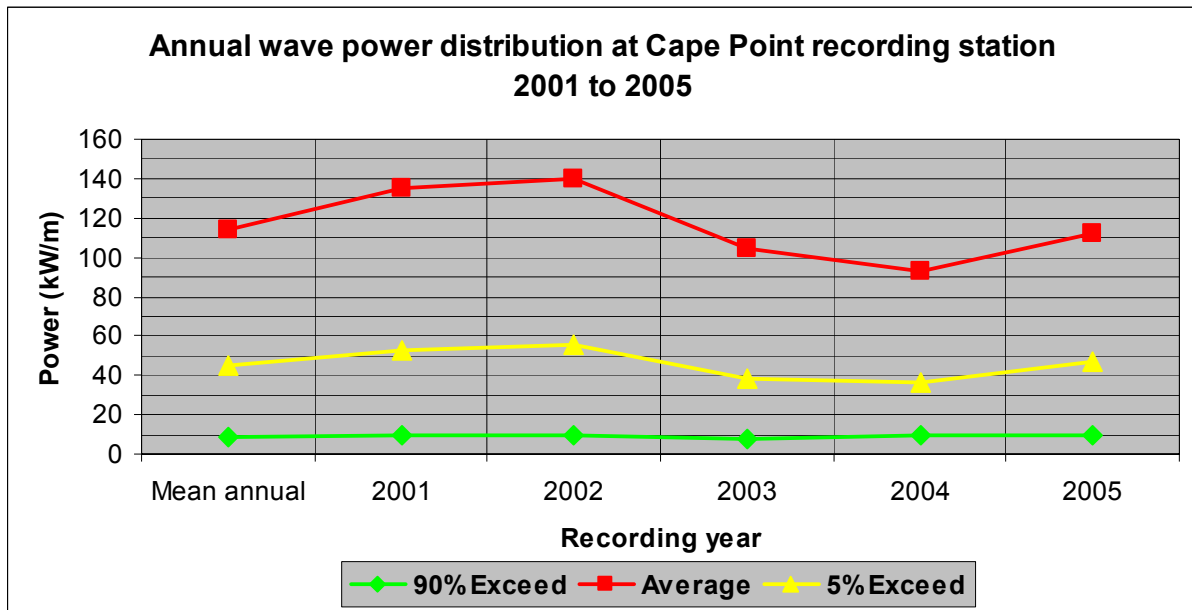


Figure 3-19: Annual- and mean annual wave power at Cape Point recording station

Figure 3-20 and Table 3-12 show that the seasonal distribution of wave power at Cape Point recording station is very similar to that of Slangkop recording station.

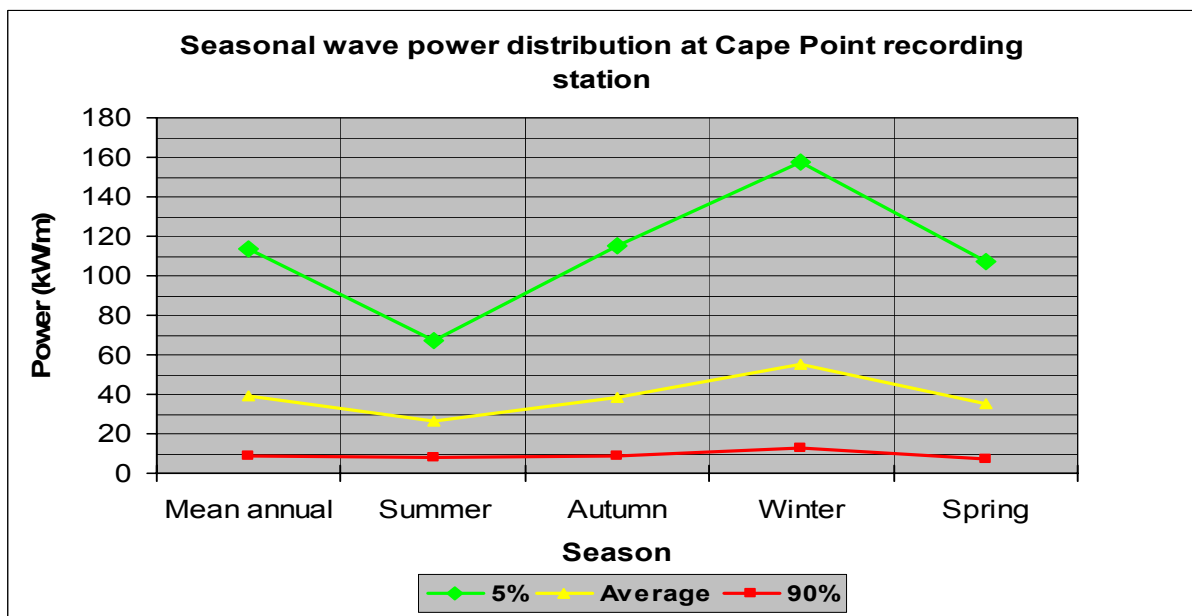


Figure 3-20: Available seasonal wave power at Cape Point recording station

Table 3-12: Statistical seasonal parameters of the wave power (kW/m) at Cape Point (Slangkop recording station indicated in brackets)

Season	Average	90% Exceedance		5% Exceedance	
Mean annual	39.3 (38.7)	9	(9.5)	113.8	(110.3)
Summer	26.3 (28.8)	7.7	(8.8)	67.1	(71.8)
Autumn	38.7 (37.2)	9.1	(9.3)	115.1	(108)
Winter	55.1 (52.9)	13	(13.1)	157.3	(145.1)
Spring	35.6 (36)	7.4	(8.6)	107.1	(100.1)

3.6.5. FA platform

Figure 3-21 below shows that the average wave power at the FA platform is approximately 35kW/m; which is only slightly lower than that of Slangkop and Cape Point.

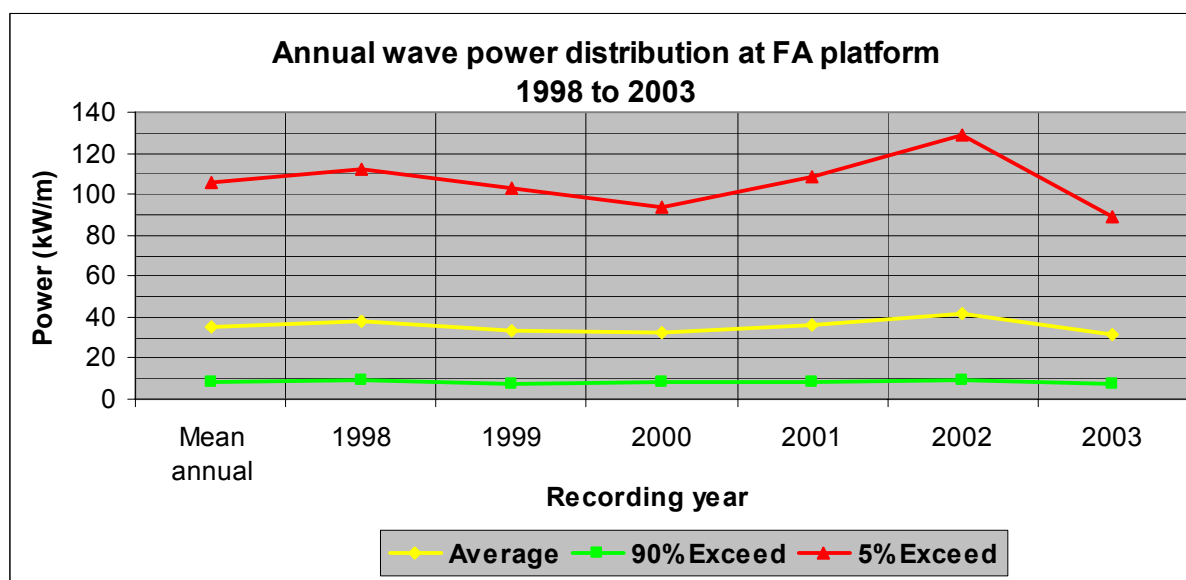


Figure 3-21: Annual- and mean annual wave power at FA platform

Similarly to the comparison drawn between Slangkop- and Port Nolloth recording station a comparison can also be made between Cape Point recording station and FA platform during their overlapping recording period.

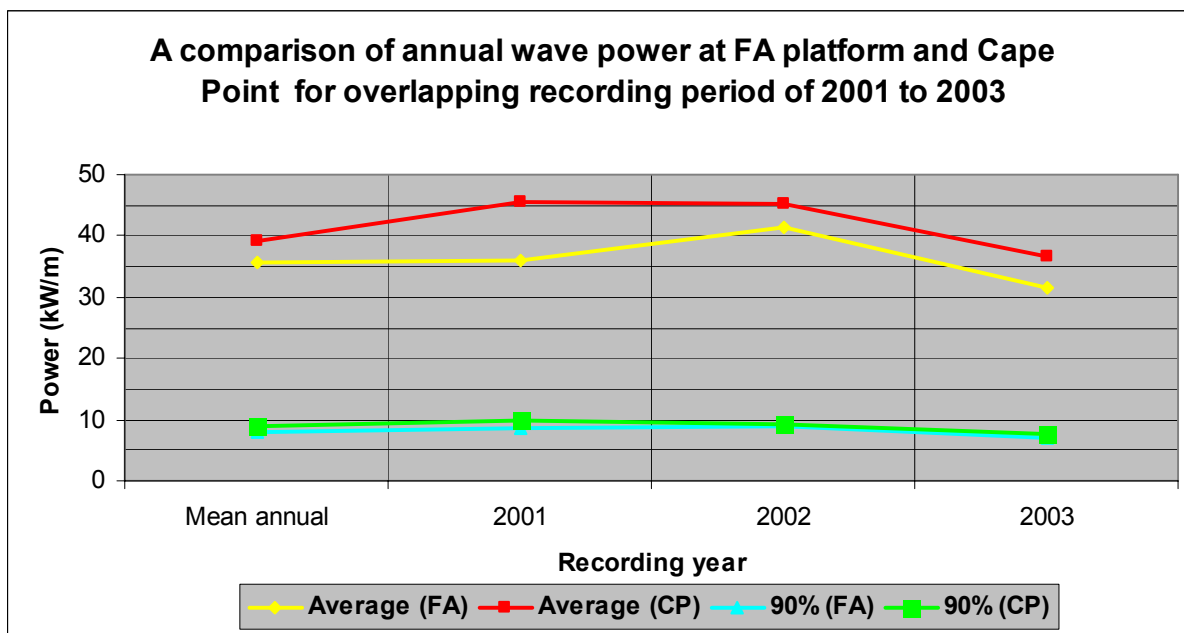


Figure 3-22: A comparison of wave power at Cape Point (CP) and FA platform (FA) during overlapping recording years

Figure 3-22 shows that Cape Point, in general, is exposed to greater wave power than FA platform during the three overlapping recording years considered (this is not expected and could be due a number of reasons as discussed under §3.9.4). The 90% probability of exceedance of the two stations are however very similar. The seasonal fluctuation of wave power at FA platform is demonstrated in Figure 3-23 and Table 3-13 below.

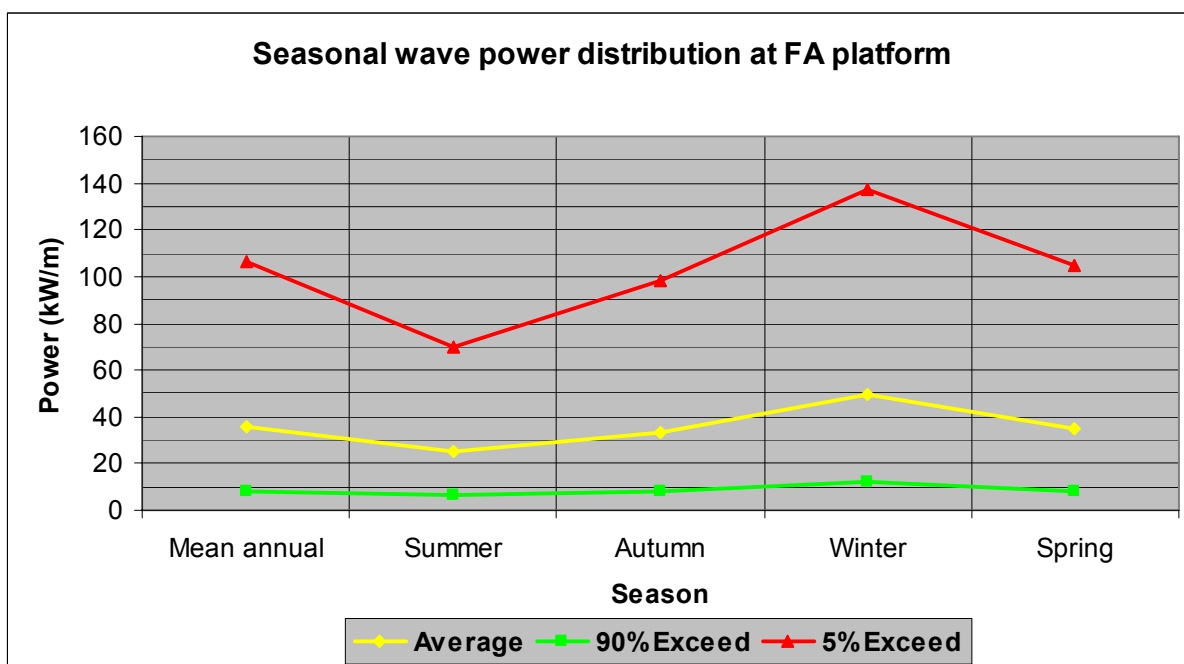


Figure 3-23: Seasonal wave power at FA platform

Table 3-13: Statistical parameters of the wave power (kW/m) at FA platform

Season	Average	90% Exceedance	5% Exceedance
Mean annual	35.6	8.1	106.6
Summer	25.4	6.6	69.7
Autumn	33.1	8.3	98.1
Winter	49.7	11.9	137.3
Spring	34.8	7.8	104.4

The seasonal statistical parameters of wave power of all the wave recording stations analysed thus far are very similar with a maximum in winter, minimum in summer and similar wave power conditions for spring, autumn and for the mean annual record.

3.6.6. Durban

The data obtained from the Durban wave recording station indicates the most variable annual wave power of all the recording stations considered. This is mainly due to the frequent malfunctioning of its Waverider buoy. Statistical parameters derived from incomplete annual records will give unrealistic results.

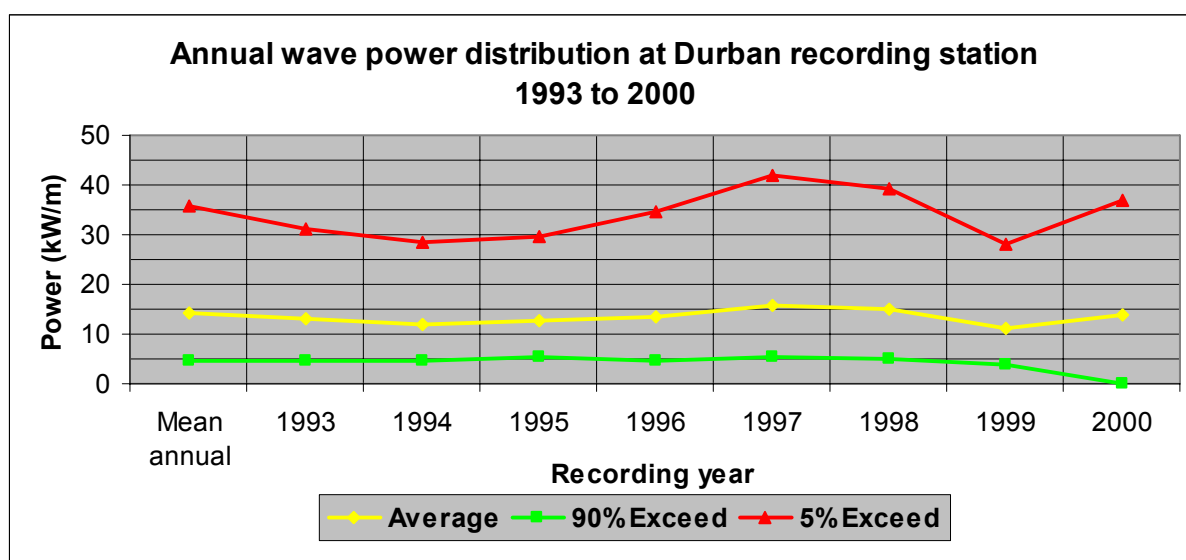


Figure 3-24: Annual- and mean annual wave power at Durban

The seasonal statistical parameters of wave power for Durban differs from that of the other stations with a maximum wave power in autumn followed by spring and then winter. This

could be due to the direct influence of tropical storms or inaccurate measurements in winter months.

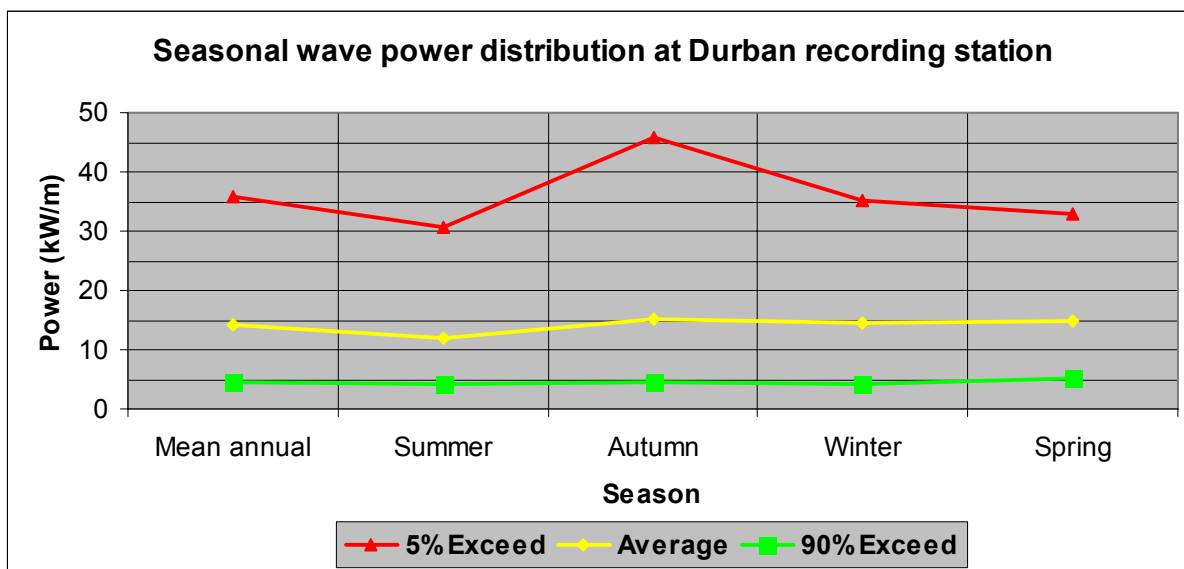


Figure 3-25: Seasonal variability of wave power at Durban recording station

Table 3-14: Statistical parameters of the wave power (kW/m) at Durban recording station

Season	Average	90% Exceedance	5% Exceedance
Mean annual	14.1	4.5	35.8
Summer	11.9	4.1	30.6
Autumn	15.3	4.7	45.9
Winter	14.5	4.1	35
Spring	14.7	5.1	32.8

An analysis of the monthly wave power distribution of all the wave recording stations is presented in Appendix C.

3.7. Wave energy development index (WEDI) = $\frac{\bar{P}}{P_{\max}}$

The wave energy development index (WEDI) is defined by (Hagerman, 2001) as the ratio of average annual wave energy flux to the maximum storm wave energy flux (which represents the energy that any wave power plant platform or hull structure and foundation or mooring would have to absorb and survive during the service life of the power plant). According to (Hagerman, 2001) a lower WEDI reflects a more severe design penalty that has to be paid in terms of capital cost for a wave power plant to harness the annual average wave energy resource available at a particular location. Values of WEDI were determined for all the wave recording stations (see Figure 3-26 and Table 3-15 below).

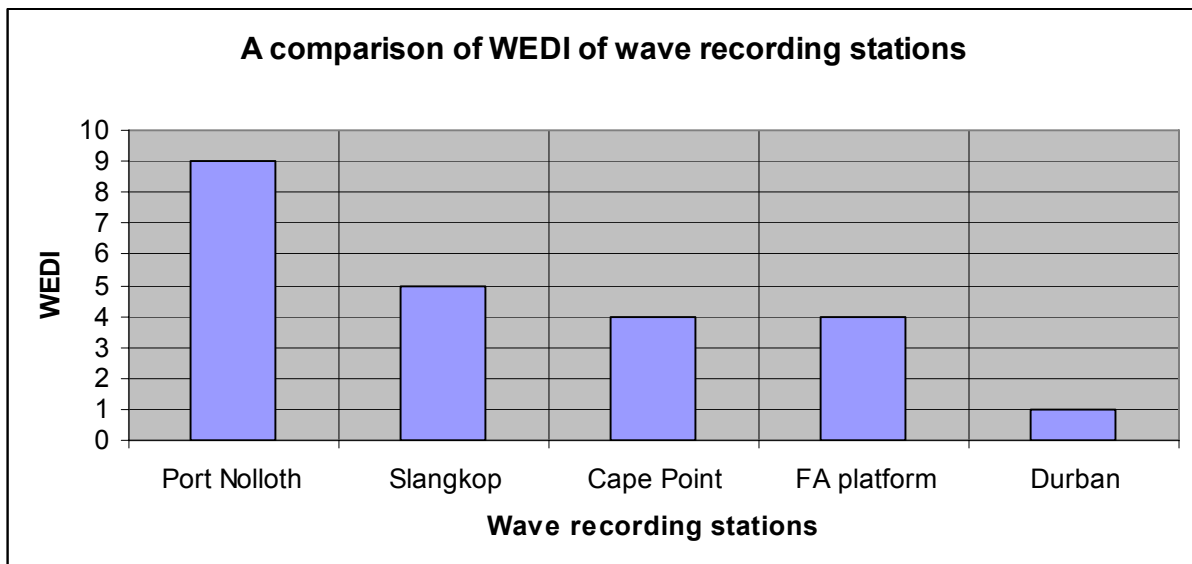


Figure 3-26: A comparison of the WEDI of each station

Table 3-15: WEDI of the various recording stations

Stations	Maximum	Average	WEDI (ave/max*100)
Port Nolloth	295	26	9
Slangkop	776	39	5
Cape Point	1023	39	4
FA platform	970	36	4
Durban	1246	14	1

It is important to note that Port Nolloth-, Cape Point- and Durban recording station all operate at three hourly recording intervals and the stations' WEDI can therefore be directly

compared. Slangkop and FA platform on the other hand, record wave parameters at six and one hourly intervals, respectively. A shorter recording interval (finer recording resolution) increases the probability of recording larger wave heights (e.g. during a storm event). It is therefore expected that the FA platform will record greater maximum storm wave energy flux than Slangkop due to its finer recording resolution. For comparative purposes it is assumed that the wave conditions obtained from the different recording stations are independent of the recording interval.

The bar graph in Figure 3-26 and Table 3-15 show that Port Nolloth has the highest WEDI due to its low storm wave energy flux (three times smaller than that of Cape Point and FA platform). Slangkop has the second highest WEDI due to its high annual average wave power. The WEDI values of the South African wave recording stations are significantly larger than that of near shore locations on the North American east coast (WEDI = 1.8 to 2.5, Hagerman 2001).

From this WEDI analysis in this thesis, the South West- and West coast of South Africa are identified as the coastal regions most favorable for wave energy conversion and the Natal coast in the Durban region the less favorable.

3.8. Probability of exceedance- and frequency of occurrence of wave power

3.8.1. Introduction

The previous section demonstrated the annual and seasonal variability of wave power at each recording station. This section deals with the probability of exceedance of different wave power levels and also with the frequency of occurrence of wave power values within specified ranges. Both these statistical parameters present an indication of the seasonal wave power distribution at each wave recording station.

The upper limit of 100 kW/m was used since a relative small percentage of power occurs above this value for all the recording stations considered. Since the bulk of the wave power at the recording stations occurs below 100 kW/m, the results of this analysis present the bulk of available power and can be of assistance in the selection of optimal locations for different WEC units.

A similar study of the exceedance and occurrence statistics of wave power of various recording stations was done in the 1980's (Geustyn, 1983) with the wave data available at the time. A significant amount of additional wave data became available since 1983 and the analysis presented in this report was done with a larger data base and serves therefore as an update of the above referred study.

3.8.2. Port Nolloth

As expected, the probability of exceedance of wave power at Port Nolloth is significantly higher in winter than in summer as presented in Figure 3-27 and Figure 3-28.

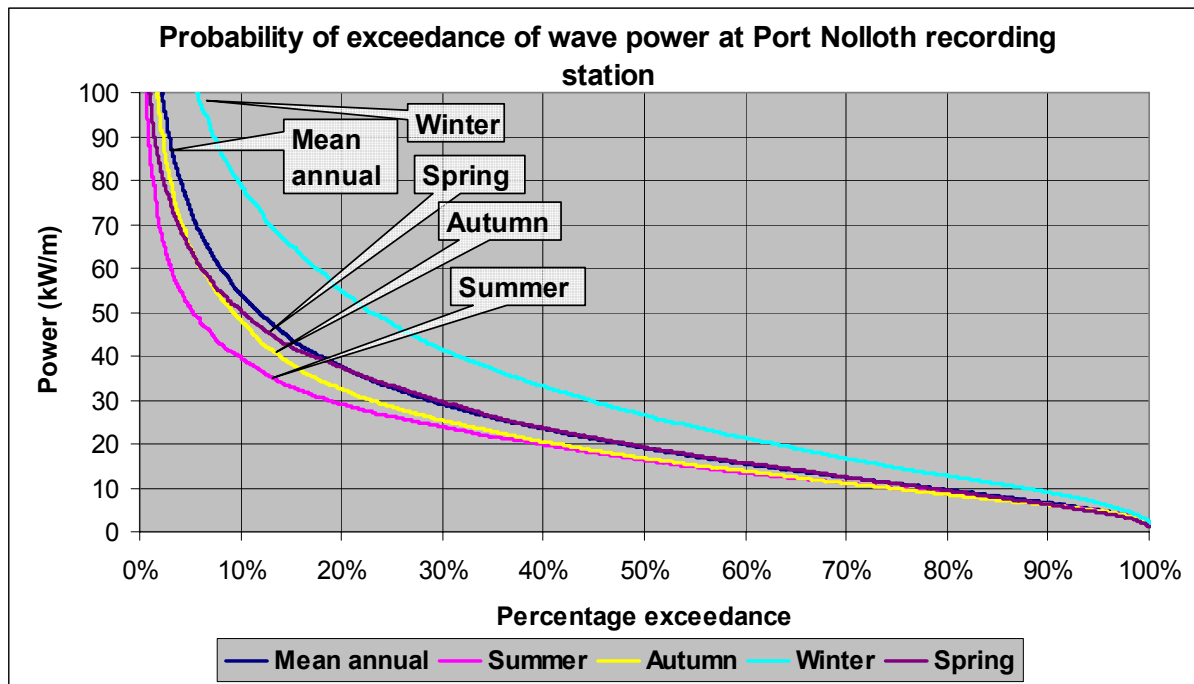


Figure 3-27: Probability of exceedance of different power levels at Port Nolloth recording station

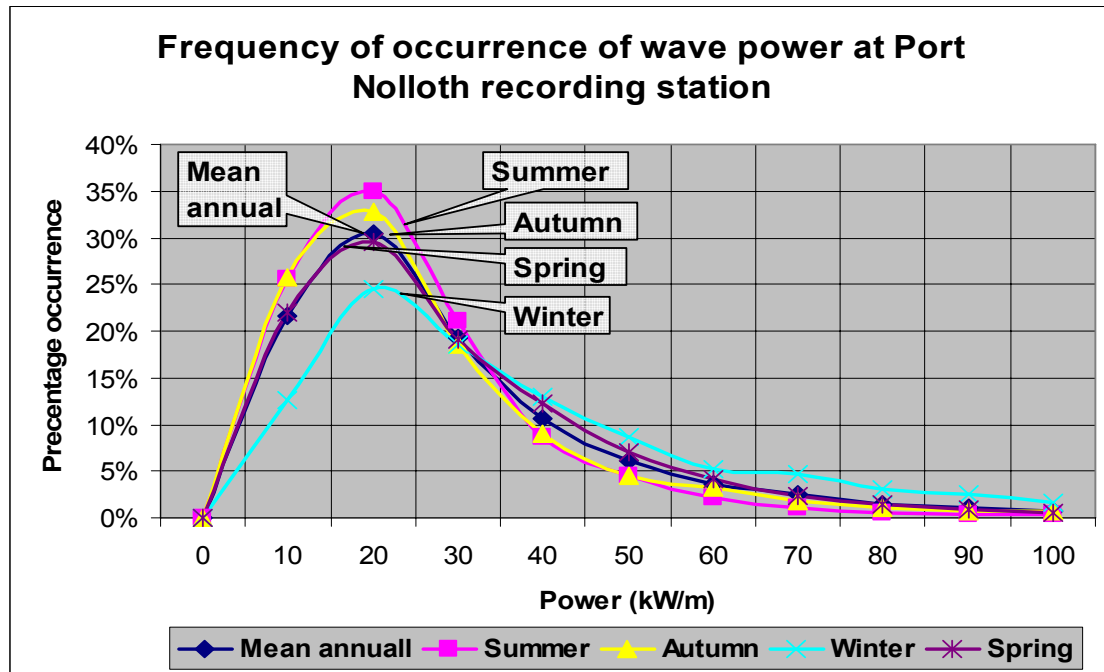


Figure 3-28: Frequency of occurrence of different power levels at Port Nolloth recording station

The frequency of occurrence curves in Figure 3-28 indicate that summer has the highest peak over the narrowest range of wave power values. Therefore low wave power values occur more frequently in summer than in winter, as expected.

3.8.3. Slangkop

The envelope of exceedance curves in Figure 3-29 for Slangkop recording station has the winter curve as the upper limit and the summer curve as the lower limit. The remaining three curves of mean annual, spring and autumn are all very similar. The large difference between the winter curve and the other seasonal curves indicates why the WEDI value of Slangkop is considerably lower than that of Port Nolloth recording station (see Figure 3-26). Survivability of a WEC unit deployed in the Slangkop area during the severe exposure of the winter months is therefore a very important design consideration.

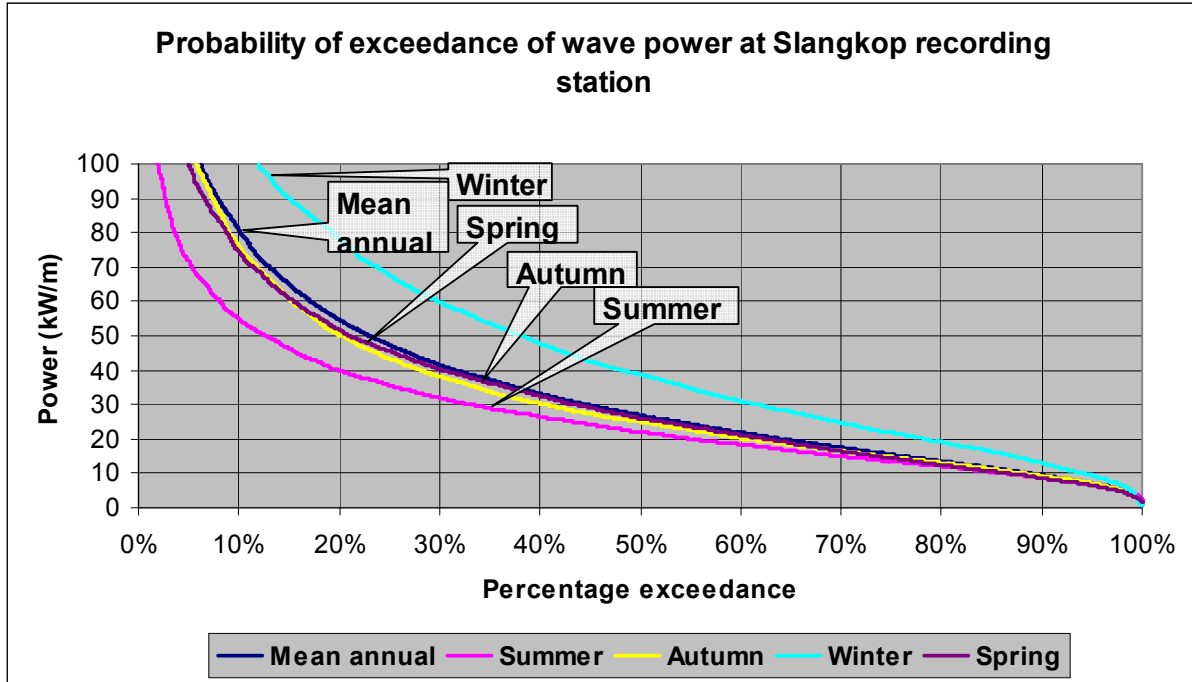


Figure 3-29: Probability of exceedance of different power levels at Slangkop recording station

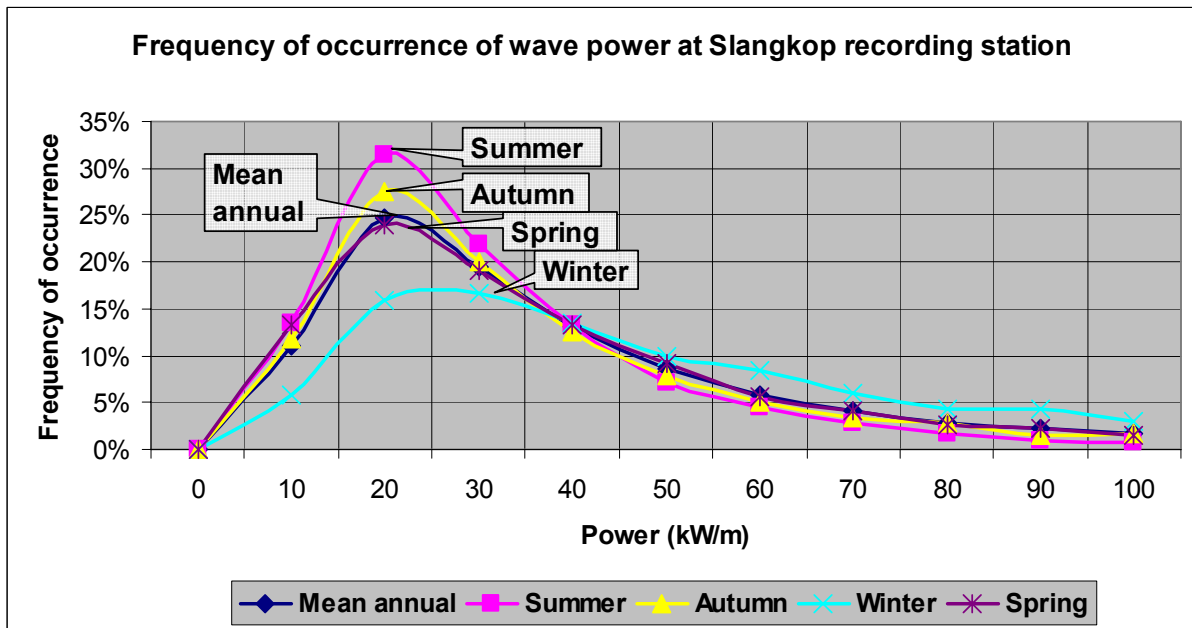


Figure 3-30: Frequency of occurrence of different power levels at Slangkop recording station

The frequency of occurrence curves in Figure 3-30 indicate a peaked summer curve and a winter curve that is well distributed over a range of wave power values. This is an

indication that high wave power conditions occur frequently in winter at Slangkop recording station.

3.8.4. Cape Point

The probability of exceedance curves of Cape Point recording station, presented in Figure 3-31 and Figure 3-32, are very similar to that of Slangkop recording station.

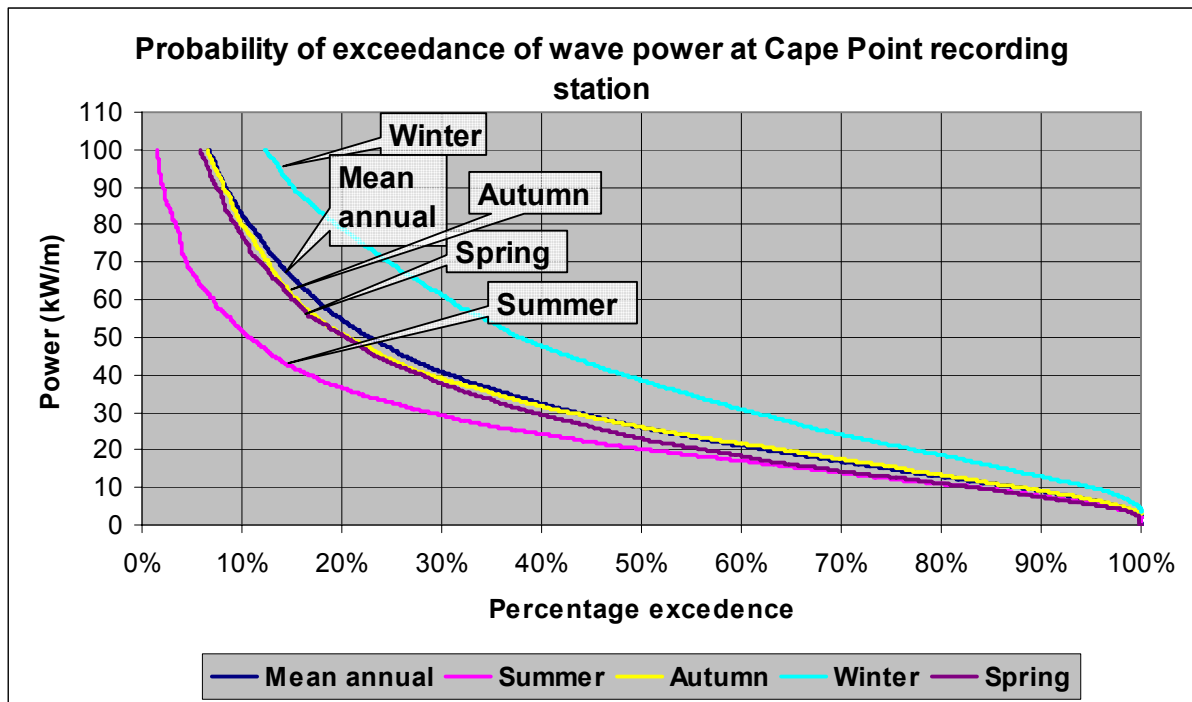


Figure 3-31: Probability of exceedance of different power levels at Cape Point recording station

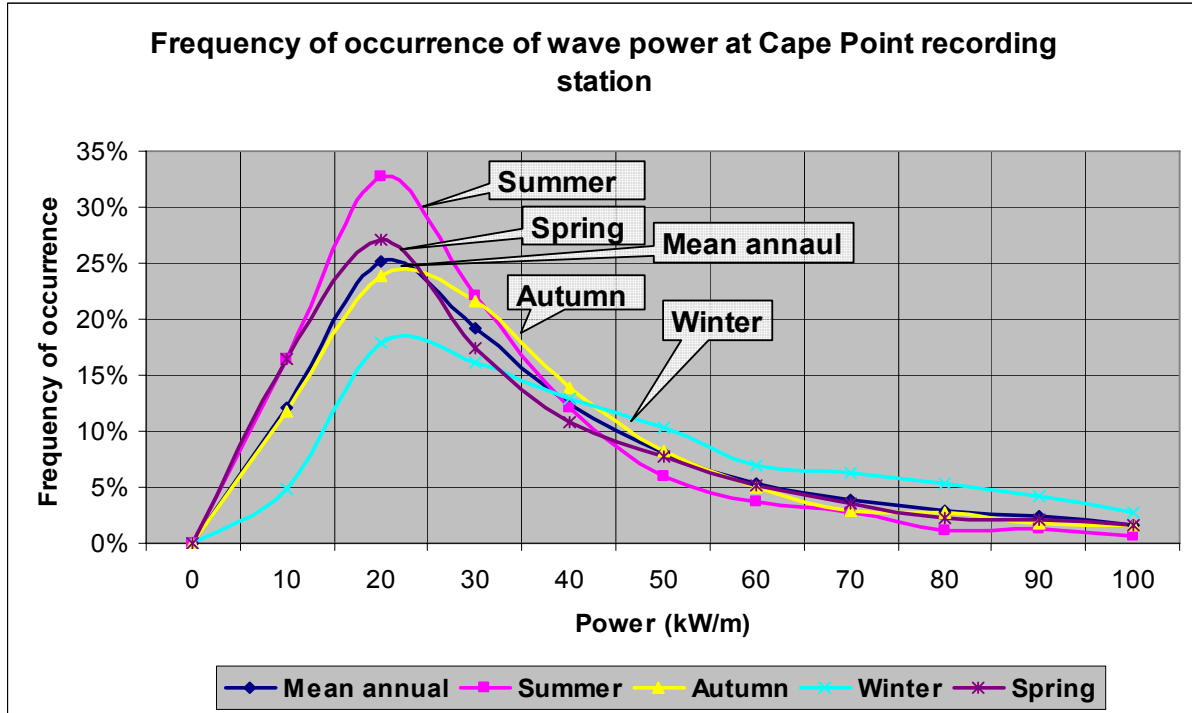


Figure 3-32: Frequency of occurrence of different power levels at Cape Point recording station

3.8.5. FA platform

The probability of exceedance- and frequency of occurrence of wave power at FA platform are presented in Figure 3-33 and Figure 3-34 below.

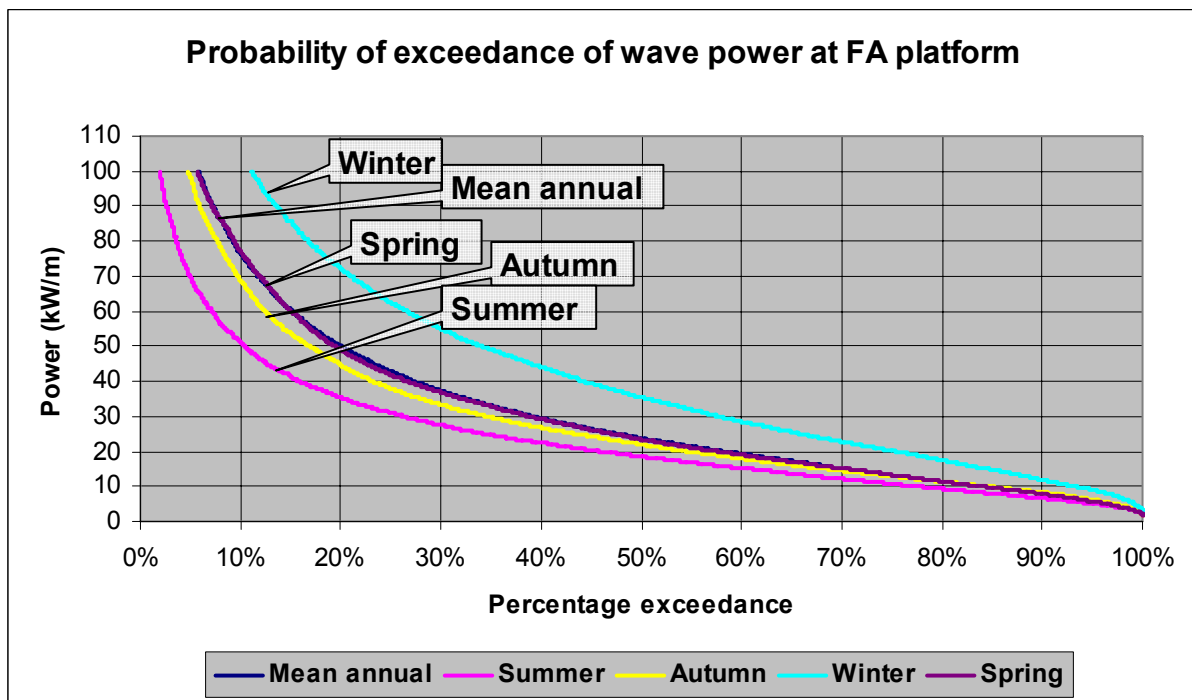


Figure 3-33: Probability of exceedance of different power levels at the FA platform

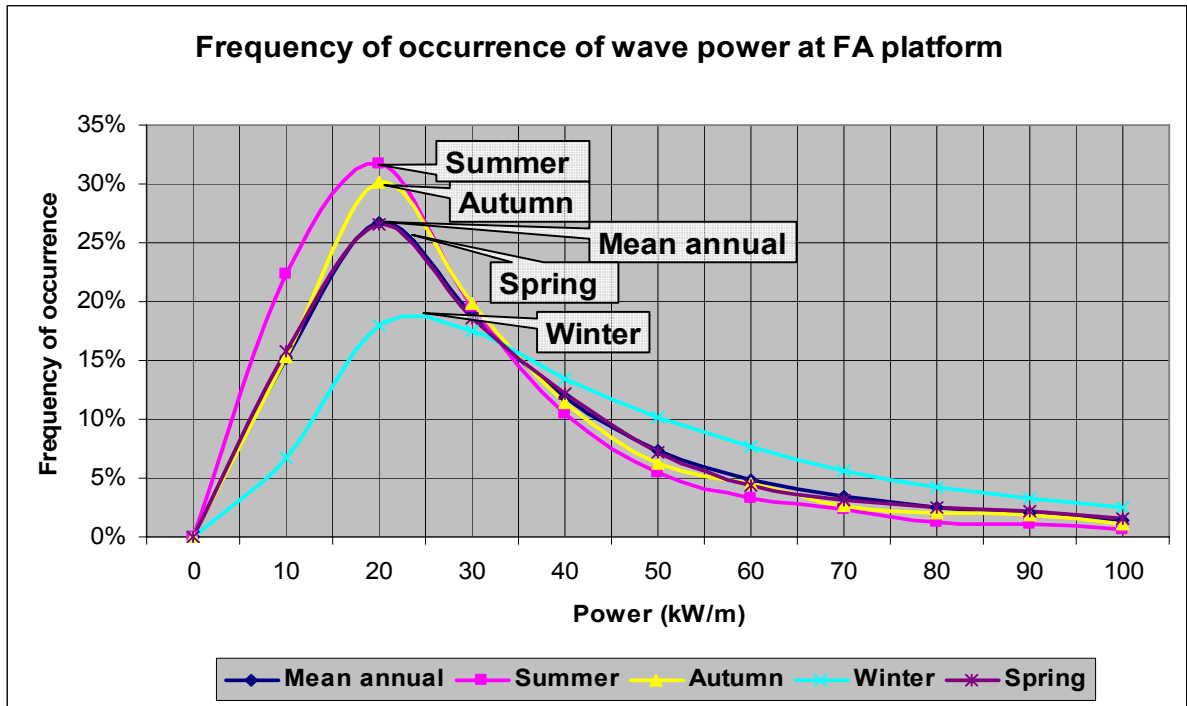


Figure 3-34: Frequency of occurrence of different power levels at FA platform

3.8.6. Durban

Figure 3-35 and Figure 3-36 below indicate a much lower wave power distribution at Durban compared to the other recording stations considered.

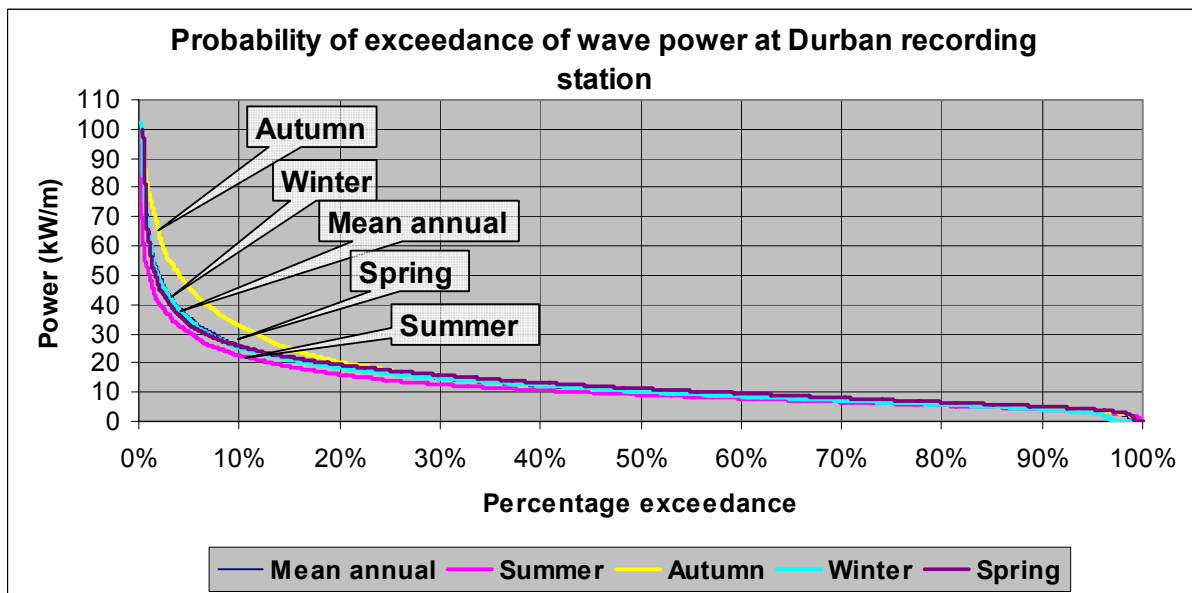


Figure 3-35: Probability of exceedance of different power levels at the Durban recording station

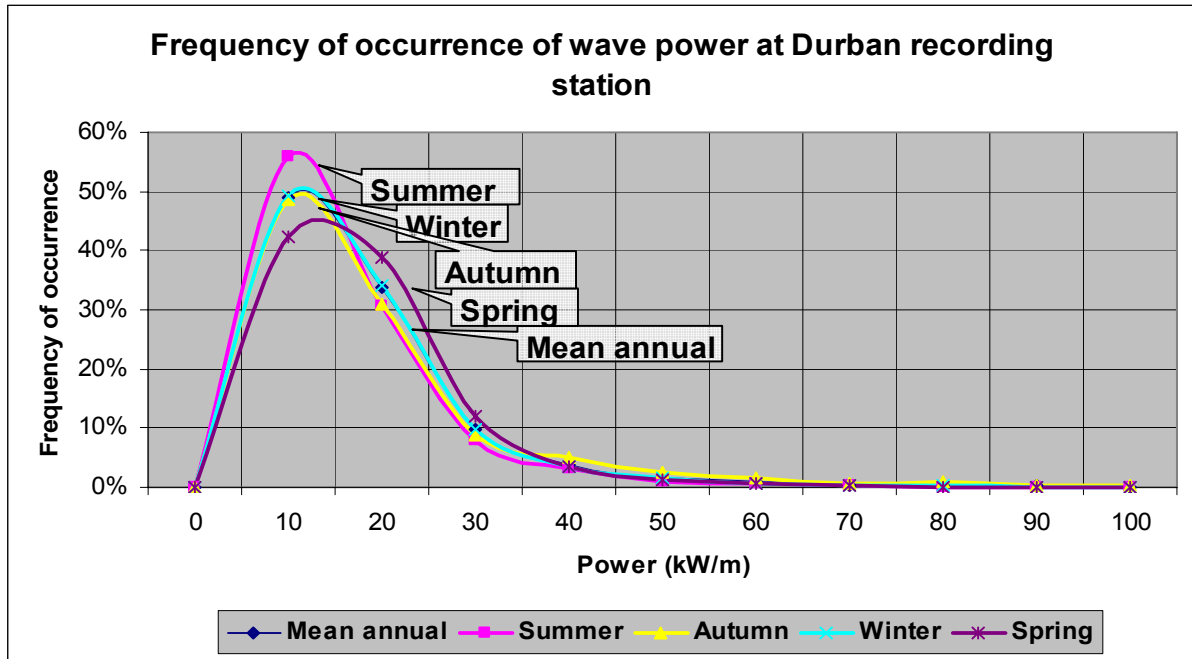


Figure 3-36: Frequency of occurrence of different power levels at Durban

3.9. Wave energy scatter diagrams

A wave energy scatter diagram is a surface, contour graph showing the frequency of occurrence and concurrent wave power of combinations of H_s and T_p values. From a scatter diagram the most dominant H_s and T_p combinations can be identified. This information is important in the establishment of the efficiency in power extraction of WEC units. The power extraction efficiency of WEC units can be predetermined by comparing the dominate wave conditions and consequent available wave power resource to the performance curves of WEC units. In order to produce a scatter diagram the following procedure was followed for each recording station's wave data:

- a) Determination of the number of concurrent H_s and T_p records.
- b) Conversion of occurrence to an equivalent number of hours per year
- c) Determination of the amount of power generated by each concurrent H_s and T_p value.
- d) Determination of the available mean annual wave energy (kWhr/m) per year per H_s , T_p bin (pre-selected H_s and T_p ranges).

The wave energy scatter analysis procedure is based on an E2I EPRI report (Bedard and Hagerman, 2003). The wave energy scatter diagrams for each wave recording station are presented below.

3.9.1. Port Nolloth

The wave energy scatter diagram for Port Nolloth recording station in Figure 3-37 indicates that the most frequent and powerful T_p , H_s values range from 12 to 14s and 2 to 3m, respectively. The latter wave condition range produces total energy of approximately 17MWhr/m/yr.

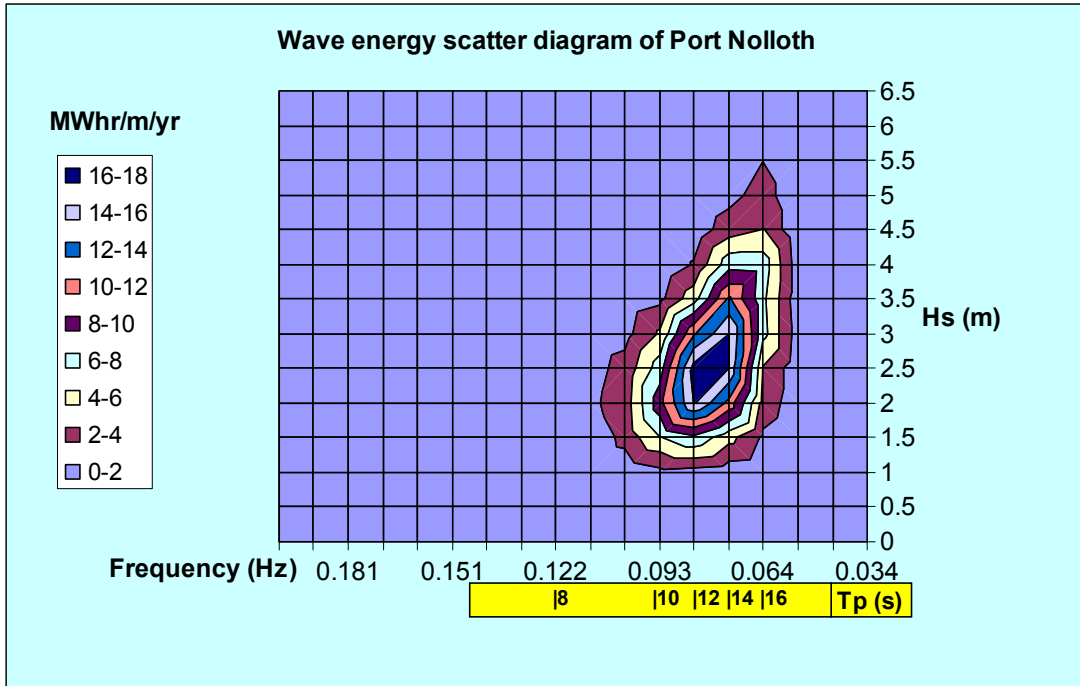


Figure 3-37: Wave energy scatter diagram at Port Nolloth recording station

3.9.2. Slangkop

Similarly to Port Nolloth recording station, Slangkop’s most dominant T_p values range from 12 to 14s (refer to §3.9.1). The associated peak energy is 18 to 20MWhr/m/yr. This is higher than the peak energy of Port Nolloth, due to the fact that the dominant T_p values occur more frequently and the dominant H_s values are larger and range from 2.5 to 3.5m.

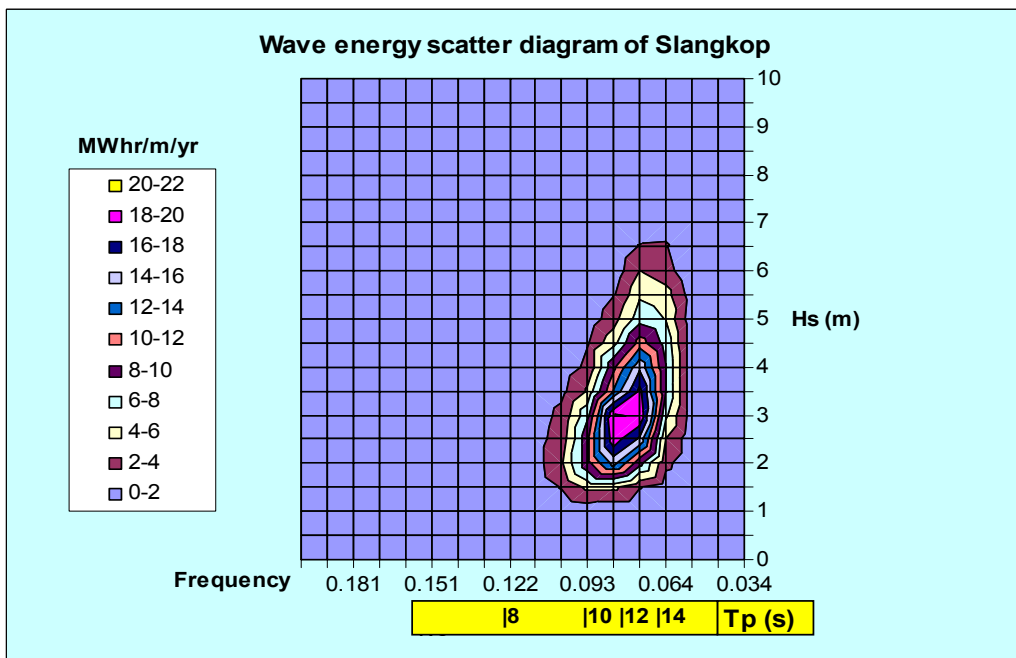


Figure 3-38: Wave energy scatter diagram at Slangkop recording station

3.9.3. Cape Point

The wave energy scatter diagram of Cape Point recording station indicates that the peak power occurs for T_p equal to 12s and H_s equal to 2.5m. Cape Point's peak energy is slightly higher than that of Slangkop and ranges from 20 to 22 MWhr/m/yr.

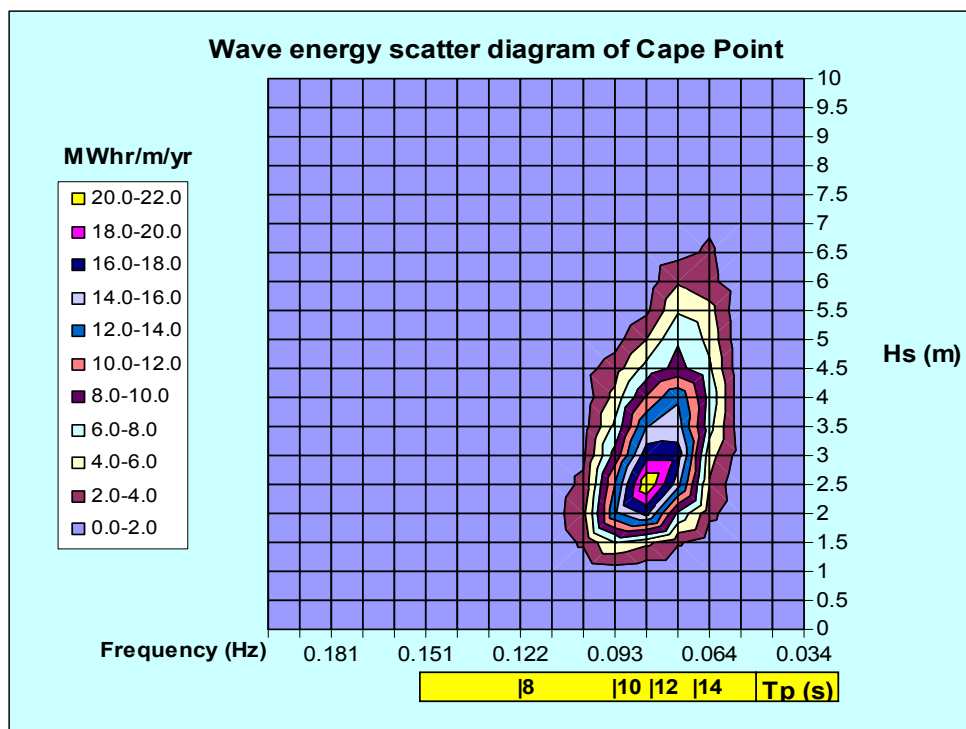


Figure 3-39: Wave energy scatter at Cape Point

3.9.4. FA platform

The wave energy scatter diagram of FA platform shows that the dominant T_p value is lower than that of the other stations and ranges between 9 and 10s (see § 3.3.2 for T_p analysis of recording stations). These lower apparent T_p values, in combination with H_s values, produces less power than the higher T_p and H_s combinations of Slangkop and Cape Point. This difference in wave power for each T_p and H_s combination accumulates and produce apparent lower wave energy scatter at the platform. This is the reason why the peak wave energy at the platform is only a relatively small 10 to 12 MWhr/m/yr even though the average wave power of the platform is of similar magnitude to that Slangkop- and Cape Point recording station.

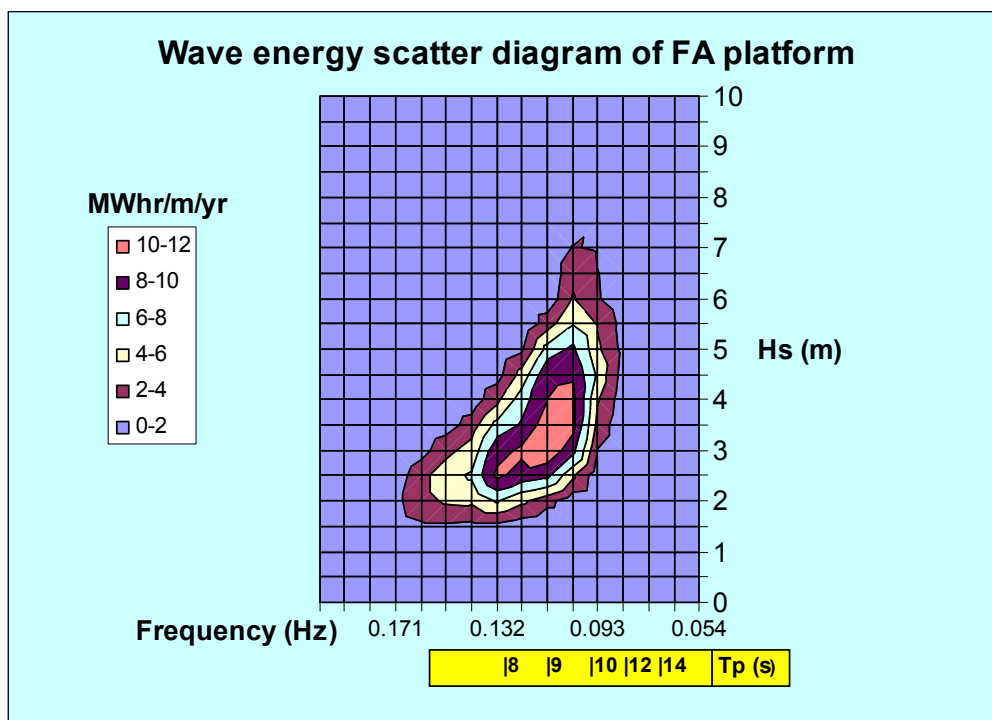


Figure 3-40: Wave power scatter at FA platform

Possible reasons for the lower apparent T_p values and consequent lower scatter energy distribution at the platform are presented below.

- i. The shortest fetch surrounding the FA platform is 72.5km. This implies that, unlike the other wave recording stations exposed at 180° due to their close proximity to shore, the platform is exposed to multidirectional locally generated wind- and wave fields. Locally generated wave fields are short period waves still being created by winds (also known as seas, CEM 2002). The platform's lower dominant wave period conditions can therefore be ascribed to the platform's frequent exposure to short period seas. The platform is also exposed to waves propagating out of the generating area (swell). Swell-sea interaction and its influence on the wave energy density spectrum measured at the platform are demonstrated in Figure 3-41 below. Deriving a value of T_p from the dual peaked spectrum, shown in the bottom left corner of Figure 3-41, would therefore not be entirely representative of the combined swell-sea conditions at the platform.

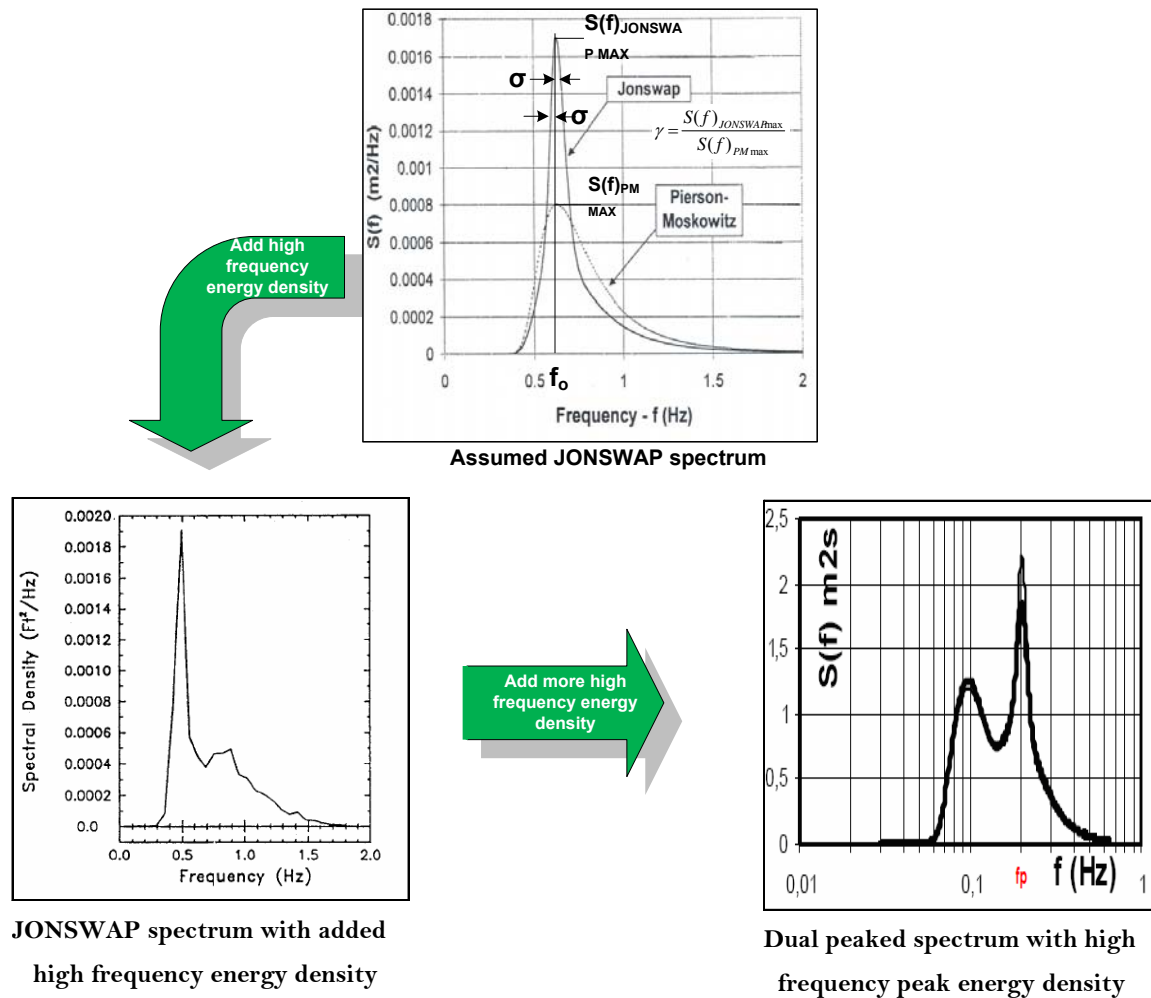


Figure 3-41: High frequency spectrum development

- ii. The FA platform and the Durban recording station are the only two stations exposed to waves generated by cut-off low pressure systems on the east coast and to a lesser extent to tropical storms in the north east. The platform's dual exposure to swells from the dominant south west and from the east will therefore also influence the actual measured spectrum. Examples of the platform's dual wave field exposure are presented in Figure 3-42 and Figure 3-43 below.

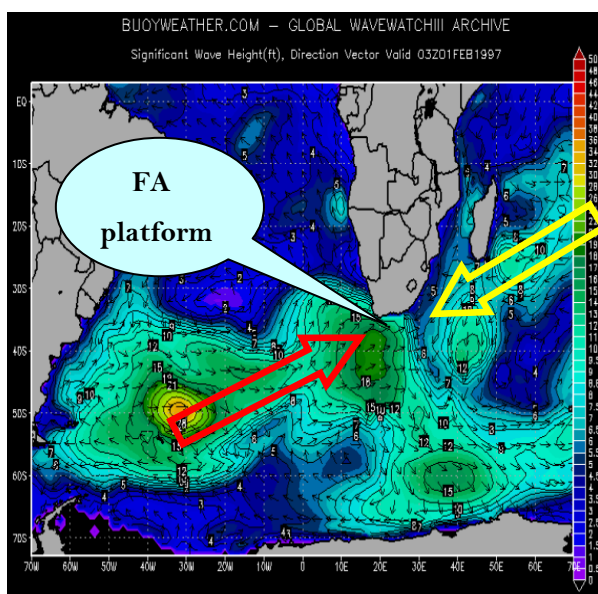


Figure 3-42: Wave exposure from opposing directions at the platform (www.buoyweather.com, 01/02/1997)

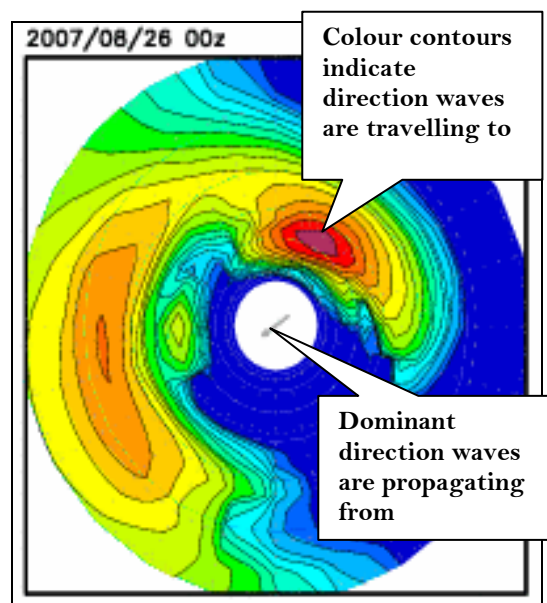


Figure 3-43: Dual directional exposure at the FA platform (http://polar.ncep.noaa.gov/waves/main_t_ext.html, 26/08/2007)

- iii. In § 3.3.2 it was mentioned that a relationship was assumed between T_z and T_p . This assumption will become inaccurate whenever the measured wave spectrum deviates from the Bretschneider spectrum.
- iv. A big difference between the platform and the other recording stations is the fact that the platform uses radar to measure wave conditions as opposed to Waverider buoys. The radar is mounted below the platform and records water surface level variations. The radar will therefore better capture short period conditions compared to the buoy type recording devices.
- v. North flowing return currents (splitting of the south going Agulhas current) could reduced the apparent wave periods of the dominantly south westerly waves at the FA platform (located on the continental shelf near the main Agulhas current).

3.9.5. Durban

The wave energy scatter diagram of Durban indicates a very low wave power distribution. Conclusions drawn from the Durban data set is questionable due to certain discrepancies within the data set. An example of such a discrepancy is presented below:

The maximum value of the Durban data set was recorded on 17 November 2000. On this day, H_s increased from 1.4 to 9.3m and T_p increased from 8 to 28 within three hours. It is not possible to study the build up to this severe storm, because the buoy was not operational before and after this event. This could be due to a tropical cyclone, but there is no evidence of such an event occurring at the FA platform during the corresponding period.

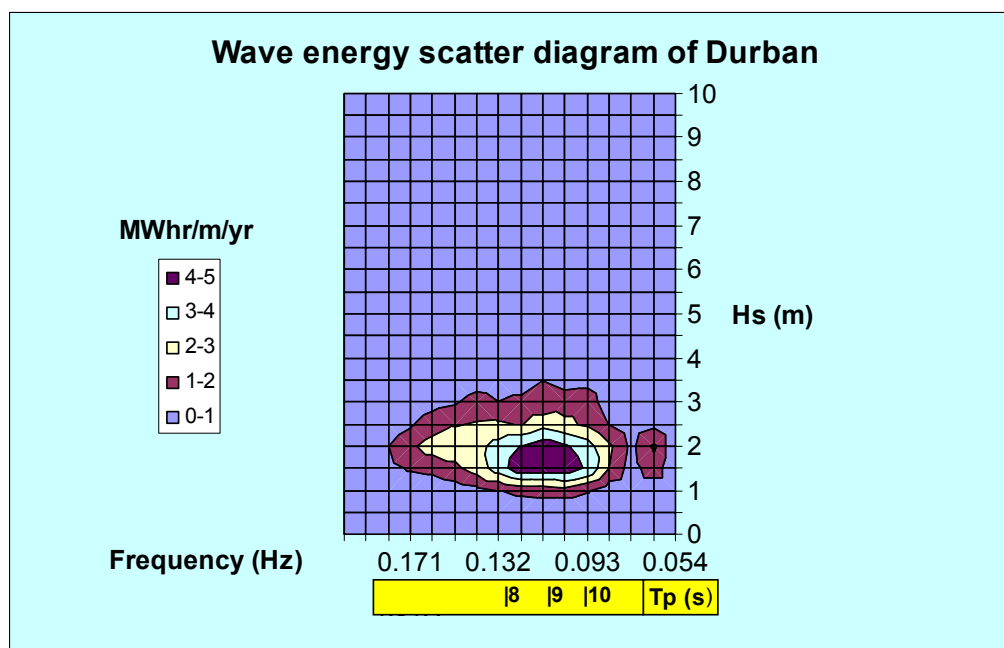


Figure 3-44: Wave energy scatter at Durban

3.10. Summary and conclusions of recorded wave data analysis

3.10.1. Summary

A brief summary of the results of the recorded wave data analysis is presented below.

3.10.1.1. Port Nolloth

- i. The wave period distribution at Port Nolloth recording station is favorable, from a wave power perspective, with a dominant T_p value of 12s.
- ii. The wave height and -power analysis indicated that Port Nolloth recording station is exposed to an energetic wave regime, but wave power does decrease in magnitude with increasing distance from the storm generation zone in the southern seas.
- iii. The WEDI of Port Nolloth recording station ($WEDI = 9$) was the highest of all the wave recording stations analysed. This indicates that

less capital investment is required to ensure the survivability of a wave power plant in the Port Nolloth region while harnessing the average annual wave power compared to, for example, Cape Point (WEDI = 4).

3.10.1.2. Slangkop

- i. Similarly to Port Nolloth, the wave period analysis of Slangkop recording station indicated a dominant T_p value of 12s.
- ii. The wave height and -power analysis indicated that Slangkop station is exposed to high levels of wave power. This implies Slangkop station has a favorable wave power resource for power generation, but WEC units deployed in the region would require the functionality to detune in case of extreme loadings during storm events to ensure survivability.
- iii. The Slangkop station had the second highest WEDI value due to its high average wave power of 39kW/m.

3.10.1.3. Cape Point

- i. The wave period, -height and -power distributions of Cape Point recording station is very similar to that of Slangkop, because of the stations' close proximity. The wave power distribution at Cape Point is slightly higher than Slangkop, but no overlapping of recording periods exist to directly compare data.

3.10.1.4. FA platform

- i. The wave period distribution at the platform was considerable lower than that of the more western stations due to mechanism discussed in §3.9.4 . This greatly influenced the platform's wave energy scatter distribution.
- ii. The wave height conditions at the platform were similar and slightly higher than that of Slangkop and Cape Point.
- iii. The wave energy distribution at the platform, as determined in the scatter analysis, was considerably lower than that of the Slangkop and Cape Point due to reasons discussed in § 3.9.4. The platform's multi-directional exposure could benefit point absorber type WEC units. WEC units designed to optimally generate power through maximum relative motion in short period conditions are well suited to the prevailing conditions at the platform.

3.10.1.5. Durban

- i. The analysis of the Durban data indicated a severe reduction in wave power compared to the other stations. This could be ascribed to the sheltering of Durban from swell propagating from the dominant south westerly direction.
- ii. The intermittent recordings of the Durban data set make any conclusions based on the analysed data questionable.

3.10.1.6. Comparison of wave power distribution at all recording stations

Figure 3-45 below presents statistical parameters of wave power for the mean annual record of each wave recording station. The figure indicates that the two southwesterly recording stations have the highest wave power resource followed by the FA platform. The average wave power of these three stations is approximately 40kW/m. The west coast station of Port Nolloth and the east coast station of Durban have an average wave power of approximately 23 and 18 kW/m respectively.

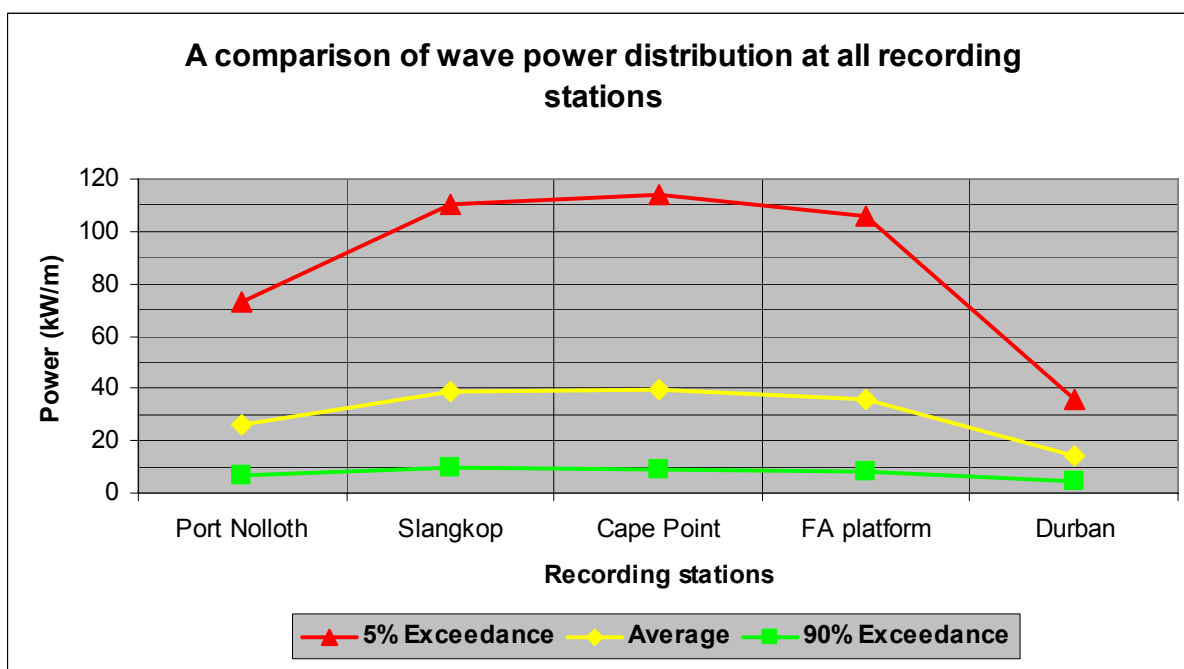


Figure 3-45: A comparison of statistical parameters of wave power of all stations

The average and 5% and 90% exceedance levels of wave power at all the wave recording stations is shown in Figure 3-46 below. The wave power curves for Cape Point- and Slangkop recording station are very similar which implies that these two stations experience similar wave power conditions. The wave power at FA platform is slightly less than that of Cape Point and Slangkop.

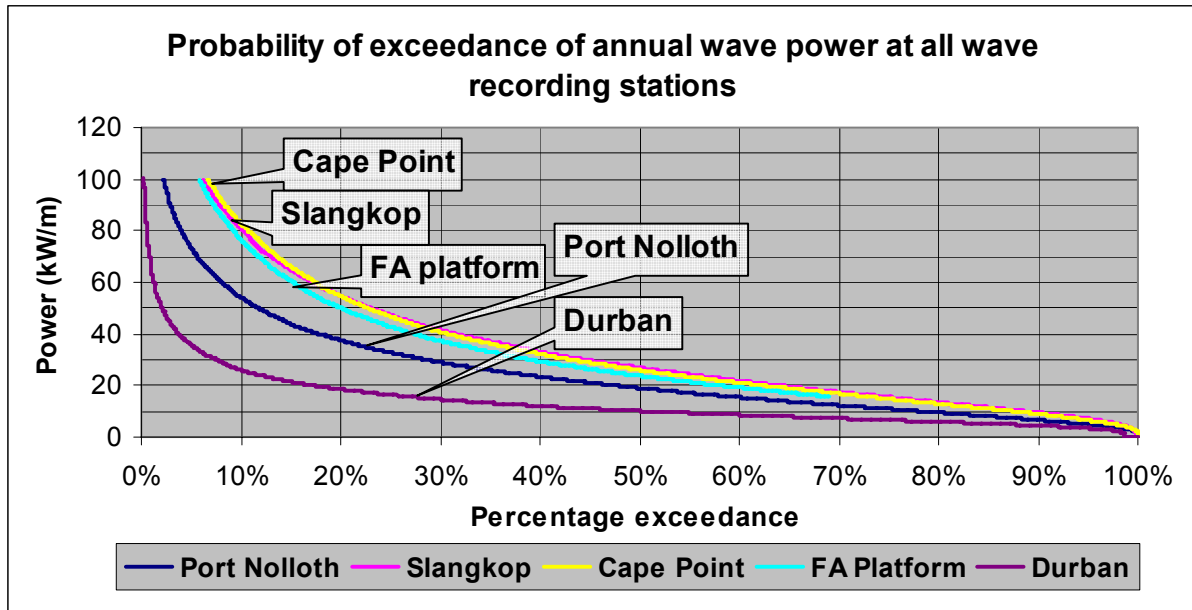


Figure 3-46: Probability of exceedance comparison of all stations

Figure 3-47 below presents the frequency of occurrence of wave power at all the wave recording stations. The frequency of occurrence analysis again confirms similar wave power conditions at Slangkop, Cape Point and FA platform.

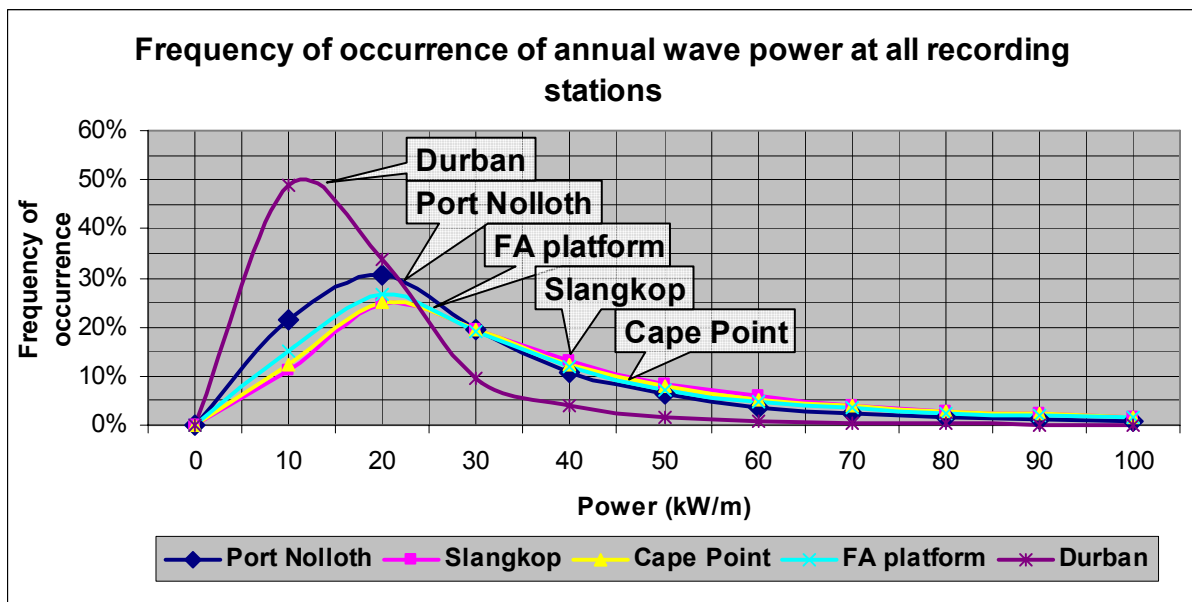


Figure 3-47: Frequency of occurrence comparison of all stations

3.10.2. Conclusions

Considering the findings of this analysis, as outlined in the previous section, the following conclusions can be drawn:

- The two southwesterly wave recording stations of Cape Point and Slangkop have the largest wave power resource, due to its close proximity to the storm generation area in the Southern Atlantic Ocean.
- The magnitude of wave power at FA platform is slightly less than that of Cape Point and Slangkop.
- From the WEDI analysis, Port Nolloth was identified as the most favorable (of all the wave recording stations analysed) for wave power generation due to its moderate average wave power and relatively low storm wave energy flux.
- The wave power resource of the east coast and the Durban recording station is relatively low with an average wave power of approximately 14kW/m.

The identification of the South African coastal region with the largest wave power resource, i.e. the South West Coast, serves as the achievement of the objective of this portion of the study. A detailed description of the wave power resource of this region is presented in the following chapter.

4. SPATIAL WAVE POWER DISTRIBUTION ON THE SOUTH AFRICAN SOUTHWEST COAST BASED ON HINDCAST DATA

4.1. Introduction

The results of the measured wave data analysis, presented in Chapter 3, provide a general description of the wave power conditions at locations with available wave data. From the analysis it was found that the South West coast has the greatest wave power resource. The analysis of the wave data recorded at the wave recording stations of Slangkop and Cape Point is an indication of the expected wave power exposure of the South West coastal region. In order to identify locations suited for wave energy conversion a detailed description of the spatial wave power distribution of the whole area is required.

This objective is achieved through the numerical simulation of ocean wave propagation over the above mentioned coastal region. In order to simulate wave transformation from deep water (offshore) to near-shore, deep sea wave data is required as input into the numerical model. The deep sea input wave data must be at sufficiently deep water depths at which little or no wave-bottom interaction occurs. The Slangkop and Cape Point recording stations are situated near-shore and its wave data is therefore not considered to be ideally suitable. Global wave models, on the other hand, describe wave conditions at deep sea locations over the entire globe. Historic output of global wave models (which are normally validated and adjusted if necessary), is known as hindcast wave data and is used in the numerical simulation application of this study. The advantages of hindcast wave data are presented below:

- Freely available (<http://www.ncep.noaa.gov/>)
- 100% coverage over a 10 year recording period (three hourly recording intervals)
- Wave data is offshore in sufficiently deep water depths
- Data includes peak wave direction (wave recording stations on the South African coast which data was analysed in Chapter 3, are non-directional recorders)
- Data is validated

This investigation quantifies the wave power resource of Cape Point to Elands Bay and is the focus area of this part of the study. Figure 4-1 below presents the objective, planned methodology and the desired output of this part of the study.

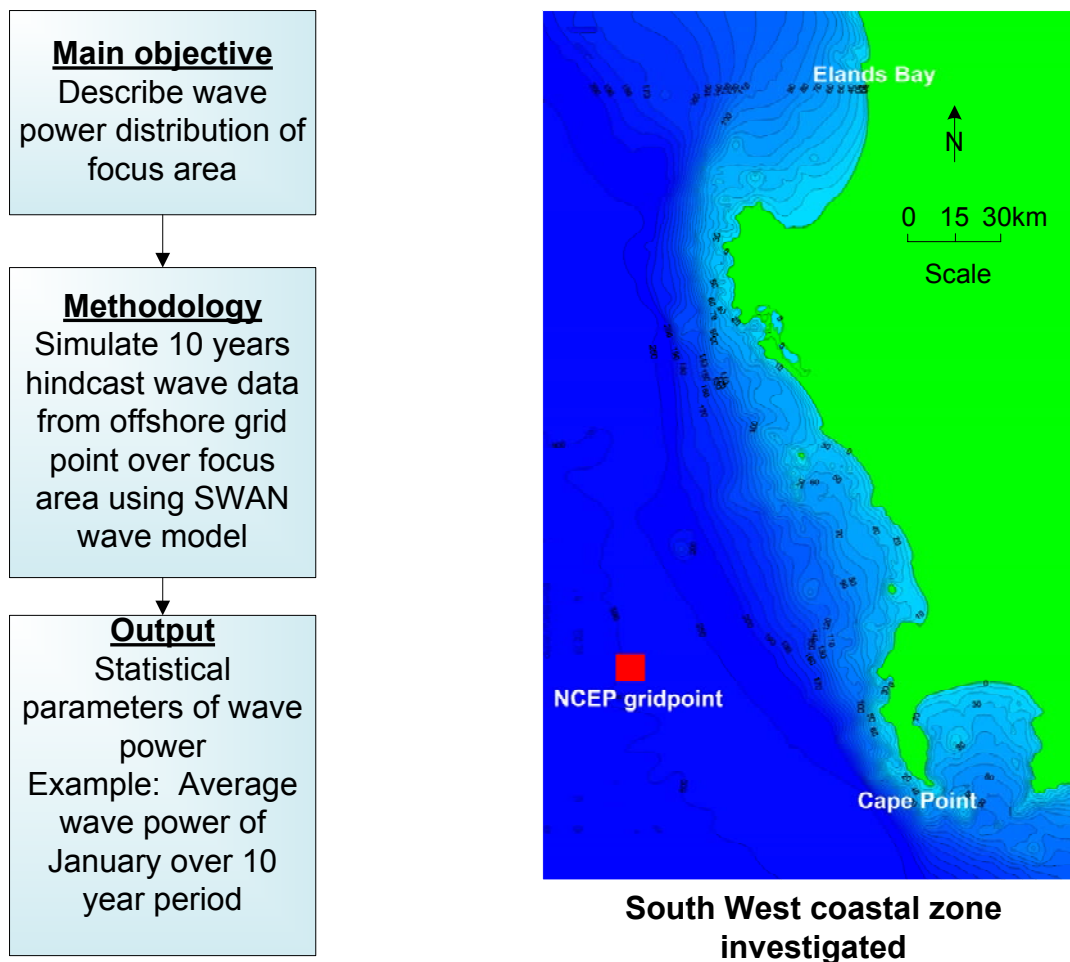


Figure 4-1: Presentation of objective, methodology, output and investigation area

The wave power climate of the focus area will be quantified by simulating wave propagation from deep sea (using 10 years of hindcast data) to shore using the SWAN wave model. The SWAN wave model and the simulation process will be discussed in § 4.4 to 4.7 below. An analysis of the 10 year hindcast wave data will be treated in the following section.

4.2. Hindcast wave data used in the study

Hindcast wave data for 10 years (1997 to 2006) was obtained from the American National Centre for Environmental Prediction (NCEP) for a selected location in deep sea as presented in Figure 4-1 (“NCEP gridpoint”) for the study of the focus area.

The role of the NCEP is best described by the organisation’s mission statement:

The Environmental Modelling Centers (EMC) improves numerical weather, marine and climate predictions at the National Centre for Environmental Prediction (NCEP), through a broad program of research in data assimilation and modelling. In support of the NCEP operational forecasting mission, the EMC develops, improves and monitors

data assimilation systems and models of the atmosphere, ocean and coupled system. (<http://www.emc.ncep.noaa.gov/mission.html> (28/08/07))

The hindcast NCEP wave data used in this investigation is the product of global wave modelling using the WAVEWATCH III wave model. A brief description of this model is presented in the WAVEWATCH III website, as follows:

WAVEWATCH III (Tolman 1997, 1999a) is a third generation wave model developed at NOAA/NCEP in the spirit of the WAM model (WAMDIG 1988, Komen *et al.* 1994). It is a further development of the model WAVEWATCH I, as developed at Delft University of Technology (Tolman 1989, 1991) and WAVEWATCH II, developed at NASA, Goddard Space Flight Center (e.g., Tolman 1992).

WAVEWATCH III solves the spectral action density balance equation for wavenumber-direction spectra. The implicit assumption of this equation is that properties of medium (water depth and current) as well as the wave field itself vary on time and space scales that are much larger than the variation scales of a single wave. A constraint is that the parameterizations of physical processes included in the model do not address conditions where the waves are strongly depth-limited. These two basic assumptions imply that the model can generally be applied on spatial scales (grid increments) larger than 1 to 10 km, and outside the surf zone. Tolman, H. 2006 <http://polar.ncep.noaa.gov/waves/wavewatch/wavewatch.html>, (05/09/2007)

As stated in the model description above the output from the NCEP global model is at offshore (deep sea) locations. Therefore, in order to describe the wave climate of the focus area of this study from offshore to near-shore, further numerical modelling is required as stated in the methodology in Figure 4-1. The NCEP global model output is calibrated and validated with buoy data and with European Remote-Sensing Satellites (ERS2) fast-delivery altimeter (instrument that measures altitude above a certain datum) and scatterometer (measures scatter from the ocean surface) data. The NCEP wave data used in this investigation (at the selected location - Figure 4-1) was analysed and the results of this analysis is discussed in the following section.

4.3. Analysis of NCEP deep sea data at selected deep sea location

The offshore NCEP data used as input to the numerical simulation portion of this research is located at 34°S 17.5°E, 176 644.89m Easting 6 232 306.93m Northing (UTM) and will from here on be referred to as Base. Base is located in approximately 500m water depth and the hindcast wave data was obtained for the period February 1997 to August 2006 (i.e. approximately for a 10 year period). Wave data is available at 3 hourly intervals which results in a total of 27 992 wave records at a 100% coverage over the recording period. A record consists out of the date- and time of recording, H_s , T_p and peak wave direction (D_p). This directional data was analysed to determine the dominant wave direction of wave fields propagating from the storm generation zones in southern ocean. The results of this analysis are presented below.

4.3.1. Directional distribution

The frequency of occurrence of wave direction presented in Figure 4-2, shows that the wave direction predominately ranges from south-south west to west-south west. The dominant wave direction is however from the south west. This graph is also shown in the form of a directional wave rose in Figure 4-3 below

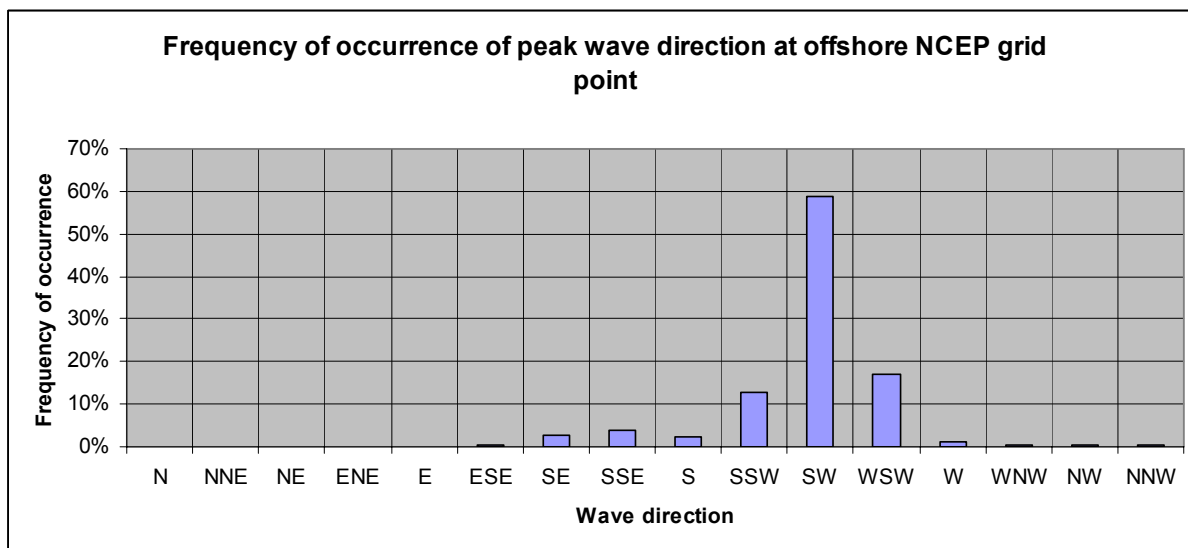


Figure 4-2: Frequency of occurrence of wave direction

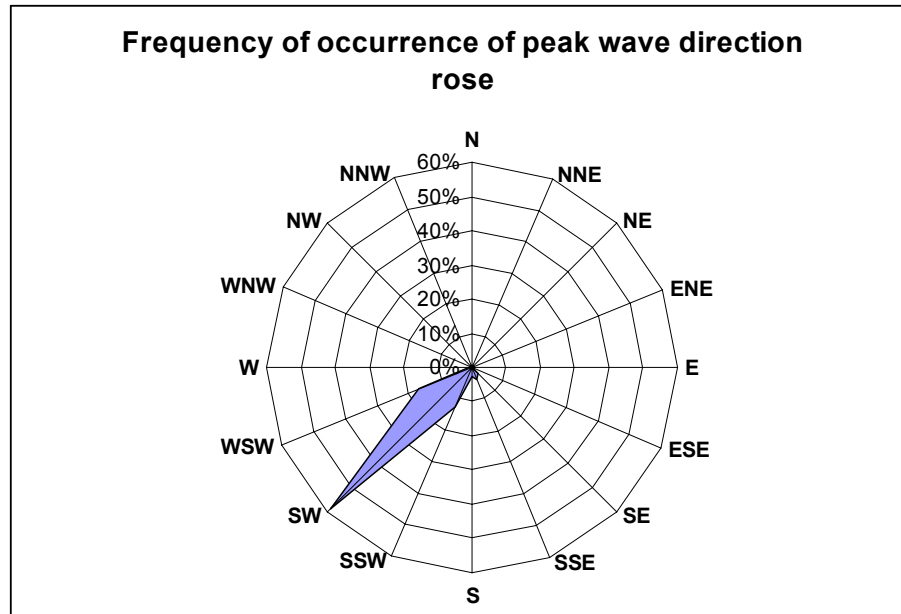


Figure 4-3: NCEP wave direction rose

A general description of the wave power conditions at Base was obtained from a wave energy scatter analysis similar to what was done for the wave recording stations in § 3.8. It is expected that the wave energy scatter at Base will be of larger magnitude compared to the coastal wave recording stations (Slangkop and Cape Point) due to Base's offshore (deep sea) location.

4.3.2. Wave energy scatter analysis

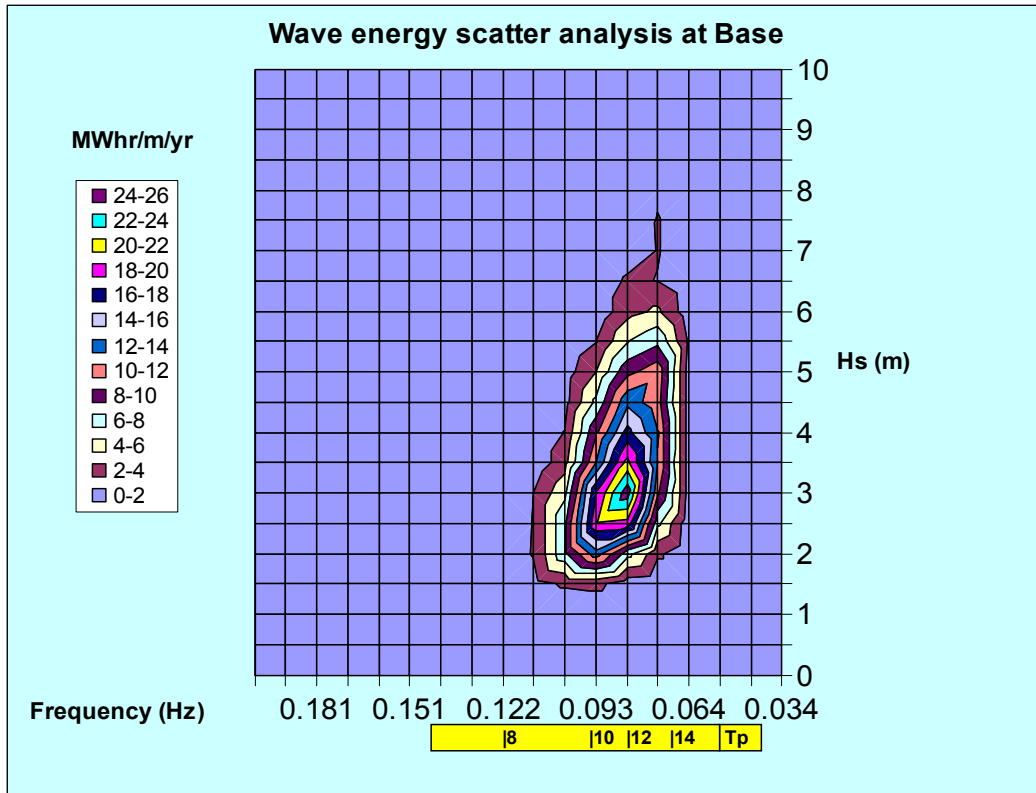


Figure 4-4: Wave energy scatter diagram of Base

The wave energy scatter diagram of Figure 4-4 shows that the most frequent and powerful H_s and T_p combination is 3m and 12s respectively. This combination produces peak wave energy of 24 to 26 MWhr/m/yr. This is the highest peak energy of all the stations analysed thus far and confirms higher wave power offshore in deep sea.

4.3.3. Frequency of occurrence of concurrent wave period and wave direction

A frequency of occurrence analysis of concurrent T_p and D_p values, contained in the Base data set, was conducted. Results of the analysis are presented below in Table 4-1 (highlighted values indicate available data for T_p and D_p conditions). This analysis further confirms the dominant concurrent T_p and D_p values of 12s and SW, respectively. The results also indicate that 90% of the Base data set occurs for T_p values ranging from 10 to 14s and D_p from SSW to WSW.

Table 4-1: Frequency of occurrence of concurrent values of T_p and D_p

T_p/D_p	0	22.5	45	67.5	90	112.5	135	157.5	180	202.5	225	247.5	270	292.5	315	337.5
	N	NNE	NE	ENE	E	ESE	SE	SSE	S	SSW	SW	WSW	W	WNW	NW	NNW
0																
2																
4							0%	0%	0%	0%		0%		0%	0%	0%
6	0%	0%				0%	2%	3%	1%	0%	0%	0%	0%	0%	0%	0%
8						0%	1%	1%	1%	1%	2%	1%	0%	0%	0%	0%
10						0%	0%	0%	1%	5%	22%	6%	0%	0%	0%	0%
12						0%	0%	0%	0%	5%	28%	8%	0%			
14						0%	0%	0%	0%	2%	7%	2%	0%	0%	0%	
16										0%	0%	0%			0%	
18										0%	0%	0%				
20																
22																
24																
26																
28																
30																

Further analysis of the Base data set is done in the following section by comparing it to the measured data of Cape Point recording station during the overlapping recording period.

4.3.4. A comparison of wave power at Base and Cape Point recording station

The recording period of Base overlaps with that of the Cape Point recording station from July 2000 to July 2006. An analysis of these seven years of overlapping data should give a good indication of the expected reduction in wave power as wave fields propagate from deep sea to shallower waters, and if true, will further confirm the general accuracy of the NCEP data. The results of the comparison of mean annual- and monthly wave power of Base and Cape Point are shown below in Table 4-2 and Figure 4-5.

Table 4-2: A comparison of mean annual wave power (kW/m) at Base and Cape Point

Station	Average	90% Exceedance	5% Exceedance
Cape Point	39.0	9.0	113.8
Base	42.0	11.5	116.8

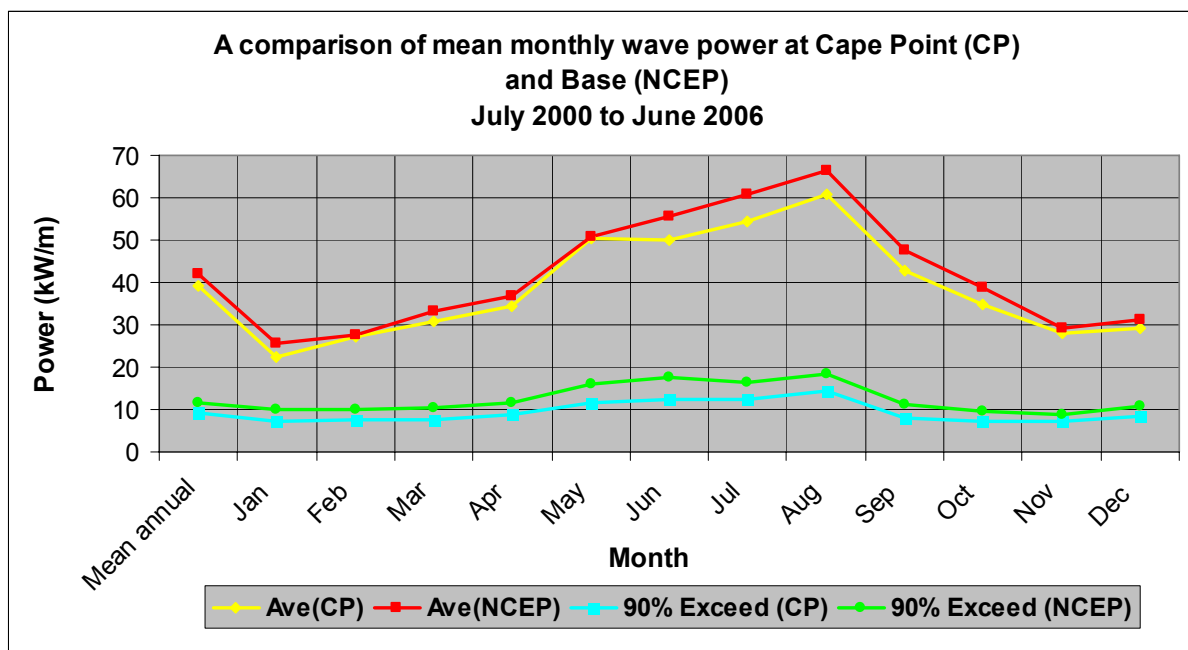


Figure 4-5: A comparison of monthly wave power distribution at Cape Point (CP) and Base (NCEP)

Figure 4-5 and Table 4-2 further confirm the expected reduction of wave power as waves propagate from 500m (at Base) to 70m (at Cape Point recording station) deep water.

Further investigation into the accuracy of the NCEP wave data and the simulation process will be done in §4.10 and Appendix D. The next step in the wave power resource mapping process in the focus area is to simulate the offshore wave inputs from Base to shore using the SWAN wave model. This model and the modelling procedure used in this investigation will be discussed in the following sections.

4.4. Background of the SWAN wave model

SWAN is a numerical wave model, used to obtain realistic estimates of wave parameters for given wind-, bottom- and current conditions, therefore the name: Simulating Waves Nearshore (SWAN). The SWAN model was developed by the Delft University of Technology (Booij et.al, 2004).

4.4.1. Functionality of SWAN

The following propagation processes are incorporated in SWAN:

- propagation through geographic space,
- refraction due to spatial variations in bottom and current,
- shoaling due to spatial variations in bottom and current,
- blocking and reflections by opposing currents,
- transmission through, blockage by or reflection against obstacles.

The model also accounts for the following generation and dissipation processes:

- generation by wind,
- dissipation by white-capping,
- dissipation by depth-induced wave breaking,
- dissipation by bottom friction,
- wave-wave interactions (quadruplets and triads).

4.4.2. General formulation

SWAN uses the two-dimensional wave action density spectrum to describe waves. Action density ($N(\sigma, \theta)$) is used rather than energy density in order to preserve energy in the presence of currents. The governing spectral action balance equation used by SWAN follows:

$$\frac{\partial}{\partial t} N + \frac{\partial}{\partial x} c_x N + \frac{\partial}{\partial y} c_y N + \frac{\partial}{\partial \sigma} c_\sigma N + \frac{\partial}{\partial \theta} c_\theta N = \frac{S}{\sigma} \quad \text{Eqn 4.1}$$

Terms: 1 2 3 4 5 6

Where: $\frac{\partial}{\partial t} N$ = change of action density in time

c_x, c_y = propagation velocity in the x- and y-space. Terms 2 and 3 represent the propagation of action density through geographical space

c_σ = propagation velocity in the σ -space. Term 4 represents the shifting of relative frequency due to variation in depth and currents

c_θ = propagation velocity in the θ -space. Term 5 represents depth- and current induced refraction

$$\frac{S}{\sigma} = \text{source term of action density representing effects of generation,}$$

dissipation and non-linear wave-wave interaction.

(Booij et.al, 2004)

4.5. SWAN assumptions

As mentioned earlier, the main focus of this study is to develop a general description of the expected wave power conditions of the study focus area. Time dependant simulations were deemed unnecessary for this purpose and are more applicable to site specific designs and real time simulations. This implies that the term 1 of Eqn 4.1 becomes zero. Similarly, wind and current inputs were also excluded from all simulations.

The most direct method for obtaining the desired output from the simulation process (as specified in Figure 4-1) is to conduct a SWAN simulation for each NCEP record and then extract statistical parameters from the collective output. This exercise would be computationally expensive with 110 days required to simulate the entire 27 992 record data set. In order to reduce the number of computer simulations it was assumed that wave transmission is independent of wave height. This assumption is clearly unrealistic, but it will be shown later that the consequential discrepancies are marginal. This assumption significantly simplified the SWAN simulation process, in that wave height variation is only determined for boundary inputs of $H_s = 1\text{m}$ and not for the entire H_s range occurring in the NCEP data set. The simplified simulation procedure and the application of the computer model, SWAN, to obtain the desired results of this study is presented diagrammatically in Figure 4-6 below. Figure 4-6 shows that there are three dissipation processes incorporated in SWAN that are dependent on wave height. These include:

White-capping

White-capping occurs when the maximum wave steepness of $H_{\text{max}}/L \approx 0.14$ (Holthuijsen, 2007) is exceeded. Energy dissipation due to white-capping occurs more frequently in the presence of wind fields and it is therefore expected that this dissipation process will have a small impact on the simulation output of this study.

Depth-induced breaking

Wave breaking due to wave-bottom interaction in shallower water and the consequential energy loss is incorporated in SWAN's surf-breaking source term (S_{surf}), with:

$$S_{surf}(f, \theta) = \bar{D}_{surf} E(f, \theta) / m_0. \text{ (Holthuijsen, 2007)}$$

$E(f, \theta)$ and m_0 are dependent on H_s inputs on the model boundaries.

Bottom friction

Energy dissipation through wave-bottom interaction is incorporated in SWAN by the

$$\text{source term: } S_{ds,b}(\sigma, \theta) = -c_{bottom} \frac{\sigma^2}{g^2 \sinh^2(kd)} E(\sigma, \theta) \text{ (Booij et.al, 2004)}$$

The source term for bottom friction ($S_{ds,b}$), is dependent on the energy density spectrum and therefore also dependent on H_s .

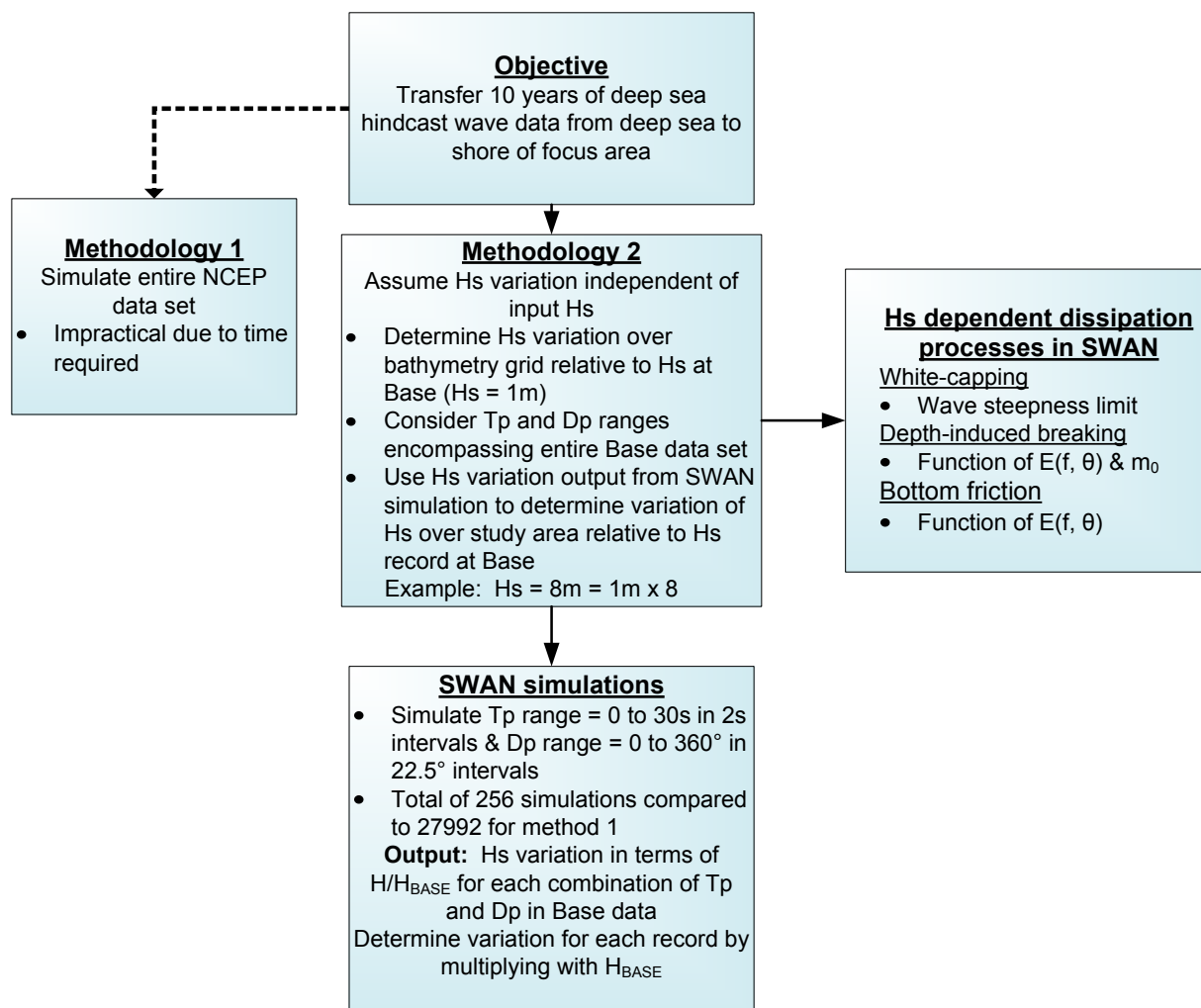


Figure 4-6: An overview of the wave transfer process with SWAN

The simplified simulation procedure, outlined in Figure 4-6, was validated by a sensitivity analysis of the influences of the three dissipation processes. The results of this analysis are presented in Appendix D.

In the next section the actual wave transfer process will be discussed in detail with focus on the input requirements for the SWAN wave model.

4.6. Input requirements for SWAN model analyses

The first step in the simulation process is to define the computational area over which wave conditions are to be modelled.

4.6.1. Computational grid for SWAN simulations

As stated earlier, this part of the investigation will focus on quantification of the wave power resource of Cape Point to Elands Bay. A uniform, rectangular (regular) computational grid was specified for the SWAN simulation, containing a 166 km by 272 km area of the South West coastal region, including its 300 km coastline. This area covers approximately 2° latitude (32.1 to 34.6°S) and 2° longitude (17.2 to 19°E).

The grid resolution was set equal to 1x1 km², which implies 167 and 273 grid lines in the x- and y-directions, respectively. This results in a total of 45 591 grid points (about 50% on land) over the entire grid. SWAN's computational limits are set to a maximum grid resolution of 250 x 250. The specified resolution is thus within SWAN's capabilities. A 1km x 1km mesh is considered sufficient for wave energy transfer in deep water, but too coarse in shallower water (i.e. water depths less than approximately 50 m). For the purpose of this study it is considered that the chosen grid spacing is sufficient to achieve the project objective since the main zone of interest was from deep sea to a depth of 50m. (In water depths shallower than 50m the chosen grid spacing is relatively coarse and for WEC site specific design in shallower water, a finer nested grid within the chosen 1km x 1km grid will be necessary).

After the computational grid was specified the next step was to prepare the other essential SWAN input parameters. These include:

- A bathymetry grid of the seabed inside the defined computational grid.
- Wave conditions on computational boundaries

- Boundary conditions to be prescribed in terms of wave parameter inputs at Base.

The bathymetric grid below, in Figure 4-7, illustrates the computational- and bathymetric grid resolution.

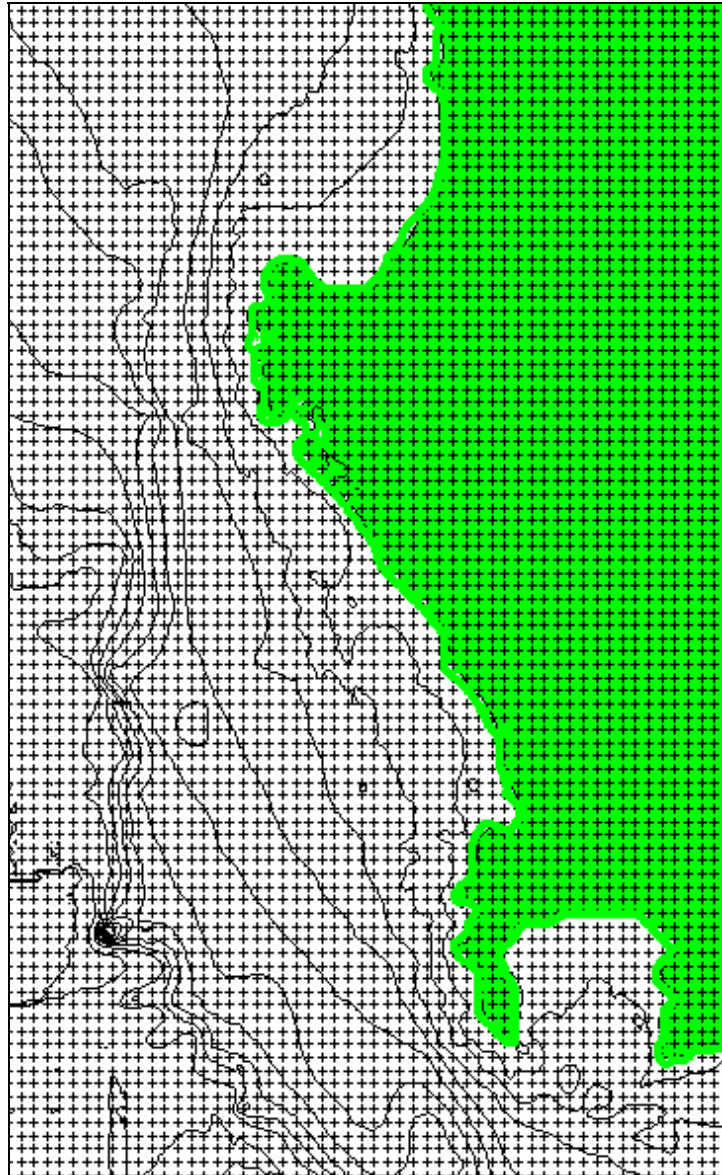


Figure 4-7: Illustration of the SWAN model grid spacing relative to seabed depth contours

4.6.2. Bathymetric grid

In order to generate a bathymetric grid over the computational area the following procedure was followed:

- i. A hand copy of the Naval chart SAN 79, Cape Deseada to Table Bay was obtained to define the seabed topography.

- ii. The naval chart was scanned, depth contours were traced and spot depths were recorded using AutoCAD.
- iii. The depth contours were exported to SURFER 8 to generate a bathymetric grid with a 1x1km² resolution. (See Figure 4-7)
- iv. The generated grid under (iii) is then ready to be used in SWAN applications. Using SURFER 8, a contour map of the bathymetric grid can be drawn.

A schematic diagram of the digitisation process is presented in Figure 4-8 below.

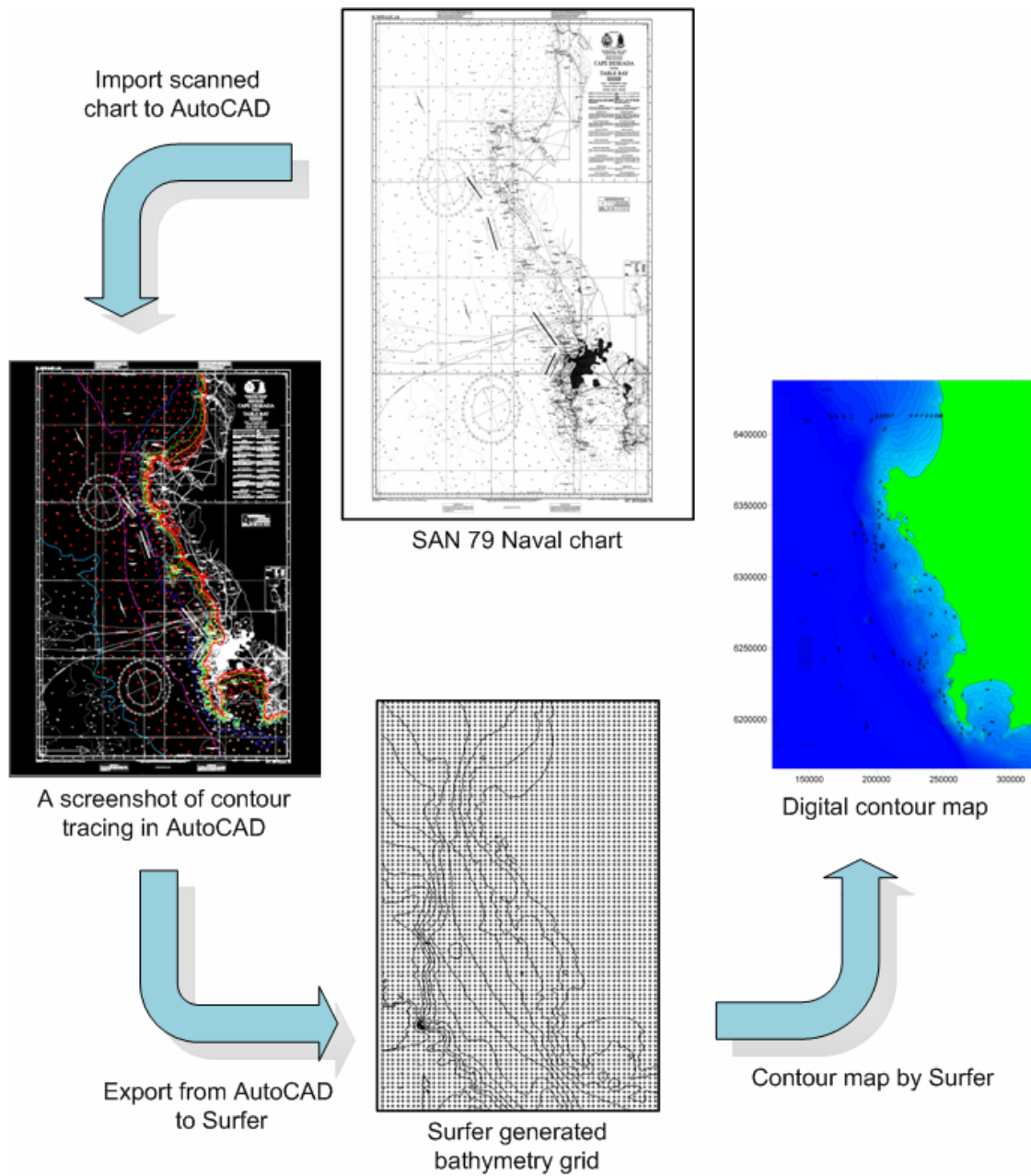


Figure 4-8: Digitisation and bathymetric grid generation process

According to the South African Naval chart (SAN 79), the maximum tidal range of Table Bay is about 1.8m Mean High Water Spring (MHWS). The datum of the seabed depths on the SA Naval chart is Chart Datum which is about 1m below Mean Sea Level (MSL). MSL was chosen as the water level for the SWAN analysis, since this is the dominant water level with a tidal range of about 1m above and 1m below MSL.

4.6.3. Boundary conditions

The final requirement for the simulation process is to prescribe the wave conditions on the boundaries of the computational grid. The computational grid shown in Figure 4-1 and Figure 4-7 has three water- (south, west and north) and one land boundary (east). The coastline in the study area was defined as fully absorbent in SWAN.

Wave conditions on the model boundaries are prescribed in terms of:

4.6.3.1. Peak wave period (T_p)

As stated in the simulation overview of Figure 4-6, the wave period input conditions was prescribed in terms of T_p . The T_p range of 0 to 30s in 2s intervals was simulated, encapsulating the entire T_p range recorded at Base.

4.6.3.2. Peak wave direction (D_p)

The full directional spectrum of D_p ranging from 0 to 360° in 22.5° intervals were prescribed on the model boundaries.

4.6.3.3. Peak-enhancement factor (γ) and wave directional spreading (m)

The shape of the energy density spectrum and the directional spreading must be specified on the model boundaries. These two parameters were prescribed as discussed in § 3.4 and §3.5. The associated distributions of these two parameters are presented in Figure 4-9 and Figure 4-10 below.

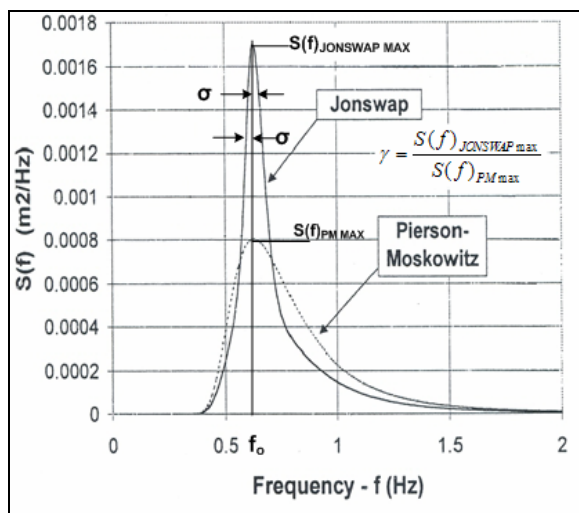


Figure 4-9: Peak-enhancement factor (CEM, 2002)

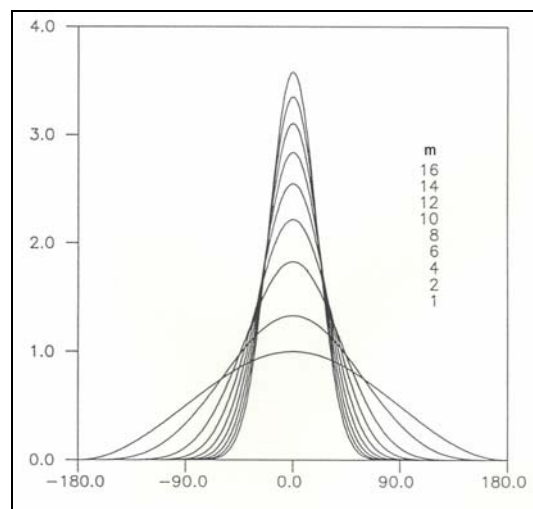
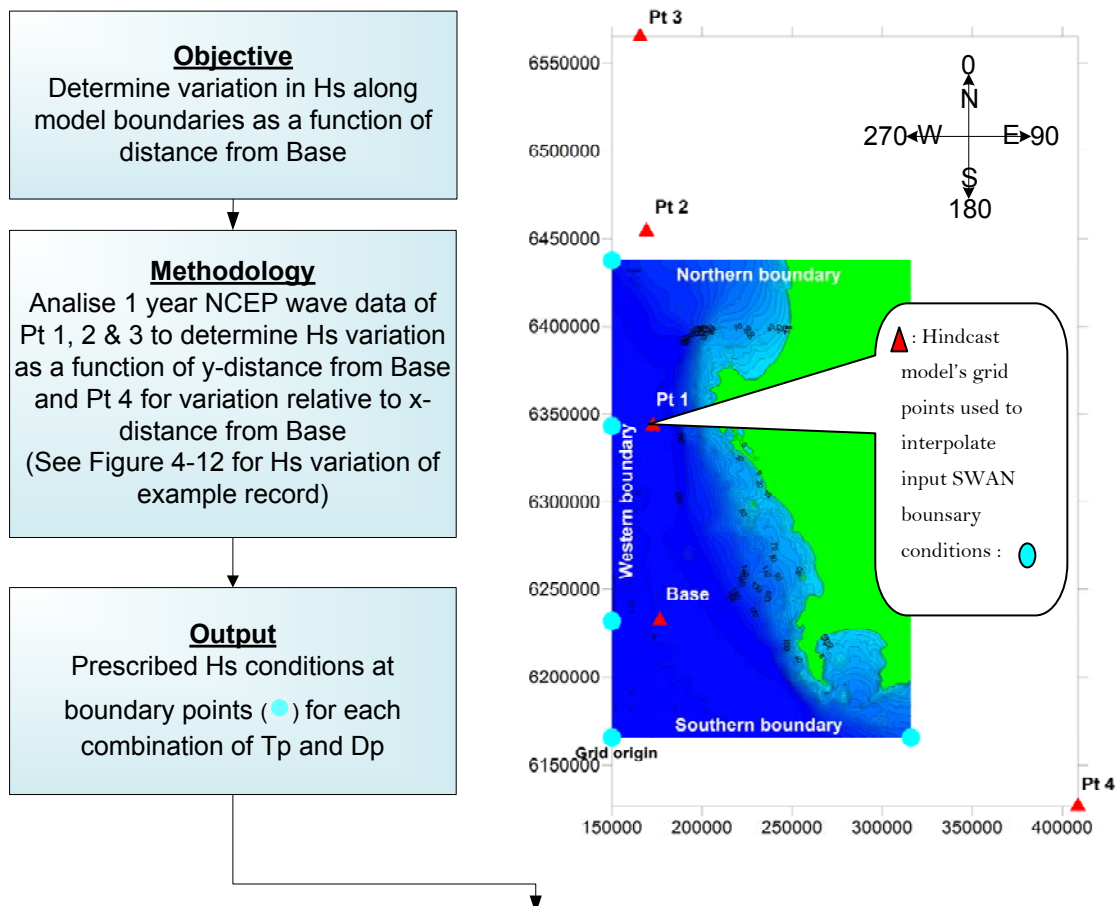


Figure 4-10: Directional spreading (van Tonder, 1992)

4.6.3.4. Significant wave height (H_s)

Similarly to the simulation process defined in §4.5 and Figure 4-6, wave height conditions on the SWAN model boundaries were prescribed relative to wave heights at Base. The procedure employed to determine the variation of H_s , on the model boundaries, as a function of distance from Base for input conditions of T_p and D_p is presented diagrammatically in Figure 4-11 and Figure 4-12 below.



Example of prescribed H/H_{BASE} ratios at grid origin

Origin	Northing	150000	Easting	6165500													
Tp/Dp	0	22.5	45	67.5	90	112.5	135	157.5	180	202.5	225	247.5	270	292.5	315	337.5	
	N	NNE	NE	ENE	E	ESE	SE	SSE	S	SSW	SW	WSW	W	WNW	NW	NNW	
0	1	1	1	1	1	1	1	1	1	1	1	1	1	1	1	1	
2	1	1	1	1	1	1	1	1	1	1	1	1	1	1	1	1	
4	1	1	1	1	1	1	1	1	0.932	1	1	1	1	1	1.000	1	
6	1.040	1	1	1	1	1	1.043	1.007	0.958	1	0.986	1.001	1.006	0.997	1.026	1.012	
8	1	1	1	1	1	0.813	1.044	1.014	1.013	0.990	1.002	0.991	1.037	1.039	0.982	1	
10	1	1	1	1	1	1	1	0.992	0.989	1.013	1.010	1.017	1	0.998	1	1	
12	1	1	1	1	1	1	1	1	1.009	1.011	1.017	1.014	1	1	1	1	
14	1	1	1	1	1	1	1	1	1	1.007	1.021	1.029	1	1	1	1	
16	1	1	1	1	1	1	1	1	1	1.012	1.045	1.029	1	1	1.041	1	
18	1	1	1	1	1	1	1	1	1	1	1	1	1	1	1	1	
20	1	1	1	1	1	1	1	1	1	1	1	1	1	1	1	1	
22	1	1	1	1	1	1	1	1	1	1	1	1	1	1	1	1	
24	1	1	1	1	1	1	1	1	1	1	1	1	1	1	1	1	
26	1	1	1	1	1	1	1	1	1	1	1	1	1	1	1	1	
28	1	1	1	1	1	1	1	1	1	1	1	1	1	1	1	1	
30	1	1	1	1	1	1	1	1	1	1	1	1	1	1	1	1	

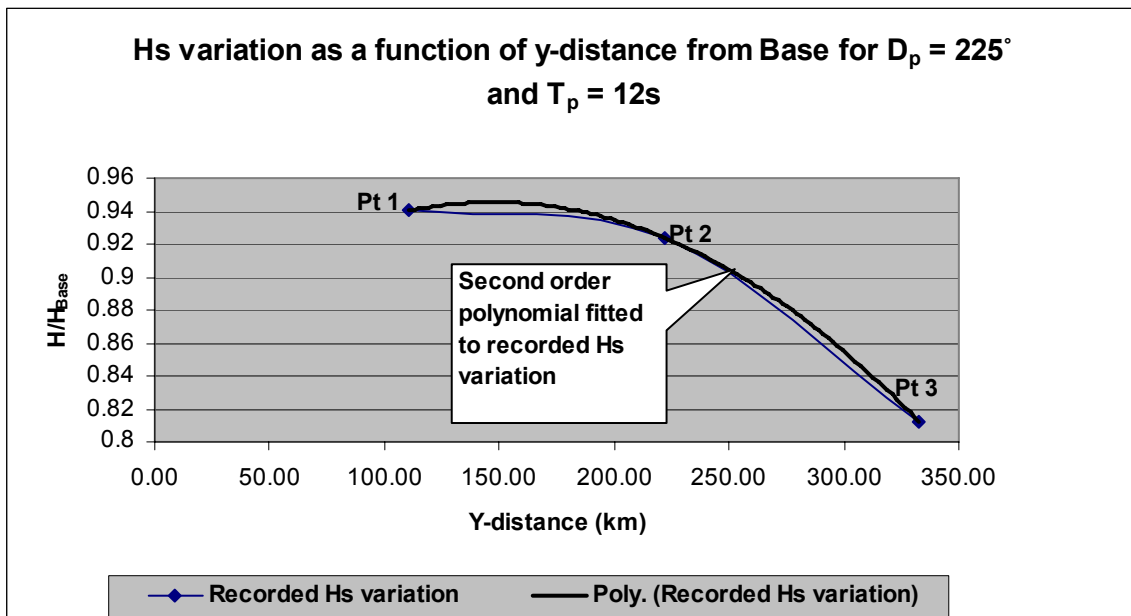
Figure 4-11: Procedure employed to determine Hs conditions on model boundaries (“1” in table means no data was available for the relevant $T_p|D_p$ bin)

The procedure methodology outlined in Figure 4-11 is applied to an example NCEP record and presented in Figure 4-12 below.

H_s variation as a function of distance from Base for example NCEP record

EXAMPLE	Base			Pt1			
Date	H _s	T _p	D _p	H _s	T _p	D _p	y-distance (km)
01 Aug 05 00	2.93	12.06	232.40	2.84	12.10	228.09	111.00

Determine H_{Pt1}/H_{Base} if T_p and D_p values correspond at Base and Pt1. Determine H_s variation as a function of y-distance by analysing wave data of Pt 1, 2 and 3



Repeat process for H_s variation as a function of x-distance from Base by analysing data of Pt 4.

Figure 4-12: Determination of H_s variation for example NCEP record

An example of prescribed wave height conditions for input values of T_p and D_p at the grid origin is shown at the bottom of Figure 4-11. The highlighted values indicate available data for those particular T_p and D_p conditions. The highlighted values correspond to the most frequently occurring T_p and D_p values of the Base data set (see Table 4-1).

Where no data was available constant wave height conditions of 1m were assumed on the model boundaries. This assumption will have little impact on the final result of the study due to the small probability of occurrence of these T_p and D_p combinations in the Base data set. The SWAN wave model interpolates linearly between prescribed values on the model boundaries in order to determine the wave conditions at each boundary grid point.

In SWAN applications wave conditions on the model boundaries are often unknown. No wave inputs or uniform conditions are assumed along such boundaries. These erroneous boundary conditions are then propagated into the model. Areas affected by these unrealistic boundary conditions are indicated by the shaded areas in Figure 4-13 and are generally found 30° from the mean wave direction. To overcome this complication the computational grid is specified in such a way that the area of interest is far away from the model boundaries.

In this study, wave conditions at certain boundary grid points were known and prescribed as determined by the procedure defined in Figure 4-11. These prescribed conditions are reasonable estimates of actual wave conditions and are more realistic than assuming no or uniform boundary conditions. The areas most affected by the estimated boundary conditions are located close to the boundaries and in this application will include False Bay and St Helena Bay in the south east- and northern region of the study area, respectively.

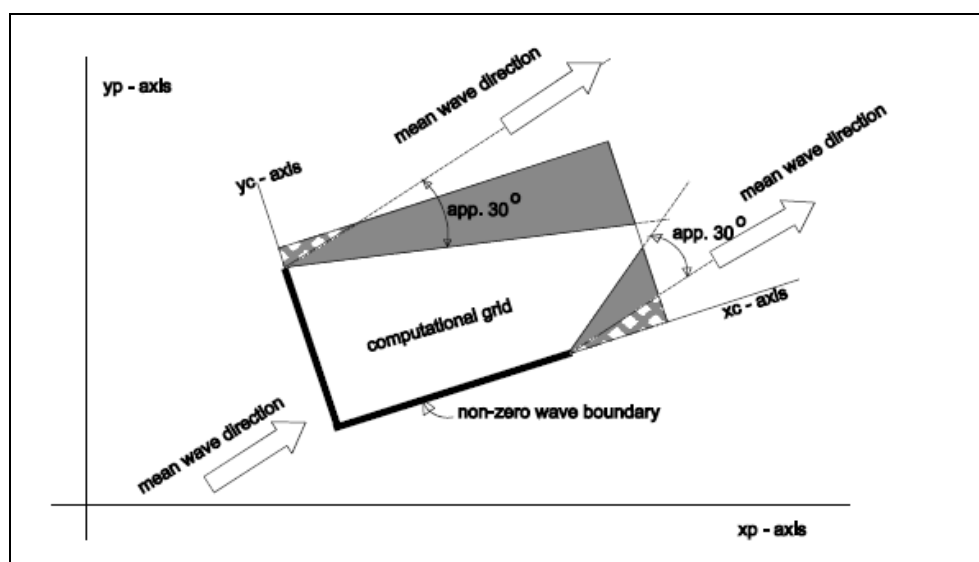


Figure 4-13: Areas affected by erroneous boundary conditions (Shaded zones)
(Booij et. al 2004)

With all the required SWAN input parameters defined, the next step was the simulation based on the 10 year hindcast wave data.

4.7. Simulation process

The simulation process is outlined in the “SWAN simulations” box of Figure 4-6 and the wave conditions to be simulated were discussed in § 4.6.3. A brief summary of the simulation process is:

SWAN wave model was used to simulate 256 combinations of T_p and D_p and the associated H_s as determined through the process outlined in § 4.6.3.4. That implies that 256 SWAN (*.swn) input files were created; each with its own unique input parameters. For the sake of convenience and saving time, the file generation process was automated. A brief discussion of this automation follows in the next section.

4.7.1. Automated file generation and simulation

The automated file generation and simulation process was implemented after consultation with experts in this field (personal communication C. Rossouw, 2007). This automated process is outlined- and was achieved as demonstrated in Figure 4-14 below. Figure 4-14 shows that the 256 *.swn files were generated by first copying the constant input parameters from the master copy *.swn file and then adding the boundary conditions unique to each *.swn file. The programming code required for this exercise was coded in Visual Basic for Applications (VBA) in Excel.

After the *.swn file generation process was completed the files were automatically executed in the DOS environment. It took 24 hours to simulate all 256 *.swn files. The next step in wave power mapping procedure was to simulate the 10 year NCEP wave data (Base) as discussed in Figure 4-6.

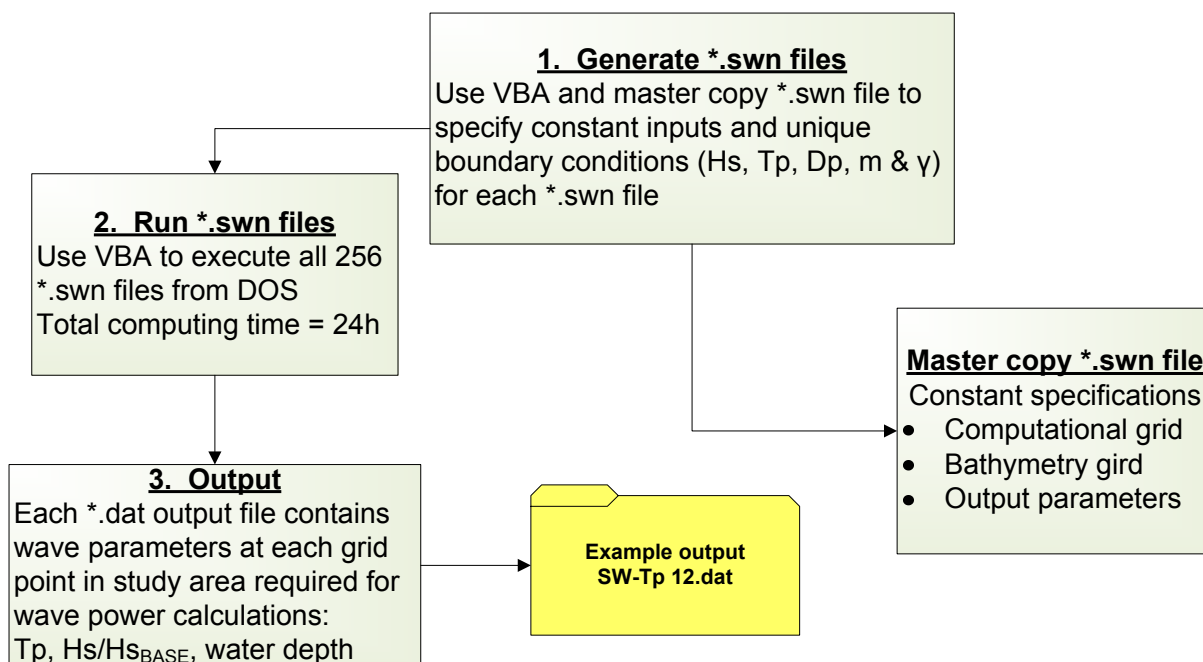


Figure 4-14: Automated file generation and simulation process

4.8. Simulate NCEP wave data

As described in Figure 4-6, each record in the NCP wave data will be simulated by first extracting the associated H_s ratios (H/H_{BASE}) from the SWAN output for that particular record's combination of T_p and D_p , and then multiplying H/H_{BASE} by H_{BASE} . The process is demonstrated diagrammatically for an example NCEP record in Figure 4-15 below.

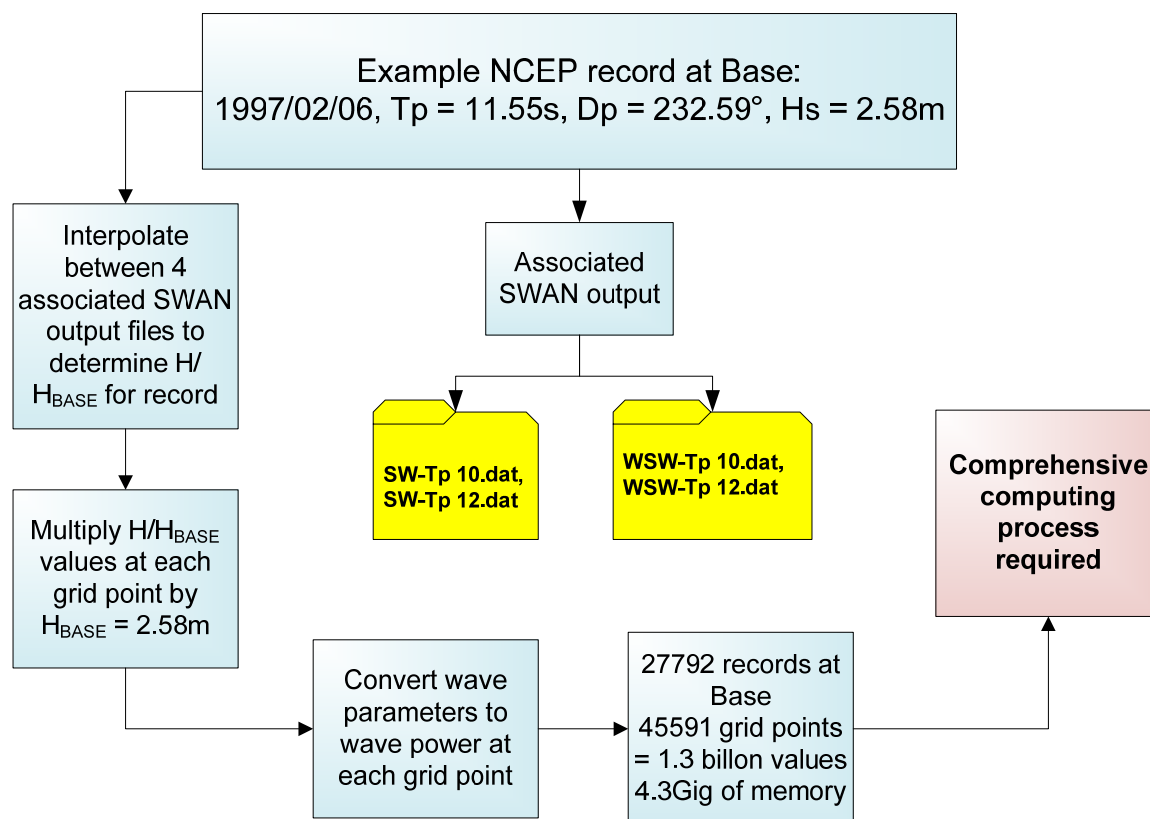


Figure 4-15: NCEP simulation process for an example case

The final outcome from Figure 4-15 is that an extensive computing process is required in order to manage and extract statistical parameters from this large amount of generated data. For the coding of the latter process, computer programming expertise was consulted (personal communication A. Strasheim, 2007).

The exact schematic process, as outlined in Figure 4-15, was programmed in the object oriented, programming environment of Java. This program was the final development required to achieve the project objective: to quantify the wave power resource spatially in the study focus area in terms of statistical parameters. These statistical outputs are discussed and presented in the following section.

4.9. Results of model study

The main purpose of the statistical output from the NCEP simulations is to assist in locating suitable coastal areas in the study area for different types of Wave Energy Converters (WEC's). Using the statistical output in conjunction with the bathymetric contour map, wave farm developers can identify areas with suitable water depth, depending on the specific type of WEC. The wave power resource capacity of a WEC in a selected area can then be determined from the statistical wave power output of this study. The opposite of this process is possible by first identifying areas of high wave power; its associated water depth then determines which type of WEC is best suited for the area. The bathymetry of the study focus area is shown in Figure 4-16 below.

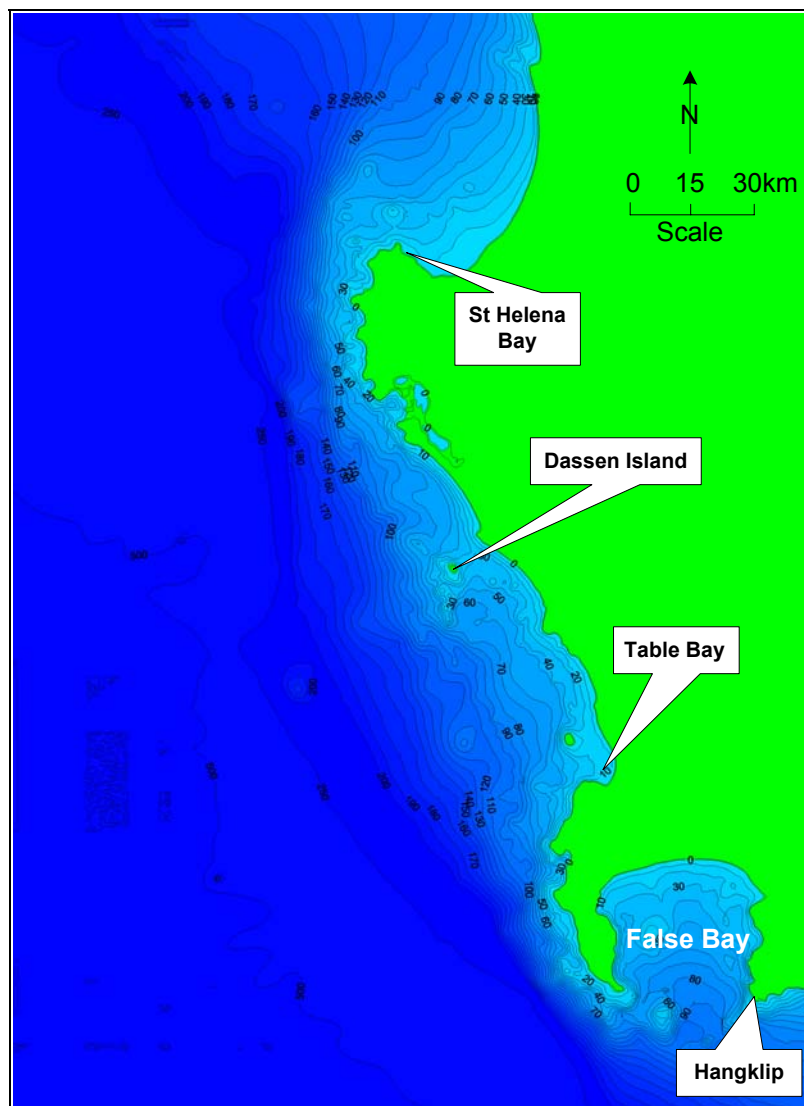


Figure 4-16: Bathymetry contour map of the study area

Similarly to the data analysis of Chapter 3, it was decided to only consider three statistical parameters of wave power namely: Average, 90% and 5% probability of exceedance. These parameters describe the expected average conditions, the lower limit power levels and the extreme conditions, respectively. The statistical parameters were determined monthly and annually. The monthly average wave power spatial maps are presented in the Appendix F.

The output data from this investigation for the study area (South West Coast) is extensive and most of it (spatial wave power maps of individual months and years) is therefore attached to this thesis in electronic format. From the 10 year hindcast data the following mean wave power spatial distribution maps for the study area were derived:

- (i) Mean monthly (i.e. mean of 10 January months, 10 February months etc. = 12 mean monthly maps).
- (ii) Annual (10 annual maps for the 10 year hindcast data).
- (iii) Mean annual (mean of all 10 year's data).

4.9.1. Mean annual wave power

The mean annual spatial distribution of average wave power in the study area over a 10 year period is presented as a wave power contour map in Figure 4-17 below. Some important conclusions drawn from Figure 4-17 are presented below:

- (i) The Southern Atlantic Ocean is the main source of wave power in the South West coastal zone. Note the reduction in wave power along the western boundary from a maximum in the south. The wave power distribution along the southern boundary is relatively uniform.
- (ii) The orientation of the contours depicts the influence of the dominant south westerly swell. This is demonstrated by the wave power penetration into False Bay and the calm zone at St Helena Bay.
- (iii) Definite wave power concentration zones are found at Cape Point, entrance of False Bay, Dassen Island and Hangklip.
- (iv) The deep sea wave power resource ranges from 33 to 41 kW/m.

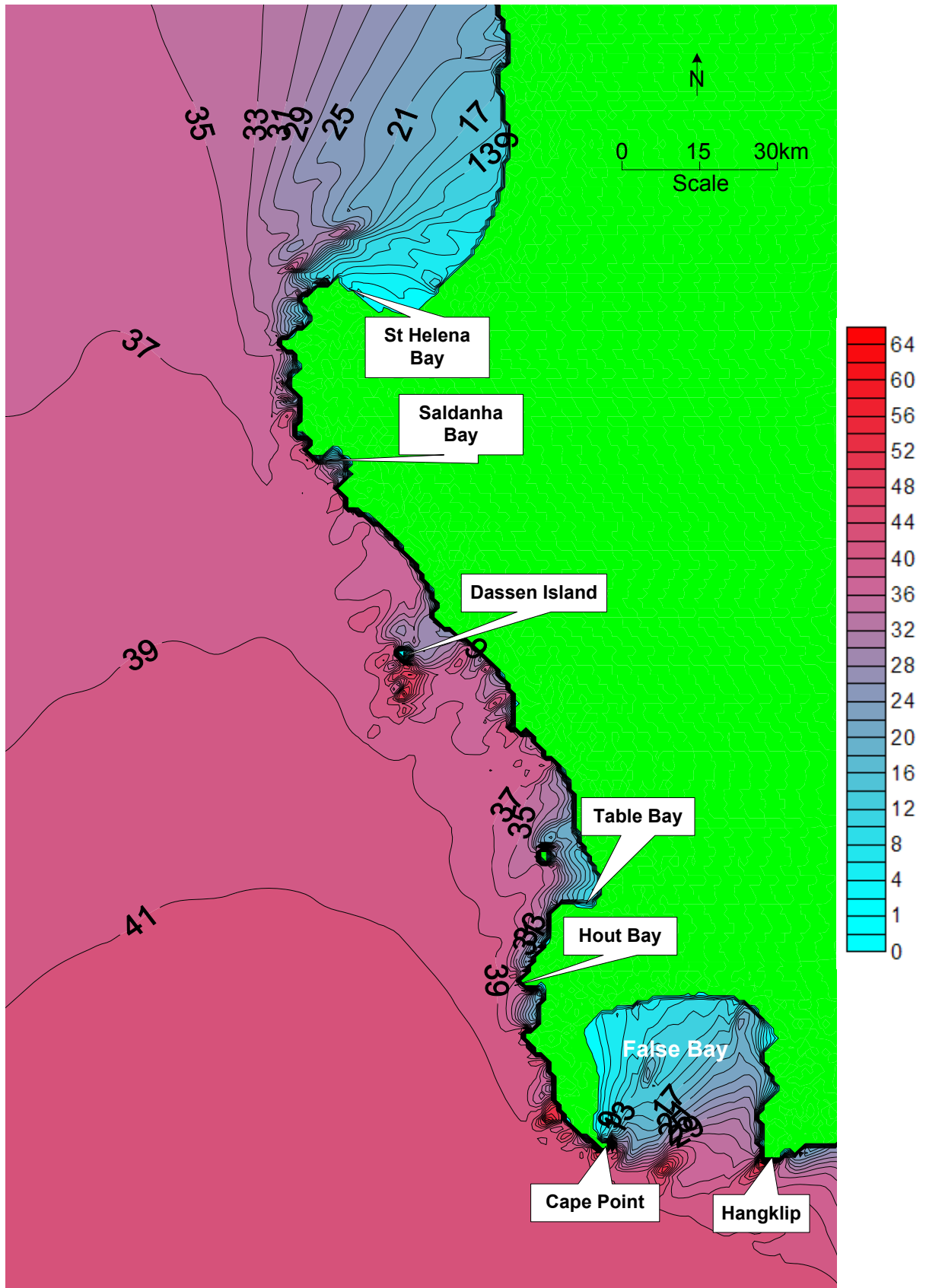


Figure 4-17: Mean annual average wave power distribution (kW/m) of the South West coastal zone based on 10 years of hindcast wave data

4.9.2. Mean seasonal wave power

The mean seasonal spatial distribution of average wave power for the South West coastal area over a 10 year period is presented for each season below in Figure 4-18 to Figure 4-21. The wave power contour map for summer in Figure 4-18 indicates that this season has the lowest average wave power exposure with a deep sea resource ranging from 20 to 27kW/m. In order to produce power consistently throughout the year WEC units must be designed to generate power optimally during exposure to such low power levels.

Figure 4-19 and Figure 4-20 indicate that spring and autumn have very similar average wave power distributions. A WEC unit will therefore generate power optimally for half the year if it is designed for these seasons. The deep sea average wave power resource for spring and autumn range from 31 to 39 kW/m.

Survivability of WEC units deployed in the study area will be tested during the winter months due to large wave power exposure as presented in Figure 4-20 below. The deep sea average wave power resource of winter ranges from 50 to 61 kW/m. This is double the summer wave power resource.

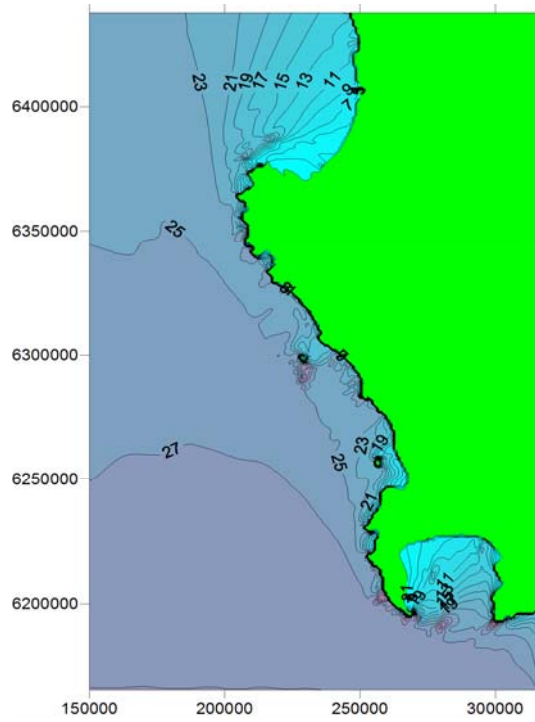


Figure 4-18: Spatial distribution of mean seasonal average wave power (kW/m) for summer

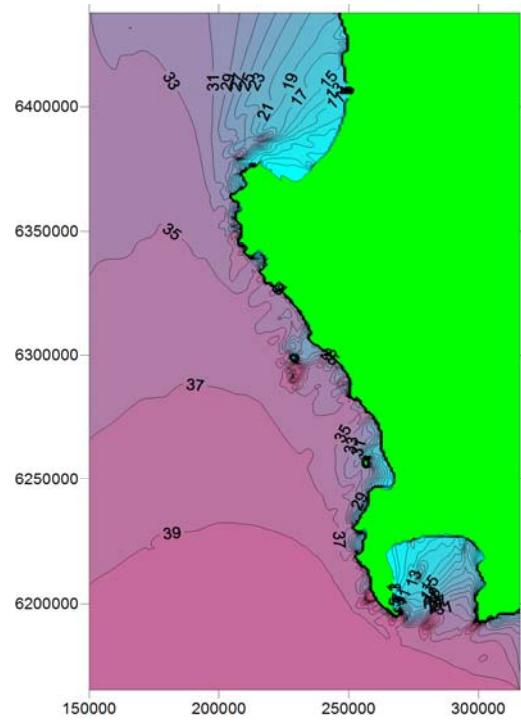


Figure 4-19: Spatial distribution of mean seasonal average wave power (kW/m) for autumn

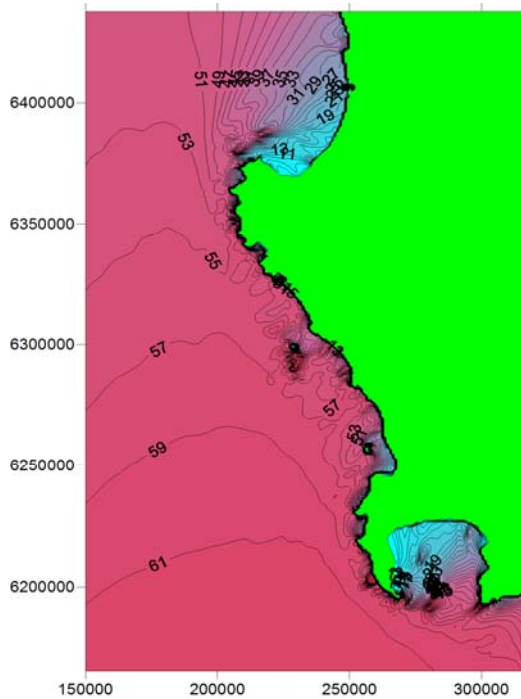


Figure 4-20: Spatial distribution of mean seasonal average wave power (kW/m) for winter

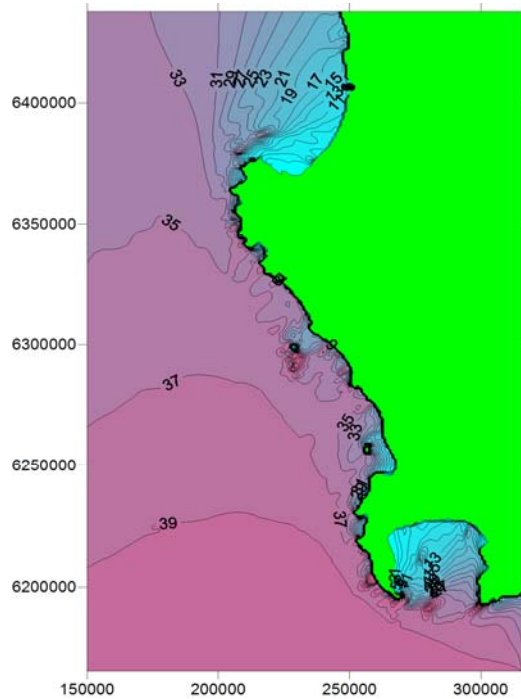


Figure 4-21: Spatial distribution of mean seasonal average wave power (kW/m) for spring

The model hindcast data is compared to measured data of Cape Point recording station in §4.10 for the overlapping recording period. The seasonal probability of exceedance of wave power at the model grid point closest to Cape Point recording station for the total 10 year period is therefore presented in Figure 4-22 below. The upper limit of wave power conditions considered was 100 kW/m for the reasons defined in §3.8. Figure 4-22 indicates that winter has the highest wave power resource. The mean annual, autumn and spring probability of exceedance curves are very similar. 5% and 1% probability of exceedance for extreme seasonal wave power events are presented in Table 4-3 below.

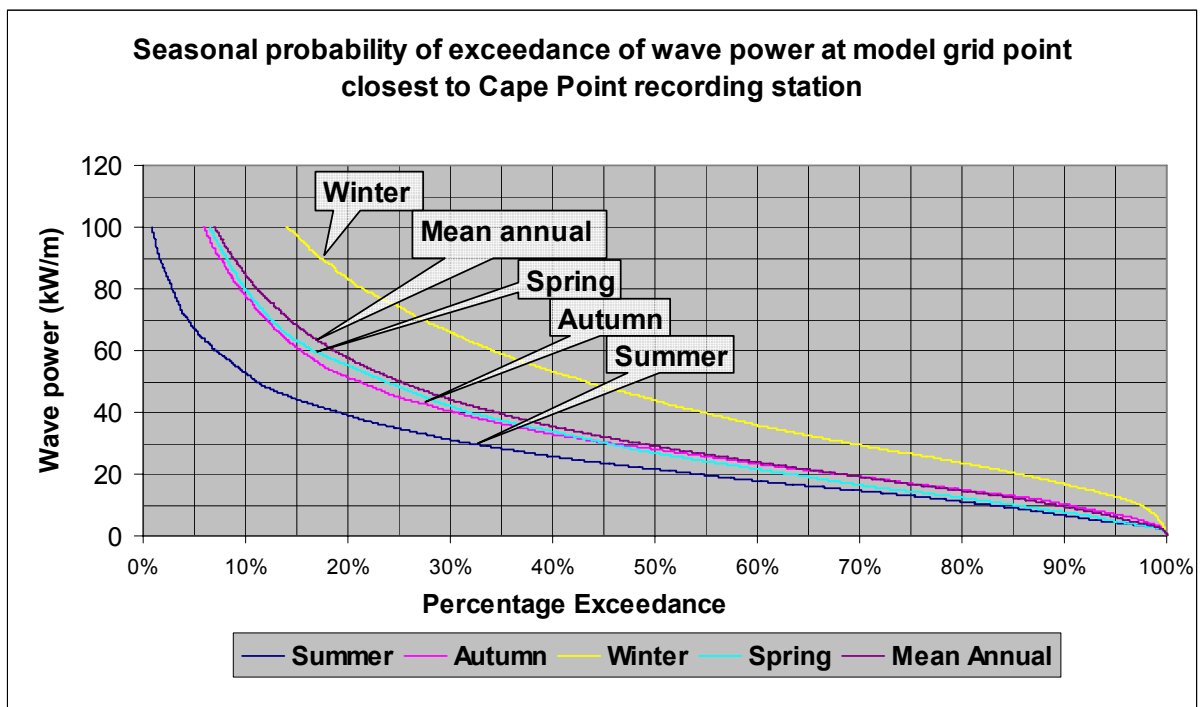


Figure 4-22: Seasonal probability of exceedance of wave power at model grid point closest to Cape Point recording station

Table 4-3: 5% and 1% probability of exceedance for extreme seasonal wave power events at model grid point closest to Cape Point recording station

Season	1% Exceed	5% Exceed
Summer	97.77	67.09
Autumn	168.73	106.63
Winter	272.47	153.30
Spring	174.49	112.22
Mean annual	194.53	114.62

4.9.3. Mean monthly wave power

The mean monthly spatial distribution of average wave power for the South West coastal region over a 10 year period is presented for the months of January, April, July and October. These months are representative of summer, autumn, winter and spring, respectively. Note the similarity between the mean monthly spatial maps and its associated mean seasonal spatial maps.

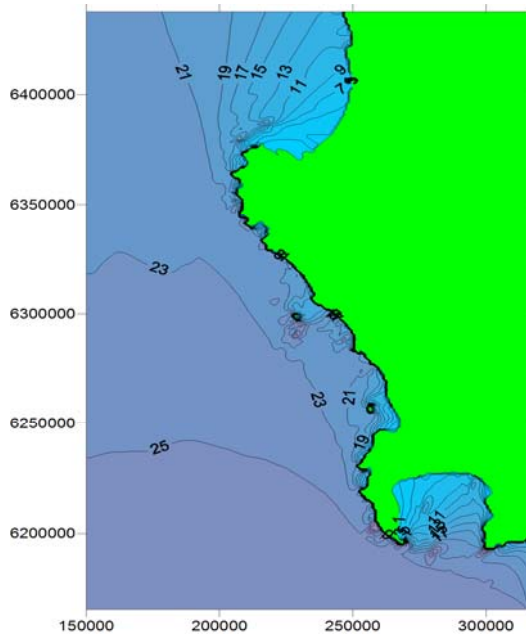
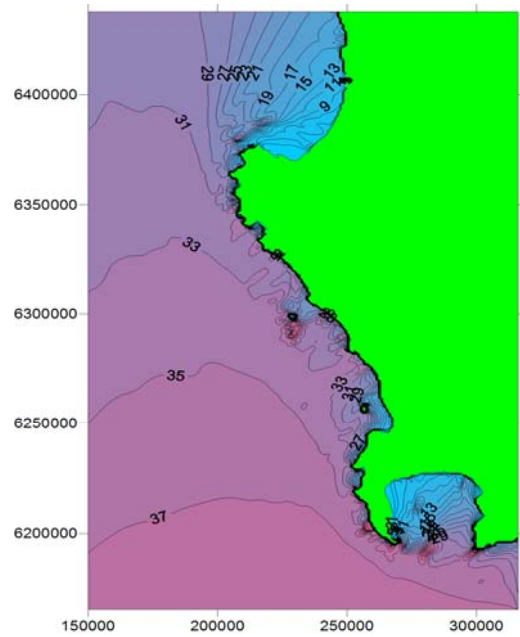


Figure 4-23: Mean monthly average wave power distribution (kW/m) for January



Statistical parameters of mean monthly wave power at the model grid point closest to Cape Point recording station for the 10 year period are presented in Figure 4-27 below.

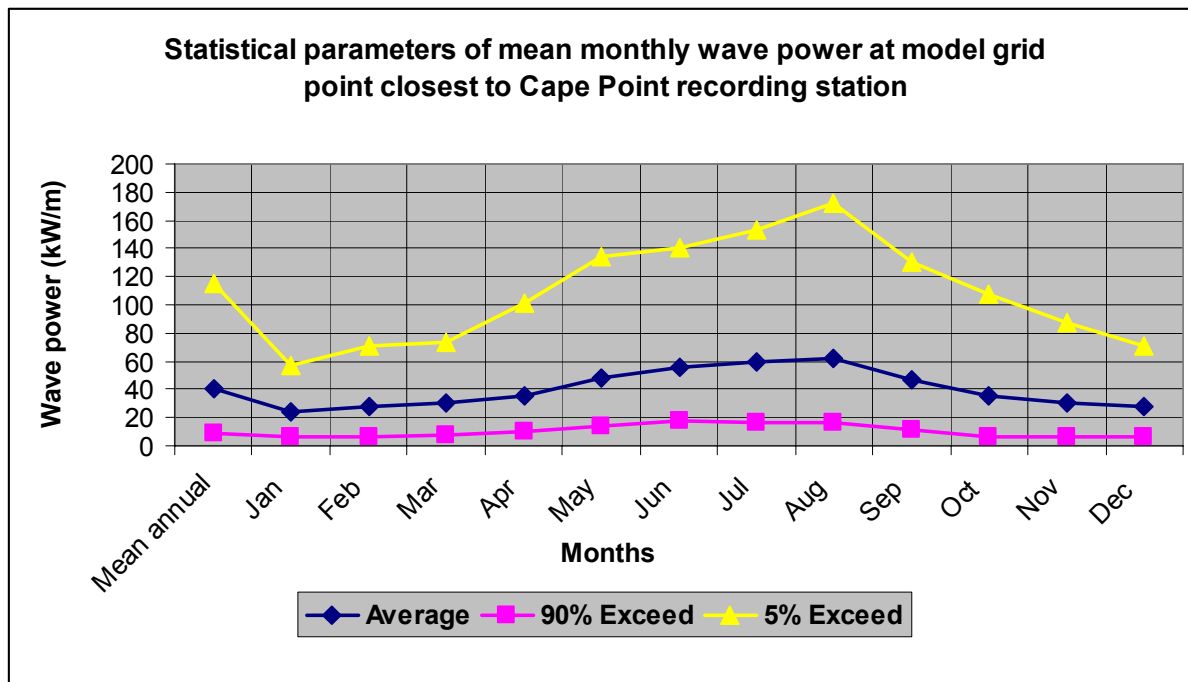


Figure 4-27: Statistical parameters of mean monthly modeled wave power

The accuracy of the model output is investigated by comparing it to the measured data of Cape Point recording station for the overlapping recording period in the following section.

4.10. Comparison of model hindcast- to measured data

The accuracy of the model output data was investigated by comparing it to the measured data of Cape Point recording station. The closest model grid point to Cape Point recording station is located at 250 000m Easting 6 211 500m Northing. The grid point is 390m south of Cape Point station at a depth of 78m compared to 70m water depth at Cape Point. As indicated in §4.3, the recording period of the Cape Point recording station and Base NCEP data overlaps for a six year period from July 2000 to July 2006. Data recorded during this period will be used for comparison purposes. This comparison is an investigation into the accuracy of the NCEP hindcast wave data and also the SWAN wave modelling process.

A comparison of the monthly measured wave data of Cape Point with the transferred hindcast data from Base to the model grid point nearest to Cape Point recording station is presented in the following section.

4.10.1. A comparison of monthly wave power distribution at Cape Point with SWAN transferred hindcast data close to the latter recording station

The statistical parameters of monthly wave power of Cape Point recording station and the model grid point closest to Cape Point for the six year overlapping recording period is presented in Figure 4-28 below. Figure 4-28 indicates that the model slightly overestimates wave power during the winter months of June, July and August, but in general the model estimates wave power sufficiently accurate compared to the measured wave power of Cape Point recording station.

The percentage difference in monthly average wave power of the modelled and measured data is presented in Table 4-4 below. Table 4-4 shows that the model overestimates monthly average wave power by a maximum of 9% for the winter months of June and July and underestimates the average wave power of February by 6%. The model overestimates the mean annual average wave power by a relatively small 5%.

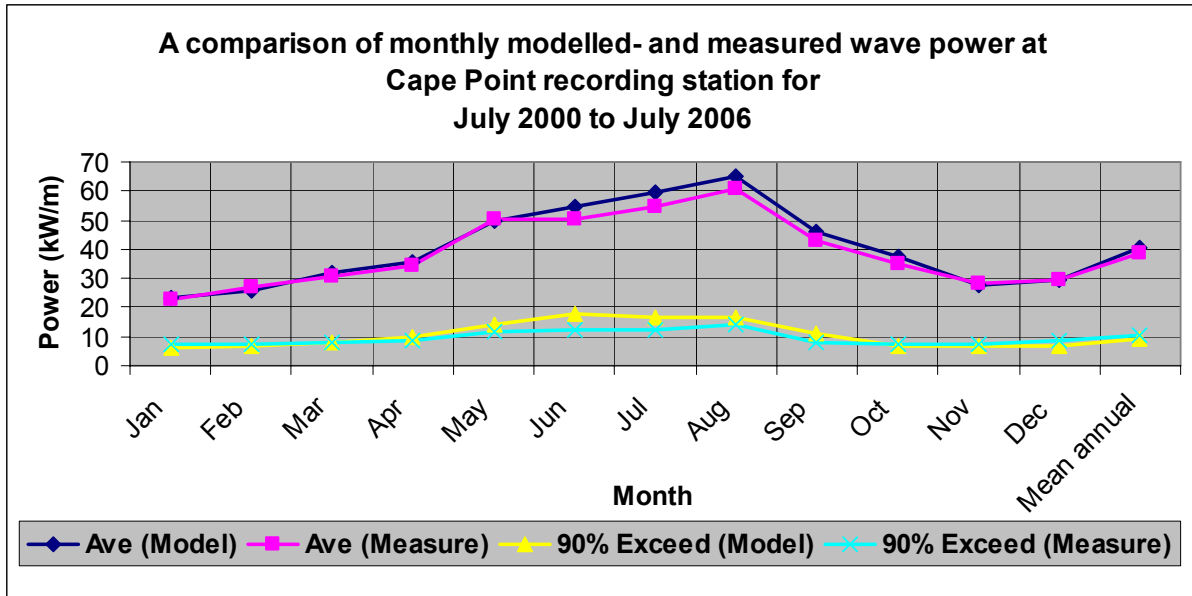


Figure 4-28: Monthly measure and modeled wave power

Table 4-4: Percentage difference in mean monthly average wave power of measured and modelled data

Jan	Feb	Mar	Apr	May	Jun	Jul	Aug	Sep	Oct	Nov	Dec	Mean annual
4%	-6%	3%	4%	-1%	9%	9%	6%	8%	7%	-2%	1%	5%

Further investigation into the accuracy of the model output was done by comparing it to the probability of exceedance of wave power of the measured data of Cape Point recording station. The probability of exceedance of wave power of the measured and modelled data is presented in Figure 4-29 below. Figure 4-29 indicates that the model estimates wave power sufficiently accurate for the purpose of the study, but slightly overestimates the wave power for the bulk of the data with probability of exceedance ranging from 20 to 80%. The wave power of extreme events with small probability of exceedance of 1% and 5% for the measured and modelled data is presented in Table 4-5 below.

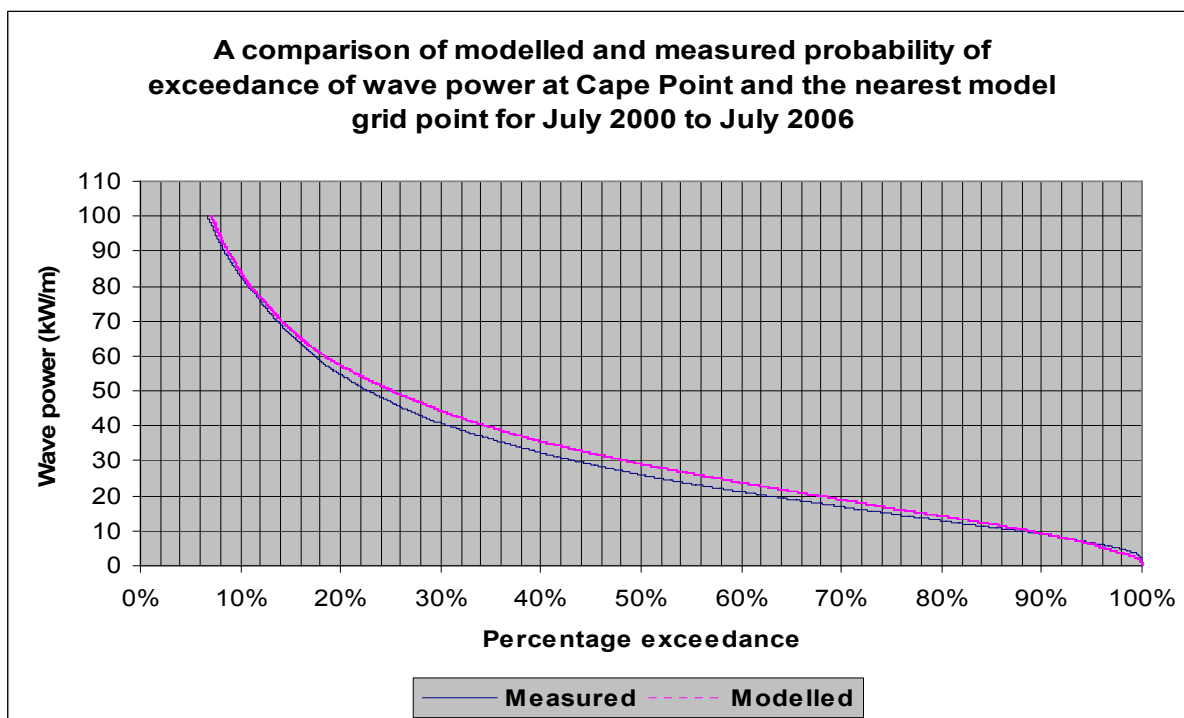


Figure 4-29: Probability of exceedance of wave power measured at Cape Point recording station and modeled data (hindcast data transferred)

Table 4-5: 1% and 5% probability of exceedance of extreme wave power events for the modelled and measured data

	1%	5%
Measured	213.78	113.76
Modelled	197.78	115.72

The monthly probability of exceedance curves for the measured- and modelled data further confirms the general accuracy of the model output (see Appendix G for the monthly probability of exceedance of measured and modelled wave power).

5. SUMMARY AND CONCLUSIONS OF STUDY

A summary of the findings of this study and conclusions drawn are presented below.

5.1. Literature study

- a) South Africa has a substantial wave power resource on a global scale due to its close proximity to the storm generation areas in the Southern Atlantic Ocean and its prevailing meteorological conditions. (See Figure 2.1 and § 2.2).
- b) The study aimed to update the wave power resource mapping of (Geustyn, 1983) by analysing the addition 23 years of recorded wave data.
- c) The applicable wave theory and wave power related parameters were identified and outlined in a wave power calculation procedure (refer to § 2.4.6). This procedure was employed during the wave power analysis of measured and modelled hindcast wave data.
- d) Each type of WEC has unique wave power resource- and site requirements. The dominant South African wave power conditions and local bathymetry will therefore be better suited to particular types of WEC's. Such WEC types should be designed to generate power optimally while exposed to relatively long period waves from the dominant South West direction.

5.2. Wave power conditions on the South African coast based on recorded data

- a) For this portion of the study wave parameters recorded at five wave recording stations along the South African coast were converted to wave power. This analysis provided a general description of the wave power conditions at locations for which wave data exist. The monthly, seasonal and annual variability of the South African wave power climate was demonstrated.
- b) Refer to Appendix B for the design wave heights at the above mentioned wave recording stations for the survivability analysis of WEC units (MacHutchon, 2006).

- c) From the wave power analysis of measured wave data it was found that the Slangkop and Cape Point wave recording stations have the highest wave power resource with a mean annual average wave power of approximately 40kW/m (refer to Figure 5-1). The FA platform also has a substantial wave power resource which is slightly lower than that of the Slangkop and Cape Point recording stations due to the platform's exposure to shorter dominant wave period conditions (refer to § 3.9.4 for reasons for short period exposure). The multi-directional wave exposure of the platform makes it suitable for power generation by direction independent WEC types (point absorbers).
- d) Based on this part of the study the South West Coast was identified as the coastal zone exposed to the highest wave power (refer to Figure 5-1) and was therefore selected as the focus study area for which detailed spatial wave power distribution statistics were determined.

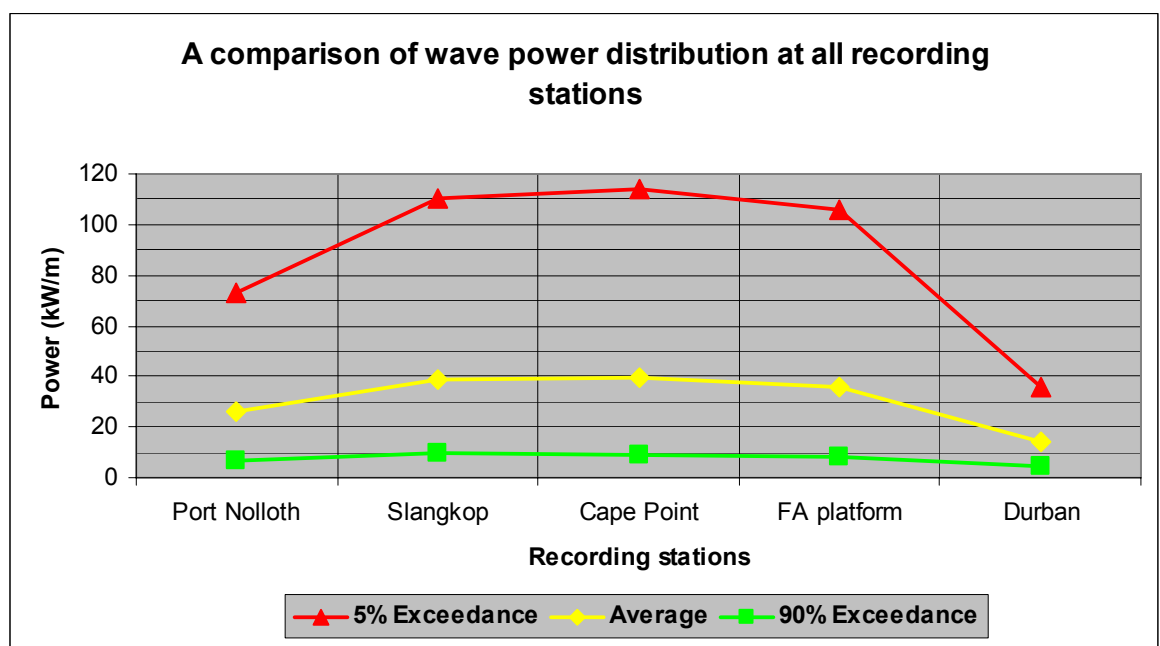


Figure 5-1: Wave power exposure of each wave recording station

5.3. Spatial wave power distribution on the South African South West Coast based on hindcast data

- a) The methodology employed to achieve the main objective of the study was to simulate 10 years of modelled hindcast wave data over the South African coastal region with the highest wave power i.e. the South West Coast stretching from Cape Point to Elands Bay. The SWAN wave model was applied in this analysis.
- b) An initial analysis of the hindcast wave data, to be simulated from deep sea to nearshore, confirmed dominant wave period and direction conditions of 12s and wave approach direction of South West, respectively. The deep sea hindcast wave data was also compared to the measured wave data in the shallower water location of Cape Point recording station for the overlapping recording period. This analysis indicated a greater wave power resource offshore and confirmed the general accuracy of the hindcast wave data.
- c) In order to successfully employ the proposed methodology certain assumptions in the simulation procedure were required. The most significant of these being that wave height variation due to wave propagation from deep sea to nearshore is independent of the input deep sea wave height. This assumption was however unavoidable due to computer limitations. The simulation methodology was validated through a sensitivity analysis (see Appendix D for results of sensitivity analysis) which indicated that the model gives sufficiently accurate estimates of wave power in deep water and nearshore regions for the dominant wave conditions. The model does however slightly overestimate wave power in shallow water regions due to the underestimation of energy dissipation.
- d) The SWAN wave model was used to simulate 256 wave conditions (T_p and D_p combinations) in the study area (defined by a computational grid). Its output was generated in terms of wave height variation relative to the wave height at the deep sea location of the hindcast wave data. The hindcast wave data was subsequently simulated, incorporating the simulation assumption and utilising the generated SWAN output. A Java program was developed and used to extract statistically parameters of wave power in the study area from the simulated hindcast data. These statistical parameters are presented in the form of wave power contour maps of the study area (South West Coast) and represent the achievement of the

study's main objective. An example of such a map is shown in Figure 5-2 below. Figure 5-2 is the average mean annual wave power distribution for the 10 year hindcast data (July 1997 to July 2006). The main conclusions that can be drawn from this particular map include the following:

- The average offshore wave power resource ranges from 35kW/m in the north to 41 kW/m in the south.
 - There is a clear reduction of offshore wave power from south to north.
 - Wave power focal zones can be identified at locations such as along the western coast of Cape Point, the tip of Hangklip, at the entrance of False Bay and the southern part of Dassen Island.
- e) The accuracy of the simulated output was investigated by means of a comparison with the measured wave data of Cape Point wave recording station. This comparison indicated that the model overestimated average wave power of the total record by a relatively small 5% which is sufficiently accurate for the purpose of the study.

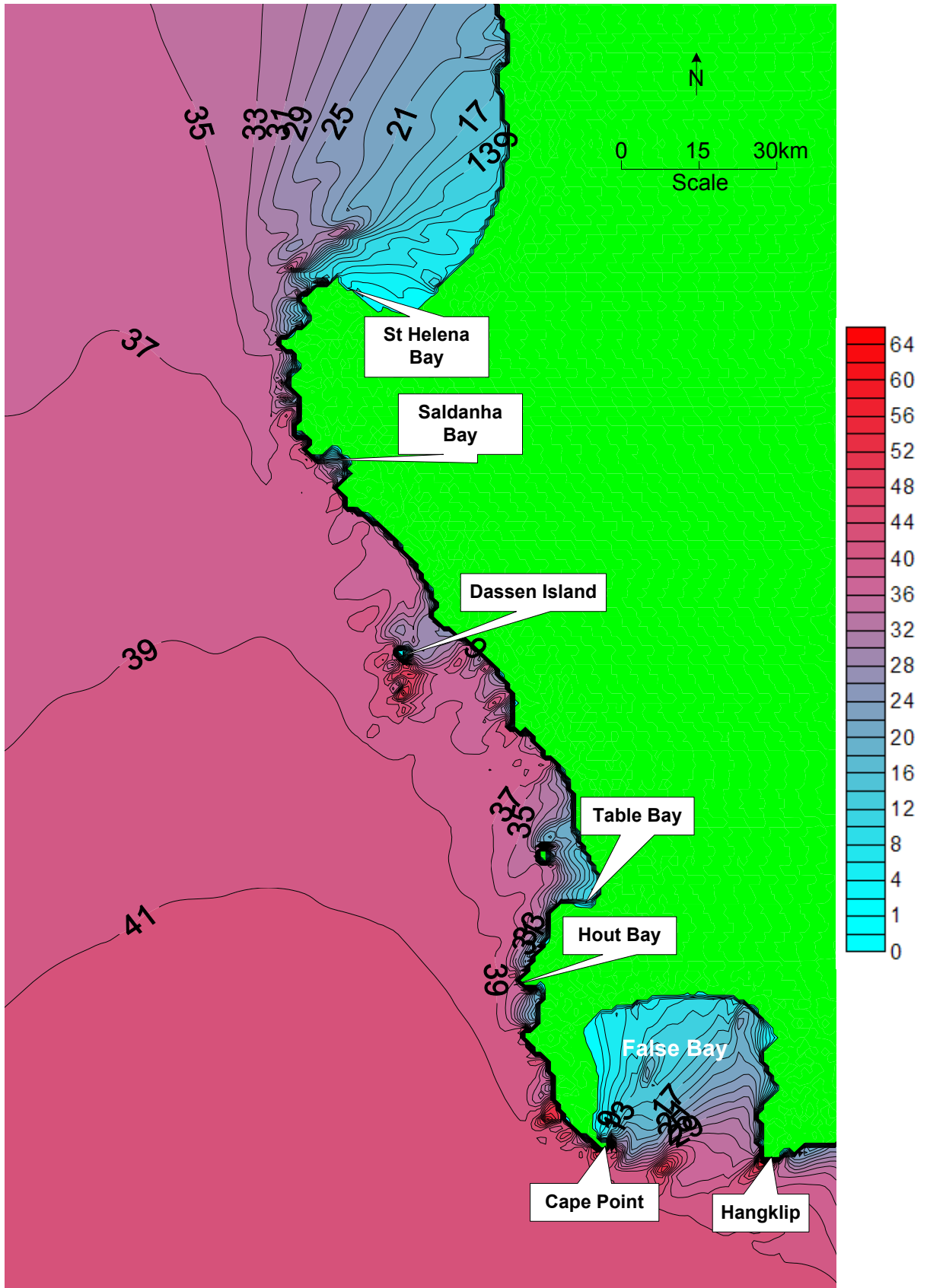


Figure 5-2: Mean annual average wave power distribution (kW/m) of the South West coastal zone based on 10 years of hindcast wave data

6. RECOMMENDATIONS

Based on the summary made and conclusions drawn from the findings of this study, the following recommendations are made with regard to the implementation of this description of the South African wave power resource.

- a) The resulting description of the South African wave power climate obtained from this study can serve as a representative indicator of wave power conditions. The results could be used to identify areas of wave power concentration in the study area for the location of WEC units. It was shown that the model accurately estimates the offshore wave power resource, but slightly overestimates the shallow water wave power resource. Correction factors can therefore be determined for concurrent values of T_p and D_p and applied to the study output in order to better estimate the wave power resource in shallow water locations. Further numerical modelling is required for detailed design of wave farms especially for survivability analyses. Such analysis will also provide more accurate estimates of wave power conditions in shallow water locations (less than approximately 50 m).
- b) The model can also be used to describe real time wave power conditions in the study area by directly simulating NCEP input data, available three hourly, from the deep water location. This system can be used to monitor the power generation performance and efficiency of deployed WEC units by comparing actual generated power to the real time available resource. Resource monitoring can ensure device survivability by enforcing generation cut off during extreme loadings of storm events.
- c) After the identification of potential wave farm sites in the study area, various statistical parameters of wave power can be extracted from the output of this study. An analysis of the wave power distribution, similar to the measured wave power analysis of this study, can be conducted for any of the 45 991 grid points.

7. REFERENCES

Booij N, Haagsma IJG, Holthuijsen LH, Kieftenburg ATMM, Ris RC, van der Westhuysen AJ, Zijlema (2004) **“SWAN Cycle III version 40.41 User Manual”** Delft University

Boud R (2003) **“Status and research and development priorities | 2003, Wave and marine current energy”** technical paper prepared for the UK Department of Trade and Industry.

Coastal Engineering Manual (CEM), US Army Corp of Engineers (2002)

Carbon Trust UK, **“Ocean waves and wave energy device design”** website describing wave parameters related to wave power.

http://www.carbontrust.co.uk/technology/technologyaccelerator/ME_guide2.htm

(01/11/2007)

Falnes J (2005), presentation on wave energy for Noregs University.

Geustyn L. (1983) **“Seegolfenergie langs die Suid-Afrikaanse kus: ‘n Evaluasie van die tyd en ruimtelike verspreiding”**, M.Sc thesis at Stellenbosch University.

Hagerman G. (2001) **“Southern New England wave energy resource potential”**, technical Paper presented at the Building Energy 2001 conference in Boston in March 2001

Hagerman G and Bedard R (2003) **“Guidelines for preliminary estimation of power production by offshore wave energy conversion devices”** technical paper published as E2I EPRI specifications

Holthuijsen LH (2007) **“Waves in oceanic and coastal waters”** book published by Cambridge University Press

Journée JMJ and Massie WW (2001) **“Offshore hydromechanics”** electronic book developed at Delft University.

MacHutchon K. (2006) **“Charaterisation of South African sea storms”**, M.Sc thesis at Stellenbosch University.

Previsic M. (2004) “**Offshore Wave Energy Conversion Devices**” technical paper published as an assessment by E2I EPRI.

Retief G de F, Prestedge GK, Müller FPJ (1982) “**A proposal for wave energy conversion near Cape Town**”, a technical paper published in ICCE, Volume 1 p.245 – 260.

Retief G de F (2007) “**Ocean energy in South Africa**”, a presentation hosted by the Centre for Renewable and Sustainable Energy Studies of the University of Stellenbosch.

Rossouw C (2007), personal communication relating to γ values.

Rossouw C (1999), “**The probability of occurrence and intensity of tropical cyclones along the Southern African east coast**”, MSc thesis at Stellenbosch University.

Rossouw J (1989) “**Design waves for the South African coastline**”, PhD thesis at Stellenbosch University.

Rossouw M (2007), personal communication relating to recorded wave data.

Strasheim A (2007), personal communication relating to computer programming.

The Queen’s University of Belfast (2002) “**Islay LIMPET wave power plant**”, technical report.

Van der Westhuysen A. J (2002) “**The application of the numerical wind-wave model SWAN to a selected filed case on the South African coast**”, Ph.D thesis at Stellenbosch University.

van Tonder A. (1992) “**A software package for the simulation of three-dimensional seastates in the laboratory**”, report on wave generation for physical modelling for the CSIR.

World Meteorological Organisation (WMO) (1998) “**Guide to wave analysis and forecasting**”, coastal engineering guidelines.

APPENDICES

APPENDIX A

Calculation of wave energy and wave power related parameters

A Calculation of wave energy and wave power related parameters

In this section the wave power calculation procedure will be derived from a simplified first principle method and applied to a typical measured wave data record and -spectrum (see Figure A-3 and Figure A-4).

A.1 Derivation of wave energy density for a sinusoidal wave (linear wave theory)

Two special cases are used here:

- (i) A sinusoidal wave reflected 100% from a vertical wall forms a standing wave (Figure A-1). There is a stage in the standing wave cycle when all energy in the wave is potential energy i.e. when no kinetic energy is present in the wave. This occurs at the stage when the standing wave crest and trough are at their maximum deviation from mean level (Figure A-2). The wave energy of one wave length is then contained over a distance of $L/2$. To derive the potential energy over one wave length is a simple procedure as presented below.
- (ii) There also exist a stage of the above standing wave when no water deviation from the mean level exist. During this stage all potential energy in the wave is converted to kinetic energy. The logic conclusion made from (i) and (ii) is that for a normal (non-reflected) sinusoidal linear wave the potential energy = kinetic energy in the wave:

$$E = E_{potential} + E_{kinetic} = \frac{\rho g H^2 L}{8}$$

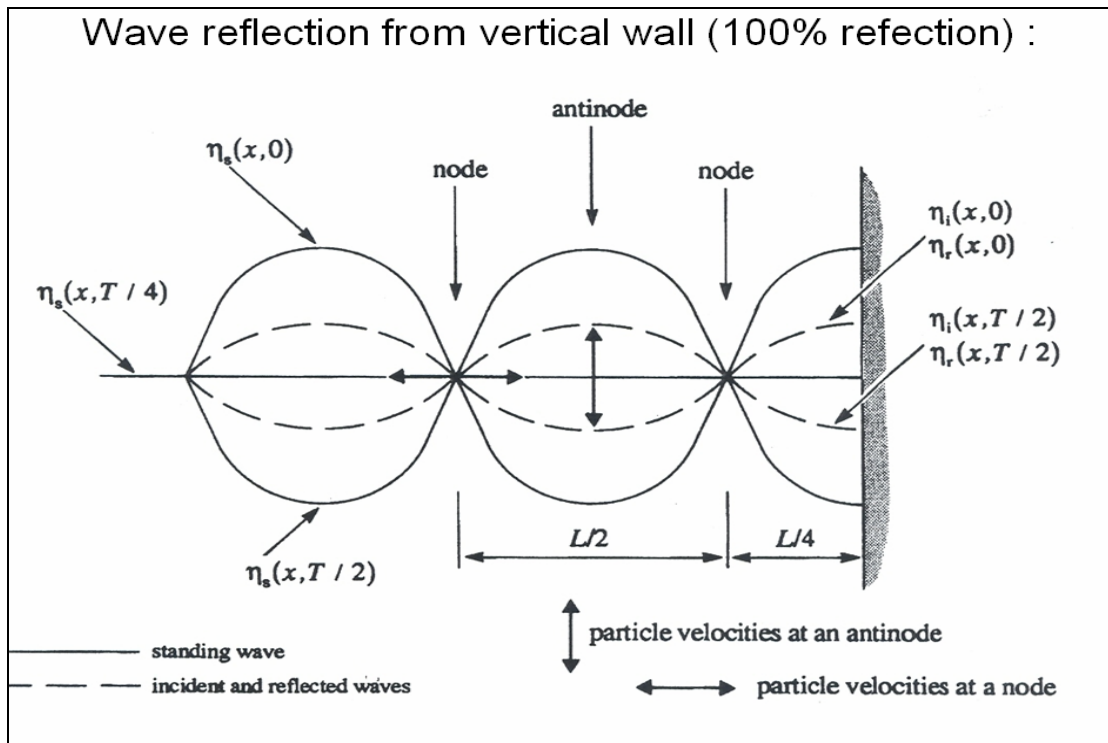


Figure A-1: 100% wave reflection by non-absorbing vertical barrier (Chadwick et.al, 2004)

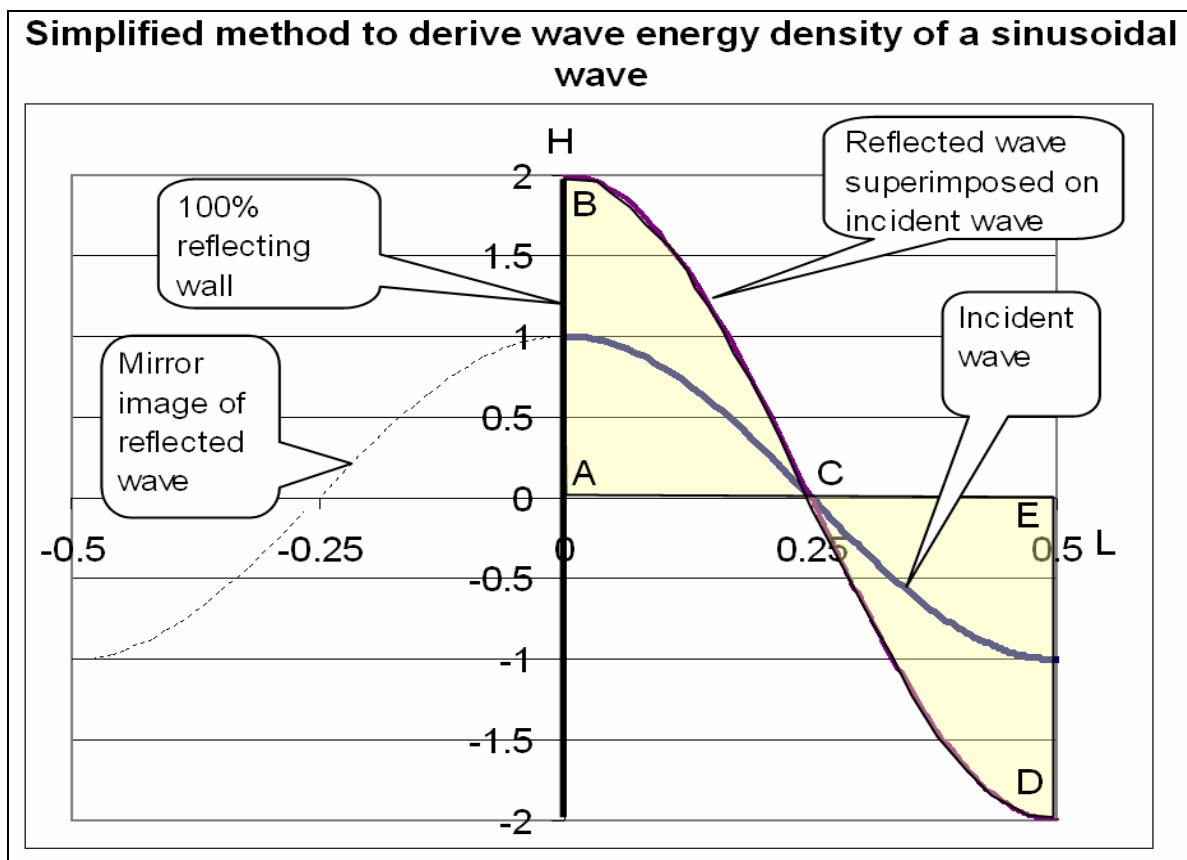


Figure A-2: Superimposed wave due to 100% reflection (Port and Coastal Engineering lecture notes, 2007)

Derivation of energy density

equation

In order to determine the energy density of the superimposed sinusoidal wave when the potential energy is a maximum and the kinetic energy is zero the centre of gravity (CG) is required. In order to determine CG the total area of half of the superimposed wave is determined by:

$$Area = \int_0^{\pi} (H \cdot \sin x) dx$$

$$Area = -[H \cdot \cos x]_0^{\pi}$$

$$Area = -[H \cdot (-1) - (H \cdot (1))] \quad Area = 2.H$$

The first moment of the superimposed wave is determined by:

$$First \ Moment = \int_0^{\pi} \frac{y}{2} dx$$

$$First \ Moment = \int_0^{\pi} (H/2)^2 \cdot \sin^2 x dx$$

$$First \ Moment = \frac{H^2}{4} \cdot [x - \cos x \cdot \sin x]_0^{\pi}$$

$$First \ Moment = \frac{H^2}{4} \cdot [(\pi - \cos \pi \cdot \sin \pi) - (0 - \cos 0 \cdot \sin 0)]$$

$$First \ Moment = \frac{H^2}{4} \cdot [(\pi - 0) - (0 - 0)]$$

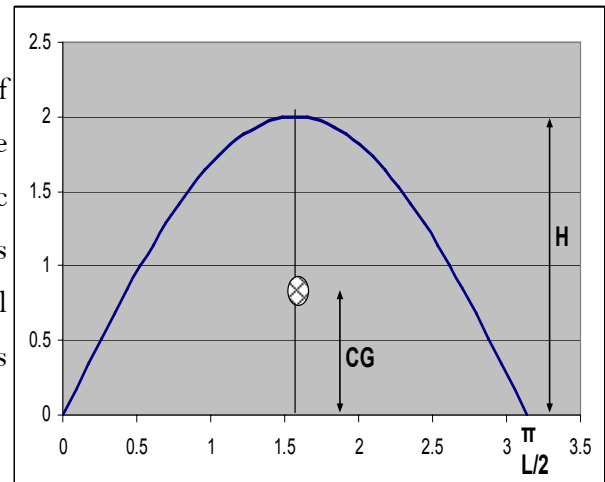
$$First \ Moment = \frac{H^2}{4} \cdot \pi$$

The centre of gravity is defined as $\frac{1stMoment}{Area} = \frac{\frac{H^2}{4} \cdot \pi}{2.H} = \frac{\pi}{8} \cdot H$

At the point of maximum elevation the kinetic energy of the superimposed wave is zero and

$$the \ total \ energy \ of \ the \ standing \ wave \ is \ thus = m \cdot g \cdot h = 2.H \cdot \rho \cdot g \cdot \frac{\pi}{8} \cdot H = 2.H \cdot \rho \cdot g \cdot \frac{L}{8} \cdot H =$$

$$\frac{H^2}{8} \cdot \rho \cdot g \cdot L \text{ in N/meter wave crest}$$



The energy density of the standing wave is defined as: $\frac{H^2}{8} \cdot \rho \cdot g$. in N/m² of unit surface area.

A.2 Root-mean-square wave height (H_{RMS})

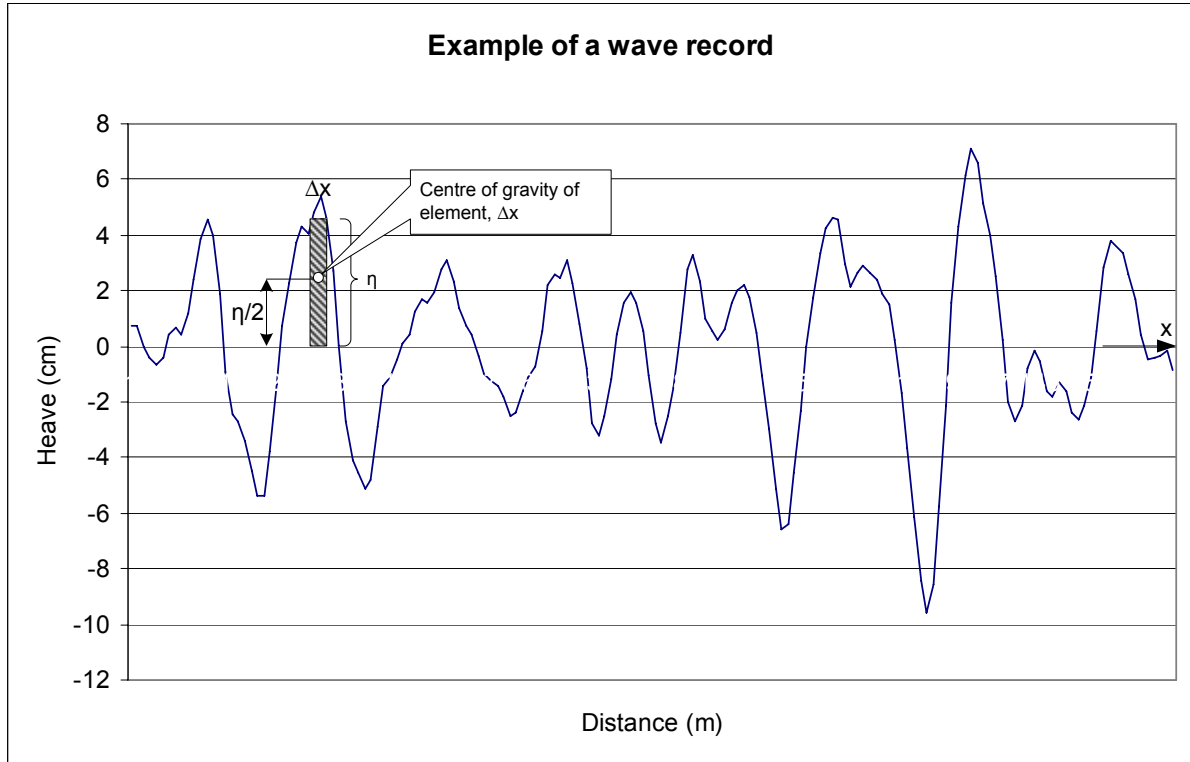


Figure A-3: Typical “snap-shot” of an ocean wave train

In order to determine the wave energy density and consequent wave power of a wave train (“snap-shot”) an equivalent, regular wave height (H_{eq}) is required containing the same wave energy density as the measured irregular wave record. In this section an equation for H_{eq} will be derived by dividing the recorded surface elevation into a series of finite elements and then determining the total energy density of the wave train through the summation of the energy density of all elements of the wave train. Considering an element of length (Δx), mean height (η) and 1 meter crest width (refer to Figure A-3):

$$\text{Volume of water element, } \Delta x, \text{ per meter wave crest} = V = \Delta x \eta$$

$$\text{Potential energy} = E_p = \Delta x \eta \frac{\eta}{2} \rho g$$

Since E_p = E_k:

$$\text{Energy density per meter wave crest in one } \Delta t \text{ element} = \bar{E} = \Delta x \eta^2 \rho g$$

$$\text{Energy density of the entire time series} = \bar{E} = \frac{\sum \Delta x \eta^2}{N \Delta x} \rho g = \frac{\sum \eta^2}{N} \rho g = \sigma^2 \rho g$$

$$\text{From (CEM, 2002)} \quad \bar{E} = \frac{H_{eq}^2}{8} \rho g = \sigma^2 \rho g$$

$$\text{Therefore: } \frac{H_{eq}^2}{8} = \sigma^2$$

$$\text{Equivalent energy wave height} = H_{eq} = \sqrt{8\sigma^2} = 2\sqrt{2}\sigma \quad \text{Eqn. A- 1}$$

$$\text{From (CEM, 2002) significant wave height} = H_s \approx 4\sigma \quad \text{Eqn. A- 2}$$

$$\text{Relationship between } H_{eq} \text{ and } H_s \text{ from Eqn. A- 1 and Eqn. A- 2: } H_{eq} = \frac{H_s}{\sqrt{2}}$$

H_{eq} is referred to as H_{RMS} in the literature (WMO, 1998).

A.3 A comparison of wave power results obtained by numerical integration and defined power calculation procedure

The accuracy of the wave power calculation procedure is investigated by comparing the results obtained by the procedure, as employed throughout the study and outlined in §2.4.6, to that of numerical integration over each frequency bin of the recorded wave spectrum.

The two methods are compared by calculating wave power for the dominant wave spectrum of Slangkop recording station (see Figure A-4 below). The dominant wave parameters include: $H_s = 3\text{m}$, $T_p = 12\text{s}$ and $\gamma = 3.3$. The frequency range considered is 0.03 to 1 Hz, divided into frequency intervals of 0.005 Hz.

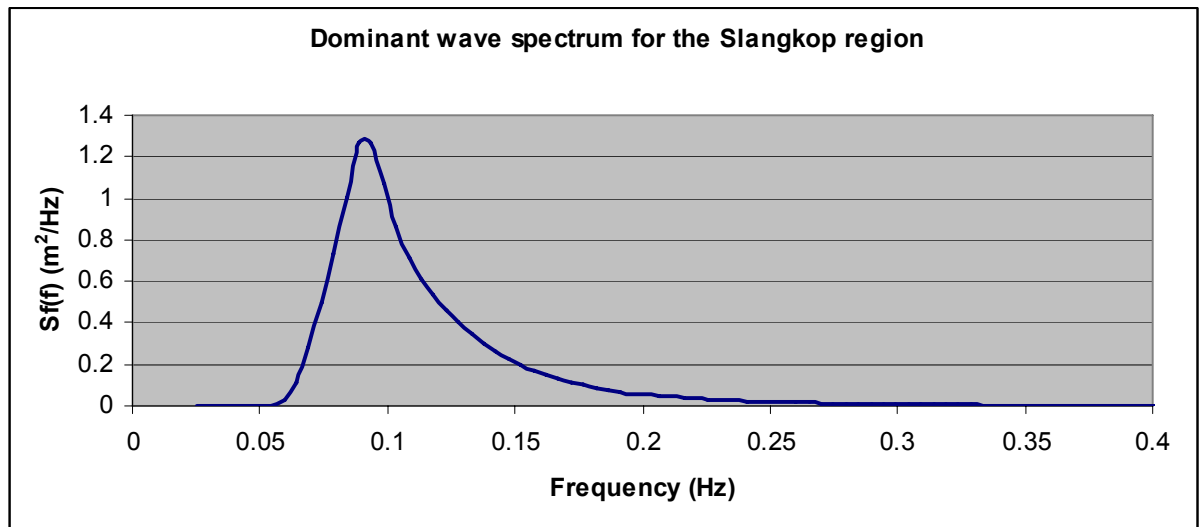


Figure A-4: Dominant measured wave spectrum for Slangkop

It was assumed that deep sea wave conditions apply and wave power for each frequency bin was therefore determined by:

$$P_i = E_i C_{gi} = S_f(f_i) \Delta f \rho g \frac{g}{4\pi f_i}$$

The total power of the measured spectrum is determined through the summation of the wave power contained in each frequency bin. The results obtained through integration (direct method) and the defined calculation procedures are presented in Table A-1 below. A good comparison between the two methods for the case investigated here was found (only a 0 to 0.02% difference in wave power). Calculating wave power using H_s and T_e was included to indicate that this parameter greatly overestimates the actual wave power of a measured wave spectrum even though it is used in the various literature sources to determine wave power. The comparison of the case here also confirms that the energy period (T_e) better represents the wave power of a wave spectrum compared to peak period (T_p).

Table A-1: Wave power calculation results

Defined calculation procedure used in this study							Direct method
H_{RMS}	E_{RMS}	E_s	T_e	C_{og}	P_{RMS}	P_s	P
2.12	5.66	11.31	10.84	8.46	47.86	95.72	47.87

APPENDIX B

Design wave heights at wave recording stations along the South African coast as determined by (MacHutchon, 2006)

B Design wave height conditions

Design wave height conditions at the wave recording stations are presented in Figure B – 1 to B - 4 (MacHutchon, 2006) for the purpose of survivability of selected WEC units at different locations on the South African coastline.

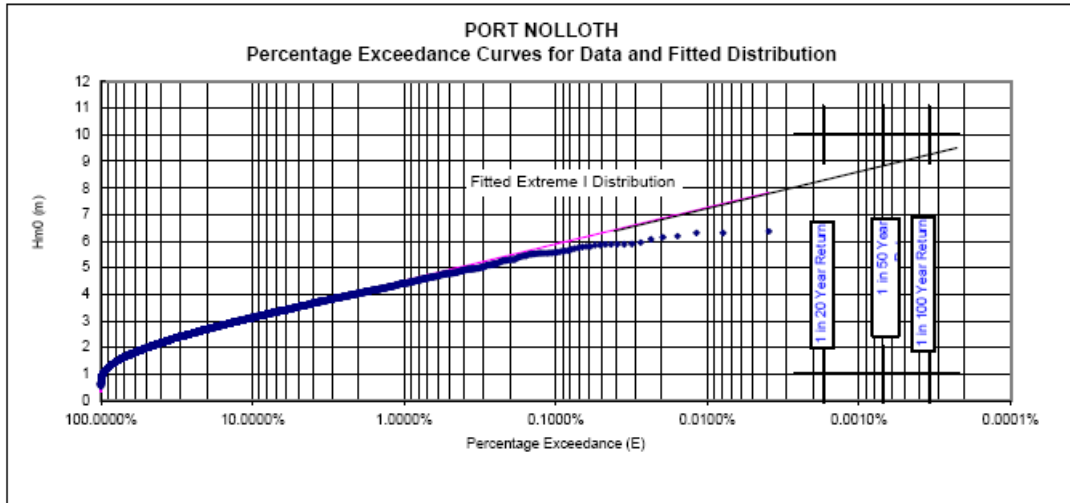


Figure B-1: Design wave heights for Port Nolloth recording station

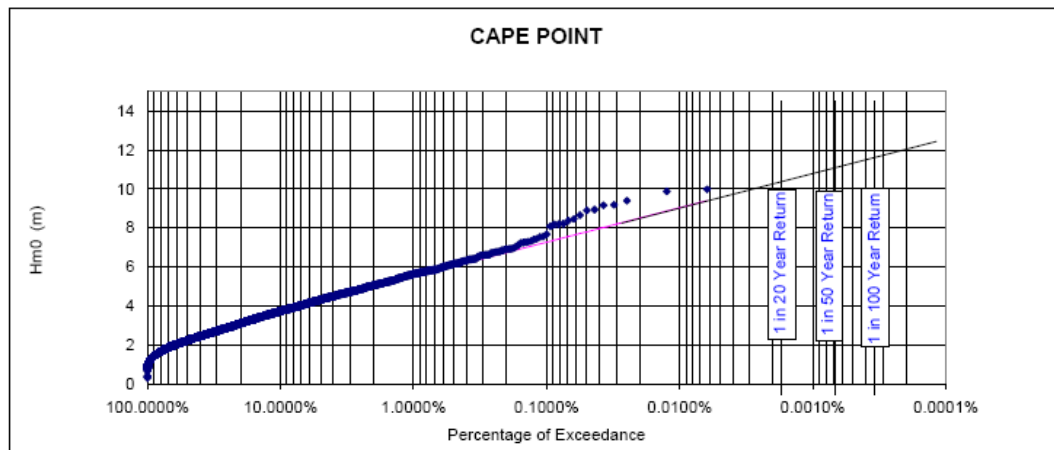


Figure B-2: Design wave heights for Cape Point recording station

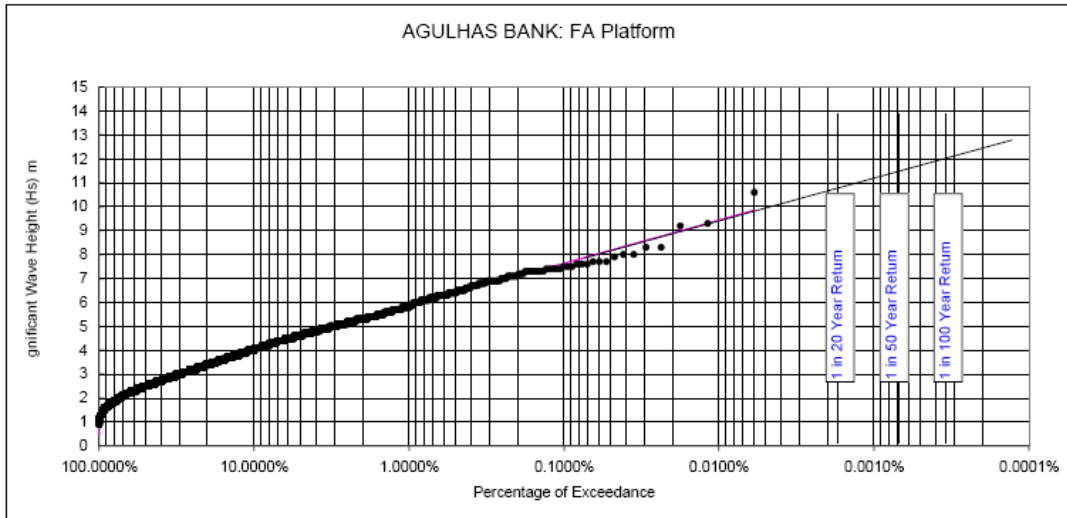


Figure B-3: Design wave heights for FA platform wave recording station

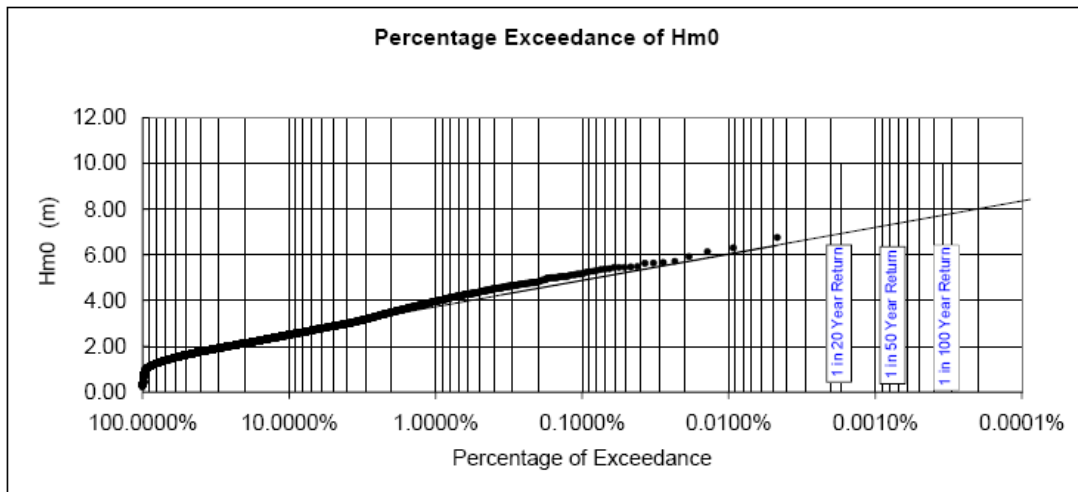


Figure B-4: Design wave heights for Durban recording station

APPENDIX C

Monthly wave power distribution at wave recording stations

C Comparison of mean monthly wave power distribution at wave recording stations

The mean monthly average wave power at each wave recording station is presented in Figure C-1 below. Figure C-1 indicates that Slangkop recording station has the highest average wave power for the majority of the months. Figure C-1 is also an indication of the seasonal and annual variability of wave power.

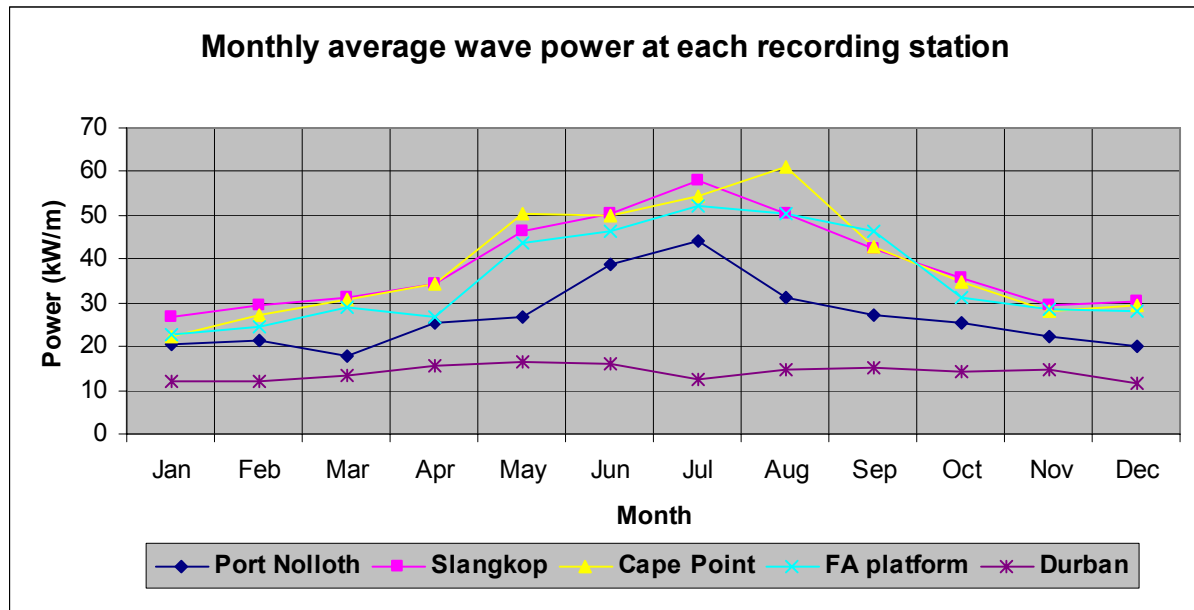


Figure C-1: A comparison of monthly average wave power

The standard deviation of monthly wave power at each wave recording station is presented below in Figure C-2. Figure C-2 indicates large variability in wave power during the winter months.

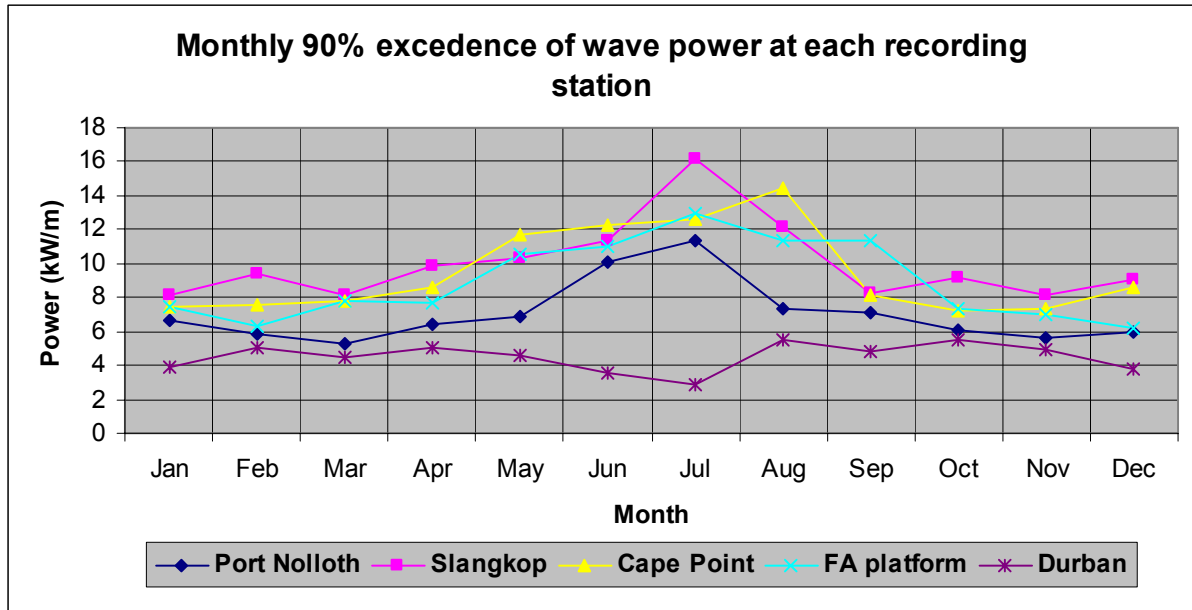


Figure C-2: Comparison of monthly 90% probability of exceedence of wave power

The 90% probability of exceedence of monthly wave power at all the wave recording stations are presented below in Figure C-3. Figure C-3 again indicates that Slangkop recording station has the highest wave power resource for the majority of the year.

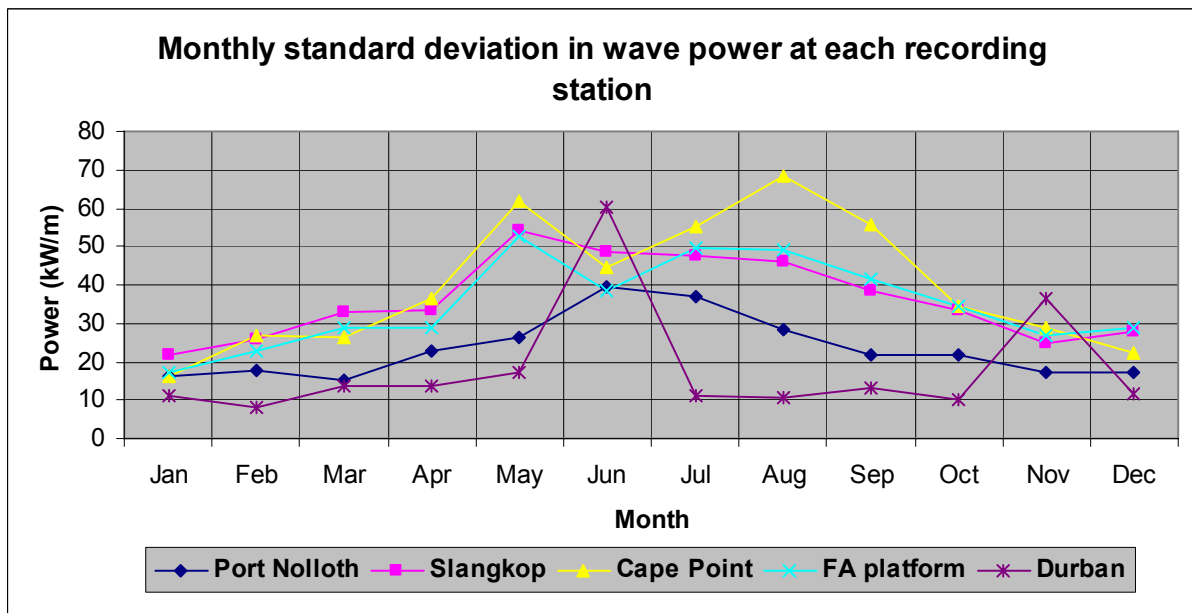


Figure C-3: Comparison of monthly standard deviation of wave power

APPENDIX D

Validation and sensitivity analysis of simplified simulation procedure
and the consequential impact on energy dissipation

D Sensitivity analysis of numerical modelling exercise

It was mentioned in § 4.5 that the most significant assumption used in the simulation process was that wave height variation is independent of the input wave height. It was indicated that this assumption is influenced by energy dissipation processes such as bottom friction, white-capping and depth induced-breaking. The influence of the dissipation processes on wave power was investigated by comparing the results of the simulation of general wave conditions by the direct- and simplified simulation procedure (methodology 1 and 2 as outlined in Figure 4-6). The general wave conditions were determined from the Base data and comprise of a range of H_s , T_p and D_p values.

D1 Wave conditions and comparative locations

Significant wave height (H_s)

The average and median wave heights of the Base data represent the dominant wave height conditions. There is a relatively small difference of 0.1m between these two values and it was therefore opted to simulate the median value of 2.6m. The frequency of occurrence of wave heights at Base showed that the most frequently occurring H_s values ranges from 2 to 3m. It was also decided to simulate the 10% probability of exceedance wave height of 4m, to investigate energy dissipation during extreme events. It is expected that this larger wave height will loose more energy to the dissipation processes than the median value.

Peak period (T_p)

From the data analysis in Chapter 3 and the scatter analysis in § 4.3.2, it is clear that the dominant wave period propagating from the storms in the southern ocean is equal to 12s. It was thus decided to simulate the dominant T_p values of 10, 12 and 14s.

Peak direction (D_p)

The analysis of the directional wave data at Base in § 4.3 indicated that the dominant wave direction from the South Atlantic Ocean generation zone is from the south west. South west and west-south west peak direction was therefore simulated. With the general wave conditions defined, all that remains is to define locations in the study area at which to compare results.

Comparative locations

Energy dissipation processes (especially bottom friction and depth induced-breaking) are depth dependent and it is expected that the model will overestimate wave power in shallow water. The impacts of energy dissipation relative to water depth were investigated by considering wave power at locations in deep-, intermediate- and shallow water depths. The effect of dissipation at a sheltered location was also considered. These locations, and its UTM coordinates, considered in this sensitivity analysis are shown in Figure D-1 and Table D-1.

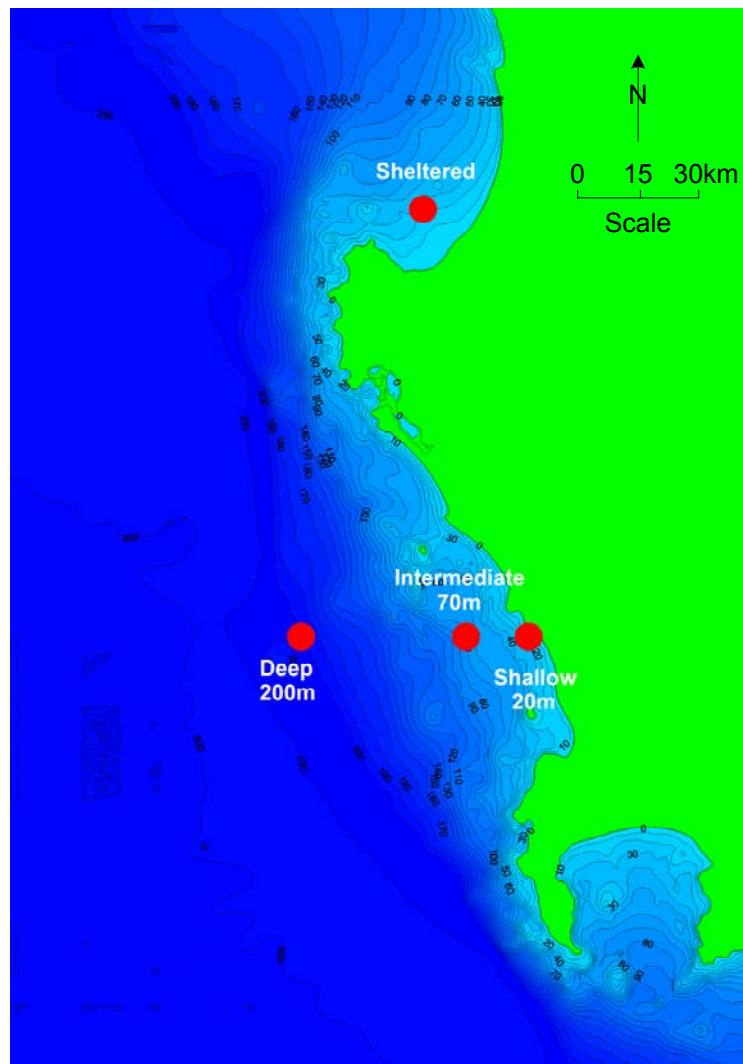


Figure D-1: Locations in deep, intermediate, shallow and sheltered water considered in the sensitivity analysis

Table D-1: UTM coordinates of comparative locations

Location	Easting	Northing	Depth (m)
Deep	190 000	6 325 500	201
Intermediate	211 000	6 325 500	72
Shallow	222 000	6 325 500	21
Sheltered	229 000	6 385 500	21

D2 Results of sensitivity analysis of simulation methodology

To recap, a brief description of method 1 and 2 is presented below.

- **Method 1** (unschematised method): actual wave height is used in the simulation process
- **Method 2** (schematised/simplified method): 1m wave height is used to determine ratio: H/H_{BASE} and H is then derived from this ratio with actual wave height at Base (H_{BASE}). Refer to Figure 4-6 for detailed method description.

The wave power as determined by method 1 and 2 at the deep-, shallow water and sheltered location for H_s equal to 2.6m is presented in Figure D-2 to Figure D-4 below. These figures indicate that the model (Method 2) slightly overestimates wave power for short period conditions ($T_p = 10s$), but is sufficiently accurate for longer period waves. The difference could be due to the lower allowed wave steepness for short period waves, but is most likely caused by energy dissipation through bottom friction. The bottom friction source term in § 4.5 indicates that it is dependent on $1/\sinh^2(kd)$. Short period waves have short wave lengths which reduces k , which reduces $\sinh(kd)$ and so doing increases the bottom friction source term.

The results also indicate that the model's overestimation of wave power increases for shallower water depths, confirming greater energy dissipation in shallow water regions. It is interesting to note that the wave power at the shallow water location is of a greater magnitude than at the deep water location. This is due to local bathymetric conditions and is confirmed in Figure 4-17 which indicates the average annual wave power resource of the study area. Figure D-4 indicates that greater wave power propagates towards St Helena Bay from west-south west swell than from south west. This is due to the Cape Columbine landmass blocking the south west swells.

The percentage difference in wave power, as determined by method 1 and 2, for the general wave conditions at the comparative locations is presented in Table D-2 below.

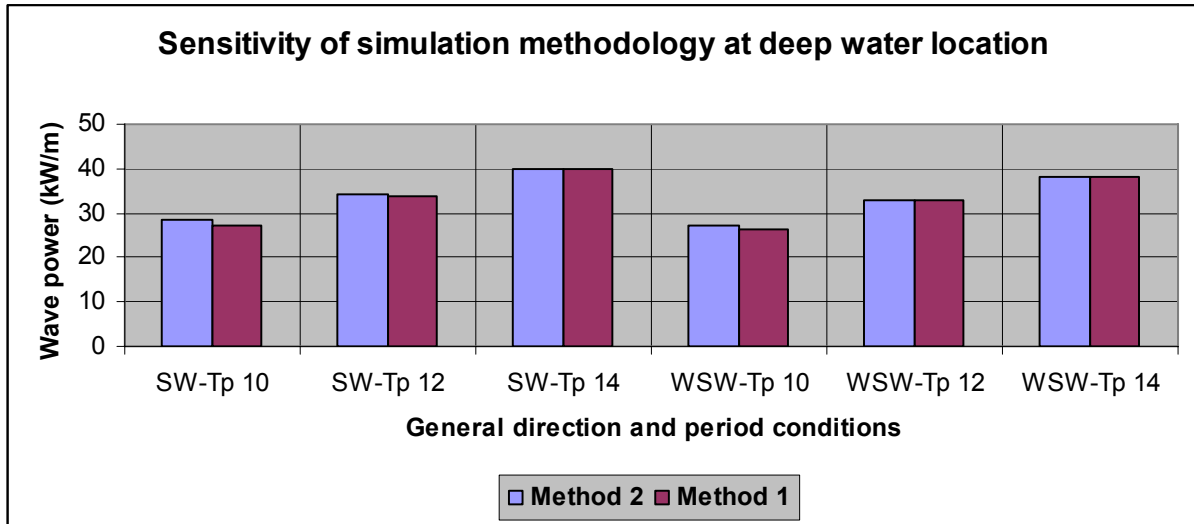


Figure D-2: Wave power at deep water location as determined by method 1 and 2 for $H_s = 2.6\text{m}$

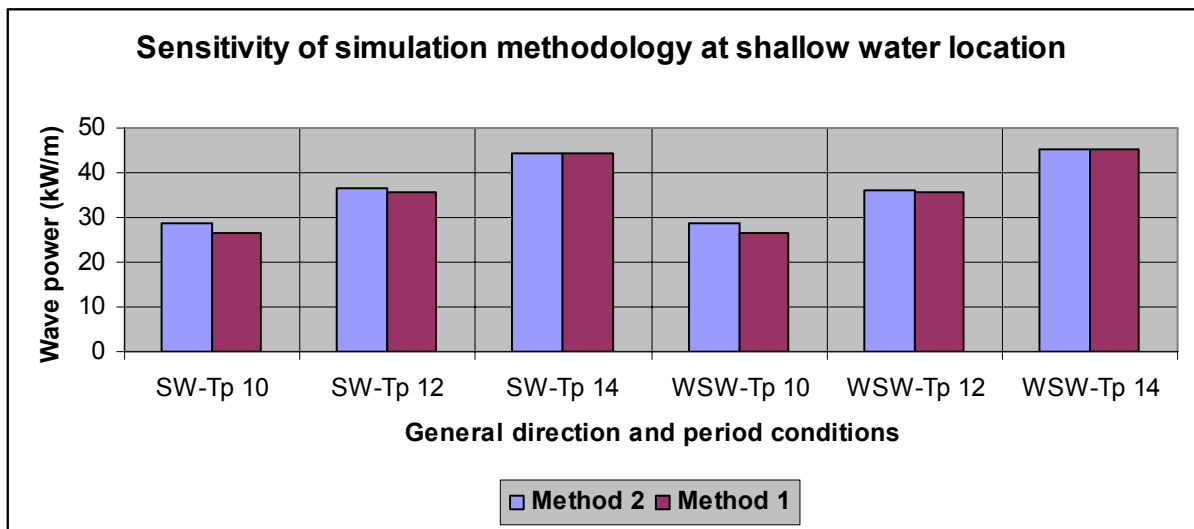


Figure D-3: Wave power at shallow water location as determined by method 1 and 2 for $H_s = 2.6\text{m}$

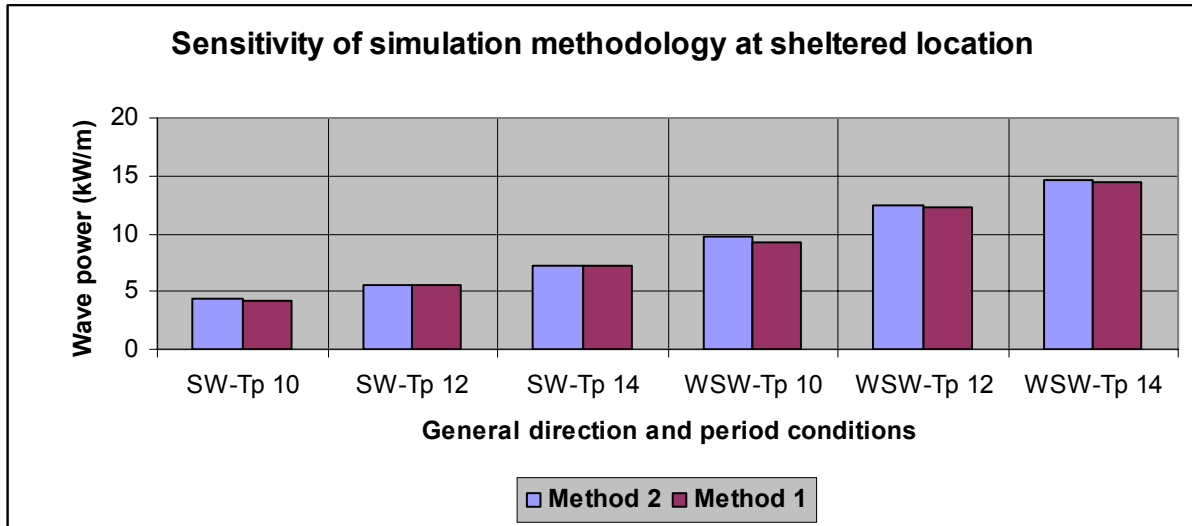


Figure D-4: Wave power at sheltered location as determined by method 1 and 2 for Hs = 2.6m

Table D-2 below indicates that the greatest overestimation of wave power occurs at the shallow water location for short period wave conditions. Table D-2 also shows that the model’s overestimation of wave power increases for greater wave heights with a maximum overestimation of 31% for the extreme wave height of 4m. 90% of the simulated wave height conditions are however smaller than 4m. The results of the sensitivity analysis indicate that the simplified simulation procedure produces sufficiently accurate estimates of wave power for the dominant wave conditions and the bulk of the data to be simulated.

Table D-2: Percentage overestimation of wave power as determined by method 2

	Hs = 2.6m				Hs = 4m			
	Deep	Inter	Shallow	Shelter	Deep	Inter	Shallow	Shelter
SW-Tp10	5%	8%	9%	5%	20%	28%	31%	19%
SW-Tp12	1%	2%	2%	1%	5%	8%	9%	8%
SW-Tp14	0%	0%	1%	1%	1%	2%	3%	7%
WSW-Tp10	4%	7%	9%	6%	16%	24%	28%	19%
WSW-Tp12	1%	2%	2%	2%	4%	7%	8%	7%
WSW-Tp14	0%	0%	0%	1%	1%	2%	2%	4%

The concluding portion of the sensitivity analysis deals with the investigation into the input peak-enhancement factor (γ) and its impact on wave power.

D3 Impact of the peak-enhancement factor (γ) on wave power

The impact of the peak-enhancement factor (γ) on wave power was investigated by comparing the results of an empirical relationship of γ and T_p (personal communication C. Rossouw, 2007) and a second order polynomial derived from the measured γ -values of Cape Point recording station to a constant γ -value of 1.5. The empirical relationship of Rossouw and the measured relationship are presented below as Eqn. D- 1 and Eqn. D- 2, respectively.

$$\gamma = 0.0002T_p^2 + 0.0193T_p + 0.9754 \quad \text{Eqn. D- 1}$$

$$\gamma = -0.0126T_p^2 + 0.4149T_p + 0.8512 \quad \text{Eqn. D- 2}$$

Table D-3 below indicates the various γ -values as determined by Eqn. D- 1 and Eqn. D- 2. Employing method 1 and comparing the results of wave power at the comparative locations, as defined in the previous section, indicates that wave power is insensitive to such small variation of γ with virtually 0% difference in wave power for the various γ -values. A constant γ -value of 1.5 was therefore deemed acceptable for the numerical modelling process.

Table D-3: Peak-enhancement factor values

T_p	Rossouw	Measured	Assumed
6	1.1	1.2	1.5
8	1.1	1.7	1.5
10	1.2	2.0	1.5
12	1.2	2.3	1.5
14	1.3	2.5	1.5
16	1.3	2.6	1.5
18	1.4	2.5	1.5
20	1.4	2.4	1.5

APPENDIX E

Wave height conditions on model boundaries for concurrent wave
period and –direction conditions

APPENDIX F

Spatial maps of monthly average wave power of the study area

F Mean monthly average wave power distribution

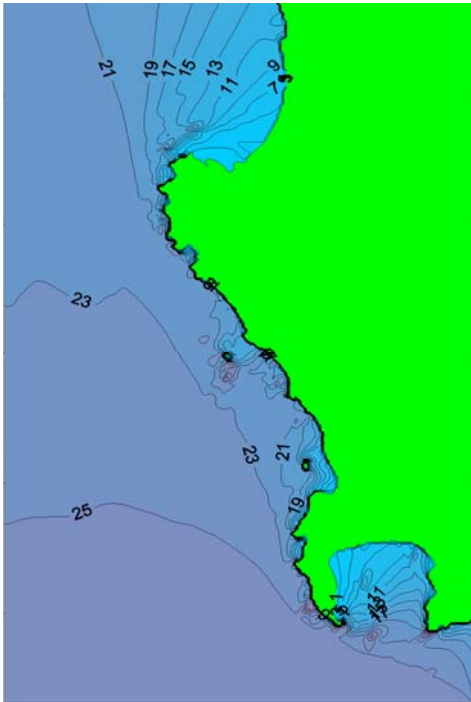


Figure F-1: Mean monthly average wave power distribution (kW/m) for January

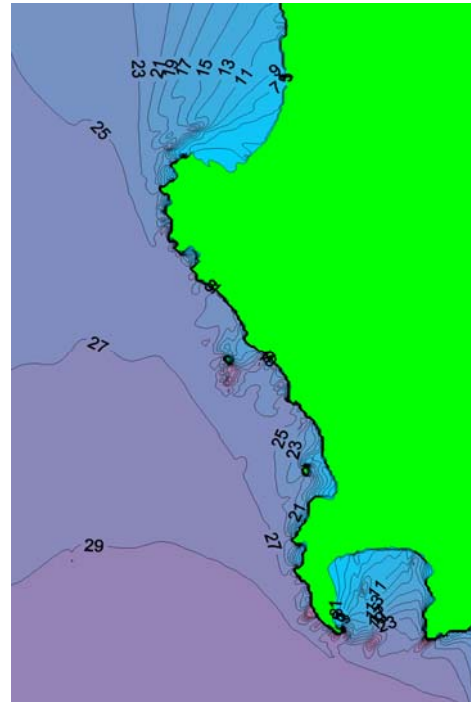


Figure F-2: Mean monthly wave average power distribution (kW/m) for February

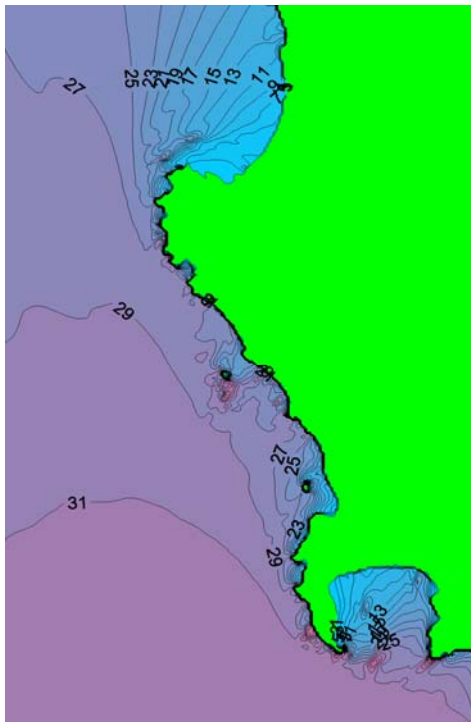


Figure F-3: Mean monthly average wave power distribution (kW/m) for March

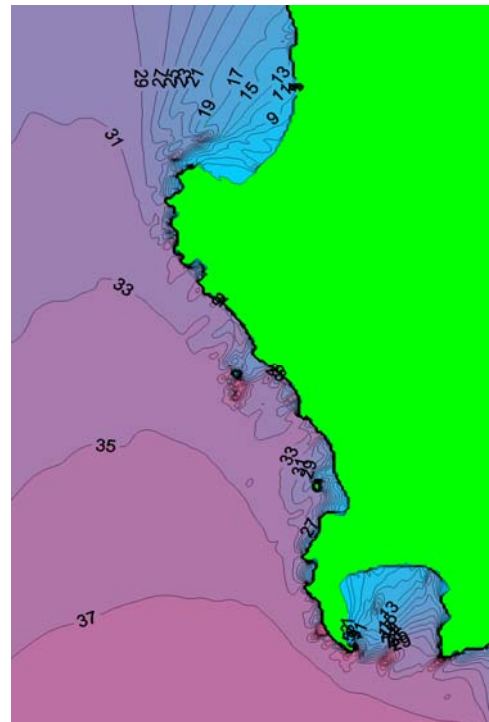


Figure F-4: Mean monthly average wave power distribution (kW/m) for April

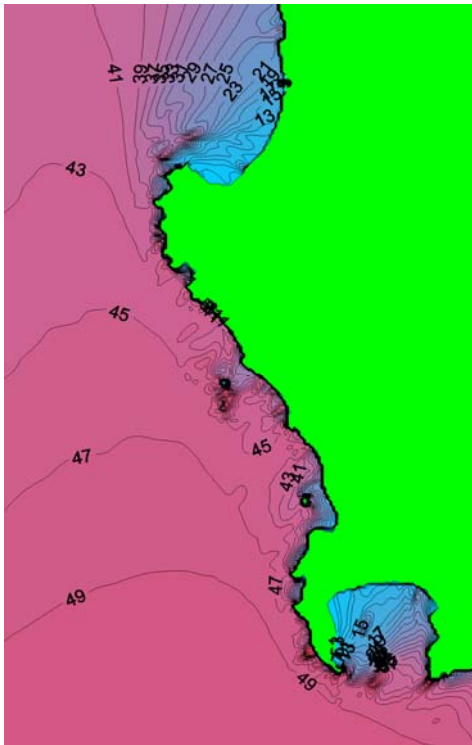


Figure F-5: Mean monthly average wave power distribution (kW/m) for May

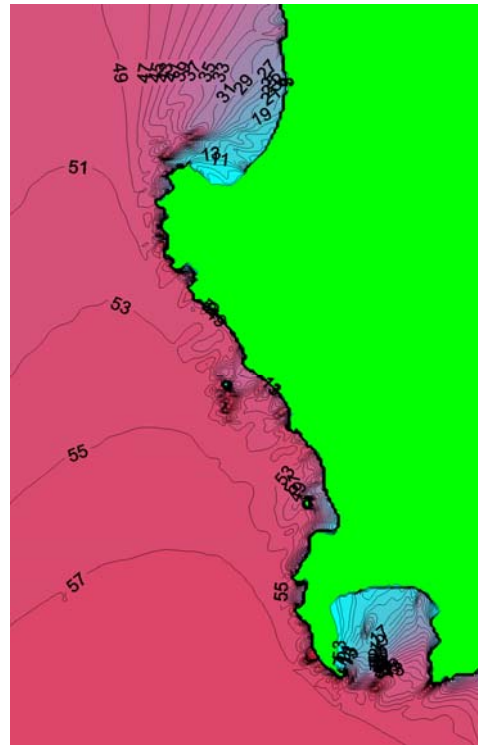


Figure F-6: Mean monthly average wave power distribution (kW/m) for June

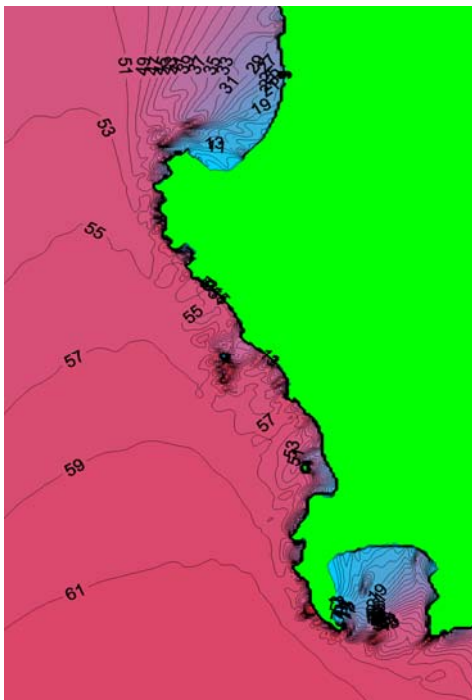


Figure F-7: Mean monthly average wave power distribution (kW/m) for July

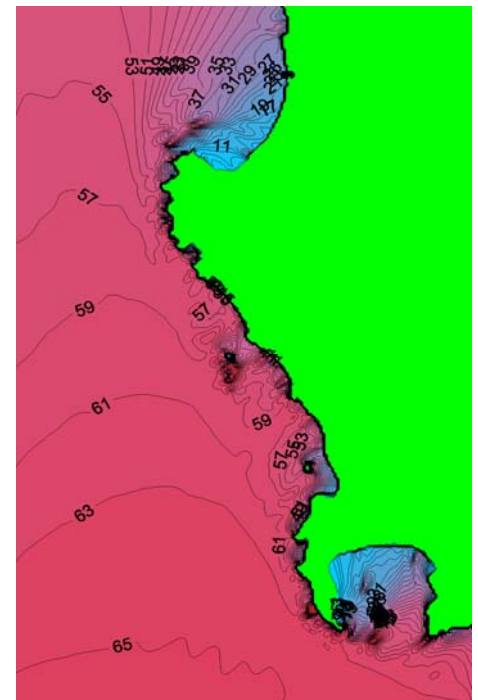


Figure F-8: Mean monthly average wave power distribution (kW/m) for August

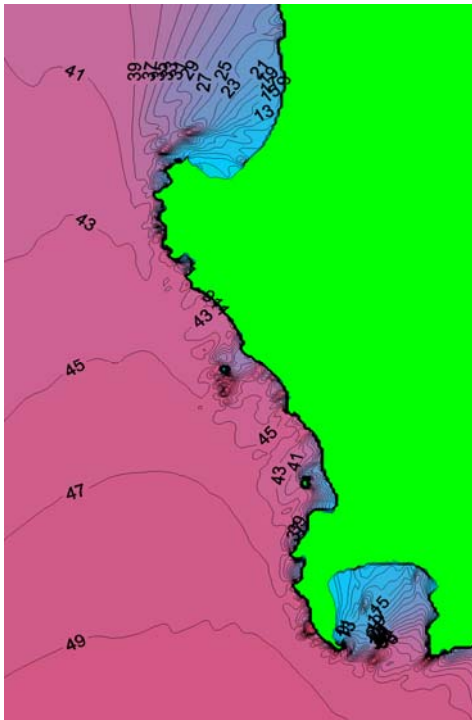


Figure F-9: Mean monthly average wave power distribution (kW/m) for September

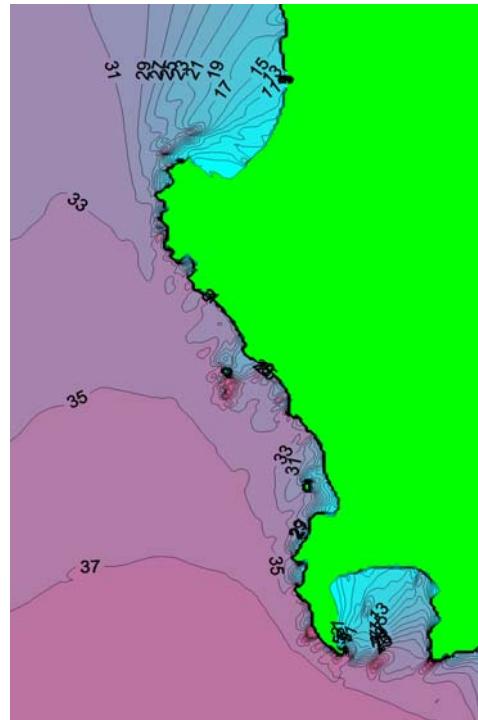


Figure F-10: Mean monthly average wave power distribution (kW/m) for October

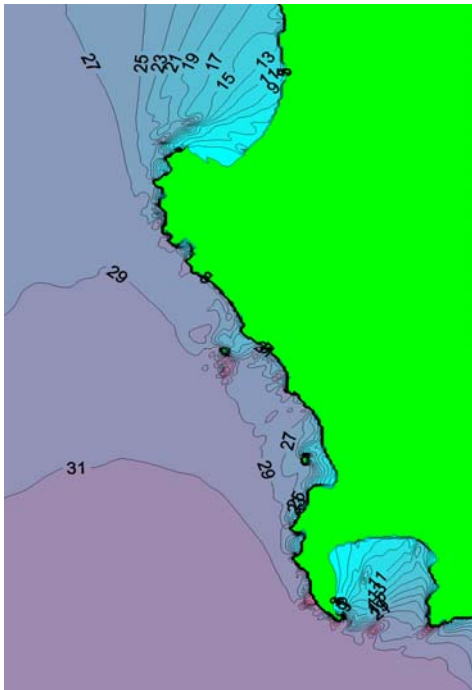


Figure F-11: Mean monthly average wave power distribution (kW/m) for November

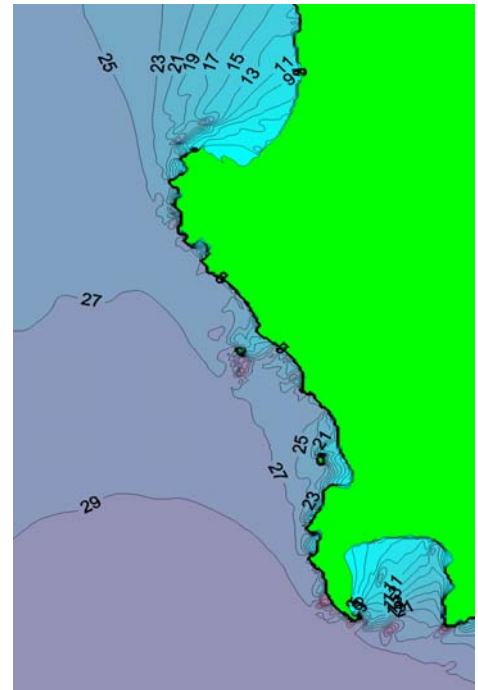
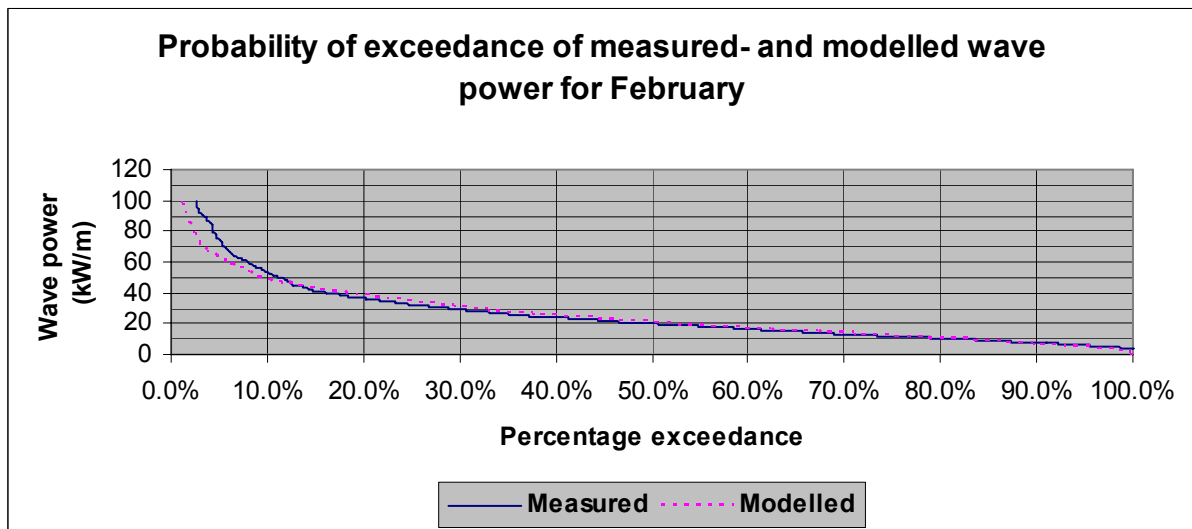
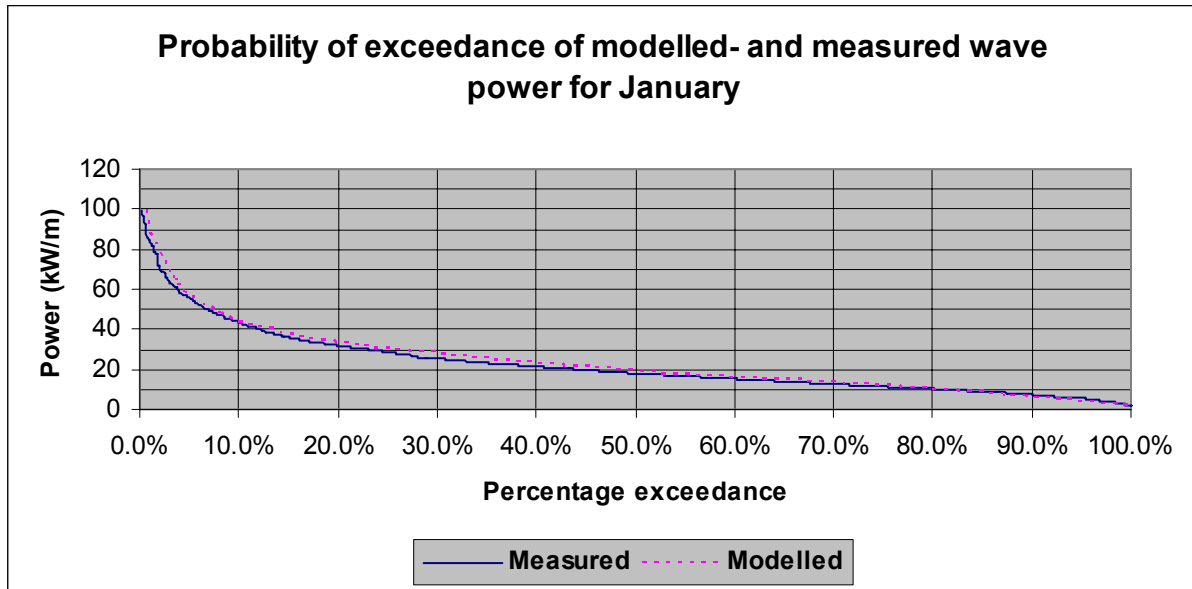


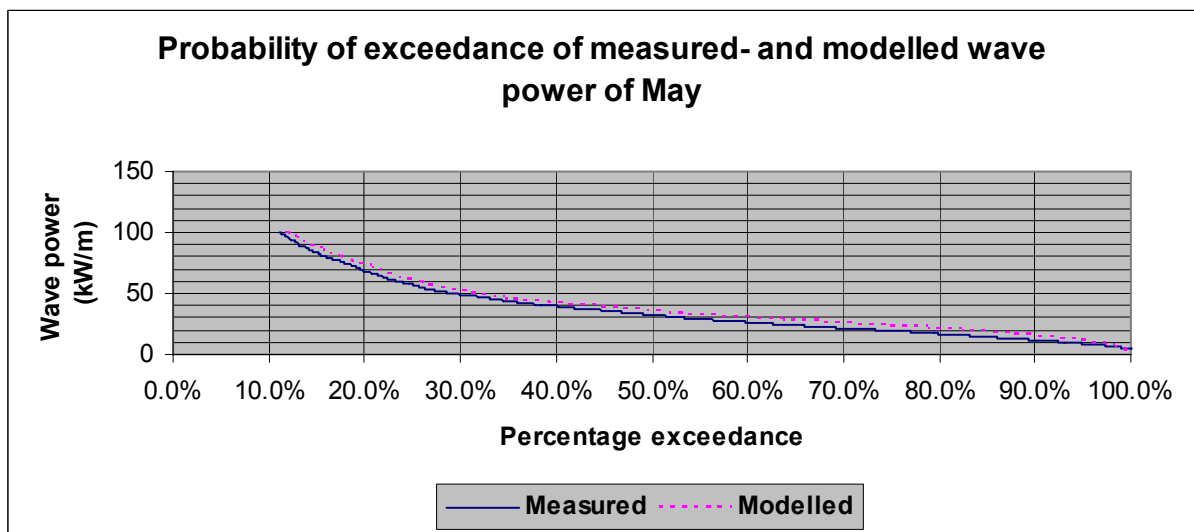
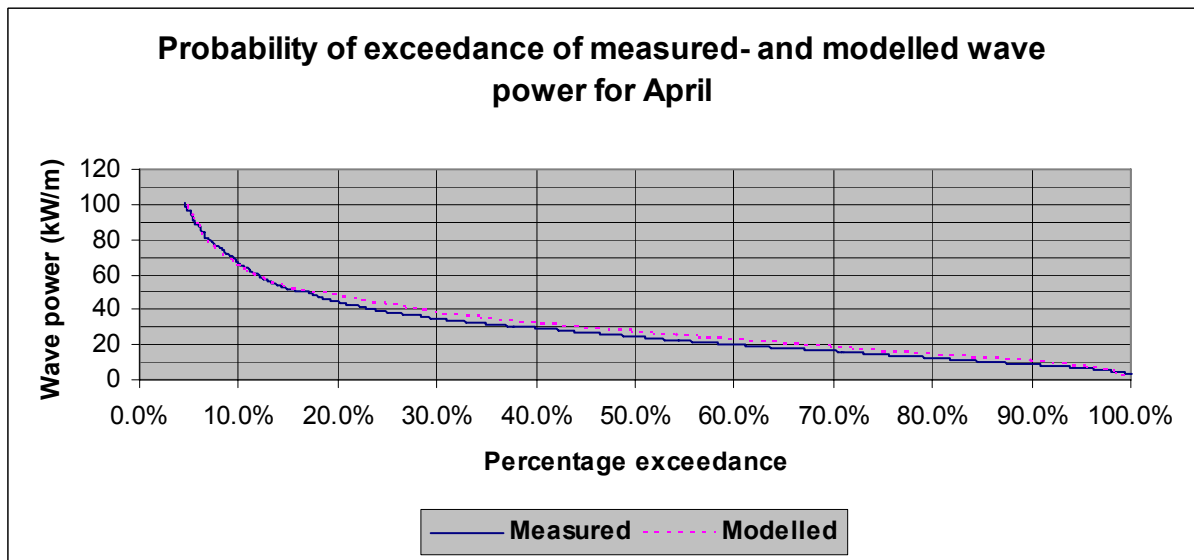
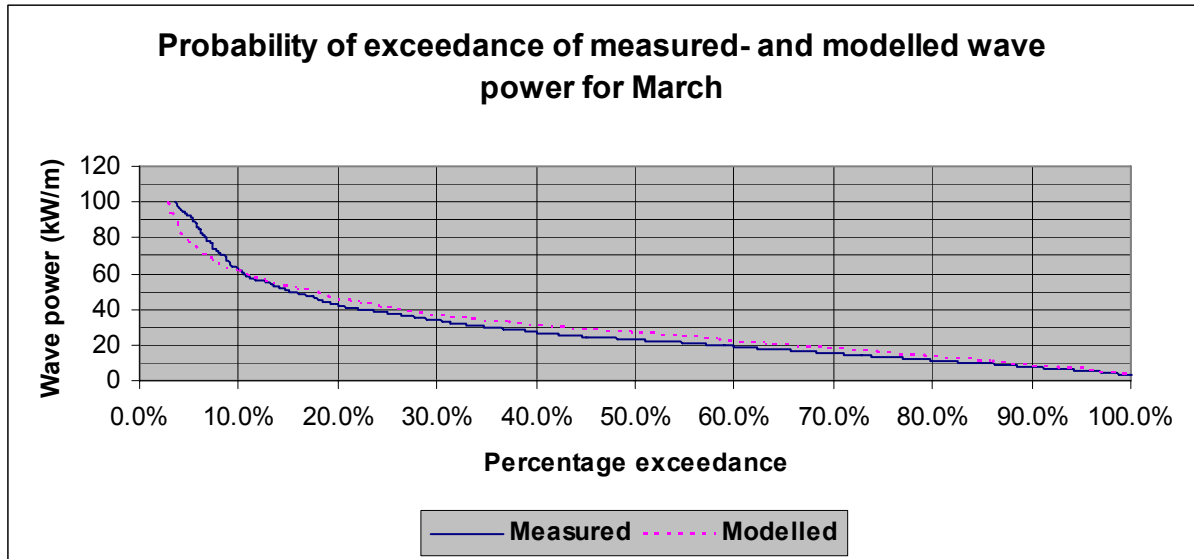
Figure F-12: Mean monthly average wave power distribution (kW/m) for December

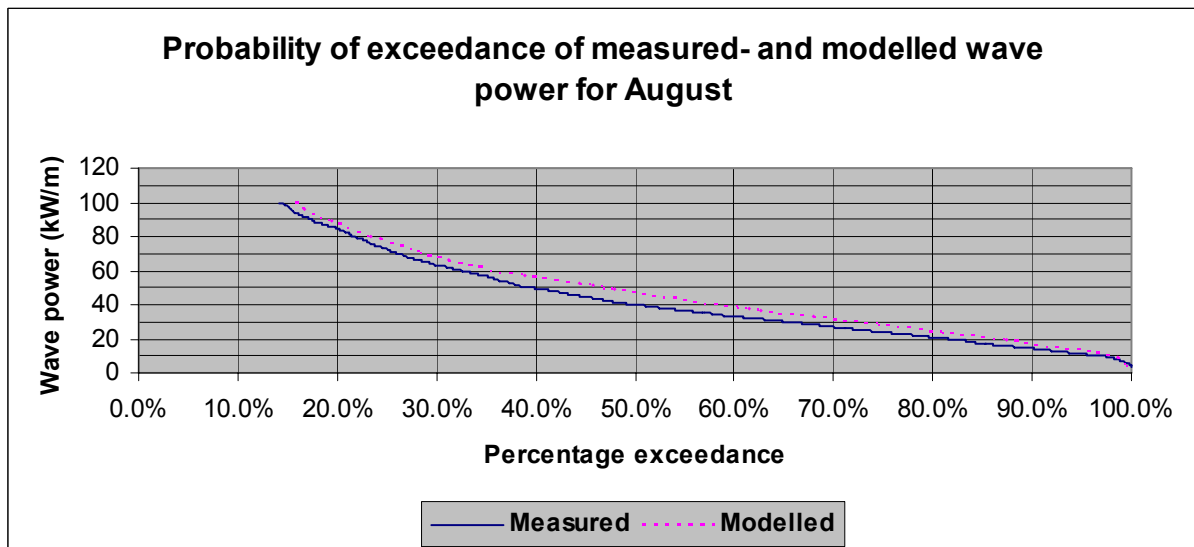
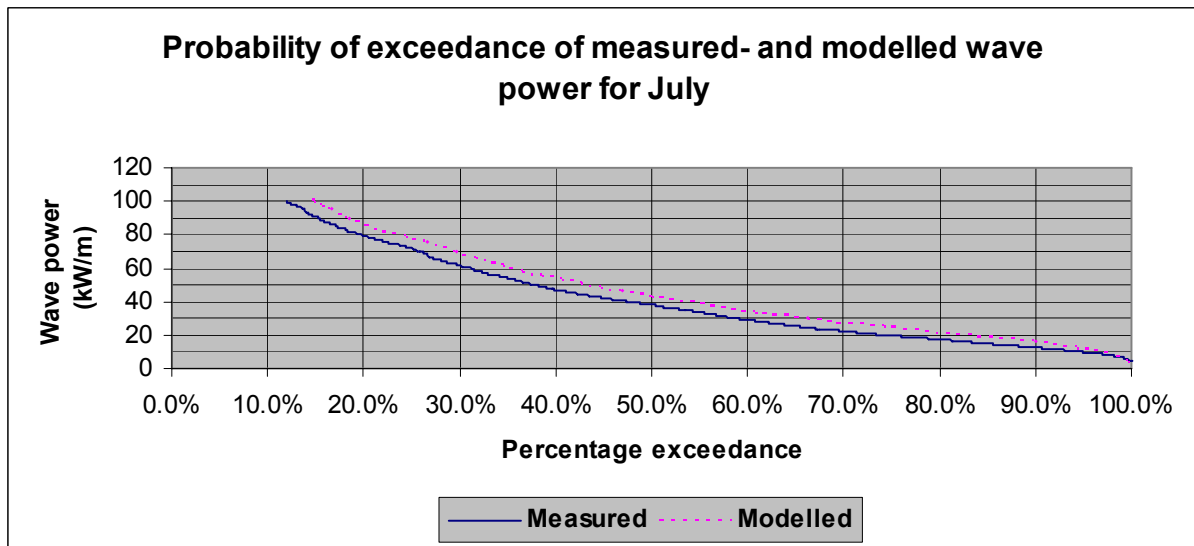
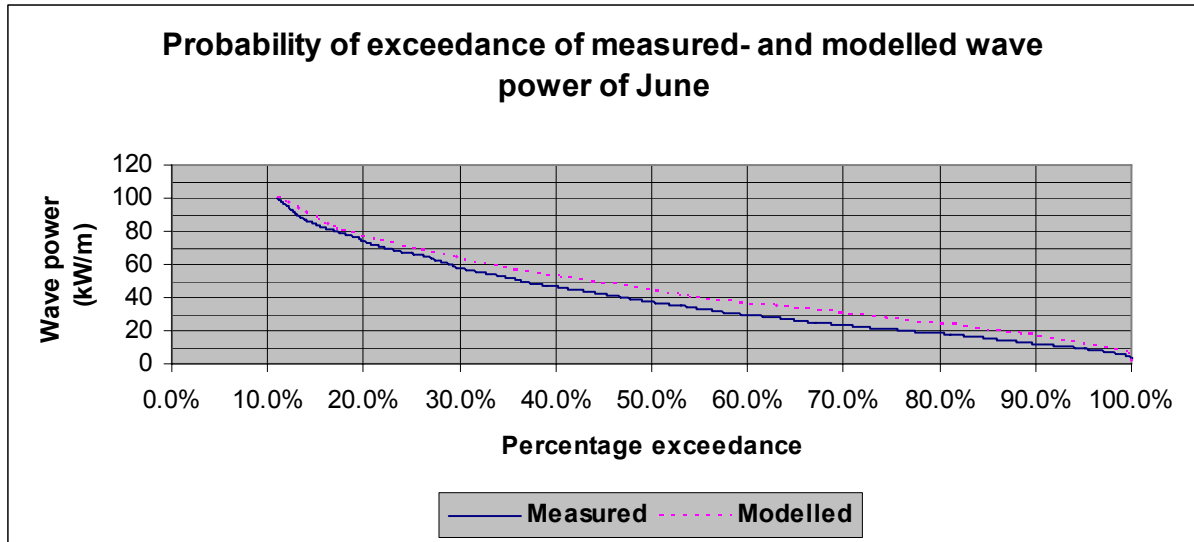
APPENDIX G

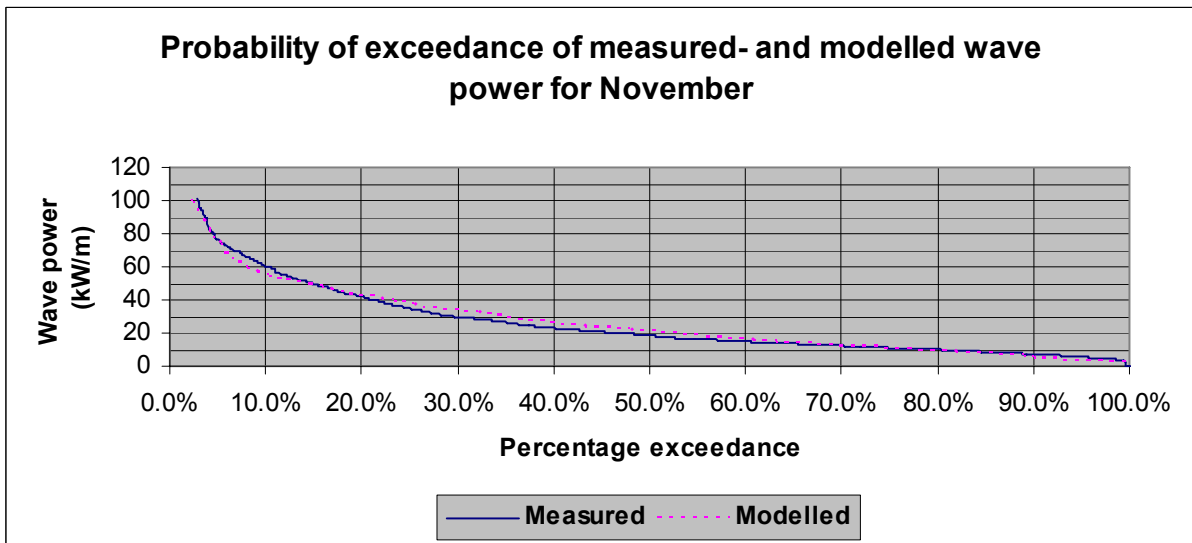
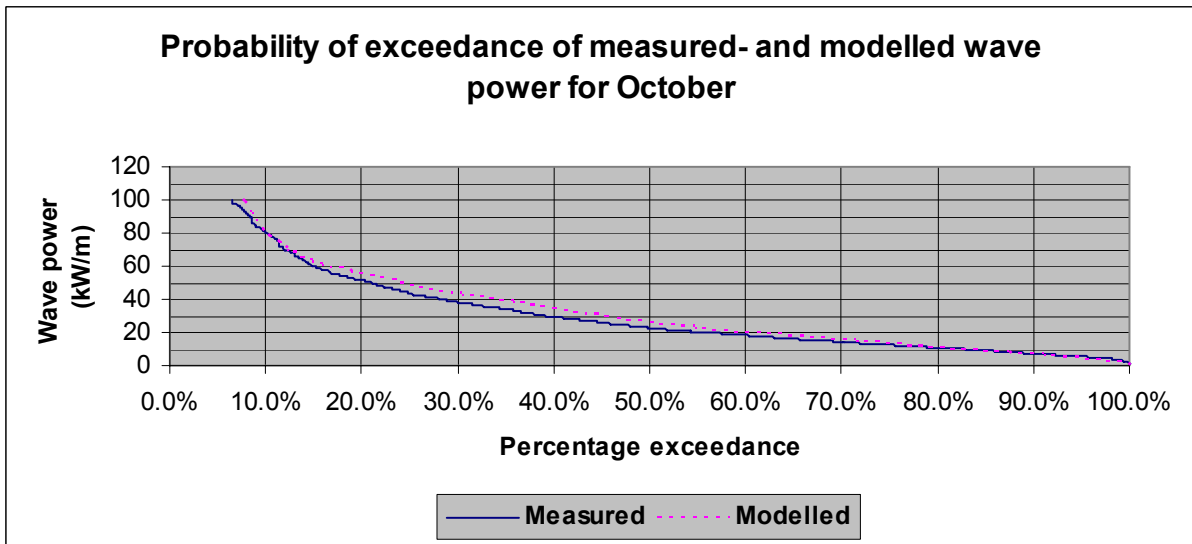
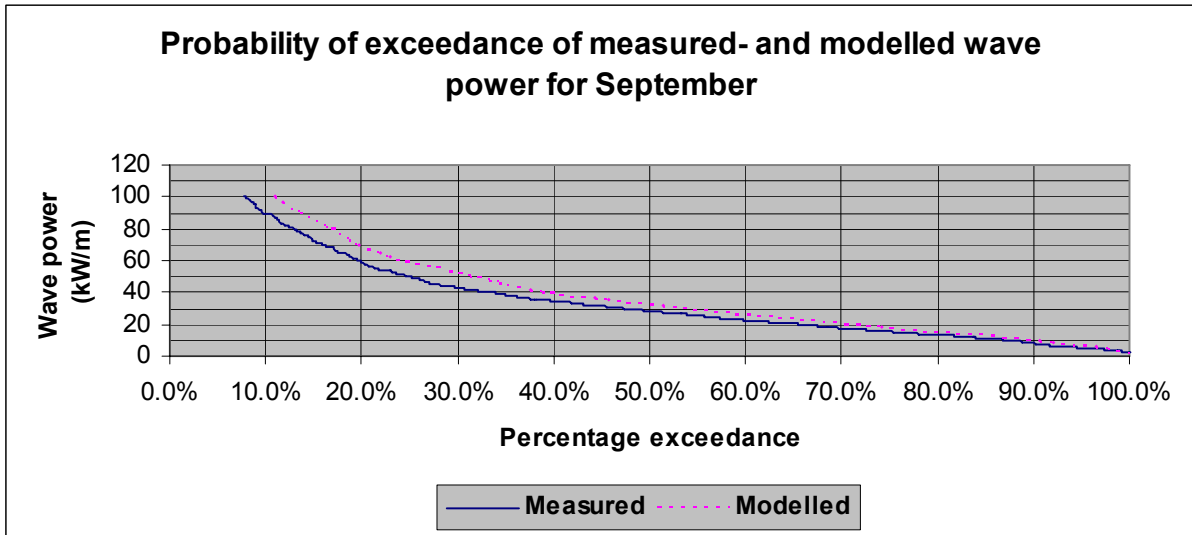
A comparison of monthly average probability of exceedance of
measured- and modelled wave power

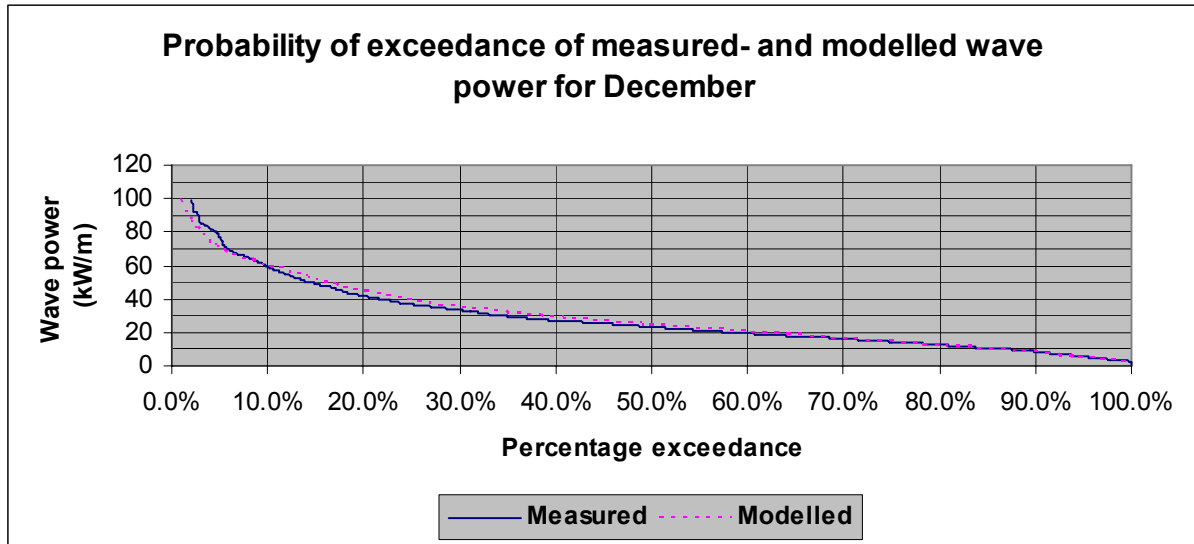
G Monthly probability of exceedance of measured and modelled wave power











APPENDIX H

Index of electronic appendix

H Index of Electronic appendix

H1 Model output

Monthly wave power

12 Mean monthly spatial distribution maps of average wave power of the study area. The *AveMonth.kmz* file is included which overlays the monthly average spatial maps on to Google Earth.

12 Mean monthly spatial distribution maps of 90% probability of exceedance of wave power of the study area.

Raw data is included of the 50% and 5% probability of exceedance of monthly wave power over the study area that can be converted to spatial distribution maps using SURFER 8.

Annual wave power (complete years of 1998 to 2005)

10 Mean annual spatial distribution maps of average wave power of the study area.

The raw data of the 90% and 5% probability of exceedance of annual wave power over the study area can be converted to spatial distribution maps using SURFER 8.

H2 References

The following electronic references relevant to study are also included.

Hagerman G. (2001) **“Southern New England wave energy resource potential”**, technical paper presented at the Building Energy 2001 conference in Boston in March 2001

Hagerman G and Bedard R (2003) **“Guidelines for preliminary estimation of power production by offshore wave energy conversion devices”** technical paper published as E2I EPRI specifications

MacHutchon K. (2006) **“Charaterisation of South African sea storms”**, M.Sc thesis at Stellenbosch University.

Previsic M. (2004) “**Offshore Wave Energy Conversion Devices**” technical paper published as an assessment by E2I EPRI.

Retief G de F, Prestedge GK, Müller FPJ (1982) “**A proposal for wave energy conversion near Cape Town**”, a technical paper published in ICCE, Volume 1 p.245 – 260.

World Meteorological Organisation (WMO) (1998) “**Guide to wave analysis and forecasting**”, technical report.

